ANALYSIS OF HEAT PARTITIONING DURING SLIDING CONTACT AT HIGH SPEED AND PRESSURE

DISSERTATION

Gracie Y. Paek-Spidell, Civilian

AFIT- ENC-DS-14-M-02

DEPARTMENT OF THE AIR FORCE

AIR UNIVERSITY

AIR FORCE INSTITUTE OF TECHNOLOGY

Wright-Patterson Air Force Base, Ohio

The views expressed in this dissertation are those of the author and do not reflect the official policy or position of the United States Air Force, Department of Defense, or the U.S. Government.

AFIT- ENC-DS-14-M-02

ANALYSIS OF HEAT PARTITIONING DURING SLIDING CONTACT AT HIGH SPEED AND PRESSURE

DISSERTATION

Presented to the Faculty

Department of Mathematics and Statistics

Graduate School of Engineering and Management

Air Force Institute of Technology

Air University

Air Education and Training Command

In Partial Fulfillment of the Requirements for the

Degree of Doctor of Philosophy in Applied Mathematics

Gracie Y. Paek-Spidell, Civilian

March 2014

AFIT- ENC-DS-14-M-02

ANALYSIS OF HEAT PARTITIONING DURING SLIDING CONTACT

AT HIGH SPEED AND PRESSURE

Gracie Y. Paek-Spidell, B.S., M.S.
Civilian

Approved:

//signed//	
Dr. William P. Baker Dissertation Advisor	Date
//signed//	
Dr. Anthony N. Palazotto Dissertation Co-Advisor	Date
//signed//	
Dr. Alan V. Lair Committee Member	Date
//signed//	
Lt.Col. John R. Dea, Ph.D Committee Member	Date

Accepted:

Adedeji B. Badiru, PhD Dean, Graduate School of Engineering and Management	Date

Abstract

This research develops a mathematical formulation and an analytical solution to frictional heat partitioning in a high speed sliding system. Frictional heating at the interface of sliding materials impacts temperature and the wear mechanisms. The heat partition fraction for a sliding system is an important parameter in calculating the distribution of frictional heat flux between the contacting surfaces

Lacking an analytical solution, a constant heat partitioning coefficient was typically used, particularly with the slipper-rail contact surface at the Holoman High Speed Test Track. This assumption was non-physical as frictional heat partitioning is influenced by the slipper velocity and the contact pressure profile as well as the material properties. The solution presented in this dissertation considers the characteristics of the slipper's frictional heat partition values along with the experimental loading data.

With a physics based, rather than a phenomenological approach, this solution improves the estimate for the slipper's heat partition function. Moreover, this analytical solution is practical in calculating the average surface temperature and estimating the total melt wear volume. The heat partition function compares favorably with existing experimental and analytical data. Using the Strang's Splitting and ADI methods, a numerical method for surface temperature and corresponding wear percentage under dynamic bounce conditions was extensively developed.

Acknowledgements

I could not have accomplished this task without the support and encouragement of my husband, who is my best friend and eternal companion, my brother, and my family. During my doctoral studies, my husband has shown great love, encouragement, patience, and support during the long hours at the school. I hope that my pursuit of education will inspire and encourage my family to continue to seek further knowledge.

Additionally, I'd like to thank my research advisors, Dr. William Baker and Dr. Anthony Palazotto, for their guidance in this research project. They spend much of their personal time researching articles, developing theory, and asking pointed questions to help me gain a better understanding of the analysis of heat partitioning values in sliding contact at high speed and high pressure. Their experiences with the numerical and analytical mathematical knowledge on partial differential equations and the high velocity wear phenomenon kept me focused on the final goal.

Gracie Y. Paek-Spidell

Table of Contents

Page

Page

Page

Page

List of Figures

Page

Page

List of Tables

List of Symbols

k	Thermal conductivity ($cal / m \cdot sec \cdot K$)
κ	Thermal diffusivity ($k / c\rho$, m^2 / sec)
$Q(t)$	Heat source ($cal / m^2 \cdot sec$)
T	Temperature (K)
T_m	Melting temperature (K)
T_0	Initial temperature (K)
T_a	Ambient temperature (K)
T_r	Reference temperature (K)
T_1 , T_2	Temperature before/after melting (K)
ρ	Density (g / m^3)
ℓ	Latent heat (cal / g)
c	Specific heat
t	Time (sec)
t_m	Melting time (sec)
$\mathcal{L}$	Laplace transform
$\sigma(t)$	Interface boundary
U	Moving velocity
$q(t)$	Heat flux
A	Surface area
$e(x,t)$	Thermal energy density
$\delta(t)$	Penetration depth / Thermal layer
(x, y, z)	Space variables in x, y, z – axis

$v(t) = at + q_0$	Velocity of Slipper (a, q_0 acceleration and initial velocity)
μ	Frictional Coefficient
P	Pressure
l	Slipper's length
α	Slipper's heat partitioning fraction values

ANALYSIS OF HEAT PARTITIONING DURING SLIDING CONTACT AT HIGH SPEED AND PRESSURE

1. Introduction

The very rapid friction of two thick bodies produces fire.

Leonardo Da Vinci

Tribology is the study of interactions between a material's surface and other materials or environments in relative motion. Because the subject is vague and complicated, numerous moderately successful attempts with different numerical, analytical, and experimental solving techniques have been examined to better understand the connection among friction, lubrication and wear in various fields of study. Current interest and knowledge on tribology is substantial, and many applications of tribology are beneficial to our daily life. The core of the tribological discipline is the development of practical design algorithms needed by engineers to overcome the failure of tribological components.

The major branches of tribology are mechanical engineering, material science, and chemistry. In addition, the mathematics of frictional heat partition fractions (the ratio describing how much frictional heat energy flows into one sliding surface and the other) and surface temperatures at the interface due to sliding, the mathematics of liquid lubricant behavior for various shapes of sliding surfaces, the mathematics of the atomic and micro-scale wear mechanisms whereby solid surface degradation or alterations

occurs during sliding, and the reactivity between lubricants and solid surfaces respectively are essential to understanding and demonstrating tribological problems.

1.1 Experimental Background

The Holloman High Speed Test Track (HHSTT), located at Holloman Air Force Base (AFB), NM, is a U.S. Air Force rocket powered sled track facility used for investigating hypersonic environments, aircraft munitions, egress systems, and aerodynamic related effects. The HHSTT performs the hypervelocity aerospace testing using rocket-propelled sleds that travel on steel rail tracks at speeds approaching 3,000 m/s.(1)(2)(3) To date, the fastest sled on record reached a velocity of 2,885 m/s in April 2003 on a newly developed dual rail sled system.

Figure 1. World Land Speed Record : 30 April 2003 (2,885m/s) (1)

While performing the high velocity test, the high-energy impact creates gouging at the interface of a slipper/rail boundary brought about by contact of the test sled on the track. These gouges typically are a result of a high pressure core developing at the slipper/rail interface and high viscoplasticity that leads to material mixing. (4)(5)(6)

Irregularities in the rail and varying aerodynamic loads cause a dynamic bounce. Two contact-driven hypervelocity phenomena that limit sled velocity are slipper wear and rail/slipper gouging, both of which have been known to cause catastrophic failure of the system. The development of these phenomena is affected by a combination of conditions, temperature, oxidation, loading pressure, etc.

In particular, this research into wear and gouging focuses on surface temperature of the slipper and thus requires consideration of the thermal state. While in sliding contact with the rail, the slipper is subject to intense frictional heating. The slipper quickly reaches a state of elevated temperature. As the slipper travels along the rail, the rail is subjected to near instantaneous frictional heating. The major task in this research is to understand how the thermal distributions of rail and slippers are characterized due to sliding at high speeds with a dynamic bounce, and to investigate its thermal effects on the slipper. To describe these physical phenomena, a mathematical model needs to characterize the heat transfer from the hypervelocity contact surface into the rail and slippers.

A simple model of the thermal transport caused by a moving source at high speeds along an infinite half-space was developed in one dimension and used the steady-state solution to determine the effects of source velocity on the effective thermal penetration depth.(7)

1.2 Wear and Friction

The existing literature reveals many different definitions of wear. Bayer (8)(9)(10) lists some of the more general aspects of wear behavior. "Wear is a system property, not a material property. Materials can wear by a variety of mechanisms and combinations of mechanisms, depending on the tribosystem in which it is used. Wear behavior is frequently nonlinear. Transitions can occur in wear behavior as a function of a wide variety of parameters."

Slipper wear at the Holloman High Speed Test Track can be seen as melt wear because slipper melted material at the sliding interface is removed due to induced temperatures that surpass the material's melting temperature. It may be considered dry sliding wear (two solid sliding surfaces in contact) because no intentional lubricant or moisture is introduced into the slipper/rail contact area with a relative sliding velocity. Or, it may be considered compound impact wear as a result of the slipper's combined effect of both sliding on and impacting the rail during the bouncing or skipping motion. According to Kato, the mechanisms of wear can be grouped into three types of wear: thermal, mechanical, and chemical. The various mechanisms of wear contribute to the overall coefficient of friction μ. (11)

Several of the wear mechanisms were briefly described in Chad Hale's Dissertation. (1)(8)(11) Abrasive wear occurs when hard particles or asperities are forced against and move along a solid surface. Adhesive wear occurs when the contacting asperities from two different sliding surfaces bond or adhere together. Melt wear occurs

when the conditions at the interface are sufficient to cause localized melting of the sliding material. Typically, these conditions are high normal load coupled with high sliding velocity. The melting temperature T_{melt} of the material also plays a role. In the case of metals, as the sliding velocity increases, a film of liquid or molten metal forms at the interface which provides melt layer and a lower coefficient of friction. This study will primarily focus on melt wear, caused by high sliding velocity and high pressure to the total slipper wear.

"Friction" is the force resisting the relative tangential/lateral motion (slipping or smooth sliding) of solid surfaces, fluid layers, or material elements in contact, and there are several subdivided categories; (12)

1. Dry friction : The force resisting relative lateral motion of two solid surfaces in contact, and also subdivided into static friction between non-moving surfaces, and kinetic friction (also called sliding friction) between moving surfaces
2. Lubricated friction : the force resisting relative lateral motion of two solid surfaces separated by a layer of gas or liquid
3. Fluid friction : the friction between layers within a fluid that are moving relative to each other
4. Internal friction : the force resisting motion between the elements making up a solid material while it undergoes deformation

The magnitude of friction is expressed in terms of the coefficient of friction,(13) which is the force to slide divided by the force or load pressing the two solid bodies

together.(14)(15) In other words, the coefficient of friction is the ratio of the frictional resistance force to the normal force pressing the surfaces together.

1.3 Thermal Effects on Melt Wear and Frictional Energy

Solid friction occurs whenever two solid bodies slide against each other generating a mechanical deformation, which is transformed into internal energy. Heat produced upon the sliding of two solid materials, called frictional heat, is among the most important contributors to of wear. Solid friction and resulting frictional heating is concentrated within the real contact area between two materials in sliding. In a micro-scale interaction, these mechanisms occur at the asperities on the contacting surfaces. In a macro-scale interaction, most heat energy dissipates into the contact surfaces of a solid by heat conduction and deformation processes. Experimental work has shown that at least 95 percent of the energy dissipation occurs within the top 5 μm of the contacting bodies(16)(17) and most tribologists agree that nearly all of the energy dissipated in frictional contact is transformed into heat.(18) This frictional heat raises the temperature of the sliding surfaces. The ability to predict the surface temperatures of contacting bodies is important to avoid a failure of tribological components. In addition, frictional heating has such an important influence on the tribological behavior of so many sliding systems that all tribotests (physical tests of friction, lubrication and wear) must be designed with thermal considerations in mind and frictional heating must be considered in interpreting the results of tribotests. For the purposes of our discussion, it is assumed that all frictional energy is dissipated as heat.

With the agreement that most frictional energy is transformed into heat at contact surface areas, frictional heating and contact temperatures of sliding materials produce a strong effect on the tribological behavior and failure of sliding materials. This in turn means high surface temperatures and leads the cause of changes in the friction and wear behavior of the materials, such as changes in the structure and properties of the sliding materials and melting of the contacting solids.

During tribological processes, frictional heating produces the following outcomes;(19)

1. Due to the high sliding velocities, sliding frictional heat of metallic components can increase contact temperatures high enough to melt the sliding face. This results in a thin layer of molten material which lowers the friction significantly but at the cost of increased wear. Such a condition can occur with rocket sleds or with projectiles traveling in gun barrels.
2. Frictional heating can cause surface temperatures to reach the melting or softening temperature of thermoplastic polymers. The combination of contact pressure and sliding velocity causes the surface temperature to reach the critical temperature of the material.
3. Contact temperatures and the resulting thermal stresses can play an important role in the wear of sliding metallic components. The fact that temperature gradients at and near the contact surface are very large can be responsible for the softening and shear failure of the near-surface layer of the material in many situations. The

thermo-mechanical stress field around a sliding contact can be responsible for wear of the contacting materials.

1.4 Heat Transfer Mechanisms

Heat is transferred between any two particles which are at different temperatures. These two particles may be part of the same solid body, of two different solids, or of a mass of fluid. There are three distinct methods by which heat transfers: Conduction, Radiation and Convection. The mechanism of heat transfer depends on the nature of the system and on the character of the material state surrounding the two particles.

Conduction: Between two particles of a solid body which are at different temperatures, heat is transferred by conduction. Consider a solid plate of thickness d with surface area A and upper and lower surface temperatures, $T_{higher} > T_{lower}$. Since a temperature difference $(T_{higher} - T_{lower})$ exists between the surfaces, heat flows from the upper surface T_{higher} to the lower one T_{lower} through the plate. Intuitively, the greater temperature difference and surface area yield the greater heat flow rate and the shorter the distance (in a homogenous solid) between surfaces yields a faster heat flow rate. Therefore, the rate of heat flow q is

$$q = kA\frac{T_{higher} - T_{lower}}{d} \tag{1.1}$$

where q is heat flux, the positive constant k is thermal conductivity of the solid, A is surface area, T_{higher} is higher surface temperature, T_{lower} is lower surface temperature, and d is thickness of a solid plate.

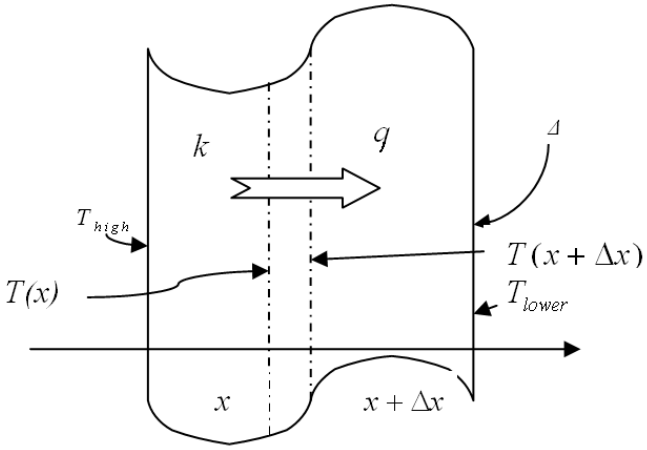

Figure 2. One-Dimensional Heat Conduction Through a Flat Plate (20)

Consider the same solid plate with the temperatures $T(x)$ at x and $T(x+\Delta x)$ at $x+\Delta x$, then

$$q = kA\frac{T(x)-T(x+\Delta x)}{\Delta x}\ . \tag{1.2}$$

Since the limit is the derivative of temperature with respect to x

$$\lim_{\Delta x\to 0} q = -kA\lim_{\Delta x\to 0}\frac{-T(x)+T(x+\Delta x)}{\Delta x}, \tag{1.3}$$

the expression of the rate of heat flow above reduces to

$$q = -kA\frac{dT}{dx} \tag{1.4}$$

where k is defined as the thermal conductivity of the solid, known as Fourier's law of heat conduction for a one-dimensional steady system.(20)

The heat flux is the quantity of heat transferred per unit time across a unit area, and using Equation (1.4) the heat flux in one dimension can be written as

$$q'' = \frac{q}{A} = -k\frac{dT}{dn} = -k\frac{dT}{dx} \tag{1.5}$$

where $q"$ is the heat flux in the direction of $\boldsymbol{n}$ at a point **P** of a solid.(20) In Equation (1.5), $\boldsymbol{n}$ is the normal vector of the surface at a given point **P**, so the direction of $\boldsymbol{n}$ is only x direction and $\boldsymbol{n} = \hat{\boldsymbol{\imath}}$.

Radiation: If two particles at different temperature are separated by a vacuum, then heat can be transferred between them not by conduction but by radiation. If the two particles are separated by an opaque solid or liquid medium, the amount of heat transferred through it by radiation is usually negligible. Typically, radiant heat transfer is of chief interest in gasses.

Convection: Heat transfer takes place by mass motion of a fluid such as air or water when the heated fluid is caused to move away from the source of heat, carrying energy with it. Convection above a hot surface occurs because hot air expands, becomes less dense, and rises.

Because materials have wavy and rough surfaces, their surfaces are uneven and irregular. Friction occurs on those asperities whenever two materials slide against each

other. Accordingly, contact between two materials can only occur at a limited number of asperity points. Since the number of contact points depends on the load, the roughness of the surface, and the total area of those contact points (typically about the top 5μm of the contacting bodies), very high pressures are concentrated on those points. During contact between surfaces, there are two interactions taking place, which is between the asperities externally and inside of materials internally. The interaction between rubbing contact surfaces results in formation of friction, which is the resistance to the sliding of one solid body over or along another. Through frictional processes, mechanical energy is transformed into internal energy or heat, which causes the temperature of the sliding bodies to increase.

Because of contact surface roughness at the sliding rail and shoes, frictional processes due to high velocities and heavy loads occur on the asperities. Frictional heat energy is concentrated on those solid-to-solid contacting areas. Thus, it may be assumed that most frictional energy is transformed into heat energy, and this heat energy transfers between two sliding solid materials conductively. Therefore, the conduction is the dominant mechanism of heat transfer between two sliding solids.

1.5 Heat Partitioning Coefficient On Sliding Surfaces

Hale (1) assumed that frictional heating was split evenly between the slipper and rail with 50 % of the frictional heating entering the slipper and 50% entering the rail. He also assumed that the slipper and rail are in contact while sliding. The slipper and rail were assumed to be made out of the same material. However, the balance of frictional

heating is actually a function of the temperature gradients of the slipper and the rail, the relative velocity (sliding time and distance), and material properties.

Farrell, Eyre (24), Lim and Ashby (25) suggested that heat partitioning values have strong correlation with loading pressure, relative velocity and frictional coefficient. Thermal physics suggests that the heat gradient is determined by temperature difference between rail and slipper as well as change in material properties when melt occurs. Because the slipper is traveling along the rail, the front edge of the slipper always enters a cooler region of the rail and the temperature difference at the front edge of the slipper is larger. So, the gradient of frictional heat energy is greater at the front edge. While the slipper is sliding on the rail, the slipper is in contact in a cooler region of the rail and more heat energy tends to flow into the lower temperature region. This leads that the gradient of heat flux of the slipper is smaller than that of the rail.

Frictional heat energy on the sliding contact is a function of heat partitioning coefficient, pressure, relative velocity and material properties. While sliding, one fraction of the frictional heat energy flows into the contact surface of slipper and the other fraction of the frictional heat energy flows into the contact surface of rail. The frictional heat energy increases the temperature at the contact surfaces of slipper and rail and eventually the slipper may reach a melt temperature. Once the slipper starts melting at the interface, the melt layer is continuously removed by sliding contact.

1.6 Literature Review on Heat Partitioning Values

The leading works on the thermal analysis of sliding systems are those by Blok (26) and Jaeger (21). At the interface of two sliding materials, the temperature of both contacting surfaces should be continuous and the frictional heat energy must be conserved. The temperature distributions of sliding surfaces at the interface should be non-uniform. Thus, heat partitioning values should be non-uniform along the slipper and rail at the contact surfaces and change with time. The heat partitioning values balance the thermal energy between a slipper and rail. This non-uniform temperature distribution of sliding surfaces and non-uniform heat partitioning values at the interface, make the thermal analysis of a sliding system difficult. Furthermore they make the analytical approach of developing a heat partitioning function complex.

Instead of matching the surface temperature of the two materials at all points along the contact interface, Blok (26) matched the maximum surface temperature of two sliding bodies along the contact region and determined the distribution of heat partitioned into each bodies. Jaeger (21) used a Green's function to develop steady-state solutions of moving and stationary bodies, matched the averaged temperature of the two bodies at the contact interface. Kennedy and Tian (27) used a finite element analysis technique to develop approximate solutions of surface temperature and heat partitioning fractions for several sliding problems. Komanduri and Hou (28) used a Green's function to find contact-surface temperature distributions of moving and stationary bodies to determine variable heat partitions along the interface between two bodies.

1.6.1 Analytical Analysis Approach

Francis (29) developed a steady-state solution for the temperature distribution on a sliding contact interface using Hertzian contact. He assumed that each body would get all of the frictional heat energy and that the temperature would only be influenced by the frictional heat energy of each point of the body.

Iwand et al. (30) found analytical solutions by assuming a constant heat flux flowing into the moving body over a circular area of radius *a* given by $q = (1-\alpha)\, p\mu V$ where *q* is the heat flux into the moving body, α the heat partition factor which is the fraction of the total friction heat generated that flows into the rail, *p* the surface pressure taken as uniform, μ the coefficient of friction, and *V* is the slide velocity. A steady-state value of heat partitioning value α is determined analytically by the formula

$$\alpha = \frac{1}{1+1.474\sqrt{\kappa / aV}} \tag{1.6}$$

where κ the thermal diffusivity.

Sun et al. (31) considers a semi-infinite body with a uniform heat flux on a rectangular area with assumptions of a uniform pressure and the gradient of heat flow being normal to the surface. Using Jaeger's method, equating expressions for the average temperatures of two bodies, they developed a transient heat partition factor in the form

$$\alpha(t) = 1 - \mathcal{L}^{-1}\left[\frac{J_1}{s^{1/2}+j_1} + \frac{J_2}{s^{1/2}+j_2} + \frac{J_3}{s^{1/2}+j_3}\right] \tag{1.7}$$

where $\mathcal{L}^{-1}$ the inverse Laplace transform, s the Laplace transform variable, J_i , j_i the functions of the contact area dimensions, slide velocity and thermal properties. The development of Equation (1.7) and the definitions of each term are well derived and explained in Sun's paper, *Progress in the reduction of wheel spalling*.(31)

1.6.2 Functional Analysis Approach

Komanduri and Hou (32) use the functional analysis approach to investigate the temperature distribution and the heat partition at the chip-tool interface in machining. They assume a uniform heat flux distribution along the sliding contact area to develop the best fit curve of heat partition values. They consider the functional relationships for the heat partition fractions as a function of the heat intensity distribution, contact length of interface, the velocity of the moving heat source, and the thermo-physical properties of the two bodies of the sliding system.

They consider the case of uniform heat intensity distribution and adopt the solutions for an infinitely long stationary and an infinitely long moving band heat sources (21). They observe that it takes much longer for a stationary heat source to reach a quasi-steady-state than a moving heat source. The moving heat source is considered as quasi-steady-state while the stationary heat source is considered as transient. They determine the time for a moving heat source to reach the quasi-steady-state given by

$$t_{qs} = \frac{20\kappa}{v^2} \tag{1.8}$$

where t_{qs} is the time for a moving heat source to reach the quasi-steady-state, κ is the thermal diffusivity, and *v* is the velocity of heat source.

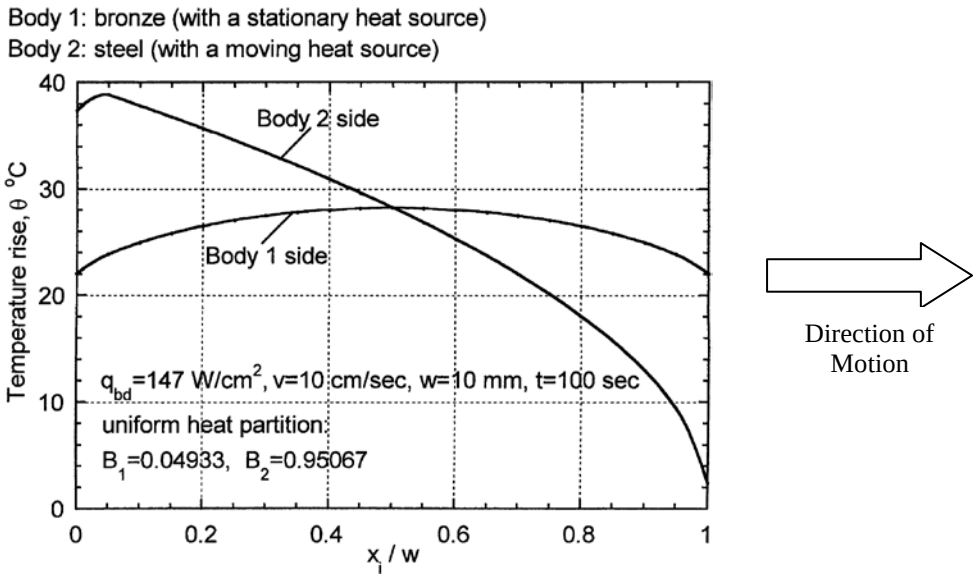

Figure 3. Surface Temperature Rise Along the Contact Interface for the Moving and Stationary Bodies Considering Uniform Heat Partitioning Fraction (32)

In Figure 3, for Body 1 with a stationary band heat source, the distribution of temperature rise is symmetric and the maximum value of the temperature rise is at the mid-point of the contact length. However, for the moving body, it is not symmetric and the maximum temperature rise is towards the trailing edge. The higher the velocity of the moving heat source, the closer is the maximum value of temperature rise to the trailing edge. This is the characteristic form of the temperature rise distribution on the surface caused by a moving heat source as originally shown by Carslaw and Jaeger (21). Furthermore, the numerical result, which will be presented in Chapter 7, will show the same pattern.

From the results of the calculation of temperature rise for moving and stationary bodies for a uniform heat partition as shown in Figure 3, it is clear that matching of the temperatures at all points on either side along the width of contact would be impossible. Consequently, when two bodies are in sliding contact, the heat partition would be non-uniform along the width of contact. Therefore, it is necessary to match the temperature rise everywhere along the width of contact on either side of the interface and not merely the average temperature rise.

Komanduri and Hou (32) developed the function for the non-uniform distribution of heat partition function B_i using the curve-fit analysis approach with trial-and-correction terms. They use a polynomial curve-fit because it is easy to adjust the parameters for matching the two temperature rise distribution curves at the sliding contact interface on each body. By increasing the number of terms of the polynomial function, a high degree of accuracy could be obtained. The resulting functional relationships of the local heat partition fractions is given

$$\begin{aligned} B_{i1} &= (B_1 + \Delta B) - 2\Delta B\left(\frac{x_i}{w}\right)^m \\ B_{i2} &= (B_2 - \Delta B) + 2\Delta B\left(\frac{x_i}{w}\right)^m \end{aligned} \tag{1.9}$$

where B_1 , B_2 the averaged heat partition fractions over the sliding contact area for Body 1 and Body 2, B_{i1} , B_{i2} the local heat partition fraction for Body 1 or Body 2 at the point x_i , ΔB the maximum trial-and-correction factor at $x_i = 0$, w the width of contact area, and m determined by a trial and error.

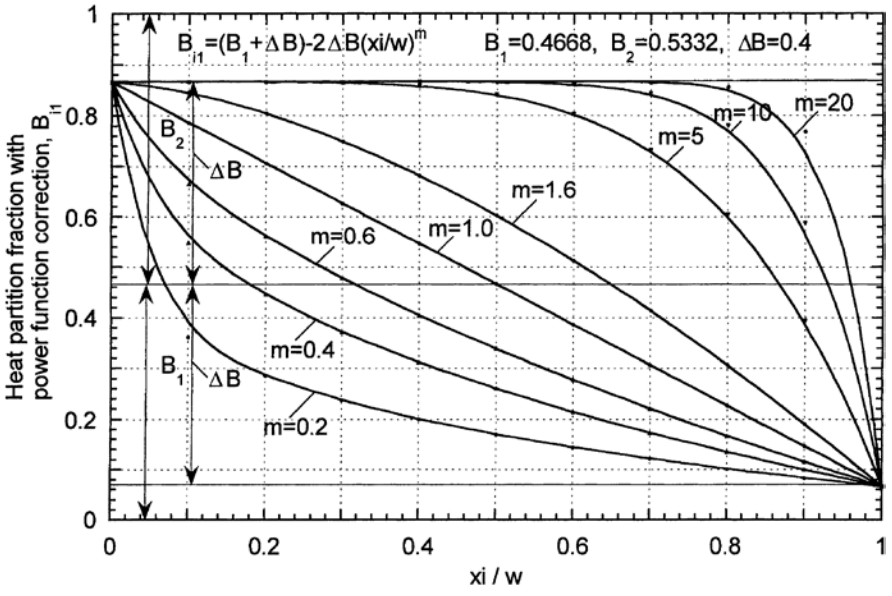

Figure 4. Variation in the Heat Partition Fraction with Power Function Correction (32)

Komanduri and Hou plotted a pair of temperature rise equations for stationary and moving band heat sources with a non-uniform distribution of heat liberation intensity, equations B_{i1} and B_{i2} in Equation (1.9). Figure 4 shows the variation of the heat partition fraction with power function correction, B_{i1} as a function of the width of the heat source x_i / w for different values of m. They observed that for smaller values of $m\,(<1)$, the compensation effect on the left wide of the temperature rise distribution curves as a whole can be lowered keeping the effect on the extreme left end $(x_i / w \to 0)$ still sufficiently large. Therefore, they stated that it is necessary to select an appropriately small value of $m\,(<1)$ such that the portion of the curve near the left end would have sufficient compensation without causing over compensation to the remaining left part. For large values of $m\,(10 \le m \le 30)$, the compensation effect is concentrated towards the

extreme right end while its effect is very small or negligible near the middle or at the left side.(32)

For matching the remaining part on the right side, a third term with a large exponent is needed. Thus, Komanduri and Hou discovered the functional relationships of the local heat partition fractions shown below

$$B_{i1} = (B_1 + \Delta B) - 2\Delta B\left(\frac{x_i}{w}\right)^m - C\Delta B\left(\frac{x_i}{w}\right)^k$$
$$B_{i2} = (B_2 - \Delta B) + 2\Delta B\left(\frac{x_i}{w}\right)^m + C\Delta B\left(\frac{x_i}{w}\right)^k \quad (1.10)$$

where m, k, C determined by a trial and error, i.e. for large values of the *Peclet number* (≈ 20), $m \approx 0.03$, $k \approx 35 \sim 45$, and $C \approx 0.5$.(32)

1.6.3 Numerical Analysis Approach Using FEA Model

Gupta et al. (33) assumed 50% of the frictional heat entering the contact surface of rolling wheel and another 50% of the frictional heat entering the rail, equally distributed between the wheel and rail. They used finite element analysis to study the frictional heat energy in a rolling and sliding system. Kennedy et al. (34) consider a Hertzian pressure distribution over the contact area rather than a uniform one and use a finite element analysis to determine the heat partition factor by matching the temperature everywhere between the wheel and rail. They simplify assumptions to determine the transient solutions for the railcar wheel sliding problem.

Figure 5 shows the comparison between Sun et al.'s analytical transient solutions (dotted line), Equation (1.7) (31), and the numerical solution using a transient finite element analysis. Kennedy et al. have chosen the case presented by Sun et al.(31) which consists of a BR Mark II coach wheel with a wheel load of 42,000 N and a sliding velocity of 40 m/s. The contact patch is a square area with sides of length 0.01m. The coefficient of friction is 0.075. The thermal conductivity of the wheel and rail steel is 40W/mC, and the thermal diffusivity is 10×10^{-6} m^2/s. The heat generated is assumed to be uniform across the contact interface and given by $q = \mu pV$. A transient finite element analysis was performed for this case assuming an initial temperature of $0^o C$.(34)

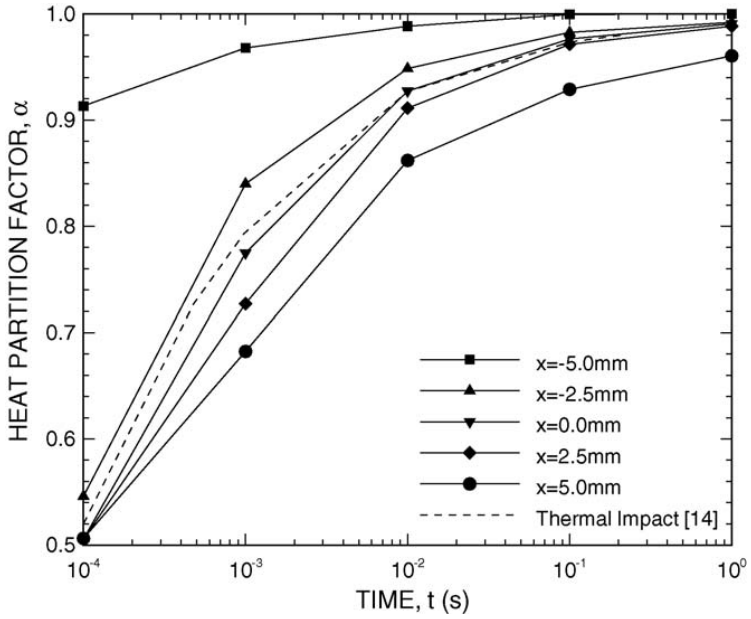

Figure 5. Heat Partition Factor vs. Time at Positions Along the Contact Patch (34)

Figure 5 shows that for all points on the interface, the heat partition factor rises rapidly with time to a value close to one. The results of the analytical model by Sun et al.

(31), in which the heat partition factor α is treated as being uniform across the contact patch, are shown in Figure 5. This simplified analytical solution is very close to the FEA results at the center $(x = 0)$ of the contact patch.(34)

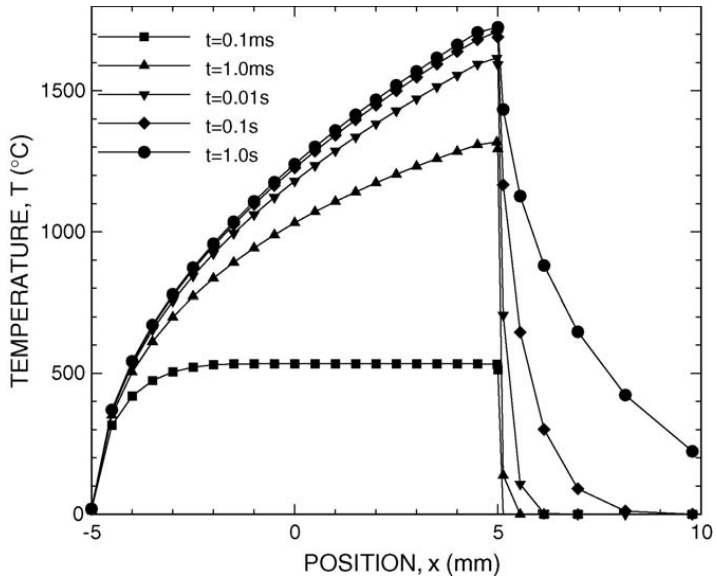

Figure 6. Temperature Distribution Along the Contact Patch at Various Times (34)

Figure 6 shows temperature profiles on the wheel surface near the contact patch at various values of time. At $t = 0.1$ ms, the temperature distribution along the contact patch is approximately uniform and is zero outside the contact patch. As time progresses, the temperature distributes in a non-uniform manner with a peak value near the tailing edge. The numerical model using ADI and Strang Splitting methods will present similar behavior, and the numerical results developed are compared in Chapter 7.

Malinowski, Lenard and Davies (35) used the mechanical models of the hot/warm forging process. The method for the determination of the heat-transfer coefficients in bulk metal-forming process consisted of two steps. The first involved measuring the

temperature distributions within two dies, one of which simulated the cold forming tool and the other the hot workpiece. The second step made use of the finite-element simulation of the resulting heat-transfer problem. The two stainless steel 303 dies of 25.4 mm diameter each are instrumented with four Type K thermocouples of 1.6 mm outside diameter, with INCONEL sheaths and exposed beads, located 2, 4, 10 and 25 mm from the contact surface and embedded to a depth of 10 mm. The dies are connected to the water-cooled heat exchangers of a servohydraulic testing system. One of the dies is heated to a pre-selected temperature in a split, openable furnace. When the desired temperature is reached, the furnace is removed and the cold die is brought into contact with the hot die under closely controlled conditions. The velocity of approach is selected at 0.83 mm/s. The initial temperature of the hot die is varied from 300 to 900 ^{o}C. They used the heat-transfer coefficient as an unknown function of the time of contact, the pressure and the temperature, and the heat-transfer coefficient function was determined using a least-squares approximation. They developed empirical relations of the heat-transfer coefficients as a function of the three parameters, the interfacial pressure, the time of contact, and the initial temperature of the hot die. Equation (1.11) is the heat-transfer coefficient function they estimated

$$\begin{aligned} \alpha &= 1000[(A - 2BQ)t + Bt^2] \quad \text{for } 0 < t \le Q \\ \alpha &= 1000[At - BQ^2] \quad \text{for } Q < t < 40 \end{aligned} \quad . \tag{1.11}$$

The predictions of Equation (1.11) are valid for pressures in the range of $30-90$ MPa and temperatures from 300 to $900\,^{o}C$. The parameters *A*, *B* and *Q* are defined as follows

$$A=[-0.99861+1.39288\overline{p}+4.16282\overline{T}-1.93378\overline{p}^{2}-7.58453\overline{T}^{2}+4.85524\overline{T}^{3}]^{2}$$
$$B=[-1.40191+1.50341\overline{p}+5.51342\overline{T}-0.89550\overline{p}^{2}-5.71863\overline{T}^{2}+1.19936\overline{T}^{3}]^{2}$$
$$Q=[-18.81105+24.37649\overline{p}-55.55330\overline{T}+35.30695\overline{p}^{2}+45.07317\overline{T}^{2}+40.67235\overline{T}^{3}$$
$$-16.59242\overline{p}^{3}-42.08732\overline{T}^{4}]^{2}+4$$

where $\overline{p}=P/100$ and $\overline{T}=\dfrac{T+273}{1000}$.

They discovered that the interfacial heat-transfer coefficient is strongly related to the contact pressures, but not strongly related to the temperature of the hot die. The calculated temperature distribution does not depend on the magnitude of the coefficient of heat transfer as strongly.(35)

Iqbal, Mativenga and Sheikh (36) developed an experimental setup using Finite Element modeling of dry sliding metals to estimate interface heat transfer coefficient. Rubbing tests were performed where the end surface of a cylindrical pin made of tool material was pressed against the end surface of a rotating workpiece. For these tests, a pin of 2.5 mm diameter and 15 mm length was made of cemented tungsten carbide. The mass of the pin was measured using a precision electronic balance to calculate the amount of weight loss during the rubbing process. The rubbing experiments were performed at the rubbing speeds up to 776 m/min. The rubbing time was set to one minute for all rotational speeds in order to achieve a steady state temperature in the pin.

The thermal imaging camera was used and this camera can capture and store thermal images and data. They observe that the estimated interface heat transfer coefficient decreases at low speeds and then becomes approximately steady for high speeds based on their experimental results. Also, they estimated values of interface heat transfer coefficient highly depend on temperature at very low speed but do not show a dependence on any parameter at high speed over 600 m/min (equivalent to 10 m/sec).

1.7 Research Objectives

The objectives of this dissertation are to develop an analytical solution for the slipper's frictional heat partitioning (the function evaluating how much frictional heat energy flows into the slipper while sliding) in order to describe the interaction and melt wear mechanism on the sliding surfaces at high velocity and high pressure, to develop the mathematical model to calculate the distribution of the frictional heat partitioned into a slipper numerically, and to analyze its effects on a sliding surface of material such as the surface temperate and melt wear. Understanding the distribution of heat partitioned into sliding materials and the resulting surface temperatures is critical to develop designs that minimize material failure due to melt wear. The problem may be split in two parts: pre-melting problem and post-melting problem. Before melting during sliding contact the frictional heat energy influences the temperature profile raising the temperature at sliding surfaces. When the surface temperature of the material reaches its melting temperature, the material changes phase from solid to liquid at the sliding surface, i.e. creating the melt layer. Due to high sliding velocity and turbulence flow between two contact surfaces,

this melted layer is removed so the melt layer does not stay on the sliding contact interface. This process is called the melt wear.

The surface temperature profile during the pre-melting period is developed using Green's function. The heat partitioning function is developed using the Laplace Transform and Incomplete Gamma Function analytically and is evaluated numerically. The heat partitioning values on the sliding interface demonstrate the surface temperature of a one dimensional half space region in sliding contact with various velocities and pressures, and calculate the wear percentage due to melting process. Because the frictional heat partitioning values determine the amount of frictional heat energy flowing into the sliding surface over the other, these values are important factor to evaluate the surface temperature distribution and to find the time required for the sliding interface to reach the melt temperature at one surface.

With the immediate melt layer removal, the surface temperature at the contact area never exceeds its melt temperature and is assumed to hold at melt temperature after melting occurs. When the melt layer is created at the sliding surface due to the frictional heat energy, the liquid is formed at the outer layer and the boundary between the liquid and solid (the melt front) moves in the direction of the material's depth. The liquid layer (melt layer) is removed instantaneously while sliding. This process explains how melt wear at high sliding velocities and pressure influences is directed to either surface.

Chapter 2 discusses the mathematical development and formulation of the heat transfer problem using partial differential equations and different initial boundary

conditions. It then presents the mathematical approach to find the temperature distribution solution to heat transfer problem using Green's function and the error function. In Chapter 3, the mathematical models of rail and slipper are developed for a two dimensional heat transfer problem to the high speed sliding system. Carslaw and Jaeger's approach, matching the averaged surface temperatures of rail and slipper, is adopted to develop the analytical solution of frictional heat partitioning. There are some assumptions made in order to formulate and solve slipper and rail's two dimensional heat transfer problem analytically, which are the sum of the frictional heat energy flowing into the slipper and rail being equal to the total frictional heat energy, the uniform heat partitioning value and uniform pressure distribution along the contact surface. No change in thermal properties due to temperature change and phase change may be assumed. Because of these assumptions, the analytical solution to the two dimensional heat transfer problem is only valid until the melt layer on sliding contact occurs. It is important to find melt time, i.e. when the melt layer is first generated. As such, in Chapter 4, the slipper's one dimensional heat transfer problem is formulated using a partial differential equation and solved using Green's function. For the melt temperature of slipper given, the melt time formula is developed for two velocity cases: constant velocity and linearly increasing velocity. In order to verify the analytical heat partitioning solution of the two dimensional heat transfer problem, the two dimensional numerical heat partitioning solution is sufficient and necessary. In Chapter 5, the slipper and rail's two dimensional heat transfer numerical models are developed using ADI and Strang Splitting Methods. Then, in Chapter 6, the slipper and rail's numerical models calculate their surface

temperature distributions and match the averaged surface temperatures, which is Carslaw and Jaeger's approach in order to develop the numerical solution of frictional heat partitioning for two dimensional heat transfer problem. After verifying the analytical solution with the numerical solution, the melt wear percentage is estimated numerically for different scenario in Chapter 7. Finally, the numerical results of melt wear percentage are compared and analyzed and the final considerations of the analytical and numerical solutions for frictional heat partitioning are discussed.

2 Analytical Modeling

2.1 One Dimensional Heat Conduction Problem

Conservation of energy assumptions are foundational to modeling heat flow with partial differential equations. The heat equation is derived from the conservation of heat energy. In Section 1.4, the solid used to formulate differential equations of heat conduction is assumed isotropic (i.e. homogeneous material) having isothermal surfaces (i.e. same temperature at every point at this instant upon it), as well as linear heat flow. Since temperature distribution of the very thin layer on local sliding contact areas is of interest with high velocities and pressures in this research, the heat flux vector at an inter-boundary surface may be considered in only one direction. Accordingly a one-dimensional heat transfer example will be used to demonstrate the simplified heat conduction problem in order to understand how frictional heat input affects the equation of heat conduction.

Suppose a thin rod of length *h* satisfies following assumptions:

1. The rod is isotropic solid (made of a single homogeneous material).
2. The lateral surface area of the rod is insulated perfectly (heat flows only in the ***x*** direction).
3. The temperature of the cross sectional area at x is constant.

Conservation of heat energy says that the heat energy between x and $x + \Delta x$ changes in time due only to heat energy flowing across the edges at x and $x + \Delta x$, and

heat energy generated inside. Applying the principle of conservation of heat to the segment $[a,b]$, the conservation of heat energy is

Rate of change of heat energy in time	= Heat energy flowing across boundaries per unit time	+ Heat energy generated inside per unit time

Let $e(x,t)$ be the thermal energy density, the amount of the thermal energy per unit volume and assumed to be constant throughout the volume. Then the total heat energy in the slice from x to $x+\Delta x$ is $e(x,t)A\Delta x$.

In a finite segment $[a,b]$, the total heat energy is $\int_a^b Ae(x,t)dx$, the sum of the contributions of the infinitesimal slices. So the rate of change in heat energy is equivalent to the following;

$$\frac{d}{dt}\int_a^b [e(x,t)Adx] = [q(b,t)A - q(a,t)A] + \int_a^b QAdx \qquad (2.1)$$

where $q(x,t)$ is defined as heat flux (the amount of thermal energy per unit time flowing to the right per unit surface area), $Q(x,t)$ or Q is heat source (heat energy per unit volume generated per unit time), and $e(x,t)$ is thermal energy density (the amount of thermal energy per unit volume).

The total thermal energy in a thin slice, $e(x,t)A\Delta x$, can be defined as the energy required to raise the temperature from a reference temperature T_r to its actual temperature $T(x,t)$,

$$e(x,t)A\Delta x = c(x)\rho(x)(T(x,t)-T_r)A\Delta x \tag{2.2}$$

where $c(x)$ is the heat capacity or specific heat (the measure of the heat energy per a unit mass necessary to raise the temperature of a substance by one unit temperature), and $\rho(x)$ is mass density (mass per unit volume). Based on this definition, the specific heat $c(x)$ of a material depends on the temperature $T(x,t)$ making the heat equation nonlinear and mathematically complex. Under some conditions, such as restricted temperature intervals and homogeneous rod, the specific heat may be assumed to be constant c having a mass density ρ. Using Equations (2.1) and (2.2), the conservation equation results in a partial differential equation;

$$c\rho\frac{\partial T}{\partial t} = \frac{\partial}{\partial x}\left(k\frac{\partial T}{\partial x}\right) + Q \tag{2.3}$$

If there are no internal heat sources $Q = 0$ and the thermal conductivity *k* is constant, then Equation (2.3) becomes

$$\frac{\partial T}{\partial t} = \kappa\frac{\partial^2 T}{\partial x^2} \tag{2.4}$$

where κ is the thermal diffusivity and defined as $\frac{k}{c\rho}$.

2.2 Simple Heat Conduction Problem Due to Sliding Contact Flux

Carslaw and Jaeger introduced the solution when heat was a moving source. They used

$\frac{1}{\kappa}\frac{\partial T}{\partial t} = \Delta T$ for the differential equation of conduction of heat in 3 dimensions, and this equation is satisfied by $T = \frac{q}{8(\pi\kappa t)^{3/2}} e^{-[(x-x')^2+(y-y)^2+(z-z')^2]/4\kappa t}$ for $t > 0$.

As $t \to 0$ this expression tends to zero at all points except (x', y', z'), where it becomes infinite. Also the total quantity of heat in the infinite region is

$$\int_{-\infty}^{\infty}\int_{-\infty}^{\infty}\int_{-\infty}^{\infty} \rho c T dx dy dz = \frac{q\rho c}{8(\pi\kappa t)^{3/2}} \int_{-\infty}^{\infty}\int_{-\infty}^{\infty}\int_{-\infty}^{\infty} e^{-[(x-x')^2+(y-y)^2+(z-z')^2]/4\kappa t} dx dy dz = q\rho c \ . \qquad (2.5)$$

Suppose that heat is generated at the origin for times $t > 0$ at the rate q heat units per unit time, and that an infinite heat generator uniformly moves by the origin with velocity v_0 parallel to the axis of x. In the element of time dt' at t', qdt' heat unit were generated at the origin; also the point where the heat is generated, which at time t is at (x, y, z), at time t' was at $(x - v_0(t - t'), y, z)$. Thus the temperature at t at (x, y, z) due to the heat qdt' emitted at t' is $\frac{qdt'}{8\rho c(\pi\kappa(t-t'))^{3/2}} \exp\left[-\frac{(x-v_0(t-t'))^2+y^2+z^2}{4\kappa(t-t')}\right]$. And the temperature at t due to the heat emitted at the origin from time *0* to *t* is

$$\frac{q}{8\rho c(\pi\kappa)^{\frac{3}{2}}} \int_0^t \frac{1}{(t-t')^{\frac{3}{2}}} \exp\left[-\frac{(x-v_0(t-t'))^2+y^2+z^2}{4\kappa(t-t')}\right] dt'$$

$$= \frac{q}{2Rk\pi^{3/2}} e^{\frac{v_0 x}{2\kappa}} \int_{R/2\sqrt{\kappa t}}^{\infty} e^{-\xi^2 - \left(\frac{v_0^2 R^2}{16\kappa^2\xi^2}\right)} d\xi \quad \text{where } R = x^2 + y^2 + z^2. \qquad (2.6)$$

Equation (2.6) is the solution for heat supply for a finite time *t*. If $t \to \infty$, a steady state solution is established, and the temperature at (x, y, z) is $\frac{q}{4\pi kR} e^{\frac{-v_0(R-x)}{2\kappa}}$.

If heat is produced at the constant rate q' per unit time per unit length along the *y*-axis, the temperature in the steady state at the point (x, y, z) is found by integration to be

$$\frac{q'}{4\pi k}\int_{-\infty}^{\infty} e^{\left(\frac{-v_0(\sqrt{R}-x)}{2\kappa}\right)}\frac{dy'}{R} = \frac{q'}{2\pi k} e^{\frac{v_0 x}{2\kappa}} K_0[v_0(x^2+z^2)/2\kappa] \qquad (2.7)$$

where $K_0(x)$ is the modified Bessel function of the second kind of order zero.

Consider the thermal effects of contacting surfaces of slipper and rail of Holloman High Speed Test Track (HHSTT). In this case, heat is supplied over some area, whose shape is not well-defined. A slipper is assumed to be an infinite strip heat source of $-b < x < b, -\infty < y < \infty$ in the plane *z=0* moving with constant velocity v_0. As it slides over the rail, the frictional heat is generated at the constant rate *q* per unit time per unit area over the strip.

In Section 10.7 of Carslaw and Jaeger's book *Conduction of heat in solids*, they presented the solution of the infinite strip heat source with velocity v_0. Using their approach to the solution, the temperature distribution is formed by integrating Equation (2.7)

$$T = \frac{q}{2\pi k}\int_{-b}^{b} e^{\frac{v_0(x-x')}{2\kappa}} K_0\left(\frac{v_0\left[(x-x')^2+z^2\right]^{1/2}}{2\kappa}\right)dx' \quad (1) \qquad (2.8)$$

where $K_0(x)$ is the modified Bessel function of the second kind of order zero.(44) On the sliding contact between the rail and shoe at HHSTT, the frictional heating generates the thermal energy, which flows into the rail and shoe. If it is assumed that the rail and shoe are semi-infinite solids, Equation (2.8) is applicable to find the temperature of the rail or shoe when they slide with a velocity v_0.

2.3 Initial and Boundary Conditions

Equation (2.4), the one dimensional heat conduction equation, is the partial differential equation that describes one dimensional heat flow in a homogeneous material. However, additional information is needed for a well posed and physically meaningful problem. This information is given in the form of initial and boundary conditions.

1. *Initial Condition* describes the state (temperature or concentration) of material when time is zero, $t = 0$. Simple initial condition is the prescription of the temperature at every point in the body at the initial moment and it is expressed mathematically as

$$T(x,0) = g(x) \tag{2.9}$$

where $g(x)$ is a known function. If the heat equation is satisfied for all time $t > 0$ and $T(x,t) \to g(x)$ as $t \to 0$, then its solution is said to satisfy its initial condition.

2. *Boundary Condition* describes the behavior (temperature or heat flux) at the surface (boundary). The boundary or surface in one dimensional heat conduction

problem generally consists of the endpoints $x = a$ and $x = b$ for $-\infty < a < b < \infty$. If both the temperature and heat flux are specified at both $x = a$ and $x = b$, then the problem is considered to be over specified, and generally there is no solution to the heat equation. Therefore, it is necessary in obtaining a unique solution to prescribe either the temperature or heat flux, or some relationship between the two at the endpoints $x = a$ and $x = b$.

During the sliding of two solid materials, the frictional process occurs and produces energy, mostly in the form of heat energy. A continuous supply of heat energy raises the temperatures of both contact surface areas and inside the material. After some time, the temperature of the contact surface areas eventually reaches the melting temperature. The boundary between solid material and melted region moves with time, and is called a moving boundary. Finding the speed and position of the this moving boundary is essential to determine how fast the material's surfaces melts away and how much the melt wear is created.

2.4 Moving Boundary and Conditions Due To Phase-Change

When a material reaches the melt temperature and undergoes a phase change from solid to liquid, there is energy absorbed as a result of phase change and that heat energy is stored in melt layer. During this phase change process, there is no temperature change at the melt layer and stays at the melt temperature. This energy is called latent heat of solidification or melting, and the amount of latent heat of melting determines the

thickness of melt layer. Thus the rate of heat supply to phase change is related to the rate at which the boundary moves.

Let $\rho_i, c_i, k_i, \kappa_i, T_i$ be the constant thermal properties (density, specific heat, conductivity and diffusivity) and temperature of solid ($i = solid$) and liquid ($i = liquid$). The specific heat is the measure of the heat energy required to increase the temperature of a unit quantity of a material by a unit of temperature, i.e. more heat energy is required to increase the temperature of a substance with high specific heat capacity than one with low specific heat capacity. In the problem to be considered, there is no volume change assumed. So both solid and liquid states have the same densities, $\rho_{solid} = \rho_{liquid} \equiv \rho$.

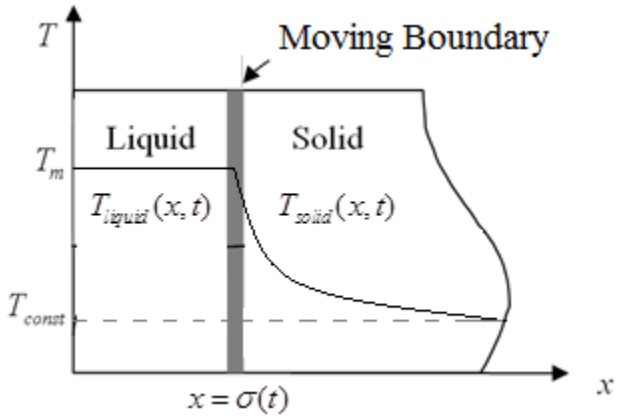

Figure 7. Melting of a Solid On the Heat-Source-Contact Surface

When a solid material is in contact with a heat source on the surface, there exists a separating interface between two phases and this interface can move as time progresses. Figure 7 illustrates how the moving boundary between a solid and a liquid is created and which direction the moving boundary moves. Solidification or melting process occurs

when the material's temperature reaches the melting temperature T_m. Figure 7 shows that the moving boundary of a solid material moves to where the temperature reaches the melting temperature T_m. From Figure 7, the position of the moving boundary can be determined by the temperature distribution inside the material, in which a phase change occurs at melting temperature.

If it is assumed that solid and liquid densities do not change significantly during phase transformation, some particle movement in a liquid phase can be ignored and heat transfer by convection does not take place. Accordingly heat transfer by conduction dominates the solid and liquid.

Let $\ell, T_m, \sigma(t)$ be the latent heat (amount of heat energy required during a change of state, in this case between solid and liquid, without changing a temperature), the melting temperature, and the separating interface location (or moving boundary, position from the initial contact surface) between the solid and liquid phases. Until such time that the temperature reaches melt (call this the melt time, t_m), the moving boundary does not move $\sigma(t) = 0$.

Temperatures of solid and liquid phases are continuous at the solid-liquid interface (moving boundary), and they are equal to its melting temperature. This leads to the boundary condition at the interface

$$T_{solid}(x,t) = T_{liquid}(x,t) = T_m \text{ , when } x = \sigma(t) \text{ for } t > 0 \text{ .} \qquad (2.10)$$

In Figure 7, a semi-infinite region $0 \le x < \infty$ contains a solid initially at a temperature T_{solid} lower than the melting temperature T_m. Where the right boundary in Figure 7 is held at a constant temperature T_{const} (lower than melting temperature), T_m is applied at the liquid surface $x = 0$ at $t = 0$. T_{const} can be either the initial temperature or the ambient (room) temperature The temperature at $x = \infty$ is maintained at this temperature T_{const} for $t > 0$. The solid starts to change phase at the boundary $x = 0$ which is treated as the separating interface located at $x = \sigma(t)$ between solid and liquid. It moves a distance $d\sigma$ in the x direction during dt. We know that the thermal conductivities k_{solid}, k_{liquid} of solid and liquid are different and the rates of heat energies which exit the liquid and enters the solid must be balanced. Therefore, the latent heat ℓ must be liberated at this interface $\sigma(t)$ of liquid and solid. Mathematically this leads to the condition,

$$k_{liquid} \left.\frac{\partial T_{liquid}}{\partial x}\right|_{x=\sigma(t)} = k_{solid} \left.\frac{\partial T_{solid}}{\partial x}\right|_{x=\sigma(t)} - \ell\rho \frac{d\sigma}{dt} \ . \qquad (2.11)$$

Equation (2.11) is known as the "Stefan condition" for the local velocity of a moving boundary as a function of quantities evaluated at both sides of the phase boundary. The Stefan condition, Equation (2.11), is usually derived from a physical constraint when considering problems of heat transfer with phase change.(22) Solving Equation (2.11) for $\frac{d\sigma}{dt}$ produces the follow

$$\frac{d\sigma}{dt} = \frac{1}{\ell\rho}\left[k_{solid} \frac{\partial T_{solid}}{\partial x} - k_{liquid} \frac{\partial T_{liquid}}{\partial x} \right]_{x=\sigma(t)} . \qquad (2.12)$$

This expression shows that the velocity of the interface, $\frac{d\sigma}{dt}$, is proportional to the difference of heat flows entering and exiting across the interface.

2.5 Green's Function Solution

Consider the one dimensional infinite space $|x| < \infty$ and the linear heat flow along the *x*-axis. The equation of linear heat flow in one dimension is

$$\kappa \frac{\partial^2 T}{\partial x^2} = \frac{\partial T}{\partial t} \tag{2.13}$$

where κ is thermal diffusivity, $T(x,t)$ is a temperature of a point x at time $t > 0$. The expression

$$T(x,t) = \frac{e^{-x^2/4\kappa t}}{\sqrt{t}} \tag{2.14}$$

is a particular solution of linear heat flow Equation (2.13).

Observe that:

1. For a fixed $t > 0$, T approaches zero as $x \to \pm\infty$ and T approaches $1/\sqrt{t}$ as $x \to 0$.
2. At $x = 0$, T approaches zero as $t \to \infty$ and T approaches ∞ as $t \to 0$.
3. For all $t > 0$, $\int_{-\infty}^{\infty} T dx = 2\sqrt{\pi\kappa}$.

If x, t, T are considered as position in the depth of solid from a surface boundary, time, and temperature distribution respectively, then Equation (2.14) captures the physical properties of heat transfer;

1 The temperature distribution is "smoothing out" over a material with the maximum temperature decreasing as time progresses, implying that heat energy stored in a material spreads to an even distribution as time progresses.

2 The maximum value of T occurs at $x = 0$ as $t \to 0$, which implies that the heat source is applied initially at the center of a material $x = 0$.

Let's integrate Equation (2.14) with respect to space variable *x* over a semi-infinite area $0 \le \xi \le x$. Introducing the change of variable $\xi = \frac{x}{2\sqrt{\kappa t}}$, $\frac{dx}{\sqrt{t}}$ is replaced with $2\sqrt{\kappa} d\xi = \frac{dx}{\sqrt{t}}$,

$$\int_0^x T dx = \int_0^x \frac{e^{-x^2/4\kappa t}}{\sqrt{t}} dx = 2\sqrt{\kappa} \int_0^{x/2\sqrt{\kappa t}} e^{-\xi^2} d\xi = \sqrt{\kappa \pi}\ erf\left(\frac{x}{2\sqrt{\kappa t}}\right) \quad \text{for } t > 0 \qquad (2.15)$$

with the error function *erf(x)* defined as

$$erf(x) = \frac{2}{\sqrt{\pi}} \int_0^x e^{-\xi^2} d\xi \ . \qquad (2.16)$$

Equation (2.16) is known as "error function solution" or "Green's function" of the heat equation. (Appendix A.1) The function given by Equation (2.14) is positive for any $t > 0$ and has a bell-shaped graph over $-\infty < x < \infty$ for a fixed t. Figure 8 shows that the

graph of the Gaussian function $\frac{1}{\sqrt{2\pi\sigma^2}}e^{(x-\mu)^2/2\sigma^2}$ is a bell-curve shape with the peak of height $1/\sqrt{2\pi\sigma^2}$ at $x=\mu$ and the bell shape gets wider as the value of σ^2 gets larger. By letting $\mu=0$ and $\sigma=\sqrt{2\kappa t}$, the Gaussian function $\frac{1}{\sqrt{2\pi\sigma^2}}e^{(x-\mu)^2/2\sigma^2}$ becomes Equation (2.14) which is a particular solution of linear heat flow Equation (2.13).

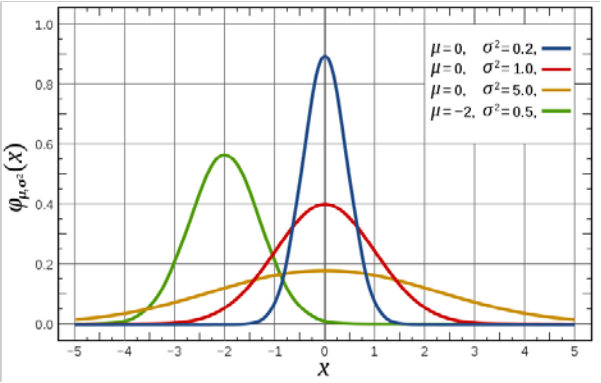

Figure 8. Gaussian Distributions With Different Parameters (23)

Thus, for some fixed time $t>0$ the peak height of Equation (2.14) $T=e^{-x^2/4\kappa t}/\sqrt{t}$ is $1/\sqrt{t}$ at $x=0$ and decays as t grows. This describes the temperature distribution of a material with one point heat source at $x=0$ over time. Since the temperature at some point x in a material at a certain time is the total sum of thermal contribution from the initial state at all points, integrating $T=\frac{e^{-x^2/4\kappa t}}{\sqrt{t}}$ over the positive x gives the temperature distribution for $t>0$.

3 Two-Dimensional Mathematical Model

The sliding system of rail and slipper is a semi-infinite solid, and the temperatures of both bodies are initially at an ambient temperature. Once the rocket-powered sled starts moving, friction generates the intensive heat energy which is applied to both contact surfaces at the interface. Because the physical geometry of slipper and rail's surfaces is rough and the sled is moving with loading pressure, dynamic bounce effects should be considered. While in contact, the frictional heat energy should be the only heat source and no frictional heat loss to environment assumed. While not in contact, there is the heat energy gain or loss due to turbulence flow between two surfaces. Therefore the conductive heat transfer mechanism is applied while in-contact and convective heat transfer mechanism is applied when not-in-contact. The frictional heat partition fraction is only engaged in conductive heat transfer while in contact.

This research employs a two dimensional heat transfer formulation to the high speed sliding system instead of a three dimensional one. It has been shown (40) that the surface temperature distribution along the centerline of a sliding contact area from a three dimensional analysis is virtually identical to its two dimensional counterpart for high velocity.

3.1 Characteristics of Heat Partition Fractions and Bounce Effects

The slipper and rail in sliding contact is illustrated in Figure 9. This sliding contact generates heat due to friction. The flow of this heat is accounted for in terms of heat flux and is partitioned into flux into the slipper and flux into the rail.

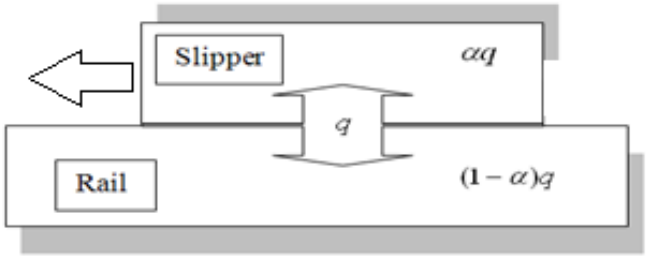

Figure 9. Frictional Heat Distribution of Slipper and Rail with Heat Partition Fraction

It is assumed that there is no heat loss at the sliding interface areas of slipper and rail. For now, the heat partitioning function $\alpha(t)$ is assumed to be the constant function α. If α $(0 \le \alpha \le 1)$ is defined as the slipper's heat partitioning value, then $1-\alpha$ is the rail's heat partitioning value. Thus, the expression for the frictional heat flowing into the rail and slipper is

$$q(t) = \mu P v(t) \Rightarrow \begin{cases} Q_{slipper}(t) = \alpha \mu P v(t) \\ Q_{rail}(t) = (1-\alpha)\mu P v(t) \end{cases} \tag{3.1}$$

where heat flux into slipper $Q_{slipper}(t)$, heat flux into rail $Q_{rail}(t)$, total frictional heat $q(t)$, sliding velocity $v(t)$, coefficient of friction μ, heat fraction flowing into slipper α, pressure P, and heat fraction flowing into rail $1-\alpha$.

Due to the aerodynamic behavior of the load, a skipping or bounce effect at the interface of slipper and rail is created. Figure 10 illustrates the bounce or skipping of the slipper along the rail. During the time of contact, frictional heating takes place and a flux is generated as given by Equation (3.1). During the time of no contact, the slipper experiences forced convection which is modeled by the boundary condition

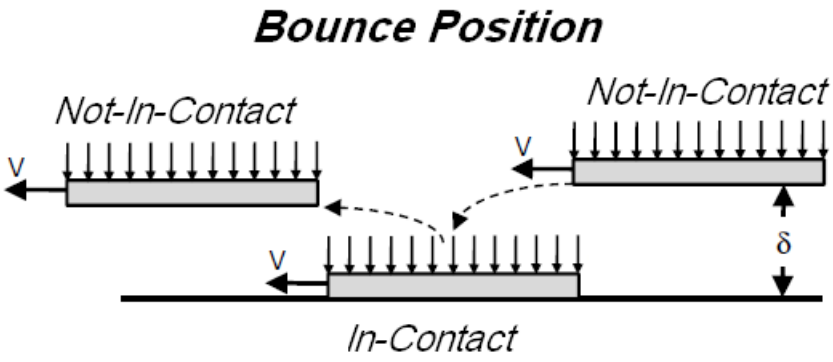

Figure 10. Slipper's Bounce Model Along a Rail (1)

$$-k\left.\frac{\partial T_s}{\partial x}\right|_{x=0} = h(T_s - T_r)\,, \tag{3.2}$$

where T_r is the forced fluid reference temperature and *h* is the surface convection coefficient. To account for the bounce effect on the flux, a switch function $m(t)$ using the Heaviside step function is

$$m(t) = \begin{cases} 1 & \text{(In-Contact)} \\ 0 & \text{(Not-In-Contact)} \end{cases}. \tag{3.3}$$

This leads to the boundary condition

$$-k\left.\frac{\partial T_s}{\partial x}\right|_{x=\sigma(t)} = m(t)\ \underbrace{\left(\alpha q(t)\right)}_{\textit{Heat Conduction}} + (1-m(t))\ \underbrace{h(T_s - T_r)}_{\textit{Heat Convection}}\ . \tag{3.4}$$

As time progresses, a melt layer may appear. This layer, as illustrated in Figure 11, is removed continuously after the temperature of slipper's sliding surface reaches its melting temperature. The latent heat of fusion stored in the slipper's melt layer must be

accounted for. To this end, the boundary condition at the sliding interface with the melt layer is modified as

$$-k\left.\frac{\partial T_s}{\partial x}\right|_{x=\sigma(t)} = m(t)\left(\alpha q(t) - \rho\ell\frac{d\sigma}{dt}\right) + (1-m(t))h(T_s - T_r) \quad . \qquad (3.5)$$

ρ : density ℓ : latent heat of fusion σ : melt front location

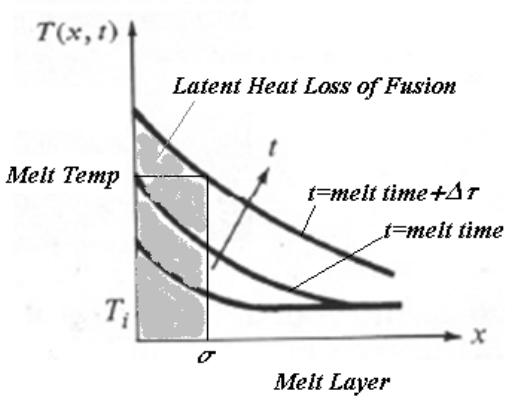

Figure 11. Dynamics of Melt Layer Removed Due to Latent Heat of Fusion

The melt wear volume is calculated using melt front, i.e.

$$\text{Melt Wear Volume} = \int_{t_m}^{t} A_s \frac{d\sigma}{dt} dt \quad \text{where} \quad A_s = \text{slipper's surface area} .$$

The bounce effect due to external loading changes the boundary condition at the interface with conductive heat transfer while in contact, but not the convective heat transfer while not in contact. It creates surface temperature changes of slipper and rail, influencing the melt wear. The results of the slipper's surface temperature and melt wear percentage due to bounce effect will be presented and analyzed in Chapter 7.

There are a few things to consider which influence the nature of the frictional heat partition function α. First, as the slipper slides along the rail's surface, the slipper's sliding surface enters into the cooler region of rail. If the frictional heating is assumed to be the only heat source, the slipper's surface temperature is always higher than the rail's. As such, the motion of slipper needs to be considered. Second, when the slipper and the rail are in contact, the frictional heat energy flows into the slipper and rail. By Equation (3.1), the pressure profile is used to calculate the flux when in contact. If there is zero pressure, it is considered as the slipper and rail are not in contact. So the convective heat transfer is used. Third, heat transfer occurs at a higher rate across materials of high thermal conductivity than across materials of low thermal conductivity. More heat flux flows into the material of high thermal conductivity. Materials of high thermal diffusivity rapidly adjust their temperature to that of their surroundings, because they conduct heat quickly. So the material properties are one of the important factors to characterize the frictional heat partition function. The last thing to consider is the sliding speed. As the difference of two sliding surface temperatures gets bigger, the more heat energy tends to flow into low temperature region. If the slipper is moving fast, the slipper generates more frictional heat energy as indicated by Equation (3.1). More heat flux tends to flow into the rail rather than the slipper because the slipper's sliding surface may be in contact with the larger region of rail. Therefore, the slipper's sliding speed influences the frictional heat partition values.

If slipper and rail are made of the same material, they have the same thermal properties. So, initially any heat input at the interface distributed between slipper and rail

is determined by the relation of the thermal properties. When the slipper is sliding along the rail with high velocity and high pressure, the frictional heat partitioning values should drop rapidly and, as melt is achieved, approach some fixed stable number.

3.2 Two-Dimensional Mathematical Model

As described in Section 3.1, the frictional heat partitioning values are influenced by material thermal properties and sliding velocity so the frictional heat partitioning can be represented as a function of material thermal properties and sliding velocity. To better understand the evolution of the frictional heat partition function α, a simplified two dimensional model for thermal evolution between the slipper and the rail is examined. Consider two semi-infinite solids, which is initially at a uniform ambient temperature T_a. During sliding processes, the surface at $y = 0$ in the interval $-l < x < l$ is subjected to a heat source at the rate of $q(t)$ due to frictional force. Suppose that T^s, T^r are the temperature distributions of slipper and rail, respectively, during the pre-melting period. It is assumed that, at the sliding surface $y = 0$ in the interval $-l < x < l$, the frictional heat generates a heat flux while in contact and the convective heat transfer occurs while not in contact. The temperatures as $|y| \to \infty$ of slipper and rail are the fixed ambient temperature T_a. There is a convective heat transfer outside of contact region on the rail. Due to aerodynamic effect, a shock wave may be created at the slipper's front-head and the convective heated air flows at the slipper's tail. Figure 12 illustrates the slipper's coordinate system relative to the rail's coordinate system. With this coordinate

transform, it leads to the following mathematical formulations of slipper and rail's thermal evolution equations for a pre-melt problem.

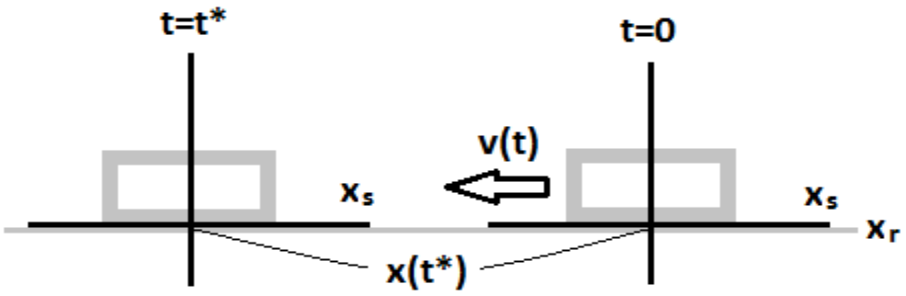

Figure 12. Slipper's Coordinate Corresponding to Rail's Coordinate System

(a) $\rho^s c^s \dfrac{\partial T^s}{\partial t} = k^s \nabla^2 T^s$ for $t > 0, |x_s| \le l, y > 0$

(b) I.C. : $T^s(x, y, 0) = T_a$ for $|x_s| \le l, 0 < y, t = 0$

(c) B.C. : $T^s(x, y, t) \to T_a$ as $y \to \infty$

Slipper (d) $$k^s \left.\frac{\partial T^s}{\partial x}\right|_{x_s=-l} = h_1 (T^s - T_1)\Big|_{x_s=-l} \quad \text{for } t > 0,\ y > 0 \qquad (3.6)$$

(e) $$-k^s \left.\frac{\partial T^s}{\partial x}\right|_{x_s=l} = h_2 (T^s - T_2)\Big|_{x_s=l} \quad \text{for } t > 0,\ y > 0$$

(f) $$-k^s \left.\frac{\partial T^s}{\partial y}\right|_{y=0} = m(t)\alpha(x_s, t) q(x_s, t) + (1 - m(t)) h_3 (T^s(x_s, 0, t) - T_3) \quad \text{for } |x_s| \le l, t > 0$$

where h_1, h_2, h_3 are the convective coefficients at slipper's heading/tailing/contact surface sides. T_1, T_2, T_3 are the temperature distribution outside of the slipper's head, tail and between the slipper and the rail's interface area when not in contact. $m(t)$ is the sign function indicating if the loading pressure exists, i.e. if $P(t) \ge 0$, $m(t) = 1$; otherwise, $m(t) = 0$.

(a) $\rho^r c^r \dfrac{\partial T^r}{\partial t} = k^r \nabla^2 T^r$ for $t > 0$, $|x_r| \le \infty$, $y < 0$

(b) I.C. : $T^r(x_r, y, 0) = T_a$ for $|x_r| \le \infty$, $-\infty < y < 0$, $t = 0$

Rail (c) B.C. : $T^r(x_r, y, t) \to T_a$ as $y \to -\infty$ or $|x_r| \to \infty$ (3.7)

(d) $k^r \dfrac{\partial T^r}{\partial y}(x_r, 0, t) =$

$$\begin{cases} m(t)(1-\alpha(x_r + x(t), t))q(x_r + x(t), t) \\ \quad + (1-m(t))h_3(T^r(x_r + x(t), 0, t) - T_3(x_r + x(t), t)) & \text{for } |x_r + x(t)| < l \\ h_4(T^r(x_r + x(t), 0, t) - T_a) & \text{for } |x_r + x(t)| \ge l \end{cases}$$

where $T_3(x_r + x(t), t) - T_a = (T_m - T_a)\phi_3(\xi, \tau)$, $v(t) =$ slipper's velocity, $x(t) = \int_0^t v(\tau) d\tau$ and h_4 the thermal convective coefficient between the air outside of interface interval and the rail's temperature. Equations (3.6b) and (3.7b) show that the initial temperature of slipper and rail is at a uniform ambient temperature. Equations (3.6f) and (3.7d) explain that only the surfaces $(y = 0)$ of slipper and rail in the interval $-l < x < l$ is subjected to the frictional heat source. Also, at sliding surface $y = 0$ in the interval $-l < x < l$, the frictional heat generates a heat flux while in contact and the convective heat transfer occurs while not in contact.

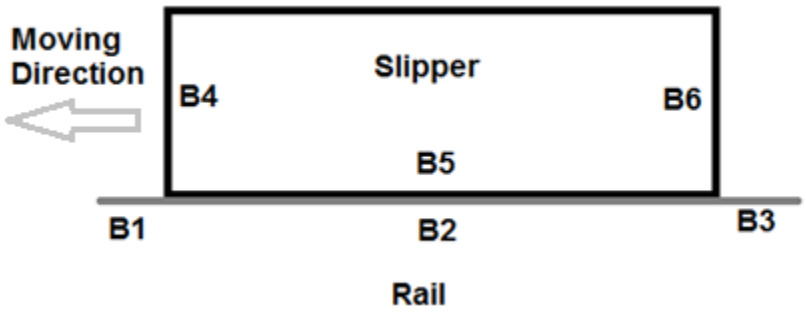

Figure 13. Boundaries of Slipper and Rail

Figure 13 shows the boundaries of rail and slipper. **B1** and **B3** indicate the rail's outside boundaries, **B2** and **B5** the rail and slipper's contact interface boundaries respectively, and **B4** and **B6** the slipper's back and front boundaries respectively. The boundaries as $y \to -\infty$ and $y \to \infty$ indicate these surfaces are far from the contact region.

Consider the rail's boundary conditions. At the contact interface **B5**, some percentage of the frictional rail when it is in contact and the convective heat flows into rail when it is not in contact. Frictional heat energy is only generated while the sliding surfaces of slipper and rail are in contact.

The slipper's PDE can be transformed to non-dimensional formulation. To do this, let $T^s(x,y,t) = T_a + (T_m - T_a)w^s(\xi,\eta,\tau)$ with dimensionless variables $\xi = \frac{x_s}{l}$, $\eta = \frac{y}{y^*}$ and $\tau = \frac{t}{t^*}$ where l is the slipper's length, t^* is the total event time and $y^* = \sqrt{\kappa^s t^*}$ is a diffusion length.

After introducing these dimensionless variables and defining the constants Nu, the Nusselt numbers, as $Nu_i = \frac{h_i l}{k^s}\,(i = 1,2,3)$ with $C^s = \frac{y^*}{k^s(T_m - T_a)}$ and $\varepsilon \equiv \frac{y^*}{l}$, Equations (3.6) become

$$\frac{\partial w^s}{\partial \tau} = \frac{\partial^2 w^s}{\partial \eta^2} + \varepsilon^2 \frac{\partial^2 w^s}{\partial \xi^2} \qquad \tau > 0\,,\ \eta > 0\,,\ -1 < \xi < 1$$

I.C.: $w^s(\xi, \eta, 0) = 0 \qquad |\xi| < 1\,,\ \eta > 0$

B.C.: $w^s(\xi, \eta, \tau) \to 0 \qquad \text{as} \quad \eta \to \infty$

$$\left.\frac{\partial w^s}{\partial \xi}\right|_{\xi=-1} = Nu_1[w^s(-1, \eta, \tau) - \phi_1(\eta, \tau)] \quad \eta > 0\,,\ \tau > 0 \tag{3.8}$$

$$-\left.\frac{\partial w^s}{\partial \xi}\right|_{\xi=1} = Nu_2[w^s(1, \eta, \tau) - \phi_2(\eta, \tau)] \quad \eta > 0\,,\ \tau > 0$$

$$-\left.\frac{\partial w^s}{\partial \eta}\right|_{\eta=0} = C^s m(\tau)\alpha(\xi, \tau)q(\xi, \tau) + (1 - m(\tau))\varepsilon Nu_3(w^s(\xi, 0, \tau) - \phi_3(\xi, \tau)) \quad |\xi| < 1\,,\ \tau > 0$$

Additionally, the functions $\phi_i(\eta, \tau)$ are defined through $T_i(\eta, \tau) = T_a + (T_m - T_a)\phi_i(\eta, \tau)$.

With $y^* = \sqrt{\kappa^s t^*}$ and material properties given in Table 1, the value of ε is approximately 10^{-2}. Furthermore, using a typical value of $h_i \approx 100$ (the reason to choose the value of h_1 is explained in Appendix 2) and material properties given in Table 1, *Nu* is approximately 0.3. The functions ϕ_1, ϕ_2 and ϕ_3 will depend on the aerodynamic heating associated with the shock front generated at high speeds. It is not the intension of this research to determine these functions.

Because $\varepsilon \ll 1$, the contribution of the boundary condition at the interface will only exist in a boundary layer of order ε. As our interest is in the behavior at the interface between the slipper and the rail, only the inner expansion solution is chosen. The solution is obtained from Equation (3.8) after setting $\varepsilon = 0$ which becomes

$$
\begin{aligned}
&\text{PDE}: \ w^s{}_{\tau} = w^s{}_{\eta\eta} \\
&\text{I.C.}: \ w^s(\xi,\eta,0) = 0 \\
&\text{B.C.}: \ w^s(\xi,\eta,0) \to 0 \qquad \text{as} \quad \eta \to \infty \\
&\qquad w^s{}_{\eta}\,|_{\eta=0} = -C^s m(\tau)\alpha(\xi,\tau)q(\xi,\tau) \qquad \left(C^s = \frac{y*}{k^s(T_m - T_a)}\right)
\end{aligned}
\tag{3.9}
$$

In this research, only the continuous contact is considered, $m = 1$. That is, it is assumed that the pressure is always positive. Using the similar process in the one-dimensional problem, which will be described in Section 4.2 for the solution to slipper's surface temperature for pre-melt problem, the solution to Equation (3.9) is

$$
w^s(\xi,\eta,\tau) = C^s \int_0^{\tau} \frac{e^{-\frac{\eta^2}{4(\tau-\tau)}}}{\sqrt{\pi(\tau-\tau')}} \alpha(\xi,\tau')q(\xi,\tau')d\tau' \tag{3.10}
$$

and Green's function for slipper is $G^s(\xi,\eta,\tau;\tau') = \frac{e^{-\frac{\eta^2}{4(\tau-\tau)}}}{\sqrt{\pi(\tau-\tau')}}$ (41). Again, this solution is the leading order inner solution and does not contain the weak contribution at the boundary layer.

Next consider the evolution of the temperature in the rail. As our interest is in the temperature in a neighborhood of the slipper, we establish a moving coordinate for the rail in reference to the fixed slipper coordinate system.

In Figure 12, x_s represents a position with respect to the moving slipper coordinates while x_r represents a position with respect to the fixed rail coordinates. If the slipper is moving to the left with a velocity $v(t)$ (assume $v(t)$ is a monotone non-

decreasing positive function), then after time t^* the slipper has moved a distance $x(t^*) = \int_0^{t^*} v(t')dt'$ along the rail coordinates. Thus any point x_r on the rail coordinates is related to a point x_s on the slipper coordinates by the Galilean transformation

$$x_r = x_s - x(t). \tag{3.11}$$

With T_r and the dimensionless variables defined in Appendix A.2, the simplified dimensionless rail's PDE is

$$\frac{\kappa^s}{\kappa^r}\frac{\partial w^r}{\partial \tau} = \frac{v(t)y^*}{\kappa^r}\left(\frac{y^*}{l}\right)\frac{\partial w^r}{\partial \xi} + \left(\frac{y^*}{l}\right)^2 \frac{\partial^2 w^r}{\partial \xi^2} + \frac{\partial^2 w^r}{\partial \eta^2} \tag{3.12}$$

where $v(t)$ is the velocity profile of slipper. Using the definition of diffusion length, $y^* = \sqrt{\kappa^s t^*}$, Equation (3.12) becomes

$$\frac{\partial w^r}{\partial \tau} = \frac{t^*}{l} v(t)\frac{\partial w^r}{\partial \xi} + \gamma\left(\frac{y^*}{l}\right)^2 \frac{\partial^2 w^r}{\partial \xi^2} + \gamma\frac{\partial^2 w^r}{\partial \eta^2} \quad \text{with } \gamma = \frac{\kappa^r}{\kappa^s} \tag{3.13}$$

Using the nominal values given in Table 1, $\gamma = \frac{\kappa^r}{\kappa^s} \approx 4.4\times10^{-1}$ and $\left(\frac{y^*}{l}\right)^2 = \varepsilon^2 \approx \mathcal{O}(10^{-4})$. The contribution of the heat diffusing in ξ axis direction, $\frac{\partial^2 w^r}{\partial \xi^2}$, is negligible. With $t = t^*\tau$, let $\bar{v}(\tau) \equiv \frac{v(t^*\tau)t^*}{l}$. Simplifying Equation (3.13) further yields

$$\frac{\partial w^r}{\partial \tau} = \bar{v}(\tau)\frac{\partial w^r}{\partial \xi} + \gamma \frac{\partial^2 w^r}{\partial \eta^2} \ . \tag{3.14}$$

If $v(t^*\tau) \approx 30m/\sec$, then $\bar{v}(\tau) = \frac{v(t^*\tau)t^*}{l} \approx \frac{30 \cdot 8}{1} = 240$. In Appendix A.2, the rail's simplified and dimensionless boundary conditions at the contact surface for Equation (3.7d) are

$$\frac{\partial w^r}{\partial \eta}(\xi, 0, \tau) = \begin{cases} \frac{y^* h_4}{k^r} w^r(\xi, 0, \tau) & |\xi| > 1 \\ C^r m(1-\alpha(\xi,\tau))q(\xi,\tau) + \frac{y^* h_3}{k^r}(1-m)[w^r(\xi,0,\tau) - \phi_3(\xi,\tau)] & |\xi| < 1 \end{cases} \tag{3.15}$$

where $C^r = \frac{y^*}{k^r(T_m - T_a)}$. With the similar analysis in the slipper PDE system, the rail's simplified reduced PDE system becomes

$$\begin{aligned} &\text{Rail's PDE}: \ \frac{\partial w^r}{\partial \tau} = \bar{v}(\tau)\frac{\partial w^r}{\partial \xi} + \gamma \frac{\partial^2 w^r}{\partial \eta^2} && |\xi| < \infty, \eta < 0, \tau > 0 \\ &\text{I.C.}: \ w^r(\xi, \eta, 0) = 0 && |\xi| < \infty, \eta < 0 \\ &\text{B.C.}: (a) \ w^r(\xi, \eta, \tau) \to 0 && \text{as } |\xi| \to \infty \text{ or } \eta \to -\infty, \tau > 0 \\ &\qquad (b) \ \frac{\partial w^r}{\partial \eta}(\xi, 0, \tau) \\ &\qquad\quad = H(1-\xi^2)C^r(1-\alpha(\xi,\tau))q(\xi,\tau) && |\xi| < \infty, \tau > 0 \end{aligned} \tag{3.16}$$

where $\bar{v}(\tau) \equiv \frac{v(t^*\tau)t^*}{l}$, $\gamma = \frac{\kappa^r}{\kappa^s}$, $C^r = \frac{y^*}{k^r(T_m - T_a)}$ and $H(\xi)$ is the Heaviside function.

Then, the solution of rail's pre-melt problem (Appendix A.2) is

$$w^r(\xi,\eta,\tau) = \sqrt{\frac{\gamma}{\pi}} C^r \int_0^\tau \frac{1}{\sqrt{\tau-\tau'}} e^{\frac{-\eta^2}{4\gamma(\tau-\tau')}} \left[H(1-z^2)\left(1-\alpha(z,\tau')\right)q(z,\tau')\right] d\tau' \qquad (3.17)$$

where $z = \bar{\xi}(\tau) - \bar{\xi}(\tau') + \xi$ and $\bar{\xi}(\tau)$, $\bar{\xi}(\tau')$ and ξ are different points on rail. $\bar{\xi}(\tau) = \int_0^\tau \bar{v}(\tau^*) d\tau^*$ and is the position on slipper, $\bar{\xi}(\tau')$ is the slipper moving distance on the rail during the time τ', $\bar{\xi}(\tau) - \bar{\xi}(\tau')$ (the slipper is moving in the negative direction in ξ-axis) is the position on rail at time $t = \tau'$, which corresponds to the contact point of slipper, and ξ is the observation point. The Green's function for the rail is

$$G^r(\eta,\tau;\tau') = \frac{1}{\sqrt{\pi(\tau-\tau')}} e^{\frac{-\eta^2}{4\gamma(\tau-\tau')}}. \qquad (3.18)$$

Let's define $\mathbf{h} \equiv \mathbf{h}(\tau,\tau') = \bar{\xi}(\tau) - \bar{\xi}(\tau')$ and consider Heaviside function in Equation (3.17), i.e. $H\left(1-\left(\xi+\bar{\xi}(\tau)-\bar{\xi}(\tau')\right)^2\right) = H(1-(\xi+\mathbf{h})^2)$. If the observation point exists in the interface interval, the frictional heat energy flows into the contact surface of the rail and slipper. Otherwise, no frictional heat energy is generated. Equation (3.17) describes that the frictional heat energy input distribution exists only along the sliding contact surface. Therefore, the values for Heaviside function in Equation (3.17) are given below

$$H(1-(\xi+\mathbf{h})^2) = \begin{cases} 1 & \text{for } -1 < \xi + \mathbf{h} < 1 \\ 0 & \text{otherwise} \end{cases}. \qquad (3.19)$$

where h in Equation (3.19) represents the value of $-\mathbf{h}$ in Figure 14. Figure 14 describes that the region where $y(x) = 1-(x-\mathbf{h})^2 > 0$ is the sliding contact surface along the

rail. The value of Heaviside function with $y(x) = 1 - (x - \mathbf{h})^2 > 0$ becomes one. If the rail and slipper are in-contact and the frictional heat is generated, the product of Heaviside function and the partitioned frictional heat flux is the heat source effecting rail and slipper.

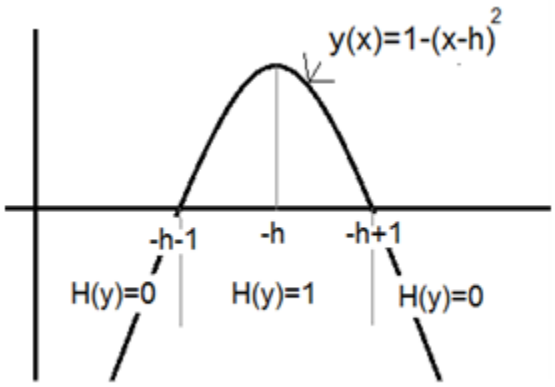

Figure 14. Graph of Heaviside Function Along Rail's Surface

Let's consider the parabolic function $y(x) = 1 - (x - \mathbf{h})^2$ and the domain of x for $y(x) \geq 0$ can be represented as slipper and rail's contact surface. If **h** moves as slipper slides along the rail and ξ is the point on the rail, the frictional heat flux influences in the interval $-1 \leq \xi \leq 1$ and no frictional heat flux outside of the interval.

Using Equations (3.10) and (3.17), the surface temperature distributions of the slipper and rail at the contact interface $\eta = 0$ are

$$w^r(\xi, 0, \tau) = \sqrt{\frac{\gamma}{\pi}} C^r \int_0^\tau \frac{H\left(1-(\xi+\mathbf{h})^2\right)\left(1-\alpha(\xi+\mathbf{h},\tau')\right)q(\xi+\mathbf{h},\tau')}{\sqrt{\tau-\tau'}} d\tau' \qquad (3.20a)$$

$$w^s(\xi,0,\tau)=\frac{c^s}{\sqrt{\pi}}\int_0^\tau \frac{\alpha(\xi,\tau')q(\xi,\tau')}{\sqrt{\tau-\tau'}}d\tau' \tag{3.20b}$$

The temperature distributions for the slipper and the rail should be continuous along the axis perpendicular to the contact interface, $|\xi|\leq 1$ at $\eta=0$. This would require $w^r(\xi,0,\tau)=w^s(\xi,0,\tau)$ over the in-contact interval even though between mirroring points of the slipper and rail along the contact surface the temperature gradient may be different. This implies the heat partition fraction would be non-uniform. If a non-uniform distribution of the heat partition fraction is considered, this equation becomes a Volterra Integral Equation of the first kind which would require a numerical method to solve. In an effort to obtain an analytical solution, the method of Carslaw and Jaeger (21) is adopted. Their method was to match the averaged contact-surface temperature distributions for the slipper and the rail. We further assume the frictional heat partition fraction value and the total frictional heat energy generated are uniformly distribution along the contact surface which is equivalent to assuming the variation in the function along the contact region is small. With these assumptions, the frictional heat partition fraction value and total frictional heat energy only depend on the sliding time, i.e. $\alpha(\xi,\tau)=\alpha(\tau)$ and $q(\xi,\tau)=q(\tau)$. Were these assumptions not made, the heat partition fraction solution would have a solution in an integral form not analytically solvable.

First define $\overline{w}(\tau)=\frac{1}{2}\int_{-1}^{1} w(\xi,0,\tau)d\xi$. Then $\overline{w}^r(\tau)$ and $\overline{w}^s(\tau)$ are respectively the averaged temperatures of rail and slipper at the interface at a given time τ. Using Equation (3.20), these values become

$$\bar{w}^r(\tau) = \sqrt{\frac{\gamma}{\pi}}\frac{C^r}{2}\int_{-1}^{1}\int_0^{\tau}\frac{H\left(1-(\xi+\mathbf{h})^2\right)\left(1-\alpha(\tau')\right)q(\tau')}{\sqrt{\tau-\tau'}}d\tau' d\xi \tag{3.21a}$$

$$\bar{w}^s(\tau) = \frac{C^s}{2\sqrt{\pi}}\int_{-1}^{1}\int_0^{\tau}\frac{\alpha(\tau')q(\tau')}{\sqrt{\tau-\tau'}}d\tau' d\xi. \tag{3.21b}$$

Next equate the averaged surface temperatures of slipper and rail at the interface using equations (3.21a) and (3.21b). Then, using Lemma A.3 given in Appendix A.3 with $K(\mathbf{h})$ define as

$$K(\mathsf{h}) \equiv \frac{1}{2}\int_{-1}^{1} H(1-(\xi+\mathsf{h})^2)d\xi = H(1-\frac{|\mathsf{h}|}{2})(1-\frac{|\mathsf{h}|}{2}), \tag{3.22}$$

and $\mathbf{h} \equiv \mathbf{h}(\tau,\tau') = \bar{\xi}(\tau) - \bar{\xi}(\tau')$, the equation reduces to

$$\int_0^{\tau}\frac{\alpha(\tau')q(\tau')}{\sqrt{\tau-\tau'}}d\tau' = \sqrt{\gamma}\frac{C^r}{C^s}\int_0^{\tau}K(\mathbf{h})\frac{\left(1-\alpha(\tau')\right)q(\tau')}{\sqrt{\tau-\tau'}}d\tau'$$

or

$$\int_0^{\tau}\frac{1}{\sqrt{\tau-\tau'}}\left(1+\beta K(\mathbf{h})\right)\alpha(\tau')q(\tau')d\tau' = \beta\int_0^{\tau}\frac{1}{\sqrt{\tau-\tau'}}K(\mathbf{h})q(\tau')d\tau' \tag{3.23}$$

where $\beta = \frac{\sqrt{\gamma}C_r}{C_s} = \frac{k^s}{k^r}\sqrt{\frac{\kappa^r}{\kappa^s}}$. The argument of the Heaviside function changes as the velocity profile changes because $\mathbf{h}(\tau,\tau') = \bar{\xi}(\tau) - \bar{\xi}(\tau')$ and $\bar{\xi}(\tau) = \int_0^{\tau}\bar{v}(\tau^*)d\tau^*$. The function $\mathbf{h}(\tau,\tau')$ represents the distance between the position on rail of the slipper at time $t=\tau$ and the position at time $t=\tau'$. This implies that the Heaviside function is a functional whose argument is velocity, $v(t)$. Thus Equation (3.23) remains a Volterra integral equation of the first kind with a weak singular kernel and would require a

numerical method to solve. However, if the velocity is constant, $\overline{v}(\tau) = v_0$, then

$\overline{\xi}(\tau) = \int_0^{\tau} \overline{v}(\tau^*) d\tau^* = v_0 \tau$ and $\mathrm{h}(\tau, \tau') = \overline{\xi}(\tau) - \overline{\xi}(\tau') = v_0(\tau - \tau')$. Further, from Equation (3.22), $K(\mathbf{h})$ becomes

$$K(\mathbf{h}) = H(1 - \tfrac{v_0|\tau-\tau'|}{2}) \left(1 - \tfrac{v_0|\tau-\tau|}{2}\right) \tag{3.24}$$

The integral equation given by Equation (3.23) now has a difference kernel and is solvable using Laplace transform methods. As shown in Appendix A.4, this leads to the solution

$$\mathcal{L}\{\alpha q\} = \mathcal{L}\{q\} B(s) \tag{3.25a}$$

where

$$B(s) = \frac{\beta\sqrt{s}\mathcal{L}\left\{\dfrac{K(\mathbf{h})}{\sqrt{\tau}}\right\}}{\sqrt{\pi} + \beta\sqrt{s}\mathcal{L}\left\{\dfrac{K(\mathbf{h})}{\sqrt{\tau}}\right\}} \tag{3.25b}$$

with $\mathcal{L}\left\{\frac{K(\mathbf{h})}{\sqrt{\tau}}\right\} = \int_0^{\infty} e^{-s\tau} \frac{1}{\sqrt{\tau}} H\left(1 - \frac{v_0|\tau|}{2}\right)\left(1 - \frac{v_0|\tau|}{2}\right) d\tau$. Thus for non-vanishing $q(t)$

$$\begin{aligned} \alpha(t) &= \frac{1}{q(t)}\left(q * \mathcal{L}^{-1}(B)\right)(t) \\ &= \frac{1}{q(t)} \int_0^t b(t-\tau) q(\tau) d\tau \end{aligned} \tag{3.26a}$$

with $b(t) = \mathcal{L}^{-1}(B)(t)$. If both the pressure and the velocity remain nonzero constants

then $q(\tau) = \mu\, P(\tau)v(\tau) = \mu\, P_0 v_0 = q_0$ is constant and, from equation (3.25a),

$$\mathcal{L}\{\alpha\} = B(s)/s \;\Rightarrow\; \alpha(t) = \int_0^t b(\tau)d\tau\,. \tag{3.26b}$$

At this point, it is necessary to determine $B(s)$ as given by Equation (3.25b) which requires the evaluation of

$$\mathcal{L}\left\{\frac{K(\mathbf{h})}{\sqrt{\tau}}\right\} = \int_0^\infty e^{-s\tau}\frac{1}{\sqrt{\tau}}H\left(1-\frac{v_0|\tau|}{2}\right)\left(1-\frac{v_0|\tau|}{2}\right)d\tau\,. \tag{3.27a}$$

Because $H(1-\frac{v_0\,|\,\tau\,|}{2}) = 0$ for $1-\frac{v_0\,|\,\tau\,|}{2} < 0$, the upper limit can be terminated at $\tau = v_0/2$. Introducing the change of variables, $z = s\tau$, $\tau = \frac{z}{s}$ and $d\tau = \frac{dz}{s}$, into Equation (3.27a) along with the reduces upper limit of integration yields

$$\mathcal{L}\left\{\tfrac{K(\mathbf{h})}{\sqrt{\tau}}\right\} = s^{-1/2}\int_0^{2s/v_0} e^{-z}z^{-1/2}dz - \tfrac{v_0}{2}s^{-3/2}\int_0^{2s/v_0} e^{-z}z^{1/2}dz. \tag{3.27b}$$

These integrals can be expressed in terms of incomplete gamma functions defined as (41)(42)

$$\begin{aligned}&(a)\quad \gamma(s,x) = \tfrac{1}{\Gamma(s)}\textstyle\int_0^x t^{s-1}e^{-t}dt\\ &(b)\quad \gamma(s,x) = (s-1)\gamma(s-1,x) - (x^{s-1}e^{-x})\end{aligned} \tag{3.28}$$

where $\gamma(s,x)$ is the lower incomplete gamma function, and $\Gamma(s) = \int_0^\infty t^{s-1}e^{-t}dt.$

Further recalling $\Gamma(1/2) = \sqrt{\pi}$ and using Equation (3.28a), Equation (3.27b) becomes

$$\mathcal{L}\left\{\frac{K(\mathbf{h})}{\sqrt{\tau}}\right\} = \frac{1}{\sqrt{s}}\sqrt{\pi}\gamma\left(\frac{1}{2},\frac{2s}{v_0}\right) - \frac{v_0}{2}\frac{1}{\sqrt{s^3}}\frac{\sqrt{\pi}}{2}\gamma\left(\frac{3}{2},\frac{2s}{v_0}\right)$$

$$= \sqrt{\frac{\pi}{s}}\left(\gamma\left(\tfrac{1}{2},\tfrac{2s}{v_0}\right) - \tfrac{v_0}{4s}\gamma\left(\tfrac{3}{2},\tfrac{2s}{v_0}\right)\right). \qquad (3.29)$$

Introducing Equation (3.28b) for $\gamma\left(\frac{3}{2},\frac{2s}{v_0}\right)$ and defining

$$\tilde{F}\left(x\right) = x^{-3/2}\left(x-\frac{1}{2}\right)\gamma\left(\frac{1}{2},x\right) + \frac{e^{-x}}{x} \qquad (3.30)$$

Equation (3.29) is more compactly written as

$$\mathcal{L}\left\{\tfrac{K(\mathbf{h})}{\sqrt{\tau}}\right\} = F(s) \equiv \sqrt{\tfrac{2}{v_0}}\tilde{F}(\tfrac{2s}{v_0}) \qquad (3.31)$$

and $B(s)$, as given in Equation (3.25b), becomes

$$B(s) = \frac{\beta^*\sqrt{s}F\left(s\right)}{1+\beta^*\sqrt{s}F(s)} \qquad \text{where} \quad \beta^* = \frac{\beta}{\sqrt{\pi}}. \qquad (3.32)$$

Using the results of the lemma from Appendix A.6, which states

$$\gamma(\frac{1}{2},x) = x^{1/2}e^{-x}\sum_{k=0}^{\infty}A_k x^k \qquad \text{where} \quad A_k = \frac{2^{2k+1}k!}{(2k+1)!}, \qquad (3.33)$$

Equation (3.30) can be written as an alternate expression for $\tilde{F}(x)$ as (Appendix A.7.)

$$\tilde{F}(x) = e^{-x}\sum_{k=0}^{\infty}(k+1)A_{k+1}x^k \quad \text{where} \quad A_k = \frac{2^{2k+1}k!}{(2k+1)!}\ . \qquad (3.34)$$

From the ratio test, it is clear that the series portion of $\widetilde{F}(x)$ converges everywhere in the complex plane so that $\tilde{F}(x)$ is an entire function.

Before proceeding to the inverse Laplace transform, consider the case of constant flux, $(t) = q_0$, and apply both the Initial and Final Value Theorem (93). For this case, the solution is given in Equation (3.26b) and the Initial Value Theorem states

$$\alpha\left(0^+\right) = \lim_{s\to+\infty} s\mathcal{L}\{\alpha\}(s) = \lim_{s\to+\infty} B(s) = \lim_{s\to\infty} \frac{\beta^*\sqrt{s}F(s)}{1+\beta^*\sqrt{s}F(s)} = \frac{\beta}{1+\beta} \tag{3.35}$$

where lemma A.5 is use along with $\beta^* = \frac{\beta}{\sqrt{\pi}}$. The Final Value Theorem states

$$\lim_{t\to+\infty} \alpha(t) = \lim_{s\to0^+} s\mathcal{L}\{\alpha\}(s) = \lim_{s\to0^+} B(s) = \lim_{s\to0^+} \frac{\beta^*\sqrt{s}F(s)}{1+\beta^*\sqrt{s}F(s)} = 0. \tag{3.36}$$

If the slipper and the rail have the same thermal properties, then $\beta = 1$ and Equation (3.35) says the initial partitioning of heat flux will be ½. As the thermal properties of the system materials vary, the initial heat flux will be bias to the slipper or rail accordingly. Further, as time progresses Equation (3.36) suggests the thermal energy generated will be bias toward the rail.

Returning to the case where the flux q_0 and the velocity v_0 are constant, the heat partition function $\alpha(t)$ is determined through the inverse Laplace transform of $\mathcal{L}\{\alpha\}$ as given in Equation (3.26b). Thus

$$\alpha(t) = \frac{1}{2\pi i}\int_{-i\infty}^{i\infty} e^{st}\frac{B(s)}{s}ds = \frac{1}{2\pi i}\int_{-i\infty}^{i\infty} e^{st}\frac{\beta^*\sqrt{s}F(s)}{s(1+\beta^*\sqrt{s}F(s))}ds \tag{3.37}$$

Analysis of this equation can be found in Appendix A.8. However, the integrand clearly contains a branch point at *s=0*. Further, the apparent simple pole at s=0 is removed by the $\sqrt{s}$ term which appears in the numerator. Using the numerical tool Matlab suggests and analysis will show $1+\beta^*\sqrt{s}F(s)$ has no roots in the complex plane. Thus, taking the branch cut along the negative real axis in *s* plane, a branch cut integral is evaluated to determine the heat partitioning function $\alpha(t)$. Referring to Appendix A. 8, the heat partitioning function $\alpha(t)$ is given by

$$\alpha(t) = \frac{1}{\pi}\int_0^\infty e^{-\frac{v_0}{2}tr}\frac{\beta^*\sqrt{r}\tilde{F}(-r)}{r(1+(\beta^*)^2 r\tilde{F}^2(-r))}dr \tag{3.38}$$

where $\beta^* = \frac{\beta}{\sqrt{\pi}} = \frac{k^s}{k^r}\sqrt{\frac{\kappa^r}{\pi\kappa^s}}$ and $\tilde{F}(-r) = e^r\sum_{k=0}^{\infty}(k+1)2^{2k+3}\frac{(k+1)!}{(2k+3)!}(-r)^k$. (See Appendix A.8.)

Equation (3.38) is the solution of the heat partition function with a non-zero constant velocity profile ($\bar{v}(\tau) = v_0 \neq 0$). This function has two parameters β and v_0, where β is determined by the thermal properties of the slipper and rail, and v_0 is the dimensionless velocity, $\bar{v}(\tau) = \frac{t^*}{l}v(t^*\tau) = v_0$, which is constant. Equation (3.38) is the slipper's frictional heat partition function $\alpha(t)$ for times prior to melting. Typical behavior of this function $\alpha(t)$ can be seen in Figure 25 found in Section 7.1.

4 One-Dimensional Mathematical Model

In this chapter, a simple one-dimensional pre and post-melting mathematical problem is formulated and the analytical solution of the pre-melt temperature distribution is developed. With some given parameters, this solution determines the time required to reach the melting temperature of the slipper.

A rocket sled slipper, where high-velocity and high-pressure are present, is governed by a coupled system of thermal and mechanical phenomena. During sliding, a localized region of high temperature yields a thin melt layer and material loss on a sliding contact area. By sliding, the rapid cooling by onrushing rail and air flow may result in the solidification of melted material forming a teardrop shaped shallow depression in both the slipper and rail material.(4)(5) Calculating the contact temperature between contacting surfaces is necessary to estimate the properties of the melt-wear layer and its resulting material failure.

Traveling along the rail, the front edge of the slipper always enters a cooler region. Accordingly, the gradient of frictional heat energy of the rail is greater at the front edge. The gradient of heat flux of the slipper is smaller than that of the rail due to the surface temperature difference between the rail and slipper's sliding interface. The frictional heat energy is a function of pressure, relative velocity, and material properties. While sliding, the frictional heat energy increases the temperature at the contact surfaces of slipper and rail and eventually the slipper reaches its melting temperature. Once the slipper starts melting at the interface, the melt layer is continuously removed by sliding

contact. All of these factors influence the temperature distributions of the slipper and the rail.

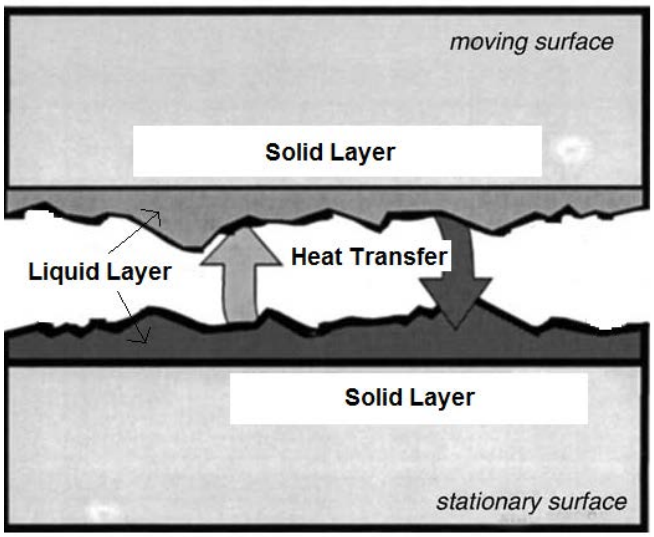

Figure 15. Heat Transfer in Liquid Layer Between the Sliding Surfaces (37)

Figure 15 illustrates a solid surface or solid-liquid interface which has a complex structure and complex properties depending on the nature of the solids and the interaction between the sliding surfaces. The surfaces contain irregularities of various orders ranging from macroscale to interatomic scale. Even the smoothest surfaces contain irregularities, asperities, whose heights exceed the interatomic distance. In addition to surface irregularities, the solid surface consists of several layers with deformed layers as the outermost layers.(37) These layers are extremely important because their mechanical behavior is influenced by the depth of deformation of the surface layers and the presence of the deformed layers affects friction and wear. Therefore, microscale and nanoscale models for the surfaces are important for tribological applications. This length scale at the surface is much smaller than the depth of material. For the numerical and

mathematical analysis at the sliding surface, we focus on the macroscale thin layer to render the present problem tractable by avoiding some of the details above. This scale is still much smaller than the material depth by 2-3 orders of magnitude. This suggests that the material could be assumed to be the half space, a semi-infinite material.

When formulating differential equations of heat transfer for this dissertation, only heat conduction is considered as a heat transfer mechanism. Other assumptions are: no changes in material properties during phase change, solids made up of homogeneous materials, no heat energy loss other than melt removal, no heat energy source other than frictional heat on sliding surfaces and fixed temperature at the other ends. More specific assumptions will be made in formulating mathematical models.

This chapter starts with simple one-dimensional mathematical formulations of pre and post-melting problems and develops the analytical solution of the pre-melt temperature distribution. This solution determines the time required to reach the melting temperature of slipper using certain parameters, frictional coefficients, sliding velocities, and heat partition values. The next chapter develops two-dimensional models and the temperature distribution of slipper and rail using Green's function for the pre-melting problem. Finally an expression for heat partitioning fractions of the pre-melting problem is developed.

4.1 One-Dimensional Mathematical Model of Pre/Post-Melting Problem

Recall Figure 7 in Section 2.4, which illustrates the melting process of a solid material when there is a heat source at the surface. Let T_{const} , T_{solid} , T_{liquid} be $T_0(x), T_1(x,t), T_2(x,t)$, and a heat source be defined as heat flux $Q(t)$.

Consider a semi-infinite solid, which has the initial temperature distribution $T_0(x)$ inside the solid in Equation (4.4).

Pre-Melting Problem

$$\text{PDE}: \quad \frac{\partial T_1}{\partial t} = \kappa \frac{\partial^2 T_1}{\partial x^2} \quad (x > 0, 0 < t < t_m) \tag{4.1}$$

$$BC1: \quad T_1(x,t) \to T_0(x) \quad as \quad x \to \infty \tag{4.2}$$

$$\text{BC2}: \quad -k \frac{\partial T_1}{\partial x} = Q(t) \quad (x = 0, 0 < t < t_m) \tag{4.3}$$

$$\text{IC}: \quad T_1(x,0) = T_0(x) \quad (x > 0) \tag{4.4}$$

where $\kappa, k, T_0(x), T_1(x,t), Q(t), t_m$ are thermal diffusivity, thermal conductivity, initial temperature, ambient temperature, pre-melt temperature, heat source, and melt time. Equation (4.3) shows that during sliding process, the surface at $x = 0$ is subjected to heat source at the rate of $Q(t)$ due to frictional force. Suppose that $T_1(x,t), t_m$ are the temperature distribution during pre-melting period and the time required for a solid to begin melting. Before the melting time, the temperature at any point inside of a material

never exceeds its melting temperature T_m. During the time prior to melt, $0 \le t < t_m$, the material remains solid, i.e. $T_0(x,t) \le T_1(x,t) < T_m$. It is assumed that only sliding surface at $x = 0$ has a heat source and as $x \to \infty$ the material temperature approaches an ambient temperature.

Now consider the melt evolution with removal of a semi-infinite solid region. The temperature distribution inside a solid material is initially at a uniform temperature $T_0(x) = T_0$. When $Q(t) > 0$, the heat source adds progressively more thermal energy at the boundary $x = 0$, the temperature of a solid increases and may eventually reach its melting point at a characteristic melting time t_m. Therefore, a material begins to melt at the sliding surface for $t > t_m$, and this melted layer is assumed to be removed immediately. After melt occurs for $t > t_m$, the following PDE system must be satisfied.

Post-Melting/Melt Removal Problem

$$\text{PDE}: \quad \frac{\partial T_2}{\partial t} = \kappa \frac{\partial^2 T_2}{\partial x^2} \quad (x > \sigma(t), t > t_m) \tag{4.5}$$

$$BC1: \quad T_2(x,t) \to T_0 \quad as \quad x \to \infty \tag{4.6}$$

$$\text{BC2}: \quad -k\frac{\partial T_2}{\partial x} = Q(t) - \rho\ell \ \frac{d\sigma}{dt} \ (x = \sigma(t), t > t_m) \tag{4.7}$$

$$\begin{aligned} &\text{Initial BC}: \quad T_2(x,t_m) = T_1(x,t_m) \ \ (x = \sigma(t_m) = 0) \\ &\text{Interface BC}: \quad T_2(\sigma(t),t) = T_m \qquad (t > t_m) \end{aligned} \tag{4.8}$$

where $T_0, T_2, T_m, \rho, \ell$ are the initial temperature, post-melt temperature, melting temperature, density and latent heat.

The phase change of a material occurs when the surface reaches the melting temperature. The thin melted layer at the boundary $x = 0$ is developing when the time is greater than or equal to its melt time. During this process, the additional energy of phase change, *latent heat* introduced in Equation (4.7), must be added for melt to continue. In the initial boundary condition of Equation (4.8), now the melt boundary location defined by $x = \sigma(t)$, must start at $t = t_m$, i.e. $\sigma(t_m) = 0$. Also, since the melt region is assumed to be removed immediately due to sliding two materials, for any $t > t_m$ the temperature on the melt boundary cannot exceed its melting temperature T_m, which implies that T_2 remains constant (T_m) at the melt boundary after the melt time t_m, shown in the interface boundary condition in Equation (4.8). In order to maintain the constant temperature on the melt boundary, melt region removal is necessary and its expression appears shown in Equation (4.7). The boundary condition as $x \to \infty$, in Equation (4.6), remains unchanged for the pre-melt state, Equation (4.2).

Note that the system is continuous from the pre-melting problem to post-melting problem. Before solving the melt evolution with removal problem, it is necessary to know the temperature distribution $T_1(x, t_m)$ because it provides the initial condition of the melt removal problem. So the temperature distribution of pre-melting problem ($t = t_m$) should be the initial temperature distribution of post-melting problem, i.e. $T_2(x, t_m) = T_1(x, t_m)$.

4.2 Model Solution Using Laplace Transforms

In this section, the PDE system to find the melt time (Melt Time Problem) along with its boundary and initial conditions is formulated. The solution of the Melt Time Problem and its development are presented. Using the Laplace transform in the time dynamic transforms a PDE system to an ODE system in one-dimension for which a closed form solution is obtained.

Let $f(t)$ be a function of *t* defined for $t > 0$. Then the Laplace transform of f with transform variable s is

$$\hat{f}(s) = \mathcal{L}(f(t)) = \int_0^\infty e^{-st} f(t)dt \ , \tag{4.9a}$$

while the Inverse Laplace transform is given by

$$f(t) = \mathcal{L}^{-1}(\hat{f}(s)) = \frac{1}{2\pi i}\int_{Br} \mathrm{e}^{st}\hat{f}(s)ds. \tag{4.9b}$$

Many of the properties of the Laplace transform and its inverse can be found in references (38),(60) and (93). Using these properties, the one-dimensional time-dependent function $T(x,t)$ and the notation $\mathcal{L}(T(x,t)) = \hat{T}(x,s) = \int_0^\infty e^{-st}T(x,t)dt$, yields

$$\mathcal{L}(\frac{\partial T}{\partial x}) = \hat{T}'(x,s) \qquad \mathcal{L}(\frac{\partial^2 T}{\partial x^2}) = \hat{T}''(x,s) \qquad \mathcal{L}(\frac{\partial T}{\partial t}) = s\hat{T}(x,s) - T(x,0) \ , \tag{4.10}$$

where $\hat{T}'(x,s) = \frac{\partial \hat{T}}{\partial x}(x,s)$ and $\hat{T}''(x,s) = \frac{\partial^2 \hat{T}}{\partial x^2}(x,s)$. Therefore with the initial condition in Equation (4.4), Equations (4.1) through (4.3) become

$$PDE: \quad s\widehat{T_1}(x,s) - T_1(x) = \kappa \widehat{T_1}''(x,s) \tag{4.11}$$

$$BC1: \quad \widehat{T_1}(x,s) \to T_0(x) \quad as \quad x \to \infty \tag{4.12}$$

$$BC2: \quad -k\widehat{T_1}'(0,s) = \hat{Q}(s) \tag{4.13}$$

where $\hat{Q}(s) = \mathcal{L}(Q(t))$. Equation (4.11) is an ordinary differential equation for $\widehat{T_1}(x,s)$, which can be written

$$\widehat{T_1}''(x,s) - \frac{s}{\kappa}\widehat{T_1}(x,s) = -\frac{T_0(x)}{\kappa}. \tag{4.14}$$

If $T_0(x) = 0$, the homogeneous solution for $\widehat{T_1}$ is given by

$$\widehat{T}_{1h}(x,s) = A(s)e^{\alpha x} + B(s)e^{-\alpha x} \qquad \text{with } \alpha \text{ defined as } \sqrt{\frac{s}{\kappa}}, \tag{4.15}$$

where the positive branch of the square root is chosen which leads to

$$\mathrm{Re}(\alpha) > 0 \ . \tag{4.16}$$

The coefficients $A(s)$, $B(s)$ are determined from boundary conditions given in Equation (4.12) and (4.13). If the initial temperature distribution does not vanish (i.e. $T_0(x) \neq 0$), a particular solution which satisfies Equations (4.12) and (4.13) is needed. Such a solution is found by using the method of variation of parameters and is given by

$$\hat{T}_{1p}(x,s) = -\int_0^x \frac{T_0(\xi)}{2\alpha\kappa}[e^{\alpha(x-\xi)} - e^{-\alpha(x-\xi)}]d\xi \ . \tag{4.17}$$

The general solution using the homogeneous solution and particular solution of Equations (4.15) and (4.17) is of the form $T_1 = T_{1h} + T_{1p}$ or

$$\hat{T}_1(x,s) = \left[A(s) - \int_0^x \frac{T_0(\xi)}{2\alpha\kappa} e^{-\alpha\xi} d\xi\right] e^{\alpha x} + \left[B(s) + \int_0^x \frac{T_0(\xi)}{2\alpha\kappa} e^{\alpha\xi} d\xi\right] e^{-\alpha x}. \qquad (4.18)$$

Now apply boundary conditions, Equations (4.12) and (4.13), to the general solution, Equation (4.18), to determine $A(s), B(s)$. Beginning with Equation (4.12), and observing Equation (4.16) implies $\lim_{x\to\infty} e^{-\alpha x} = 0$.

$$[BC1] \qquad \hat{T}_1(x,s)\big|_{x\to\infty} = \lim_{x\to\infty} \left(A(s) - \int_0^x \frac{T_0(\xi)}{2\alpha\kappa}\, e^{-\alpha\xi} d\xi\right) e^{\alpha\xi} = 0 \qquad (4.19)$$

$$\Rightarrow \qquad A(s) = \int_0^\infty \frac{T_0(\xi)}{2\alpha\kappa} e^{-\alpha\xi}\, d\xi$$

Next using Equation (4.13),

$$[BC2] \qquad -k\hat{T}_1'(0,s) = \hat{Q}(s) = -k\alpha A(s) + k\alpha B(s)$$

$$\Rightarrow \qquad B(s) = A(s) + \frac{\hat{Q}(s)}{k\alpha}. \qquad (4.20)$$

Now the solution to Equations (4.11) - (4.13) is

$$\hat{T}_1(x,s) = \int_0^\infty \frac{T_0(\xi)}{2\alpha\kappa} e^{-\alpha(x-\xi)} d\xi + \frac{\hat{Q}(s)}{\alpha k} e^{-\alpha x} + \int_0^\infty \frac{T_0(\xi)}{2\alpha\kappa} e^{-\alpha(x+\xi)} d\xi$$

$$= \int_0^\infty \frac{T_0(\xi)}{2\alpha\kappa} [e^{-\alpha(x-\xi)} + e^{-\alpha(x+\xi)}] d\xi + \frac{\hat{Q}(s)}{\alpha k} e^{-\alpha x} \qquad (4.21)$$

where $\alpha = \sqrt{s/\kappa}$ and $\mathrm{Re}(\alpha) > 0$.

To determine the solution of $T_1(x,t)$, it is necessary to invert the Laplace transform.

Using the inversion formula $\mathcal{L}^{-1}\left(\frac{1}{\sqrt{s}}e^{-x\sqrt{s}}\right)=\frac{1}{\sqrt{\pi t}}e^{-\frac{x^2}{4t}}$ from *Handbook of Mathematical Functions with Formulas, Graphs, and Mathematical Tables* (42), the solution of $T_1(x,t)$ for $0<t<t_m$ and $x>0$ is

$$T_1(x,t)=\int_0^\infty T_0(\xi)\frac{1}{2\kappa}\sqrt{\frac{\kappa}{\pi t}}\left[\exp\left(\frac{-(x-\xi)^2}{4\kappa t}\right)+\exp\left(\frac{-(x+\xi)^2}{4\kappa t}\right)\right]d\xi \\ +\int_0^t Q(\tau)\frac{1}{k}\sqrt{\frac{\kappa}{\pi(t-\tau)}}\exp\left(\frac{-x^2}{4\kappa(t-\tau)}\right)d\tau \tag{4.22a}$$

since $\mathcal{L}^{-1}\left(\frac{e^{-\alpha x}}{\alpha}\right)=\mathcal{L}^{-1}\left(\frac{e^{-x\sqrt{\frac{s}{\kappa}}}}{\sqrt{\frac{s}{\kappa}}}\right)=\frac{\sqrt{\kappa}}{\sqrt{\pi t}}e^{\frac{-x^2}{4\kappa t}}$. Thus the half-space Green's function for the Neumann boundary condition (22) is

$$G(x,\xi,t)=\frac{1}{2}\sqrt{\frac{1}{\kappa\pi t}}\left[\exp\left(\frac{-(x-\xi)^2}{4\kappa t}\right)+\exp\left(\frac{-(x+\xi)^2}{4\kappa t}\right)\right]. \tag{4.22b}$$

Using this Green's function, Equation (4.22a) is simplified to

$$T_1(x,t)=\int_0^\infty T_0(\xi)G(x,\xi,t)d\xi+\int_0^t\frac{\kappa}{k}Q(\tau)G(x,0,t-\tau)d\tau\ , \tag{4.23}$$

The first term of Equation (4.23), $\int_0^\infty T_0(\xi)G(x,\xi,t)d\xi$, shows the influence over time t due to the initial temperature distribution $T_0(\xi)$ while the second term, $\int_0^t Q(\tau)G(x,0,t-\tau)d\tau$, is the influence of the frictional heat source $Q(\tau)$.

4.3 Physical Interpretation of Mathematical Solution $T_1(x,t)$

Equation (4.22) is the solution to the pre-melting problem, Equation (4.1), under considerations of boundary and initial conditions. Equation (4.2) - (4.4) shows that the temperature distribution during the pre-melting period is influenced by the initial temperature distribution $T_0(x)$ and heat source $Q(t)$. In Equation (4.23), the temperature at time *t* in the solid at the sliding contact area is influenced by two factors, a transient heat distribution due to the initial temperature over one-dimensional space and a continuous frictional heat source over time. $G(x,\xi,t)$ influences the initial temperature distribution and $G(x,0,t-\tau)$ influences the heat source for $0 < t < t_m$ and $x > 0$. $\int_0^\infty T_0(\xi)G(x,\xi,t)\,d\xi$ describes how the initial temperature evolves over space, and $\int_0^t Q(\tau)G(x,0,t-\tau)\,d\tau$ describes how much the heat source affects the temperature distribution over time. If there is no initial temperature given, then only the frictional heat source raises the temperature requiring more time to reach melt temperature. If there is a change in the flux function $Q(\tau)$, such as an increase or decrease in heat flow rate, then the time to reach the melt temperature takes less or more time respectively.

Next we determine the time required for the temperature at the sliding contact surface to reach the melting point with given parameters, such as pressure, velocity, friction and material properties of a given material. After a material reaches melt temperature at the sliding surface, it forms a thin melt layer at the boundary as the phase change occurs. The thin melt layer creates new wear phenomena as the phase changes with resulting new material properties, friction coefficient and boundary conditions. In order to understand the relation of wear and temperature distribution, it is essential to know the temperature distributions in the two sliding materials due

to frictional heating; how quickly a material reaches melt temperature; how fast the melt front moves from the boundary; and what affects the velocity of moving boundary.

Recalling an earlier discussion, the melt layer at the sliding surface starts developing at its melt time $t = t_m$ and moves continuously into the material depending on the heat flux. Because the melt layer is removed and the melt front moves, the rate of melt removal (melt wear) is directly proportional to the rate at which the melt front moves.

With these considerations, finding the time t_m to start melting (melt time) is equivalent to solving $T_1(0, t_m) = T_m$ for t_m. Melt temperature T_m of a specific material (*VascoMax*, whose melt temperature is 1685 *K* in SI unit(39)) can be obtained from any reference book or handbook of material properties.

Heat flux being the essential factor in the melting process, it is necessary to consider the frictional heat energy to define the heat flux function $Q(t)$. It is influenced by velocity v, friction coefficient μ, partition coefficient α and pressure P. Some assumptions are needed;

1. The velocity of moving body is either constant or increasing, $\dot{v}(t) \geq 0$. There are two cases for the velocity function of interest in this research. The velocity function will be given by $v(t) = at + q_0$; constant ($a = 0$) and linear ($a \neq 0$), where q_0 initial velocity and a acceleration.
2. The frictional coefficient μ is a number related to the two specific surfaces that are in contact with each other. It is dependent on the roughness of each surface and how the materials slide against each other. The pressure or force P is the force pushing two

materials together, perpendicular to each surface. For a sufficiently small time increment, friction coefficient μ and pressure P are constant. Also, partition coefficient α is assumed to be constant (to be discussed in section 4.1).

The assumption of constant values for μ, P, α is not strictly true as the values will depend on the nature of the contacting surfaces. However, in the transient moving problem, they are assumed fixed for a small time increment.

Because frictional heat is the major contributor to the melting process, it is important to define the frictional heat flux function $Q(t)$. Consider a two-body sliding contact in which Body 1 is moving with velocity $v_1(t)$ relative to the contact area and Body 2 is moving with velocity $v_2(t)$ relative to the same contact area. The rate of total energy dissipated in the sliding contact is determined by the friction force and the relative sliding velocity. If it is assumed that all of this energy is dissipated as heat on the sliding surfaces within the real area of contact, then the rate of heat generated per unit area of contact $Q(t)$ for either Body 1 or Body 2 is defined as

$$Q(t) = \mu\alpha P v(t) = \mu\alpha P(q_0 + at) = \mu\alpha P q_0 + (\mu\alpha P a)t \qquad (4.24)$$

where μ is the coefficient of friction, α the frictional heat partitioning value, P the contact pressure or load, and $v(t) = | v_1(t) - v_2(t) | = at + q_0$ the relative sliding velocity. The sliding velocity of two materials is either accelerating at a constant rate (linearly increasing velocity with time, $a \neq 0$) or a fixed constant velocity, $a = 0$ where q_0 is the initial velocity.

Let the sliding surface ($x = 0$) temperature reach the melt temperature T_m when $t = t_m$. Since the material's melt temperature is a material property, the melt time t_m can be calculated. Let the change in temperature at the melt front be equal to the difference between the melt temperature T_m and the initial temperature T_0. Let's assume that the initial temperature distribution is the same as the ambient temperature, i.e. $T_0 = T_a$. Then solve Equation (4.23) with $x = 0, t = t_m$ for the melt time t_m, i.e.

$$\begin{gathered} T_1(0, t_m) = T_m \\ \int_0^\infty T_0(\xi) G(0, \xi, t_m) d\xi + \int_0^{t_m} \frac{\kappa}{k} Q(\tau) G(0, 0, t_m - \tau) d\tau = T_m \end{gathered} . \tag{4.25}$$

Note that if $T_0(\xi) = T_a$, then $\int_0^\infty T_0(\xi) G(0, \xi, t_m) d\xi = T_a$. Then, Equation (4.25) becomes

$$\int_0^{t_m} \frac{\kappa}{k} Q(\tau) G(0, 0, t_m - \tau) d\tau = T_m \text{ -T}_a \qquad \text{(assumed to be } T_a = T_0) \ . \tag{4.26}$$

Combining $G(x, \xi, t) = \frac{1}{2} \sqrt{\frac{1}{\kappa \pi t}} \left[\exp\left(\frac{-(x-\xi)^2}{4\kappa t} \right) + \exp\left(\frac{-(x+\xi)^2}{4\kappa t} \right) \right]$ in Equation (4.23) and $Q(t) = \mu \alpha P q_0 + (\mu \alpha P a) t$ in Equation (4.24), yields

$$\int_0^{t_m} \frac{\mu \alpha P q_0 + (\mu \alpha P a) \tau}{k} \sqrt{\frac{\kappa}{\pi (t_m - \tau)}} d\tau = T_m - T_a \ . \tag{4.27}$$

First, consider the material moving at a constant velocity, i.e. $a = 0$. The rate of heat flux is constant, $Q(t) = \mu \alpha P q_0$, and the solution of Equation (4.27) for melt time t_m, solved in Appendix A.10, is

$$t_m = \frac{\pi}{\kappa}\left(\frac{(T_m - T_a)k}{2\mu\alpha P q_0}\right)^2 . \qquad (4.28)$$

Let's apply this result to a *Holloman High Speed Test Track* experiment.

Table 1. Physical and Material Properties for the HHSTT Wear Project (1)

	Thermal Conductivity ($\frac{J}{m\cdot s\cdot K}$)	Density ($\frac{kg}{m^3}$)	Thermal Diffusivity ($\frac{m^2}{s}$)	Specific Heat ($\frac{j}{kg\cdot K}$)	Melting Temp. (K)
Slipper (VascoMax V300 Maraging Steel)	31	8000	9.2e-6	420	1685
Rail (AISI 1080 Carbon Steel)	15	8055	3.91e-6	480	1670
Slipper's Dimension	4 in (width)*8 in (length)*14.7 mm (thickness)				
Total Traveled Distance	5.8155 km				
Total Sliding Time	8.14 seconds				

The material used for the Holloman High Speed Test Track experiment (1) is *VascoMax,* whose material properties are given in Table 1. During the experiment, the ambient temperature T_a is *300* K, the initial velocity q_0 is fixed at $q_0 = 10$ m/sec , the pressure is fixed at $P = 100\ MPa$ and the frictional coefficient value μ ranges from *0.1* to *0.5*. It is assumed that half of the total frictional heat energy dissipated enters into a shoe and the other half enters into the rail.(1) In Table 2, time to reach the melting point on the sliding contact surface is evaluated for different values of frictional coefficient while considering that the rate of heat input is constant.

Table 2. Time to Reach the Melt Temperature at the Contact Surface with Various Frictional Coefficients for a Constant Fixed Velocity 10 m/sec

Coefficient of Friction (μ)	0.1	0.2	0.3	0.4	0.5
Melt time (sec)	6.295	1.574	0.699	0.393	0.252

Table 2 shows that it takes less time to reach the melting temperature if the frictional coefficient increases. The larger coefficient of friction (the increase of sliding resistance between two contact surfaces) means dissipating more frictional energy during sliding process. More frictional heat energy heats up the material faster, and the material's contact area reaches the melt temperature faster. The result of Table 1 explains that more energy input shortens the time to reach the melting point or melt temperature.

Second, consider the case where the velocity of the material is linearly increasing, i.e. $a \neq 0$. From Equation (4.24), the rate of heat input is a linearly increasing function of time. For the linearly increasing heat flux condition ($a \neq 0$) and $s^2 = t_m$, solving Equation (4.27) is reduced as following

$$s^3 + \beta s - \lambda = 0\,, \tag{4.29}$$

where $\beta = \dfrac{3q_0}{2a}$ and $\lambda = \dfrac{T_m - T_a}{\alpha \mu P a}\dfrac{3k}{4}\sqrt{\dfrac{\pi}{\kappa}}$.

The exact solution to Equation (4.29) is

$$s = \left(\frac{\lambda}{2}\right)^{1/3}\left[(\sqrt{1+M}+1)^{1/3} - (\sqrt{1+M}-1)^{1/3}\right] \qquad \text{where } M = \frac{4\beta^3}{27\lambda^2}\,. \tag{4.30}$$

With the linearly increasing value a fixed at 10 $\mathrm{m/s^2}$ and the initial sliding velocity q_0 vary from 0 to 50 m/sec, the solution to Equation (4.30) with various frictional coefficient values is presented in Table 3. In Table 3, time to reach the melting point on the sliding contact surface is calculated while the rate of heat input increases linearly. Each column represents the time to reach the melting point for different values of β which is defined as $\frac{3q_0}{2\alpha}$. So the increase in q_0 (the initial velocity) means the increase in β. Each row represents the time to reach the melting point for different values of λ which is defined as $\frac{3k(T_m-T_a)}{4\alpha\mu Pa}\sqrt{\frac{\pi}{\kappa}}$. So the increase in μ (coefficient of friction) means the decrease in λ.

Table 3. Time to Reach the Melt Temperature at the Contact Surface with Various Frictional Coefficients and Initial Velocities for Linearly Increasing Velocity

		$\beta = 0$	$\beta = 1.5$	$\beta = 3$	$\beta = 4.5$	$\beta = 6$	$\beta = 7.5$
$\mu = 0.1$	λ= 3.4624	2.289	1.413	0.821	0.482	0.302	0.202
$\mu = 0.2$	λ= 1.7312	1.442	0.649	0.279	0.139	0.081	0.053
$\mu = 0.3$	λ= 1.1541	1.100	0.378	0.136	0.064	0.037	0.024
$\mu = 0.4$	λ= 0.8656	0.908	0.246	0.079	0.036	0.021	0.013
$\mu = 0.5$	λ= 0.6925	0.783	0.172	0.052	0.023	0.013	0.009

With $\beta = \dfrac{3q_0}{2a}$, the values of β increase as the initial velocity q_0 changes from zero to $50\ m/\sec$. With $\lambda = \dfrac{T_m - T_a}{\alpha\mu Pa}\dfrac{3k}{4}\sqrt{\dfrac{\pi}{\kappa}}$, the values of λ decrease as the fictional coefficients μ change from *0.1* to *0.5*. So time (in seconds) to reach the melting point for a linearly increasing flux condition is a function of s^2 with parameters β and λ. In Table 3, the values of each

column with a fixed value for initial velocity q_0 are decreasing as the values of frictional coefficient increase. This trend is similar to the one described in Table 2 where less time is taken to reach the melting temperature if the frictional coefficient increases. The increased initial velocity contributes to increased heat energy input (or increase of heat flux $Q(t)$). More heat energy accelerates the material's melting process on the sliding contact area and shortens the time to the start of melting. Expectedly, an increase in the frictional coefficient and initial velocity provides more frictional energy which heats the material faster reducing melt time, here we have quantified it.

5 Numerical Formulation of Two Dimensional Heat Transfer Problem

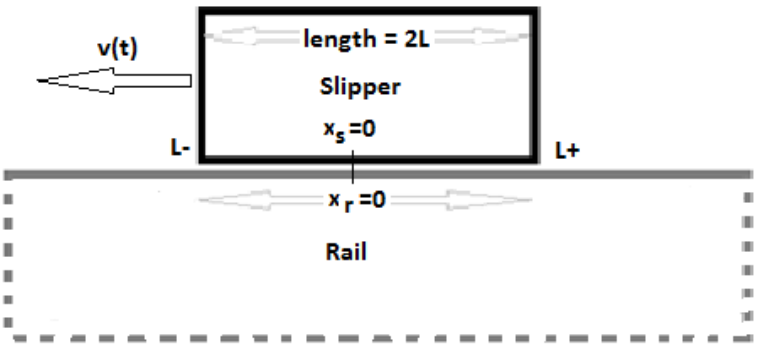

Figure 16. Rail and Slipper's Two Dimensional Heat Transfer Model

During numerical analysis, let's consider the sliding system of rail and slipper to be finite. The length of the slipper is $2L$ and the length of the rail is some multiple of the length of the slipper, i.e. Rail length $= 2kL$ for some positive constant integer *k*, and the slipper lies in the middle of the rail. In Figure 16, L^+ and L^- represent $+L$ and $-L$ respectively for some L (the half of the slipper's length). They are initially at $T_0(x, y)$. Finding the temperature distribution and melt wear of the slipper, and the slipper's frictional heat partitioning function are our interest. The length of the slipper is fixed, and the entire contact surface of the slipper is subject to the frictional heat source while sliding. So it is reasonable to set the slipper's coordinate system fixed and to make the rail's coordinate system match the sliding velocity. Treat the rail as a moving object sliding at the velocity $v(t)$ in the opposite direction of slipper's 'real world' direction in *x*-axis and treat the slipper as a stationary object. Using the coordinate change due to the slipper sliding along the rail, the rail's PDE introduces the extra term $v(t)\frac{\partial u}{\partial x}$.

While sliding, dynamic loading pressure is observed. This dynamic loading was earlier described as the *bounce effect*. This phenomenon randomly changes the interface boundary condition between rail and slipper from in-contact to not-in-contact. From Figure 16, when the slipper's surface is in contact on the rail's surface, the sliding contact surface area $-L \le x_s \le L$ at $y = 0$ is subjected to frictional heating. For $t > 0$, the position x_s on the slipper's surface corresponds to a position x_r on the rail, i.e. $x_r = \int_0^t v(t')dt' + x_s = x(t) + x_s$, where $x(t)$ is the distance that the sled has traveled on the rail for time t.

This heating generates a flux $q(x,t)$ along the contact surface. It is assumed that only the sliding surface area $|x_r| \le L$ at $y = 0$ is subjected to the heat source at a rate of $q(x,t)$. When they are not in-contact, the surfaces are subjected to convective heat transfer between the slipper's surface and the air layer in the gap. The region outside of the sliding surface area, $|x_r| > L$, at $y = 0$ is subjected to convective heat transfer. The other boundary conditions of rail $y \to -\infty$ and slipper $y \to \infty$ are a fixed boundary temperature, T_a, call it 'ambient temperature'. Later, for the discrete PDE, the domain of the *y*-axis will be finite. The slipper's head and tail boundary $x = -L$ and $x = +L$ will be subjected to convective heat transfer between the slipper's heat and tail and the surrounding air. Let the temperature surrounding the slipper head, tail and below be $T_1(y,t), T_2(y,t)$ and $T_3(x,t)$. These assumptions lead to the slipper and rail's two dimensional PDE, initial and boundary conditions as the following.

For the slipper,

$$\text{PDE}: \text{(a)} \qquad \rho c \frac{\partial u}{\partial t} = k_s \frac{\partial^2 u}{\partial x^2} + k_s \frac{\partial^2 u}{\partial y^2}$$

$$\text{I.C.}: \text{(b)} \qquad u(x, y, 0) = T_0(x, y) \qquad \text{for } |x| < L,\ y > 0$$

$$\text{B.C.}: \text{(c)} \qquad k_s \left.\frac{\partial u}{\partial x}\right|_{x=L^-} = h_1(u(L^-, y, t) - T_1(y, t)) \quad \text{for } y > 0$$

$$\text{(d)} \qquad -k_s \left.\frac{\partial u}{\partial x}\right|_{x=L^+} = h_2(u(L^+, y, t) - T_2(y, t)) \quad \text{for } y > 0 \qquad . \ (5.1)$$

$$\text{(e)} \qquad k_s \left.\frac{\partial u}{\partial y}\right|_{y=0} = \begin{cases} \alpha(t) \cdot q(t) & \text{in contact} \\ h_3(u(x, 0, t) - T_3(x, t)) & \text{not in contact} \end{cases} \quad \text{for } |x| < L$$

where $\alpha(t)$ heat flux partition flowing into slipper

$$\text{(f)} \qquad u(x, y, t) = T_a \qquad \text{as } y \to \infty$$

For the rail,

$$\text{PDE}: \text{(a)} \qquad \rho c \left(\frac{\partial u}{\partial t} - v(t) \frac{\partial u}{\partial x} \right) = k_r \frac{\partial^2 u}{\partial x^2} + k_r \frac{\partial^2 u}{\partial y^2}$$

$$\text{I.C.}: \text{(b)} \qquad u(x, y, 0) = T_0(x, y) \qquad |x| < \infty,\ y < 0$$

$$\text{B.C.}: \text{(c)} \qquad u(x, y, t) = T_a \qquad \text{as } |x| \to \infty\ y \to -\infty$$

$$\text{(d)} \qquad k_r \left.\frac{\partial u}{\partial y}\right|_{y=0} =$$

$$\begin{cases} \begin{cases} h(u(x, 0, t) - T_a) & x_r < L^- \text{ or } x_r > L^+ \\ (1 - \alpha(t)) \cdot q(t) & L^- \le x_r \le L^+ \end{cases} & \text{in contact} \\ \begin{cases} h(u(x, 0, t) - T_a) & x_r < L^- \text{ or } x_r > L^+ \\ h_3(u(x, 0, t) - T_3(x, t)) & L^- \le x_r \le L^+ \end{cases} & \text{not in contact} \end{cases} \qquad . \ (5.2)$$

$$\text{where } T_3(x, t) = \begin{cases} T_a & x_r < L^- \text{ or } x_r > L^+ \\ \frac{1}{2}\left(u(x, 0, t) + T_a\right) & L^- \le x_r \le L^+ \end{cases}$$

Equations (5.1b) and (5.2b) set the initial temperatures of slipper and rail as $T_0(x, y)$. Equations (5.1e) and (5.2d) describe the bounce effect. When in contact, the sliding contact surface area at $y = 0$ is subjected to frictional heating. When not in-contact, the surfaces are subjected to convective heat transfer between the contact surface and the air layer in the gap. Equations (5.1c) and (5.1d) are the slipper's head and tail boundary $x = -L$ and $x = +L$, subjected to convective heat transfer. Equations (5.1f) and (5.2c) are the other boundary conditions of slipper and rail, which is a fixed boundary temperature T_a.

From this point, the label x will be used instead of x_s or x_r for slipper or rail. The rail is divided into three intervals on the surface as indicated in Figure 16. The interval $|x| < L$ has either a conductive heat transfer boundary condition when in contact or a convective boundary condition when not in contact. The other two intervals $-\infty < x < -L$ and $L < x < +\infty$ have a convective heat transfer. This implies that the boundary conditions are not continuous at the endpoints $x = L$ and $x = -L$. For the numerical analysis, we take the limit at the endpoints from the positive and negative directions and set these two limits being equal. Therefore, at the endpoints L^+ and L^-, the continuous condition has to be applied, i.e.

$$\begin{aligned}
\text{In Contact: } & \lim_{x^+ \to L^+} k_r \left.\frac{\partial u}{\partial y}\right|_{y=0} = \lim_{x^- \to L^+} k_r \left.\frac{\partial u}{\partial y}\right|_{y=0} \\
& \Rightarrow\ h(L^+)(u(L^+, 0, t) - T_0) = (1 - \alpha(t))q(L^+, t) \\
& \lim_{x^+ \to L^-} k_r \left.\frac{\partial u}{\partial y}\right|_{y=0} = \lim_{x^- \to L^-} k_r \left.\frac{\partial u}{\partial y}\right|_{y=0} \\
& \Rightarrow\ h(L^-)(u(L^-, 0, t) - T_0) = (1 - \alpha(t))q(L^-, t)
\end{aligned} \quad . \qquad (5.3)$$

$$\text{Not in Contact: } \lim_{x^+ \to L^+} k_r \left.\frac{\partial u}{\partial y}\right|_{y=0} = \lim_{x^- \to L^+} k_r \left.\frac{\partial u}{\partial y}\right|_{y=0}$$
$$\Rightarrow\ h(L^+)(u(L^+,0,t)-T_0) = h_3(L^+)(u(L^+,0,t)-T_3) \quad . \qquad (5.4)$$
$$\lim_{x^+ \to L^-} k_r \left.\frac{\partial u}{\partial y}\right|_{y=0} = \lim_{x^- \to L^-} k_r \left.\frac{\partial u}{\partial y}\right|_{y=0}$$
$$\Rightarrow\ h(L^-)(u(L^-,0,t)-T_0) = h_3(L^-)(u(L^-,0,t)-T_3)$$

The following section adopts Lakoba's study (45) on development of numerical method and analysis. In the next section, numerical methods for the heat transfer problem in 2 dimension in space will be developed. The simple explicit scheme for the 2D heat equation (Crank-Nicolson scheme, CN scheme) will be presented, and it will show the stability of CN scheme of 2D heat equation. However, after analyzing CN scheme for 2D heat equation, it is discovered that CN scheme of 1D heat equation is even more time-efficient than of 2D heat equation. In order for the 2D heat equation to be stable and time-efficient, CN scheme needs to be modified using operator splitting and this modified CN scheme of 2D heat equation is called Alternating Direction Implicit (ADI) method.

Since this chapter has lots of details and computations of 2D heat equation developments using CN scheme, ADI and Strang's Splitting methods, here is a brief preview for each section. In Section 5.1, we will examine the stability and time-efficiency of CN scheme for 2D heat equation, and discover that CN scheme for 2D heat equation is not time-efficient. The ADI method for 2D heat equation will be derived by splitting operators into x and y directions, and we will prove that ADI method is stable and time-efficient. The boundary conditions need to be altered for x and y direction. So Section 5.2 will present the developments of different boundary conditions, such as Dirichlet, Neumann and Convective boundary conditions of ADI method. In

section 5.3 and 5.4, the numerical implementations of slipper and rail will be developed using ADI method and redefined boundary conditions of 2D heat equation, and presented in vector-matrix form. In Equations (5.49) and (5.76), the matrix **B** will represent the 2D heat transfer PDE, and the vectors $\mathbf{U}_j^i$, $\mathbf{b}^{n+1}$ ($i = n\,, n+1$ and $j = x, y$) will represent the temperature distribution in x or y direction and the boundary conditions of interface and the other end. Since the heat partitioning function only appears at the interface while the slipper is sliding in contact with the rail, the heat partitioning function $\alpha(t)$ will be seen in the boundary vector $\mathbf{b}^{n+1}$. Also, the accuracy and stability of ADI methods for the slipper and rail's 2D heat equations will be discussed. Since the 2D heat transfer PDE for the rail has heat flow term $v(t)\frac{\partial u}{\partial x}$, it becomes the convection-diffusion equation which has some restrictions on numerical analysis. So in Section 5.5, Strang's Splitting method will be introduced to overcome the technical problem when implementing 2D convection-diffusion equation using ADI method. Then, the numerical results of temperature distributions for the rail and slipper using ADI and Strang's Splitting methods can be found. The slipper's heat partitioning values will be calculated iteratively by matching the averaged surface temperatures of rail and slipper in Section 5.6.

5.1 Stability and Derivation of ADI for Two Dimensional Heat Problem

The general form of the two dimensional parabolic differential equation is

$$\frac{\partial u}{\partial t} = \frac{\partial^2 u}{\partial x^2} + \frac{\partial^2 u}{\partial y^2} \tag{5.5}$$

with proper boundary conditions and initial condition.

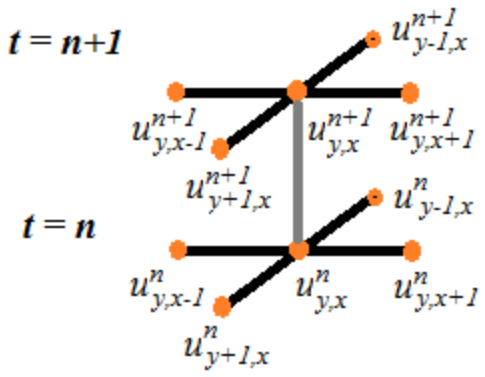

Figure 17. Crank-Nicolson Method for 2D Heat Equation

To construct a difference scheme, the space domain is partitioned into a uniform rectangular grid with the time domain. Figure 17 shows the Crank-Nicolson schematic of 2D heat equation for u_n and u^{n+1}. If the second-order difference operator δ_x^2 is defined as $\delta_x^2 u_{y,x}^n = u_{y,x+1}^n - 2u_{y,x}^n + u_{y,x-1}^n$, an explicit scheme for Equation (5.5) is

$$\frac{u_{y,x}^{n+1} - u_{y,x}^n}{\Delta t} = \frac{\delta_x^2 u_{y,x}^n}{\Delta x^2} + \frac{\delta_y^2 u_{y,x}^n}{\Delta y^2} \tag{5.6}$$

The stability of the 2 dimensional heat PDE scheme can be obtained by the von Neumann technique. Substituting $u_{y,x}^n = \lambda^n e^{i(ax\Delta x + by\Delta y)}$ for $x, y \in \mathbb{R}$ into Equation (5.6), the amplification factor λ is $\lambda = 1 - 4\frac{\Delta t}{\Delta x^2} sin^2\left(\frac{a\Delta x}{2}\right) - 4\frac{\Delta t}{\Delta y^2} sin^2\left(\frac{b\Delta y}{2}\right)$. With the condition $\frac{\Delta t}{\Delta x^2} + \frac{\Delta t}{\Delta y^2} \le \frac{1}{2}$, then $|\lambda| \le 1$ for all a and b. Therefore, this scheme is conditionally stable.

The Crank-Nicolson (CN) scheme of Equation (5.5) is obtained by averaging the spatial variation over two time steps which leads to

$$\frac{u_{y,x}^{n+1}-u_{y,x}^{n}}{\Delta t}=\frac{1}{2}\left[\frac{\delta_x^2(u_{y,x}^{n+1}+u_{y,x}^{n})}{\Delta x^2}+\frac{\delta_y^2(u_{y,x}^{n+1}+u_{y,x}^{n})}{\Delta y^2}\right]. \tag{5.7}$$

With $s_x=\frac{\Delta t}{\Delta x^2}$ and $s_y=\frac{\Delta t}{\Delta y^2}$ defined, Equation (5.7) can be rewritten as

$$\left(1-\frac{1}{2}s_x\delta_x^2-\frac{1}{2}s_y\delta_y^2\right)u_{y,x}^{n+1}=\left(1+\frac{1}{2}s_x\delta_x^2+\frac{1}{2}s_y\delta_y^2\right)u_{y,x}^{n}\ . \tag{5.8}$$

A similar stability analysis produces the amplification factor

$$\lambda=\frac{1-2s_x sin^2\left(\frac{a\Delta x}{2}\right)-2s_y sin^2\left(\frac{b\Delta y}{2}\right)}{1+2s_x sin^2\left(\frac{a\Delta x}{2}\right)+2s_y sin^2\left(\frac{b\Delta y}{2}\right)}\ . \tag{5.9}$$

Since s_x, s_y, and $\sin^2$ are positive, Equation (5.9) is always less than or equal to one for any partition size Δx and Δy. Hence Equation (5.8) is unconditionally stable.

In *The Heat equation in 2 and 3 spatial dimensions*, Lakoba (45) performed the accuracy analysis for CN scheme. Because $\frac{\delta_x^2}{\Delta x^2}\frac{\delta_y^2}{\Delta y^2}\frac{\delta_t}{\Delta t}u_{y,x}^{n}=\mathcal{O}(1)$, it follows that

$\frac{\Delta t^2}{4}\frac{\delta_x^2}{\Delta x^2}\frac{\delta_y^2}{\Delta y^2}\frac{u_{y,x}^{n+1}-u_{y,x}^{n}}{\Delta t}=\mathcal{O}(\Delta t^2)$. Since the accuracy of the scheme

$\left(1-\frac{1}{2}s_x\delta_x^2-\frac{1}{2}s_y\delta_y^2\right)u_{y,x}^{n+1}=\left(1+\frac{1}{2}s_x\delta_x^2+\frac{1}{2}s_y\delta_y^2\right)u_{y,x}^{n}$ is $\mathcal{O}(\Delta t^2+\Delta x^2+\Delta y^2)$, Lakoba (45) says that it may be added to any term of the same order without changing the accuracy of the scheme.

Using this observation, add the term $\frac{\Delta t^2}{4}\frac{\delta_x^2}{\Delta x^2}\frac{\delta_y^2}{\Delta y^2}\frac{u_{y,x}^{n+1}-u_{y,x}^{n}}{\Delta t}$ to L.H.S. of Equation (5.7)

resulting in

$$\frac{u_{y,x}^{n+1}-u_{y,x}^{n}}{\Delta t}+\frac{\Delta t^2}{4}\frac{\delta_x^2}{\Delta x^2}\frac{\delta_y^2}{\Delta y^2}\frac{u_{y,x}^{n+1}-u_{y,x}^{n}}{\Delta t}=\left(\frac{\delta_x^2}{2\Delta x^2}+\frac{\delta_y^2}{2\Delta y^2}\right)\left(u_{y,x}^{n+1}+u_{y,x}^{n}\right). \qquad (5.10)$$

Equation (5.10) still has the accuracy $\mathcal{O}(\Delta t^2+\Delta x^2+\Delta y^2)$. After multiplying by Δt, Equation (5.10) has the equivalent form

$$\left(1-\frac{s_x}{2}\delta_x^2-\frac{s_y}{2}\delta_y^2+\frac{s_x}{2}\delta_x^2\frac{s_y}{2}\delta_y^2\right)u_{y,x}^{n+1}=\left(1+\frac{s_x}{2}\delta_x^2+\frac{s_y}{2}\delta_y^2+\frac{s_x}{2}\delta_x^2\frac{s_y}{2}\delta_y^2\right)u_{y,x}^{n}. \quad (5.11)$$

Factoring the operator expressions on both sides results in

$$\left(1-\frac{s_x}{2}\delta_x^2\right)\left(1-\frac{s_y}{2}\delta_y^2\right)u_{y,x}^{n+1}=\left(1+\frac{s_x}{2}\delta_x^2\right)\left(1+\frac{s_y}{2}\delta_y^2\right)u_{y,x}^{n} \qquad (5.12)$$

which is the modified Crank-Nicolson scheme(46). For the CN scheme, a system of second-order difference operators of both *x* and *y* directions must be solved at each time step. Because it does not form the tridiagonal matrix as a 1-D problem, solving such a system can be quite laborious due to the expensive computational power and memory depth to store and solve the matrix directly systematically. A simple and efficient method, called Alternative Direction Implicit (ADI) method, for solving 2-D parabolic problems was first proposed by Peaceman and Rachford in 1955.(47) The basic idea is to break a 2-D problem into two 1-D problems solved by implicit schemes as tridiagonal.

For the ADI method, Equation (5.12) is implemented as follows

$$\begin{aligned}\left(1-\frac{s_x}{2}\delta_x^2\right)u_{y,x}^{*} &= \left(1+\frac{s_y}{2}\delta_y^2\right)u_{y,x}^{n} \quad \cdots(a)\\ \left(1-\frac{s_y}{2}\delta_y^2\right)u_{y,x}^{n+1} &= \left(1+\frac{s_x}{2}\delta_x^2\right)u_{y,x}^{*} \quad \cdots(b)\end{aligned} \qquad (5.13)$$

First, it is necessary to prove that this method is equivalent to Equation (5.12). This will imply that it satisfies the same accuracy. Apply the operator $(1-\frac{s_x}{2}\delta_x^2)$ to both sides of Equation (5.13b). Then the sequence of equations follows

$$\begin{aligned}\left(1-\frac{s_x}{2}\delta_x^2\right)\left(1-\frac{s_y}{2}\delta_y^2\right)u_{y,x}^{n+1} &= \left(1-\frac{s_x}{2}\delta_x^2\right)\left(1+\frac{s_x}{2}\delta_x^2\right)u_{y,x}^{*}\\ &= \left(1+\frac{s_x}{2}\delta_x^2\right)\left(1-\frac{s_x}{2}\delta_x^2\right)u_{y,x}^{*}\end{aligned} \qquad (5.14)$$

where the fact that the operators $\left(1+\frac{s_x}{2}\delta_x^2\right)$ and $\left(1-\frac{s_x}{2}\delta_x^2\right)$ commute is used. Next apply Equation (5.13a) and Equation (5.14) becomes

$$\left(1-\frac{s_x}{2}\delta_x^2\right)\left(1-\frac{s_y}{2}\delta_y^2\right)u_{y,x}^{n+1} = \left(1+\frac{s_x}{2}\delta_x^2\right)\left(1+\frac{s_y}{2}\delta_y^2\right)u_{y,x}^{n}. \qquad (5.15)$$

This proves that Equation (5.12) is equivalent to Equation (5.13).

5.2 Boundary Conditions for the ADI methods

The ADI methods solve a 1-dimensional heat transfer problem implicitly in one direction and repeat it in the other direction. Between these steps, the boundary conditions need to be modified. It is important to prescribe boundary conditions for the intermediate solution $u^*_{y,x}$ in Equation (5.13). There are three kinds of boundary conditions, Dirichlet, Neumann and mixed boundary conditions.

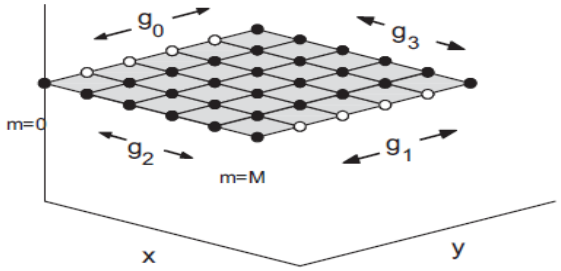

Figure 18. Two Dimensional Boundaries for the ADI Method (45)

$$\begin{cases} g_0(y,t) = u(0,y,t) \text{ or } \dfrac{\partial u}{\partial x}(0,y,t) \\ g_1(y,t) = u(M,y,t) \text{ or } \dfrac{\partial u}{\partial x}(M,y,t) \end{cases} \quad 0 \le y \le L, \quad t \ge 0$$

$$\begin{cases} g_2(x,t) = u(x,0,t) \text{ or } \dfrac{\partial u}{\partial y}(x,0,t) \\ g_3(x,t) = u(x,L,t) \text{ or } \dfrac{\partial u}{\partial y}(x,L,t) \end{cases} \quad 0 \le x \le M, \quad t \ge 0 \qquad (5.16)$$

Figure 18 shows how to label the boundaries for the ADI scheme. Equation (5.16) defines g_i for i=0,1,2,3 as a function for each boundary. M, L represent the upper endpoints of x and y domain.

In order to find the required boundary values $u^*_{y,0}$ and $u^*_{y,M}$ with $1 \le y \le L-1$, two equations in Equation (5.13) must be added to solve for $u^*_{y,x}$. This leads to the equation

$$u^*_{y,x} = \frac{1}{2}\left(u^n_{y,x} + u^{n+1}_{y,x}\right) + \frac{s_y}{4}\delta^2_y\left(u^n_{y,x} - u^{n+1}_{y,x}\right) \tag{5.17}$$

which is valid for all integers.

Here, the derivations of three intermediate boundary conditions of the *Peaceman-Rachford method* for the two dimensional heat transfer problem are demonstrated.

For the ***Dirichlet boundary condition***, the boundary values of the intermediate step $u^*_{y,x}$ at $x = 0$ and $x = M$ are

$$\begin{aligned} u^*_{y,(0,M)} &= \frac{1}{2}\left(u^n_{y,(0,M)} + u^{n+1}_{y,(0,M)}\right) + \frac{s_y}{4}\delta^2_y\left(u^n_{y,(0,M)} - u^{n+1}_{y,(0,M)}\right) \\ &= \frac{1}{2}\left(g^n_{y,(0,1)} + g^{n+1}_{y,(0,1)}\right) + \frac{s_y}{4}\delta^2_y\left(g^n_{y,(0,1)} - g^{n+1}_{y,(0,1)}\right) \\ &= \frac{1}{2}\left(g^n_{y,(0,1)} + g^{n+1}_{y,(0,1)}\right) + \frac{s_y}{4}\begin{bmatrix}\left(g^n_{y+1,(0,1)} - 2g^n_{y,(0,1)} + g^n_{y-1,(0,1)}\right) \\ -\left(g^{n+1}_{y+1,(0,1)} - 2g^{n+1}_{y,(0,1)} + g^{n+1}_{y-1,(0,1)}\right)\end{bmatrix} \end{aligned} \tag{5.18}$$

for $1 \le y \le L-1$. Here the notation $u_{y,(0,M)}$ represents the row vector $u_{y,0}$ or $u_{y,M}$ and $g_{y,(0,1)}$ represents the boundary condition $g_0(y,t)$ or $g_1(y,t)$ described in Equation (5.16).

To determine the ***Neumann boundary condition*** values at the intermediate step $u^*_{y,x}$, the central difference scheme around $u^*_{y,(1,M-1)}$ is used in conjunction with Equation (5.17) to estimate the heat flow rate. This leads to the following sequence of equations.

$$
\begin{aligned}
\frac{u^{*}_{y,(2,M)} - u^{*}_{y,(0,M-2)}}{2\Delta x} &= \frac{1}{2}\left(\frac{u^{n}_{y,(2,M)} - u^{n}_{y,(0,M-2)}}{2\Delta x} + \frac{u^{n+1}_{y,(2,M)} - u^{n+1}_{y,(0,M-2)}}{2\Delta x} \right) \\
&\quad + \frac{s_y}{4} \cdot \delta_y^2 \left(\frac{u^{n}_{y,(2,M)} - u^{n}_{y,(0,M-2)}}{2\Delta x} - \frac{u^{n+1}_{y,(2,M)} - u^{n+1}_{y,(0,M-2)}}{2\Delta x} \right) \\
&= \frac{1}{2}\left(\frac{u^{n}_{y,(2,M)} - u^{n}_{y,(0,M-2)}}{2\Delta x} + \frac{u^{n+1}_{y,(2,M)} - u^{n+1}_{y,(0,M-2)}}{2\Delta x} \right) \\
&\quad + \frac{s_y}{4}\left(\frac{u^{n}_{y-1,(2,M)} - u^{n}_{y-1,(0,M-2)}}{2\Delta x} - \frac{u^{n}_{y,(2,M)} - u^{n}_{y,(0,M-2)}}{\Delta x} + \frac{u^{n}_{y+1,(2,M)} - u^{n}_{y+1,(0,M-2)}}{2\Delta x} \right) \\
&\quad - \frac{s_y}{4}\left(\frac{u^{n+1}_{y-1,(2,M)} - u^{n+1}_{y-1,(0,M-2)}}{2\Delta x} - \frac{u^{n+1}_{y,(2,M)} - u^{n+1}_{y,(0,M-2)}}{\Delta x} + \frac{u^{n+1}_{y+1,(2,M)} - u^{n+1}_{y+1,(0,M-2)}}{2\Delta x} \right) \\
&= \frac{1}{2}\left(g^{n}_{y,(0,1)} + g^{n+1}_{y,(0,1)} \right) + \frac{s_y}{4}\left[\begin{array}{l} \left(g^{n}_{y-1,(0,1)} - 2g^{n}_{y,(0,1)} + g^{n}_{y+1,(0,1)} \right) \\ -\left(g^{n+1}_{y-1,(0,1)} - 2g^{n+1}_{y,(0,1)} + g^{n+1}_{y+1,(0,1)} \right) \end{array} \right]
\end{aligned}
\qquad (5.19)
$$

The ***Robin boundary condition*** at the intermediate step $u^{*}_{y,x}$ is derived by considering the boundary condition of n^{th} time step, $\frac{u^{n}_{y,3} - u^{n}_{y,1}}{2\Delta x} - h(u^{n}_{y,2}) = -hT_1^{n}$ for T_1^{n} the air temperature at the boundary $x = 0$ of n^{th} time step and h the convective coefficient. For the boundary condition for $u^{*}_{y,x}$, this expression becomes $\frac{u^{*}_{y,3} - u^{*}_{y,1}}{2\Delta x} - h(u^{*}_{y,2}) = -hT_1^{*}$. Using Equation (5.17) and substituting into LHS of Equation (5.19), the boundary condition for $u^{*}_{y,x}$ can be represented with n^{th} and $(n+1)^{th}$ as per the following steps

$$\frac{u^*_{y,3}-u^*_{y,1}}{2\Delta x}-h(u^*_{y,2})=\frac{1}{2\Delta x}\begin{pmatrix}\frac{1}{2}\left(u^n_{y,3}+u^{n+1}_{y,3}\right)+\frac{s_y}{4}\delta_y^2\left(u^n_{y,3}-u^{n+1}_{y,3}\right)\\-\frac{1}{2}\left(u^n_{y,1}+u^{n+1}_{y,1}\right)-\frac{s_y}{4}\delta_y^2\left(u^n_{y,1}-u^{n+1}_{y,1}\right)\end{pmatrix}-h\begin{pmatrix}\frac{1}{2}\left(u^n_{y,2}+u^{n+1}_{y,2}\right)\\+\frac{s_y}{4}\delta_y^2\left(u^n_{y,2}-u^{n+1}_{y,2}\right)\end{pmatrix}$$

$$=\frac{1}{2}\left(\frac{u^n_{y,3}-u^n_{y,1}}{2\Delta x}-hu^n_{y,2}\right)+\frac{s_y}{4}\delta_y^2\left(\frac{u^n_{y,3}-u^n_{y,1}}{2\Delta x}-hu^n_{y,2}\right)$$

$$+\frac{1}{2}\left(\frac{u^{n+1}_{y,3}-u^{n+1}_{y,1}}{2\Delta x}-hu^{n+1}_{y,2}\right)-\frac{s_y}{4}\delta_y^2\left(\frac{u^{n+1}_{y,3}-u^{n+1}_{y,1}}{2\Delta x}-hu^{n+1}_{y,2}\right)$$

$$=\frac{1}{2}\left(-hT_1^n\right)+\frac{s_y}{4}\delta_y^2\left(-hT_1^n\right)+\frac{1}{2}\left(-hT_1^{n+1}\right)-\frac{s_y}{4}\delta_y^2\left(-hT_1^{n+1}\right)$$

$$=\frac{-h}{2}\left(T_1^n+T_1^{n+1}\right)+\frac{s_y}{4}\delta_y^2\left(T_1^n-T_1^{n+1}\right) \tag{5.20}$$

Therefore, the boundary condition is reduced to

$$\frac{u^*_{y,(3,M-2)}-u^*_{y,(1,M)}}{2\Delta x}=h(u^*_{y,(2,M-1)})-\frac{h}{2}\left(T_1^n+T_1^{n+1}\right)+\frac{s_y}{4}\delta_y^2\left(T_1^n-T_1^{n+1}\right)\ . \tag{5.21}$$

In the following sections, the development of the numerical code for slipper and rail using the ADI method will be presented and analyzed. In the numerical analysis of slipper and rail, their conductive and convective boundary conditions are considered. The numerical representations of three boundary conditions, Equations (5.18), (5.19) and (5.21), are adopted when the numerical method using the ADI method is being constructed according to Lakoba's paper(45).

5.3 Numerical Analysis for Slipper using ADI method

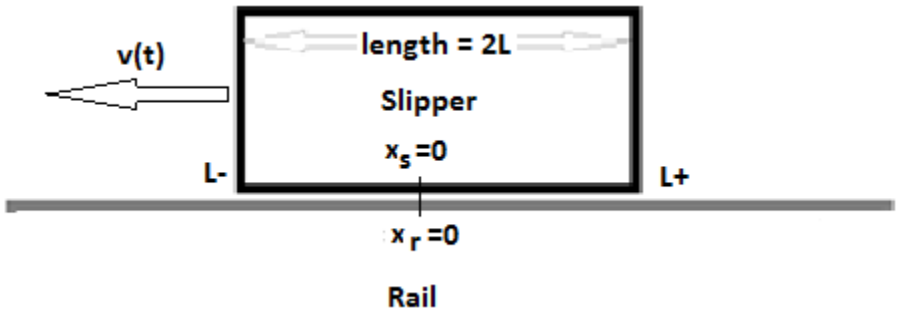

Figure 19. Slipper and Rail's Sliding System

Let's formulate *Peaceman- Rachford's* 2D ADI scheme (47) for the slipper. Use the *Crank-Nicolson* method (48) for $\nabla^2(\delta_x^2$ and $\delta_y^2)$,

$$\text{(a) PDE:} \quad \frac{u^{n+1}-u^n}{\Delta t} = \kappa_s \nabla^2 u^n \quad \text{and} \quad \frac{u^{n+1}-u^n}{\Delta t} = \kappa_s \nabla^2 u^{n+1}$$

$$\text{(b) Average:} \quad \frac{u^{n+1}-u^n}{\Delta t} = \frac{\kappa_s}{2}\nabla^2\left(u^n + u^{n+1}\right)$$

$$= \frac{\kappa_s}{2}\left[\frac{\delta_x^2(u_{y,x}^{n+1}+u_{y,x}^n)}{\Delta x^2} + \frac{\delta_y^2(u_{y,x}^{n+1}+u_{y,x}^n)}{\Delta y^2}\right] \quad . \qquad (5.22)$$

$$= \frac{\kappa_s}{2}\left[\frac{\delta_x^2}{\Delta x^2} + \frac{\delta_y^2}{\Delta y^2}\right](u_{y,x}^{n+1}+u_{y,x}^n)$$

Define $p_x = \frac{\kappa_s \Delta t}{2\Delta x^2}$, $p_y = \frac{\kappa_s \Delta t}{2\Delta y^2}$ and define the operators $A_x = p_x\delta_x^2$ and $A_y = p_y\delta_y^2$, then R.H.S. in Equation (5.22b) becomes

$$\text{R.H.S.} = \frac{1}{\Delta t}\left\{A_x + A_y\right\}\left(u_{y,x}^{n+1}+u_{y,x}^n\right) = \mathcal{O}(\Delta t) \quad . \qquad (5.23)$$

As shown in Section 5.1, and according to Lakoba's accuracy analysis (45),

$\frac{\Delta t^2}{4}\frac{\delta_x^2}{\Delta x^2}\frac{\delta_y^2}{\Delta y^2}\frac{u_{y,x}^{n+1}-u_{y,x}^{n}}{\Delta t}=\mathcal{O}(\Delta t^2)$ which is equivalent to $A_xA_y\frac{u_{y,x}^{n+1}-u_{y,x}^{n}}{\Delta t}=\mathcal{O}(\Delta t^2)$. Further, the accuracy of the slipper's 2D ADI scheme is $\mathcal{O}(\Delta t^2+\Delta x^2+\Delta y^2)$. Therefore, it is possible to add to the scheme any term of the same order without changing the accuracy of the scheme. Using this observation and add the term appearing on L.H.S of Equation (5.22b),

$$\text{R.H.S.}=\frac{u^{n+1}-u^{n}}{\Delta t}+A_xA_y\frac{u_{y,x}^{n+1}-u_{y,x}^{n}}{\Delta t}=\{1+A_xA_y\}\frac{u^{n+1}-u^{n}}{\Delta t}\ . \qquad (5.24)$$

Then, rewrite Equation (5.22b) using Equations (5.23) and (5.24)

$$\begin{aligned}\left\{1+A_xA_y\right\}\frac{u_{y,x}^{n+1}-u_{y,x}^{n}}{\Delta t}&=\frac{1}{\Delta t}\left\{A_x+A_y\right\}(u_{y,x}^{n+1}+u_{y,x}^{n})\\ \left\{1-A_x-A_y+A_xA_y\right\}u_{y,x}^{n+1}&=\left\{1+A_x+A_y+A_xA_y\right\}u_{y,x}^{n}\end{aligned}\ , \qquad (5.25)$$

and this is the slipper's 2D scheme. A_x and A_y are operators, and the operator expressions on both sides can be factored. Result in the factored form is

$$\begin{gathered}B_1B_2u_{y,x}^{n+1}=B_3B_4u_{y,x}^{n}\\ \text{where } B_1=(1-A_x),\ B_2=(1-A_y),\ B_3=(1+A_x) \text{ and } B_4=(1+A_y)\end{gathered}\ . \qquad (5.26)$$

When factoring the operator expressions, the order of operators in their product is not changed as these operators may not commute. For splitting steps, choose $u_{y,x}^{*}$ such that

$$\left\{\begin{aligned}B_1u_{y,x}^{*}&=B_4u_{y,x}^{n}\\ B_2u_{y,x}^{n+1}&=B_3u_{y,x}^{*}\end{aligned}\right\}\ \Rightarrow\ \left\{\begin{aligned}\left(1-p_x\delta_x^2\right)u_{y,x}^{*}&=\left(1+p_y\delta_y^2\right)u_{y,x}^{n} &&\cdots(a)\\ \left(1-p_y\delta_y^2\right)u_{y,x}^{n+1}&=\left(1+p_x\delta_x^2\right)u_{y,x}^{*} &&\cdots(b)\end{aligned}\right\}\ , \qquad (5.27)$$

which is Peaceman and Rachford's 2D ADI method for slipper. In order to show that Equation (5.27) is equivalent to $B_1B_2u_{y,x}^{n+1} = B_3B_4u_{y,x}^{n}$, apply the operator $\left(1- p_x\delta_x^2\right)$ to both sides of Equation (5.27b), and apply the operator $\left(1+ p_x\delta_x^2\right)$ to both sides of Equation (5.27a) to produce

$$\begin{aligned}\left(1+ p_x\delta_x^2\right)\left(1- p_x\delta_x^2\right)u_{y,x}^{*} &= \left(1+ p_x\delta_x^2\right)\left(1- p_x\delta_x^2\right)u_{y,x}^{n} \\ \left(1- p_x\delta_x^2\right)\left(1- p_y\delta_y^2\right)u_{y,x}^{n+1} &= \left(1- p_x\delta_x^2\right)\left(1+ p_x\delta_x^2\right)u_{y,x}^{*}\end{aligned} \quad . \tag{5.28}$$

Because the operators $B_1 = \left(1- p_x\delta_x^2\right)$ and $B_3 = \left(1+ p_x\delta_x^2\right)$ commute, Equation (5.28) lead to the following result

$$\left(1- p_x\delta_x^2\right)\left(1- p_y\delta_y^2\right)u_{y,x}^{n+1} = \left(1+ p_x\delta_x^2\right)\left(1+ p_y\delta_y^2\right)u_{y,x}^{n} \quad . \tag{5.29}$$

This proves that Peaceman and Rachford's 2D ADI method for the slipper is equivalent to $B_1B_2u_{y,x}^{n+1} = B_3B_4u_{y,x}^{n}$.

It is sufficient to show that the explicit heat transfer scheme is conditionally stable with very strong restrictions and the Peaceman and Rachford's 2D ADI method for slipper, Equation (5.27), is unconditionally stable using the von Neumann stability analysis. Note that this stability analysis does not consider any influence of the boundary condition, but only considers the PDE. It uses the fact that the solution of the constant-coefficient difference equation is satisfied by the Fourier harmonics $u_{y,x}^{n} = \lambda^n e^{iby\Delta y}e^{iax\Delta x}$ where λ is the amplification factor and a , b are arbitrary scaling factors.

Before examining the difference scheme, first observe

$$\text{(a)}\quad \delta_x^2 u_{y,x}^n = \lambda^n e^{iby\Delta y} e^{ia(x+1)\Delta x} - 2\lambda^n e^{iby\Delta y} e^{iax\Delta x} + \lambda^n e^{iby\Delta y} e^{ia(x-1)\Delta x}$$

$$= \left(e^{ia\Delta x} - 2 + e^{-ia\Delta x}\right)\lambda^n e^{iby\Delta y} e^{iax\Delta x}$$

$$= (-4)\sin^2\left(\frac{a\Delta x}{2}\right)\lambda^n e^{iby\Delta y} e^{iax\Delta x} \quad . \qquad (5.30)$$

$$\text{(b)}\quad \delta_y^2 u_{y,x}^n = (-4)\sin^2\left(\frac{b\Delta y}{2}\right)\lambda^n e^{iby\Delta y} e^{iax\Delta x}$$

The explicit heat transfer scheme is given by $\frac{u^{n+1} - u^n}{\Delta t} = \kappa_s \nabla^2 u^n$ and its equivalent form is

$$u_{y,x}^{n+1} = u_{y,x}^n + \kappa_s \Delta t\left(\frac{\delta_x^2}{\Delta x^2} u_{y,x}^n + \frac{\delta_y^2}{\Delta y^2} u_{y,x}^n\right). \qquad (5.31)$$

Substituting Equations (5.30a) and (5.30b) into Equation (5.31), produces

$$\lambda^{n+1} e^{iby\Delta y} e^{iax\Delta x} = \lambda^n e^{iby\Delta y} e^{iax\Delta x} + \kappa_s \Delta t \left\{ \begin{array}{l} (-4)\sin^2\left(\frac{a\Delta x}{2}\right)\frac{\lambda^n e^{iby\Delta y} e^{iax\Delta x}}{\Delta x^2} \\ +(-4)\sin^2\left(\frac{b\Delta y}{2}\right)\frac{\lambda^n e^{iby\Delta y} e^{iax\Delta x}}{\Delta y^2} \end{array} \right\}. \qquad (5.32)$$

Upon removing a common factor, the amplification factor is

$$\lambda = 1 - 4\frac{\kappa_s \Delta t}{\Delta x^2}\sin^2\left(\frac{a\Delta x}{2}\right) - 4\frac{\kappa_s \Delta t}{\Delta y^2}\sin^2\left(\frac{a\Delta y}{2}\right). \qquad (5.33)$$

In order to make this scheme stable, the stability condition $|\lambda| \le 1$ has to be imposed.

Clearly, $0 \le \sin^2\left(\frac{a\Delta x}{2}\right) \le 1$ and $0 \le \sin^2\left(\frac{b\Delta y}{2}\right) \le 1$. If the largest value of $\sin^2\left(\frac{a\Delta x}{2}\right)$ and $\sin^2\left(\frac{b\Delta y}{2}\right)$ is used, i.e. $\sin^2\left(\frac{a\Delta x}{2}\right) = 1$ and $\sin^2\left(\frac{b\Delta y}{2}\right) = 1$, then $1 - 4\frac{\kappa_s \Delta t}{\Delta x^2} - 4\frac{\kappa_s \Delta t}{\Delta y^2} \le \lambda$. If the

smallest value is used, i.e. $\sin^2\left(\frac{a\Delta x}{2}\right)=0$ and $\sin^2\left(\frac{b\Delta y}{2}\right)=0$, then $\lambda \le 1$. Since $|\lambda| \le 1$ is imposed, the stability condition for λ becomes $-1 \le 1-4\frac{\kappa_s \Delta t}{\Delta x^2}-4\frac{\kappa_s \Delta t}{\Delta y^2} < \lambda \le 1$. This leads to the following result, $\frac{\kappa_s \Delta t}{\Delta x^2}+\frac{\kappa_s \Delta t}{\Delta y^2} \le \frac{1}{2}$. In order for the scheme to be stable, the size of the time step has to satisfy $\Delta t \le \frac{\Delta x^2}{2\kappa_s}$ and $\Delta t \le \frac{\Delta y^2}{2\kappa_s}$.

Now it remains to show that the Peaceman and Rachford 2D ADI method for the slipper is unconditionally stable. Recall Equation (5.27). For the von Neumann stability analysis of the modified Peaceman-Rachford 2D ADI method scheme, set $u_{m,l}^n = \lambda^n e^{ibm\Delta y} e^{ial\Delta x}$ and $u_{m,l}^* = \lambda^* \lambda^n e^{ibm\Delta y} e^{ial\Delta x}$, where λ^* is the amplification factor for the intermediate step from the n^{th} time step. Substituting these expressions into Equation (5.27) admits the following

$$
\begin{aligned}
&\text{(a) } u_{y,x}^* - p_x \delta_x^2 u_{y,x}^* = u_{y,x}^n + p_y \delta_y^2 u_{y,x}^n \\
&\qquad \lambda^* \lambda^n e^{iby\Delta y} e^{iax\Delta x} - p_x \delta_x^2 \left(\lambda^* \lambda^n e^{iby\Delta y} e^{iax\Delta x}\right) = \lambda^n e^{iby\Delta y} e^{iax\Delta x} + p_y \delta_y^2 \left(\lambda^n e^{iby\Delta y} e^{iax\Delta x}\right) \\
&\qquad \lambda^* \left\{1+4p_x \sin^2\left(\frac{a\Delta x}{2}\right)\right\} = \left\{1-4p_y \sin^2\left(\frac{b\Delta y}{2}\right)\right\} \\
&\text{(b) } u_{y,x}^{n+1} - p_y \delta_y^2 u_{y,x}^{n+1} = u_{y,x}^* + p_x \delta_x^2 u_{y,x}^* \\
&\qquad \lambda \lambda^n e^{iby\Delta y} e^{iax\Delta x} - p_y \delta_y^2 \left(\lambda \lambda^n e^{iby\Delta y} e^{iax\Delta x}\right) = \lambda^* \lambda^n e^{iby\Delta y} e^{iax\Delta x} + p_x \delta_x^2 \left(\lambda^* \lambda^n e^{iby\Delta y} e^{iax\Delta x}\right) \\
&\qquad \lambda \left\{1+4p_y \sin^2\left(\frac{b\Delta y}{2}\right)\right\} = \lambda^* \left\{1-4p_x \sin^2\left(\frac{a\Delta x}{2}\right)\right\}
\end{aligned}
\tag{5.34}
$$

By defining $E = 4p_y \sin^2\left(\frac{b\Delta y}{2}\right)$ and $F = 4p_x \sin^2\left(\frac{a\Delta x}{2}\right)$, the results of Equations (5.34a) and (5.34b) can be written as $\lambda^* = \frac{1-E}{1+F}$ and $\lambda = \lambda^* \frac{1-F}{1+E}$ respectively. This leads to $\lambda = \lambda^* \frac{1-F}{1+E} = \frac{1-E}{1+F} \cdot \frac{1-F}{1+E} = \frac{1-E}{1+E} \cdot \frac{1-F}{1+F}$. For all positive *E* and *F*, $\left|\frac{1-E}{1+E}\right| \le 1$ and $\left|\frac{1-F}{1+F}\right| \le 1$. It follows that $|\lambda| \le 1$ for all *a* and *b*. Therefore, the Peaceman-Rachford 2D ADI method for the slipper, Equation (5.27), is unconditionally stable.

In order to solve the heat transfer problem and find the solution numerically, it is necessary to discretize the region of slipper in space and time. Let the length of the slipper be ℓ. Let *xn* be the number of gridpoints of slipper including the endpoints, and add one ghost point at each end outside of the slipper. Therefore, *xn+2* is the number of gridpoints of slipper including the ghost points along *x*-axis. Similarly, let *yn* be the number of gridpoints of slipper along *y*-axis. Therefore, *yn+2* is the number of gridpoints including the ghost points. Using this discretization in space and time and the difference operators $\delta_x^2 u_{y,x}^n = u_{y,x+1}^n - 2u_{y,x}^n + u_{y,x-1}^n$ and $\delta_y^2 u_{y,x}^n = u_{y+1,x}^n - 2u_{y,x}^n + u_{y-1,x}^n$, the finite difference Crank-Nicolson scheme of Equation (5.1) becomes

$$\text{PDE}: \ \rho c \frac{u_{y,x}^{n+1} - u_{y,x}^n}{\Delta t} = k_s \frac{\delta_x^2}{\Delta x^2}(u_{y,x}^{n+1} + u_{y,x}^n) + k_s \frac{\delta_y^2}{\Delta y^2}(u_{y,x}^{n+1} + u_{y,x}^n)$$

$$\text{I.C.}: \ u_{y,x}^1 = T_0(x, y) \qquad \text{with } 2 \le (y, x) \le (yn+1, xn+1)$$

$$
\begin{aligned}
&\text{B.C.1 (Head):} \quad k_s \frac{u^n_{y,3} - u^n_{y,1}}{2\Delta x} = h_1(u^n_{y,2} - T_1^n(y)) \qquad \text{with } 2 \le y \le yn+1 \\
&\Rightarrow\ u^n_{y,1} = u^n_{y,3} - \frac{2h_1\Delta x}{k_s}(u^n_{y,2} - T_1^n(y)) + \mathcal{O}(\Delta x^2) \\
&\text{B.C.2 (Tail):} \quad k_s \frac{u^n_{y,xn+2} - u^n_{y,xn}}{2\Delta x} = h_2(u^n_{y,xn+1} - T_2^n(y)) \qquad \text{with } 2 \le y \le yn+1 \\
&\Rightarrow\ u^n_{y,xn+2} = u^n_{y,xn} - \frac{2h_2\Delta x}{k_s}(u^n_{y,xm+1} - T_2^n(y)) + \mathcal{O}(\Delta x^2)
\end{aligned} \tag{5.35}
$$

$$
\begin{aligned}
&\text{B.C.3 (Interface):} \quad k_s \frac{u^n_{3,x} - u^n_{1,x}}{2\Delta y} = \begin{cases} -\alpha^n q^n & \text{in contact} \\ -h_3(u^n_{2,x} - T_3^n(x)) & \text{not in contact} \end{cases} \\
&\Rightarrow u^n_{1,x} = u^n_{3,x} + \frac{2\Delta y}{k_s}\begin{cases} \alpha^n q^n & \text{in contact} \\ h_3(u^n_{2,x} - T_3^n(x)) & \text{not in contact} \end{cases} \\
&\Rightarrow\ u^n_{1,x} = u^n_{3,x} + \frac{2\Delta y}{k_s}(m\alpha^n q^n - (1-m)h_3(u^n_{2,x} - T_3^n(x))) + \mathcal{O}(\Delta y^2) \\
&\text{B.C.4 (Top):} \quad u^n_{yn+1,x} = T_a \qquad \text{with } 2 \le x \le xn+1
\end{aligned}
$$

where m is the switch function depending on loading pressure. The region of slipper $u^n_{y,x}$ is within $2 \le (y,x) \le (yn+1, xn+1)$, and boundary values are $u^n_{2,x}$ and $u^n_{yn+1,x}$ with $2 \le x \le xn+1$ and $u^n_{y,2}$ and $u^n_{y,xn+1}$ with $2 \le y \le yn+1$. Given the solutions $u^n_{y,x}$ with $3 \le (y,x) \le (yn, xn)$, it is necessary to find the values at the boundary points $u^n_{y,2}$ and $u^n_{y,xn+1}$ with $2 \le y \le yn+1$ and $u^n_{2,x}$ and $u^n_{yn+1,x}$ with $2 \le x \le xn+1$.

To complete the boundary condition, four corner points of the slipper have to be added. These corner points are ghostpoints, which are not part of the slipper and exist at each corner of the slipper externally. Using Lakoba's method (45), the boundary conditions at slipper's head and tail are used to evaluate the two left endpoints and two right endpoints. For the left low

endpoint $u_{1,1}$, apply the convective boundary condition at the slipper's head $y=1$ and solve for $u_{1,1}$, i.e.

$$
\begin{aligned}
k_s\frac{u^n_{1,3}-u^n_{1,1}}{2\Delta x}&=h_1(u^n_{1,2}-T^n_1)\ \Rightarrow\ u^n_{1,1}=u^n_{1,3}-\frac{2h_1\Delta x}{k_s}(u^n_{1,2}-T^n_1)\\
k_s\frac{u^n_{1,xn+2}-u^n_{1,xn}}{2\Delta x}&=-h_2(u^n_{1,xn+1}-T^n_2)\ \Rightarrow\ u^n_{1,xn+2}=u^n_{1,xn}-\frac{2h_2\Delta x}{k_s}(u^n_{1,xn+1}-T^n_2)\\
k_s\frac{u^n_{yn+2,3}-u^n_{yn+2,1}}{2\Delta x}&=h_1(u^n_{yn+2,2}-T^n_1)\ \Rightarrow\ u^n_{yn+2,1}=u^n_{yn+2,3}-\frac{2h_1\Delta x}{k_s}(u^n_{yn+2,2}-T^n_1)\\
k_s\frac{u^n_{yn+2,xn+2}-u^n_{yn+2,xn}}{2\Delta x}&=-h_2(u^n_{yn+2,xn+1}-T^n_2)\ \Rightarrow\ u^n_{yn+2,xn+2}=u^n_{yn+2,xn}-\frac{2h_2\Delta x}{k_s}(u^n_{yn+2,xn+1}-T^n_2)
\end{aligned}
\tag{5.36}
$$

It is further necessary to determine the boundary values for the intermediate solution $u^*_{y,x}$. Recall Equation (5.27) and define $r_x=\frac{\kappa_s\Delta t}{\Delta x^2}$ and $r_y=\frac{\kappa_s\Delta t}{\Delta y^2}$. To find the expression for $u^*_{y,x}$ add Equations (5.27a) and (5.27b) and solve for $u^*_{y,x}$,

$$
\begin{gathered}
\left(1-\frac{r_x}{2}\delta_x^2\right)u^*_{y,x}-\left(1+\frac{r_y}{2}\delta_y^2\right)u^n_{y,x}+\left(1+\frac{r_x}{2}\delta_x^2\right)u^*_{y,x}-\left(1-\frac{r_y}{2}\delta_y^2\right)u^{n+1}_{y,x}=0\\
u^*_{y,x}=\frac{1}{2}\left(u^n_{y,x}+u^{n+1}_{y,x}\right)+\frac{r_y}{4}\delta_y^2\left(u^n_{y,x}-u^{n+1}_{y,x}\right)
\end{gathered}
\quad . \tag{5.37}
$$

The result $u^*_{y,x}$ in Equation (5.37) will find the intermediate boundary values of the slipper's head and tail by examining the expression $\frac{k_s}{2\Delta x}\left(u^*_{y,3}-u^*_{y,1}\right)-h_1u^*_{y,2}$. It is assumed that the temperature distributions $T^n_1(y)$ and $T^n_2(y)$ at the slipper's head and tail are uniform, so there is

no temperature difference along *y-axis*. In Section 5.2, the convective boundary condition for the slipper, Equation (5.21), with the result $u^*_{y,x}$ becomes

$$\frac{u^*_{y,3}-u^*_{y,1}}{2\Delta x}=\frac{h_1}{k_s}u^*_{y,2}-\frac{h_1}{2k_s}(T_1^n+T_1^{n+1})\equiv G_1\ . \tag{5.38}$$

Similarly, for the intermediate boundary condition of slipper's tail,

$$\frac{u^*_{y,xn+2}-u^*_{y,xn}}{2\Delta x}=\frac{h_2}{k_s}u^*_{y,xn+1}+\frac{h_2}{2k_s}(T_2^n+T_2^{n+1})\equiv G_2\ . \tag{5.39}$$

Next, use the first step in Equation (5.27) to find the intermediate solutions $u^*_{y,x}$. This step solves the heat transfer problem in the *x*-direction. Let $\mathbf{U}_y$ and $\mathbf{U}_x$ be the row vector at a fixed *y* and the column vector at a fixed *x* for slipper inside, i.e. $\mathbf{U}_y=[u_{y,2},u_{y,3},\cdots,u_{y,xn+1}]^T$ and $\mathbf{U}_x=[u_{2,x},u_{3,x},\cdots,u_{yn+1,x}]^T$, and $\mathbf{b}_y$ and $\mathbf{b}_x$ be the boundary influence vector at slipper's bottom/top and head/tail, i.e. $\mathbf{b}_y=[u_{y,2},0\cdots 0,u_{y,xn+1}]^T$ and $\mathbf{b}_x=[u_{2,x},0\cdots 0,u_{yn+1,x}]^T$ For each $2\le y\le yn+1$, solve Equation (5.27a), which is the linear system

$$(1-\frac{r_x}{2}\delta_x^2)\mathbf{U}^*_y=\mathbf{U}^n_y+\frac{r_y}{2}(\mathbf{U}^n_{y+1}-2\mathbf{U}^n_y+\mathbf{U}^n_{y-1})+\frac{r_y}{2}\mathbf{b}^*_y\ . \tag{5.40}$$

L.H.S. of Equation (5.40) is

$$\left(1-\frac{r_x}{2}\delta_x^2\right)\begin{bmatrix}u^*_{y,2}\\ \cdots\\ u^*_{y,xn}\\ u^*_{y,xn+1}\end{bmatrix}=\mathbf{A}_s\begin{bmatrix}u^*_{y,2}\\ \cdots\\ u^*_{y,xn}\\ u^*_{y,xn+1}\end{bmatrix}\ . \tag{5.41}$$

where $\mathbf{A}_s = \begin{bmatrix} 1+r_x & -r_x & 0 & \cdots & & & 0 \\ -\frac{r_x}{2} & 1+r_x & -\frac{r_x}{2} & 0 & \cdots & & 0 \\ 0 & -\frac{r_x}{2} & 1+r_x & -\frac{r_x}{2} & 0 & \cdots & 0 \\ & & & \cdots & & & \\ 0 & \cdots & 0 & -\frac{r_x}{2} & 1+r_x & -\frac{r_x}{2} & 0 \\ 0 & & \cdots & 0 & -\frac{r_x}{2} & 1+r_x & -\frac{r_x}{2} \\ 0 & & & \cdots & 0 & -r_x & 1+r_x \end{bmatrix}$.

R.H.S. of Equation (5.40) is

$$\begin{bmatrix} u^n_{y,2} \\ u^n_{y,3} \\ \cdots \\ u^n_{y,xn+1} \end{bmatrix} + \frac{r_y}{2}\left(\begin{bmatrix} u^n_{y+1,2} \\ u^n_{y+1,3} \\ \cdots \\ u^n_{y+1,xn+1} \end{bmatrix} - 2\begin{bmatrix} u^n_{y,2} \\ u^n_{y,3} \\ \cdots \\ u^n_{y,xn+1} \end{bmatrix} + \begin{bmatrix} u^n_{y-1,2} \\ u^n_{y-1,3} \\ \cdots \\ u^n_{y-1,xn+1} \end{bmatrix} \right) + \frac{r_x}{2}\begin{bmatrix} -2\Delta x G_1 \\ 0 \\ \cdots \\ 2\Delta x G_2 \end{bmatrix}, \qquad (5.42)$$

where G_1, G_2 are defined in Equations (5.38) and (5.39). Combine Equations (5.41) and (5.42), then the result of Equation (5.40) in a matrix form is

$$\mathbf{A}_s \begin{bmatrix} u^*_{y,2} \\ \cdots \\ u^*_{y,xn} \\ u^*_{y,xn+1} \end{bmatrix} + \begin{bmatrix} \frac{r_x \cdot \Delta x \cdot h_1}{k_s} u^*_{y,2} \\ 0 \\ \cdots \\ \frac{-r_x \cdot \Delta x \cdot h_2}{k_s} u^*_{y,xn+1} \end{bmatrix}$$

$$= \frac{r_y}{2} \begin{bmatrix} u^n_{y+1,2} \\ u^n_{y+1,3} \\ \cdots \\ u^n_{y+1,xn+1} \end{bmatrix} + (1-r_y) \begin{bmatrix} u^n_{y,2} \\ u^n_{y,3} \\ \cdots \\ u^n_{y,xn+1} \end{bmatrix} + \frac{r_y}{2} \begin{bmatrix} u^n_{y-1,2} \\ u^n_{y-1,3} \\ \cdots \\ u^n_{y-1,xn+1} \end{bmatrix} + \begin{bmatrix} \frac{r_x \cdot \Delta x \cdot h_1}{2k_s} (T_1^n + T_1^{n+1}) \\ 0 \\ \cdots \\ \frac{-r_x \cdot \Delta x \cdot h_2}{2k_s} (T_2^n + T_2^{n+1}) \end{bmatrix} . \quad (5.43)$$

Now the values of the intermediate solution $u^*_{y,x}$ with $2 \le (y,x) \le (yn+1, xn+1)$ are determined. In order to complete this first step, solving the heat transfer problem in the y-direction, it is necessary to determine the values of $u^*_{y,1}$ and $u^*_{y,xn+2}$ for $2 \le y \le yn+1$ using Equations (5.38) and (5.39),

$$\begin{aligned} u^*_{y,1} &= u^*_{y,3} - \frac{2h_1 \cdot \Delta x}{k_s} u^*_{y,2} + \frac{h_1 \Delta x}{k_s} (T_1^n + T_1^{n+1}) \\ u^*_{y,xn+2} &= u^*_{y,xn} + \frac{2h_2 \cdot \Delta x}{k_s} u^*_{y,xn+1} + \frac{h_2 \Delta x}{k_s} (T_2^n + T_2^{n+1}) \end{aligned} . \quad (5.44)$$

The results of Equation (5.44) are the values of the intermediate solution $u^*_{y,x}$ with $1 \le x \le xn+2$ and $2 \le y \le yn+1$, and these values are necessary and sufficient to find the solution on the $(n+1)^{st}$ time level.

The solution at the new time level, $u_{y,x}^{n+1}$ with $2 \le (y,x) \le (yn+1, xn+1)$ is determined by solving the heat transfer problem in the *y*-direction (into slipper's depth) with the values of the intermediate solution $u_{y,x}^{*}$ with $1 \le x \le xn+2$ and $2 \le y \le yn+1$.

Let's recall Equation (5.27b), $\left(1-\frac{r_y}{2}\delta_y^2\right)u_{y,x}^{t+1} = \left(1+\frac{r_x}{2}\delta_x^2\right)u_{y,x}^{*}$. Equation (5.35) shows a Dirichlet boundary condition at the slipper's top (B.C.4 of Equation (5.35)) and the Neumann boundary condition or mixed boundary condition at the interface (B.C.3 of Equation (5.35)). In this step, Equations (5.19) and (5.21) need to be considered. For each *x* for $2 \le x \le xn+1$, solve the linear system

$$\left(1-\frac{r_y}{2}\delta_y^2\right)\mathbf{U}_x^{n+1} = \mathbf{U}_x^{*} + \frac{r_x}{2}\left(\mathbf{U}_{x+1}^{*} - 2\mathbf{U}_x^{*} + \mathbf{U}_{x-1}^{*}\right) + \frac{r_y}{2}\mathbf{b}_x^{n+1}\Big|_{x=m} \quad . \tag{5.45}$$

L.H.S. of Equation (5.45) is

$$\left(1-\frac{r_y}{2}\delta_y^2\right)\begin{bmatrix} u_{2,x}^{n+1} \\ \cdots \\ u_{yn,x}^{n+1} \\ u_{yn+1,x}^{n+1} \end{bmatrix} = \mathbf{B}_s \begin{bmatrix} u_{2,x}^{n+1} \\ \cdots \\ u_{yn,x}^{n+1} \\ u_{yn+1,x}^{n+1} \end{bmatrix} \tag{5.46}$$

where $\mathbf{B}_s = \begin{bmatrix} 1+r_y & -r_y & 0 & \cdots & & & 0 \\ -\frac{r_y}{2} & 1+r_y & -\frac{r_y}{2} & 0 & \cdots & & 0 \\ 0 & -\frac{r_y}{2} & 1+r_y & -\frac{r_y}{2} & 0 & \cdots & 0 \\ & & & \cdots & & & \\ 0 & \cdots & 0 & -\frac{r_y}{2} & 1+r_y & -\frac{r_y}{2} & 0 \\ 0 & & \cdots & 0 & -\frac{r_y}{2} & 1+r_y & -\frac{r_y}{2} \\ 0 & & & \cdots & 0 & -\frac{r_y}{2} & 1+r_y \end{bmatrix}_{yn \times yn}$.

In order to solve R.H.S. of Equation (5.45), it is necessary to determine the boundary influence vector $\mathbf{b}_x^{n+1}\Big|_{x=m}$. At the interface, the on-and-off bounce effect changes the boundary condition from conductive to convective heat transfer. The boundary condition at the interface is

$$\frac{u_{3,x}^{n+1} - u_{1,x}^{n+1}}{2\Delta y} = \frac{1}{k_s}\left(m\alpha^{n+1}q^{n+1} - (1-m)h_3(u_{2,x}^{n+1} - T_3^{n+1})\right) \equiv G_3 \ . \qquad (5.47)$$

Note that G_3 contains the unknown value $u_{2,x}^{n+1}$. This definition is a convenient way to show the step from Equation (5.48) to (5.49). B.C.4 of Equation (5.35) shows that the boundary condition for $y = yn+1$ and $2 \le x \le xn+1$ (the slipper's top) is a fixed temperature boundary condition (Dirichlet boundary condition). $u_{2,m}$ and $u_{yn+1,m}$ for $b_x = [u_{2,m}, 0 \cdots 0, u_{yn+1,m}]$ are defined. Therefore, R.H.S. of Equation (5.45) is

$$\begin{bmatrix} u^*_{2,x} \\ u^*_{3,x} \\ \cdots \\ u^*_{yn+1,x} \end{bmatrix} + \frac{r_x}{2}\left(\begin{bmatrix} u^*_{2,x+1} \\ u^*_{3,x+1} \\ \cdots \\ u^*_{yn+1,x+1} \end{bmatrix} - 2\begin{bmatrix} u^*_{2,x} \\ u^*_{3,x} \\ \cdots \\ u^*_{yn+1,x} \end{bmatrix} + \begin{bmatrix} u^*_{2,x-1} \\ u^*_{3,x-1} \\ \cdots \\ u^*_{yn+1,x-1} \end{bmatrix} \right) + \frac{r_y}{2}\begin{bmatrix} -2\Delta y G_3 \\ 0 \\ \cdots \\ T_0 \end{bmatrix} \tag{5.48}$$

where G_3 is defined in Equation (5.47). Combine Equations (5.46) and (5.48), then the result of Equation (5.45) in a matrix form is

$$\begin{aligned} \mathbf{B}_s \begin{bmatrix} u^{n+1}_{2,x} \\ \cdots \\ u^{n+1}_{yn,x} \\ u^{n+1}_{yn+1,x} \end{bmatrix} + \begin{bmatrix} \frac{r_y \cdot \Delta y \cdot h_3}{k_s}(1-m^{n+1})u^{n+1}_{2,2} \\ 0 \\ \cdots \\ 0 \end{bmatrix} &= \frac{r_x}{2}\begin{bmatrix} u^*_{2,x+1} \\ u^*_{3,x+1} \\ \cdots \\ u^*_{yn+1,x+1} \end{bmatrix} + (1-r_x)\begin{bmatrix} u^*_{2,x} \\ u^*_{3,x} \\ \cdots \\ u^*_{yn+1,x} \end{bmatrix} \\ + \frac{r_x}{2}\begin{bmatrix} u^*_{2,x-1} \\ u^*_{3,x-1} \\ \cdots \\ u^*_{yn+1,x-1} \end{bmatrix} + \begin{bmatrix} \frac{r_y \cdot \Delta y}{k_s} m^{n+1}\alpha^{n+1}q^{n+1} - \frac{r_y \cdot \Delta y \cdot h_3}{k_s}(1-m^{n+1})T_3^{n+1} \\ 0 \\ \cdots \\ \frac{r_y}{2}T_0 \end{bmatrix} \end{aligned} \tag{5.49}$$

5.4 Numerical Analysis for Rail using ADI method

Recall Figure 19, *Slipper and rail's sliding system*, of Section 5.3. Peaceman and Rachford's 2D ADI method (47) for the rail is different from Equation (5.22) because the rail's PDE contains the heat flow term $v(t)\frac{\partial u}{\partial x}$ due to its moving velocity $v(t)$ (in the slipper's reference frame). Similar to the numerical analysis for slipper in Section 5.3, the Crank-

Nicolson scheme(47) is obtained by averaging both forward and backward central difference scheme (49) to produce

$$\frac{u^{n+1}-u^n}{\Delta t}=\frac{1}{2}\left(\kappa_r\nabla^2\left(u^n+u^{n+1}\right)+v^n\bullet\nabla u^n+v^{n+1}\bullet\nabla u^{n+1}\right) \tag{5.50}$$

where v is a vector valued function and $v^n=v(t_n)$ and $v^{n+1}=v(t_{n+1})$. With the Taylor series expansion around $t_{n+1/2}$, the vector functions v^n and v^{n+1} may be expressed by the common term $v^{n+1/2}$ (the averaged velocity),

$$\begin{aligned} v^{n+1}&=v^{n+1/2}+\frac{d}{dt}\left(v^{n+1/2}\right)\frac{\Delta t}{2}+\mathcal{O}(\Delta t^2)\\ v^{n}&=v^{n+1/2}-\frac{d}{dt}\left(v^{n+1/2}\right)\frac{\Delta t}{2}+\mathcal{O}(\Delta t^2)\end{aligned}\quad . \tag{5.51}$$

The heat flow term $v^n\cdot\nabla u^n+v^{n+1}\cdot\nabla u^{n+1}$ in Equation (5.50) can be rewriten using Equation (5.51) as

$$\begin{aligned} &v^{n+1}\cdot\nabla u^{n+1}+v^n\cdot\nabla u^n\\ &=\left\{v^{n+\frac{1}{2}}+\frac{d}{dt}\left(v^{n+\frac{1}{2}}\right)\frac{\Delta t}{2}\right\}\cdot\nabla u^{n+1}+\left\{v^{n+\frac{1}{2}}-\frac{d}{dt}\left(v^{n+\frac{1}{2}}\right)\frac{\Delta t}{2}\right\}\cdot\nabla u^n+O(\Delta t^2) \qquad (5.52)\\ &=v^{n+\frac{1}{2}}\cdot\nabla(u^{n+1}+u^n)+\frac{\Delta t^2}{2}\frac{d}{dt}\left(v^{n+\frac{1}{2}}\right)\cdot\frac{\nabla(u^{n+1}-u^n)}{\Delta t}+O(\Delta t^2)\end{aligned}$$

Assuming $\nabla\cdot\frac{\partial u}{\partial t}=O(1)$, then $\frac{\Delta t^2}{2}\frac{d}{dt}\left(v^{n+\frac{1}{2}}\right)\cdot\frac{\nabla(u^{n+1}-u^n)}{\Delta t}=O(\Delta t^2)$ and Equation (5.52) reduces to

$$v^{n+1}\cdot\nabla u^{n+1}+v^n\cdot\nabla u^n=v^{n+\frac{1}{2}}\cdot\nabla(u^{n+1}+u^n)+O(\Delta t^2). \tag{5.53}$$

Introducing Equation (5.53) into Equation (5.50) along the central difference operators, defined in the usual way as $\delta_x^c u_{y,x}^n = u_{y,x+1}^n - u_{y,x-1}^n$, produces

$$\frac{u_{y,x}^{n+1} - u_{y,x}^n}{\Delta t}$$
$$= \frac{\kappa_r}{2}\left[\frac{\delta_x^2(u_{y,x}^{n+1} + u_{y,x}^n)}{\Delta x^2} + \frac{\delta_y^2(u_{y,x}^{n+1} + u_{y,x}^n)}{\Delta y^2}\right] + \frac{1}{2}\left[\frac{v_x^{n+1/2}\delta_x^c\left(u_{y,x}^{n+1} + u_{y,x}^n\right)}{2\Delta x} + \frac{v_y^{n+1/2}\delta_y^c\left(u_{y,x}^{n+1} + u_{y,x}^n\right)}{2\Delta y}\right] + \mathcal{O}(\Delta t^2)$$
$$= \frac{\kappa_r}{2}\left[\frac{\delta_x^2}{\Delta x^2} + \frac{\delta_y^2}{\Delta y^2}\right](u_{y,x}^{n+1} + u_{y,x}^n) + \frac{1}{2}\left[\frac{v_x^{n+1/2}\delta_x^c}{2\Delta x} + \frac{v_y^{n+1/2}\delta_y^c}{2\Delta y}\right]\left(u_{y,x}^{n+1} + u_{y,x}^n\right) + \mathcal{O}(\Delta t^2) \qquad (5.54)$$

Next define the values $p_x = \frac{\kappa_r \Delta t}{2\Delta x^2}$, $p_y = \frac{\kappa_r \Delta t}{2\Delta y^2}$, $c_x^n = \frac{v_x{}^{n+1/2}\Delta t}{4\Delta x}$ and $c_y^n = \frac{v_y{}^{n+1/2}\Delta t}{4\Delta y}$, along with operators $A_x = p_x\delta_x^2$, $A_y = p_y\delta_y^2$, $C_x^n = c_x^n\delta_x^c$ and $C_y^n = c_y^n\delta_y^c$. It is important to observe that C_x^n changes at each time step and that v_x & v_y are respectively the horizontal and velocity and vertical velocities. If the sled slides along the rail horizontally and does not move vertically, then $C_y = c_y\delta_y^c$ is negligible as $c_y^n = 0$. Now Equation (5.54) can be simplified to

$$\frac{u_{y,x}^{n+1} - u_{y,x}^n}{\Delta t} = \frac{1}{\Delta t}\left\{A_x + A_y + C_x^n\right\}(u_{y,x}^{n+1} + u_{y,x}^n) = \mathcal{O}(\Delta t)\ , \qquad (5.55)$$

which is the rail's modified implicit 2D ADI scheme.

Once again, according to Lakoba's analysis (45),

$A_xA_y\frac{u_{y,x}^{n+1} - u_{y,x}^n}{\Delta t} = \kappa_r^2\frac{\Delta t^2}{4}\frac{\delta_x^2}{\Delta x^2}\frac{\delta_y^2}{\Delta y^2}\frac{u_{y,x}^{n+1} - u_{y,x}^n}{\Delta t} = \mathcal{O}(\Delta t^2)$. Similarly, $C_x^nA_y\frac{u_{y,x}^{n+1} - u_{y,x}^n}{\Delta t} = \mathcal{O}(\Delta t^2)$.

Because the accuracy of the rail's modified 2D ADI scheme is $\mathcal{O}(\Delta t^2 + \Delta x^2 + \Delta y^2)$, adding the

operators $A_x A_y$ and $C_x^n A_y$ to the L.H.S. of Equation (5.55) does not change the order of accuracy of the scheme, i.e. $\left\{1+A_xA_y+C_x^nA_y\right\}\dfrac{u_{y,x}^{n+1}-u_{y,x}^n}{\Delta t}=\dfrac{1}{\Delta t}\left\{A_x+A_y+C_x^n\right\}(u_{y,x}^{n+1}+u_{y,x}^n)$.

Rearranging terms Equation (5.55) becomes

$$\left\{1-C_x^n-A_x-A_y+A_xA_y+C_x^nA_y\right\}u_{y,x}^{n+1}=\left\{1+C_x^n+A_x+A_y+A_xA_y+C_x^nA_y\right\}u_{y,x}^n. \quad (5.56)$$

The operator expressions in Equation (5.56) can be factored by defining $B_1=(1-A_x-C_x^n)$, $B_2=(1-A_y)$, $B_3=(1+A_x+C_x^n)$, and $B_4=(1+A_y)$. Then, Equation (5.56) in a factored form is

$$B_1B_2u_{y,x}^{n+1}=B_3B_4u_{y,x}^n \ . \quad (5.57)$$

Notice that when factoring Equation (5.56), the order of operators in their product was not changed as the operators do not commute. Splitting steps require $u_{y,x}^*$ chosen such that

$$\left\{\begin{matrix}B_1u_{y,x}^*=B_4u_{y,x}^n\\B_2u_{y,x}^{n+1}=B_3u_{y,x}^*\end{matrix}\right\}\Rightarrow\left\{\begin{matrix}\left(1-c_x^n\delta_x^c-p_x\delta_x^2\right)u_{y,x}^*=\left(1+p_y\delta_y^2\right)u_{y,x}^n & \cdots(\text{a})\\\left(1-p_y\delta_y^2\right)u_{y,x}^{n+1}=\left(1+c_x^n\delta_x^c+p_x\delta_x^2\right)u_{y,x}^* & \cdots(\text{b})\end{matrix}\right\}, \quad (5.58)$$

which is the modified Peaceman and Rachford's 2D ADI method for the rail. To prove the equivalence of this split step method to Equation (5.57), apply the operator $(1-c_x^n\delta_x^c-p_x\delta_x^2)$ to both sides of Equation (5.58b) and the operator $(1+c_x^n\delta_x^c+p_x\delta_x^2)$ both sides of Equation (5.58a) and obtain

$$\begin{matrix}\left(1+c_x^n\delta_x^c+p_x\delta_x^2\right)\left(1-c_x^n\delta_x^c-p_x\delta_x^2\right)u_{y,x}^*=\left(1+c_x^n\delta_x^c+p_x\delta_x^2\right)\left(1+p_y\delta_y^2\right)u_{y,x}^n\\\left(1-c_x^n\delta_x^c-p_x\delta_x^2\right)\left(1-p_y\delta_y^2\right)u_{y,x}^{n+1}=\left(1-c_x^n\delta_x^c-p_x\delta_x^2\right)\left(1+c_x^n\delta_x^c+p_x\delta_x^2\right)u_{y,x}^*\end{matrix} \ . \quad (5.59)$$

Again, because $\left(1+c_x^n\delta_x^c+p_x\delta_x^2\right)$ and $\left(1-c_x^n\delta_x^c-p_x\delta_x^2\right)$ commute, Equation (5.59) leads to

$$\left(1-c_x^n\delta_x^c-p_x\delta_x^2\right)\left(1-p_y\delta_y^2\right)u_{y,x}^{n+1}=\left(1+c_x^n\delta_x^c+p_x\delta_x^2\right)\left(1+p_y\delta_y^2\right)u_{y,x}^n \quad . \qquad (5.60)$$

This proves that Equation (5.58) is equivalent to $B_1B_2u_{y,x}^{n+1}=B_3B_4u_{y,x}^n$.

To study the stability of the rail's modified 2D ADI scheme (Equation (5.58)), an approach similar to that for the implicit scheme on the sled (Section 5.3) is used. However, because the operators B_1 and B_3 are time dependent, a modified approach is necessary. Begin by setting $u_{y,x}^n=\lambda_n e^{iby\Delta y}e^{iax\Delta x}$ where λ_n may change at each time step and $u_{y,x}^*=\lambda^* u_{y,x}^n$. Further, applying the central difference operator, δ_x^c, and the two second order difference operators δ_x^2 and δ_y^2 to $u_{y,x}^n$ produces

$$\begin{aligned}
\delta_x^c u_{y,x}^n &= \lambda_n e^{iby\Delta y}e^{ia(x+1)\Delta x}-\lambda_n e^{iby\Delta y}e^{ia(x-1)\Delta x}\\
&=\left(e^{ia\Delta x}-e^{-ia\Delta x}\right)\lambda_n e^{iby\Delta y}e^{iax\Delta x}\\
&=(2i)\sin(a\Delta x)\lambda_n e^{iby\Delta y}e^{iax\Delta x} \quad . \qquad (5.61)\\
\delta_x^2 u_{y,x}^n &= (-4)\sin^2\left(\frac{a\Delta x}{2}\right)\lambda_n e^{iby\Delta y}e^{iax\Delta x}\\
\delta_y^2 u_{y,x}^n &= (-4)\sin^2\left(\frac{b\Delta y}{2}\right)\lambda_n e^{iby\Delta y}e^{iax\Delta x}
\end{aligned}$$

Using these in the rail's modified 2D ADI scheme (Equation (5.58)) and removing the Fourier terms results in

$$[1-4ic_x^n \sin(a\Delta x)+8p_x \sin^2\left(\frac{a\Delta x}{2}\right)]\lambda^*\lambda_n = [1-8p_y \sin^2\left(\frac{b\Delta y}{2}\right)]\lambda_n$$
$$[1+8p_y \sin^2\left(\frac{b\Delta y}{2}\right)]\lambda_{n+1} = [1+4ic_x^n \sin(a\Delta x)-8p_x \sin^2\left(\frac{a\Delta x}{2}\right)]\lambda^*\lambda_n \quad (5.62a)$$

Next define $E = 8p_y \sin^2\left(\frac{b\Delta y}{2}\right)$, $F = 8p_x \sin^2\left(\frac{a\Delta x}{2}\right)$ and $G_n = 4c_x^n \sin(a\Delta x)$ and observe that $0 \le \sin^2\left(\frac{a\Delta x}{2}\right) \le 1$, $0 \le \sin^2\left(\frac{b\Delta y}{2}\right) \le 1$ and $-1 \le \sin(a\Delta x) \le 1$. Thus *E* and *F* are always positive and Equation (5.62a) is reduced to

$$(1-iG+F)\lambda^* = (1-E)$$
$$(1+E)\lambda_{n+1} = (1+iG-F)\lambda^*\lambda_n \quad (5.62b)$$

Solving this equation for λ_{n+1} leads to

$$\lambda_{n+1} = \frac{1-F+iG_n}{1+E}\lambda^*\lambda_n = \frac{1-F+iG_n}{1+E}\frac{1-E}{1+F-iG_n}\lambda_n = \frac{1-E}{1+E}\cdot\frac{1-F+iG_n}{1+F-iG_n}\lambda_n . \quad (5.63a)$$

This difference equation has the solution

$$\lambda_n = \left(\frac{1-E}{1+E}\right)^n \prod_{k=1}^{n}\frac{1-F+iG_k}{1+F-iG_k}. \quad (5.63b)$$

For all *E*, *F* and *G*, $\left|\frac{1-E}{1+E}\right| \le 1$ and $\left|\frac{1-F+iG_n}{1+F-iG_n}\right| \le 1$ because *E* and *F* are positive number. It follows that $|\lambda_n| \le 1$ for all *a* and *b*. Therefore, the modified Peaceman-Rachford 2D ADI method for rail is unconditionally stable.

The rail and slipper are semi-infinite solids. In order to solve the heat transfer problem and find the solution numerically, it is necessary to discretize the regions of rail and slipper in space and time. Therefore, the semi-infinite space of rail and slipper is no longer useful and must be replaced with a finite length. For the numerical analysis, the three additional boundary conditions are added, such as the right-end-side and left-end-side boundaries, and aerodynamic boundary between the rail and slipper's contact surfaces. It is assumed that the temperature distribution at the right and left ends are fixed at an ambient temperature. Aerodynamics (movement of air) between the rail and slipper's sliding surfaces creates the bounce effect while the slipper moves along the rail with the sliding velocity. The switch function defined in Section 3.1 is used to simulate the bounce effect. Let's suppose that the length of rail is some multiples of slipper's length. For convenience and simplification to demonstrate the numerical formulation of this problem for the rail, say $k = 2$. So the number of gridpoints of rail on *x*-axis is twice that of the slipper's. Let *2xn* be the number of gridpoints to which the rail is discretized including the endpoints, and add one ghost point at each end outside of the rail. Therefore, *2xn+2* is the number of gridpoints assigned to the rail including the ghost points along the *x*-axis. Similarly, let *yn* be the number of gridpoints assigned along the *y*-axis. Therefore, *yn+2* is the number of gridpoints including the ghost points. Let $L^- = \frac{xn}{2}$ and $L^+ = \frac{3xn}{2}$ for some positive even integer xn. Accordingly these numbers represent the endpoints of the rail's contact surface. Discretizing space and time, the finite difference scheme of Equation (5.2), heat transfer problem for the rail, becomes

$$\text{PDE}: \ \rho c\left(\frac{u_{y,x}^{n+1}-u_{y,x}^{n}}{\Delta t}-v^{n+1/2}\cdot\nabla\left(u^{n+1}+u^{n}\right)\right)=k_r\frac{\delta_x^2}{\Delta x^2}(u_{y,x}^{n+1}+u_{y,x}^{n})+k_r\frac{\delta_y^2}{\Delta y^2}(u_{y,x}^{n+1}+u_{y,x}^{n})$$

$$\text{I.C.:} \quad u_{y,x}^{1}=T_0(x,y) \qquad \text{with } 2\le(y,x)\le(yn+1,2xn+1)$$

$$\text{B.C.1 (Left)}: \quad u_{y,1}^{n}=T_a \qquad \text{with } 2\le y\le yn+1$$

$$\text{B.C.2 (Right)}: \quad u_{y,2xn+2}^{n}=T_a \qquad \text{with } 2\le y\le yn+1$$

$$\text{B.C.3 (Interface)}: \quad k_r\frac{u_{3,x}^{n}-u_{1,x}^{n}}{2\Delta y}=$$

$$\begin{cases}\left\{\begin{matrix} h(u_{2,x}^{n}-T_a) & 1\le x\le L^{-}-1 \text{ and } L^{+}+1\le x\le 2xn+2\\ (1-\alpha^{n})q^{n} & L^{-}\le x\le L^{+}\end{matrix}\right\} & \text{in contact}\\ \left\{\begin{matrix} h(u_{2,x}^{n}-T_a) & 1\le x\le L^{-}-1 \text{ and } L^{+}+1\le x\le 2xn+2\\ h_3(u_{2,x}^{n}-T_3^{n}(x)) & L^{-}\le x\le L^{+}\end{matrix}\right\} & \text{not in contact}\end{cases}$$

$$\text{B.C.4 (Bottom)}: \quad u_{yn+2,x}^{n}=T_a \qquad \text{with } 2\le x\le 2xn+1 \tag{5.64}$$

The rail's PDE includes the heat flow term $v^{n+1/2}\cdot\nabla\left(u^{n+1}+u^{n}\right)$ because the rail is a moving object. This heat flow will introduce the heat front and heat tail after computing the rail's 2D ADI scheme, which was discussed in Literature Review Section, Section 1.6.3. The whole rail is initially at $T_0(x,y)$ and the only heat source is under the sliding surface. The left and right sides of rail's domain are not influenced by the frictional heat. Let the temperature distributions of both the left and right ends of the rail remain at ambient temperature T_a. Similarly, let the rail's bottom remain at T_a. From Figure 19, at the rail's top the frictional heat source is only located between L^{-} and L^{+} when the slipper and rail are in contact. As such, the boundary condition at the interface in the interval $L^{-}\le x\le L^{+}$ is the same as the slipper's interface boundary condition with the different heat partitioning value $(1-\alpha)$. In the region $1\le x\le L^{-}-1$ and $L^{+}+1\le x\le 2xn+2$, there is convective heat transfer between air and rail.

The region of the rail $u^n_{y,x}$ is within $2 \le (y,x) \le (yn+1, 2xn+1)$, and the boundaries are $u^n_{1,x}$ and $u^n_{yn+2,x}$ with $2 \le x \le 2xn+1$ and $u^n_{y,1}$ and $u^n_{y,2xn+2}$ with $2 \le y \le yn+1$. Given the solutions $u^n_{y,x}$ with $2 \le (y,x) \le (yn+1, 2xn+1)$, find the values at the boundary points $u^*_{y,1}$ and $u^*_{y,2xn+2}$ with $2 \le y \le yn+1$ and $u^*_{1,x}$ and $u^*_{yn+2,x}$ with $2 \le x \le 2xn+1$.

To complete the boundary condition, four corner points of the rail must be added. These corner points are ghostpoints, which are not part of the slipper and exist at each corner of the rail externally. This condition ensures the continuity of boundary conditions around the rail's four boundary sides. Using an approach similar to the slipper problem in Section 5.3, the values at ghostpoints are $u^n_{1,1} = T_a$, $u^n_{1,2xn+2} = T_a$, $u^n_{yn+2,1} = T_a$ and $u^n_{yn+2,2xn+2} = T_a$.

It is further necessary to determine the boundary values for the intermediate solution $u^*_{y,x}$. See Equation (5.58) and define $r_x = \frac{\kappa_r \Delta t}{\Delta x^2}$, $r_y = \frac{\kappa_r \Delta t}{\Delta y^2}$ and $c^n_x = \frac{v^{n+1/2} \Delta t}{4 \Delta x}$. To find the expression for $u^*_{y,x}$, add two Equations (5.58a) and (5.58b) and solve for $u^*_{y,x}$,

$$\left(1 - c^n_x \delta^c_x - \frac{r_x}{2}\delta^2_x\right)u^*_{y,x} - \left(1 + \frac{r_y}{2}\delta^2_y\right)u^n_{y,x} - \left(1 - \frac{r_y}{2}\delta^2_y\right)u^{n+1}_{y,x} + \left(1 + c^n_x \delta^c_x + \frac{r_x}{2}{}_x\,\delta^2_x\right)u^*_{y,x} = 0 \quad . (5.65)$$

$$u^*_{y,x} = \frac{1}{2}\left(u^n_{y,x} + u^{n+1}_{y,x}\right) + \frac{r_y}{4}\delta^2_y\left(u^n_{y,x} - u^{n+1}_{y,x}\right)$$

The boundary condition at left and right end of rail's domain is a fixed temperature $T_0(x,y)$. This implies that at any time step, the temperature at both ends is fixed at $T_0(x,y)$. So the rail's left and right end boundary condition for $2 \le y \le yn+1$ at the intermediate step is

$$\begin{aligned} \text{Left}: u^*_{y,2} &= T_a \equiv G_1 \\ \text{Right}: u^*_{y,2xn+1} &= T_a \equiv G_2 \end{aligned} \quad . \tag{5.66}$$

Formulating the numerical code for Equations (5.58a) and (5.58b), it is necessary to use the difference operator $(1-c_x^n\delta_x^c-\frac{r_x}{2}\delta_x^2)$ and $(1-c_x^n\delta_x^c-\frac{r_x}{2}\delta_x^2)$ to $u^*_{y,2}$ and $u^*_{y,2xn+1}$. Using Equation (5.66), the values at the rail's left and right end boundaries, $(1-c_x^n\delta_x^c-\frac{r_x}{2}\delta_x^2)u^*_{y,2}$ and $(1-c_x^n\delta_x^c-\frac{r_x}{2}\delta_x^2)u^*_{y,2xn+1}$ become

$$\begin{aligned} (1-c_x^n\delta_x^c-\frac{r_x}{2}\delta_x^2)u^*_{y,2} &= u^*_{y,2}-c_x^n\delta_x^c u^*_{y,2}-\frac{r_x}{2}\delta_x^2 u^*_{y,2} \\ &= u^*_{y,2}-c_x^n\left(u^*_{y,3}-u^*_{y,1}\right)-\frac{r_x}{2}\left(u^*_{y,3}-2u^*_{y,2}+u^*_{y,1}\right) \\ &= \left(c_x^n-\frac{r_x}{2}\right)u^*_{y,1}+\left(1+r_x\right)u^*_{y,2}+\left(-c_x^n-\frac{r_x}{2}\right)u^*_{y,3} \\ &= \left(c_x^n-\frac{r_x}{2}\right)T_a+\left(1+r_x\right)u^*_{y,2}+\left(-c_x^n-\frac{r_x}{2}\right)u^*_{y,3} \end{aligned} \quad . \tag{5.67}$$

$$(1-c_x^n\delta_x^c-\frac{r_x}{2}\delta_x^2)u^*_{y,2xn+1}=\left(c_x^n-\frac{r_x}{2}\right)u^*_{y,2xn}+\left(1+r_x\right)u^*_{y,2xn+1}+\left(-c_x^n-\frac{r_x}{2}\right)T_a$$

Performing the first step in Equation (5.58) finds the intermediate solutions $u^*_{y,x}$. This step solves the heat transfer problem in the *x*-direction. Let $\mathbf{U}_y$ and $\mathbf{U}_x$ be the row vector at a fixed *y* and the column vector at a fixed *x* for the interior of the rail, i.e. $\mathbf{U}_y=[u_{y,2},u_{y,3},\cdots,u_{y,2xn+1}]^T$ and $\mathbf{U}_x=[u_{2,x},u_{3,x},\cdots,u_{yn+1,x}]^T$, and $\mathbf{b}_y$ and $\mathbf{b}_x$ are the boundary

influence vector at rail's left and right, i.e. $\mathbf{b}_y = [u_{y,2}, 0 \cdots 0, u_{y,2xn+1}]^T$ and $\mathbf{b}_x = [u_{2,x}, 0 \cdots 0, u_{yn+1,x}]^T$. For each $2 \le y \le yn+1$, solve Equation (5.58a), which is the linear system

$$(1 - c_x^n \delta_x^c - \frac{r_x}{2}\delta_x^2)\mathbf{U}_y^* = \mathbf{U}_y^n + \frac{r_y}{2}(\mathbf{U}_{y+1}^n - 2\mathbf{U}_y^* + \mathbf{U}_{y-1}^*) + \mathbf{b}_y^* \tag{5.68}$$

L.H.S. of Equation (5.68) is

$$(1 - c_x^n \delta_x^c - \frac{r_x}{2}\delta_x^2)\mathbf{U}_y^* = \left(1 - c_x^n \delta_x^c - \frac{r_x}{2}\delta_x^2\right)\begin{bmatrix} u_{y,2}^* \\ \cdots \\ u_{y,2xn}^* \\ u_{y,2xn+1}^* \end{bmatrix} = \mathbf{A}_r \begin{bmatrix} u_{y,2}^* \\ \cdots \\ u_{y,2xn}^* \\ u_{y,2xn+1}^* \end{bmatrix} \tag{5.69}$$

where $\mathbf{A}_r = \begin{bmatrix} 1+r_x & -\frac{r_x}{2} - c_x^n & 0 & \cdots & & 0 \\ -\frac{r_x}{2} + c_x^n & 1+r_x & -\frac{r_x}{2} - c_x^n & 0 & \cdots & 0 \\ 0 & -\frac{r_x}{2} + c_x^n & 1+r_x & -\frac{r_x}{2} - c_x^n & \cdots & 0 \\ & & & \cdots & & \\ 0 & \cdots & -\frac{r_x}{2} + c_x^n & 1+r_x & -\frac{r_x}{2} - c_x^n & 0 \\ 0 & \cdots & 0 & -\frac{r_x}{2} + c_x^n & 1+r_x & -\frac{r_x}{2} - c_x^n \\ 0 & & \cdots & 0 & -\frac{r_x}{2} + c_x^n & 1+r_x \end{bmatrix}$

and $\mathbf{U}_y = \left[u_{y,2}, \cdots, u_{y,2xn+1}\right]^T$.

R.H.S. of Equation (5.68)

$$\mathbf{U}_y^n + \frac{r_y}{2}(\mathbf{U}_{y+1}^n - 2\mathbf{U}_y^* + \mathbf{U}_{y-1}^*) + \mathbf{b}_y^*$$

$$= \begin{bmatrix} u_{y,2}^n \\ u_{y,3}^n \\ \cdots \\ u_{y,xn+1}^n \end{bmatrix} + \frac{r_y}{2}\left(\begin{bmatrix} u_{y+1,2}^n \\ u_{y+1,3}^n \\ \cdots \\ u_{y+1,xn+1}^n \end{bmatrix} - 2\begin{bmatrix} u_{y,2}^n \\ u_{y,3}^n \\ \cdots \\ u_{y,xn+1}^n \end{bmatrix} + \begin{bmatrix} u_{y-1,2}^n \\ u_{y-1,3}^n \\ \cdots \\ u_{y-1,xn+1}^n \end{bmatrix} \right) + \begin{bmatrix} \left(\frac{r_x}{2} - c_x^n\right) G_1 \\ 0 \\ \cdots \\ \left(\frac{r_x}{2} + c_x^n\right) G_2 \end{bmatrix} \qquad (5.70)$$

where G_1, G_2 are defined in Equation (5.66). Combine Equations (5.69) and (5.70), then the result of Equation (5.68) in a matrix form is

$$\mathbf{A}_r \begin{bmatrix} u_{y,2}^* \\ \cdots \\ u_{y,xn}^* \\ u_{y,xn+1}^* \end{bmatrix} = \frac{r_y}{2} \begin{bmatrix} u_{y+1,2}^n \\ u_{y+1,3}^n \\ \cdots \\ u_{y+1,xn+1}^n \end{bmatrix} + (1 - r_y) \begin{bmatrix} u_{y,2}^n \\ u_{y,3}^n \\ \cdots \\ u_{y,xn+1}^n \end{bmatrix} + \frac{r_y}{2} \begin{bmatrix} u_{y-1,2}^n \\ u_{y-1,3}^n \\ \cdots \\ u_{y-1,xn+1}^n \end{bmatrix} + \begin{bmatrix} \left(\frac{r_x}{2} - c_x^n\right) T_a \\ 0 \\ \cdots \\ \left(\frac{r_x}{2} + c_x^n\right) T_a \end{bmatrix}. \qquad (5.71)$$

Now the values of the intermediate solution $u_{y,x}^*$ with $2 \le (y, x) \le (yn+1, 2xn+1)$ are determined. Since Equation (5.66) shows that the temperature at both left and right ends of the rail is fixed at T_a, the values of $u_{y,1}^*$ and $u_{y,2xn+2}^*$ for $2 \le y \le yn+1$ are T_a. In order to complete this first step, it is necessary to determine the values of $u_{y,x}^*$ with $1 \le x \le 2xn+2$ and $2 \le y \le yn+1$. These values are necessary and sufficient to find the solution on the $(n+1)^{st}$ time level.

The solution at the new time level, $u_{y,x}^{n+1}$ with $2 \le (y,x) \le (yn+1, 2xn+1)$ is determined by solving the heat transfer problem in the x-direction with the values of the intermediate solution $u_{y,x}^{*}$ with $1 \le x \le 2xn+2$ and $2 \le y \le yn+1$. Recall Equation (5.58b) and consider the mixed boundary conditions, the Dirichlet boundary condition at the rail's bottom and the Neumann boundary condition at the interface. For each $2 \le x \le 2xn+1$, solve the linear system

$$\left(1-\frac{r_y}{2}\delta_y^2\right)\mathbf{U}_x^{n+1} = \mathbf{U}_x^{*} + \frac{r_x}{2}\left(\mathbf{U}_{x+1}^{*} - 2\mathbf{U}_x^{*} + \mathbf{U}_{x-1}^{*}\right) + c_x(\mathbf{U}_{x+1}^{*} - \mathbf{U}_{x-1}^{*}) + \frac{r_y}{2}\mathbf{b}_m^{n+1}\ , \tag{5.72}$$

which is the matrix form of Equation (5.58b). L.H.S. of Equation (5.72) is

$$\left(1-\frac{r_y}{2}\delta_y^2\right)\mathbf{U}_x^{n+1} = \left(1-\frac{r_y}{2}\delta_y^2\right)\begin{bmatrix} u_{2,x}^{n+1} \\ \cdots \\ u_{yn,x}^{n+1} \\ u_{yn+1,x}^{n+1} \end{bmatrix} = \mathbf{B}_r \begin{bmatrix} u_{2,x}^{n+1} \\ \cdots \\ u_{yn,x}^{n+1} \\ u_{yn+1,x}^{n+1} \end{bmatrix} \tag{5.73}$$

where $\mathbf{B}_r = \begin{bmatrix} 1+r_y & -r_y & 0 & \cdots & & & 0 \\ -\frac{r_y}{2} & 1+r_y & -\frac{r_y}{2} & 0 & \cdots & & 0 \\ 0 & -\frac{r_y}{2} & 1+r_y & -\frac{r_y}{2} & 0 & \cdots & 0 \\ & & & \cdots & & & \\ 0 & \cdots & 0 & -\frac{r_y}{2} & 1+r_y & -\frac{r_y}{2} & 0 \\ 0 & & \cdots & 0 & -\frac{r_y}{2} & 1+r_y & -\frac{r_y}{2} \\ 0 & & & \cdots & 0 & -\frac{r_y}{2} & 1+r_y \end{bmatrix}_{yn \times yn}$.

Before rewriting R.H.S. of Equation (5.72), the boundary influence vector $\mathbf{b}_x^{n+1}\Big|_{x=m}$ must be determined. This boundary influence vector is similar to Equation (5.47), the slipper's boundary condition at the interface discussed in Section 5.3. The difference is that the rail's surface is partitioned into three parts and each segment has a different boundary condition which is defined at B.C.3 in Equation (5.64). The numerical expression of B.C.3 in Equation (5.64) becomes

$$k_r \frac{u_{3,x}^n - u_{1,x}^n}{2\Delta y} = \begin{cases} \left\{ \begin{array}{ll} h(u_{2,x}^n - T_a) & 1 \le x \le L^- - 1 \text{ and } L^+ + 1 \le x \le 2xn + 2 \\ (1-\alpha^n)q^n & L^- \le x \le L^+ \end{array} \right\} & \text{in contact} \\ \left\{ \begin{array}{ll} h(u_{2,x}^n - T_a) & 1 \le x \le L^- - 1 \text{ and } L^+ + 1 \le x \le 2xn + 2 \\ h_3(u_{2,x}^n - T_3^n(x)) & L^- \le x \le L^+ \end{array} \right\} & \text{not in contact} \end{cases} \tag{5.74}$$

Solving Equation (5.74) for $u^n{}_{2,x}$ is the numerical representation of the rail's interface, which is the first component of $\mathbf{b}_m^{n+1}$. Let's define Equation (5.74) as G_3. When the rail is in contact, G_3 represents the conductive boundary condition along the sliding contact area and the convective boundary condition outside of the contact area. When the rail is not in contact, there exists the convective boundary condition between two sliding surfaces along the contact area and another convective boundary condition outside of the contact area. Then R.H.S. of Equation (5.72) becomes

$$\mathbf{U}_x^* + \frac{r_x}{2}\left(\mathbf{U}_{x+1}^* - 2\mathbf{U}_x^* + \mathbf{U}_{x-1}^*\right) + c_x^n(\mathbf{U}_{x+1}^* - \mathbf{U}_{x-1}^*) + \frac{r_y}{2}\mathbf{b}_m^{n+1}$$

$$= \begin{bmatrix} u_{2,x}^* \\ u_{3,x}^* \\ \cdots \\ u_{yn+1,x}^* \end{bmatrix} + \frac{r_x}{2}\left(\begin{bmatrix} u_{2,x+1}^* \\ u_{3,x+1}^* \\ \cdots \\ u_{yn+1,x+1}^* \end{bmatrix} - 2\begin{bmatrix} u_{2,x}^* \\ u_{3,x}^* \\ \cdots \\ u_{yn+1,x}^* \end{bmatrix} + \begin{bmatrix} u_{2,x-1}^* \\ u_{3,x-1}^* \\ \cdots \\ u_{yn+1,x-1}^* \end{bmatrix}\right). \qquad (5.75)$$

$$+ c_x^n\left(\begin{bmatrix} u_{2,x+1}^* \\ u_{3,x+1}^* \\ \cdots \\ u_{yn+1,x+1}^* \end{bmatrix} - \begin{bmatrix} u_{2,x-1}^* \\ u_{3,x-1}^* \\ \cdots \\ u_{yn+1,x-1}^* \end{bmatrix}\right) + \frac{r_y}{2}\begin{bmatrix} -2\Delta y G_3 \\ 0 \\ \cdots \\ T_0 \end{bmatrix}$$

Combine Equations (5.73) and (5.75), then Equation (5.72) becomes

$$\mathbf{B}_r\begin{bmatrix} u_{2,x}^{n+1} \\ \cdots \\ u_{yn,x}^{n+1} \\ u_{yn+1,x}^{n+1} \end{bmatrix} + \begin{bmatrix} \frac{r_y \cdot \Delta y \cdot h_3}{k_s}(1-m^{n+1})u_{2,2}^{n+1} \\ 0 \\ \cdots \\ 0 \end{bmatrix} = \left(\frac{r_x}{2} - c_x^n\right)\begin{bmatrix} u_{2,x-1}^* \\ u_{3,x-1}^* \\ \cdots \\ u_{yn+1,x-1}^* \end{bmatrix} + (1-r_x)\begin{bmatrix} u_{2,x}^* \\ u_{3,x}^* \\ \cdots \\ u_{yn+1,x}^* \end{bmatrix}$$

$$+\left(\frac{r_x}{2} + c_x^n\right)\begin{bmatrix} u_{2,x+1}^* \\ u_{3,x+1}^* \\ \cdots \\ u_{yn+1,x+1}^* \end{bmatrix} + \begin{bmatrix} \frac{r_y \cdot \Delta y}{k_s} m^{n+1}\alpha_r{}^{n+1}q^{n+1} - \frac{r_y \cdot \Delta y \cdot h_3}{k_s}(1-m^{n+1})T_3^{n+1} \\ 0 \\ \cdots \\ \frac{r_y}{2}T_0 \end{bmatrix} \qquad (5.76)$$

5.5 Restrictions on Numerical Analysis of the Convection-Diffusion Problem

The beginning of Chapter 5 considered the two dimensional heat transfer PDE with a heat flow term $v(t)\frac{\partial u}{\partial x}$ for the rail. In Section 5.4, a finite difference scheme with the rail and the convection-diffusion equation was developed. Equation (5.2a) is the partial differential equation of the rail's heat transfer system, and its forward-time central-space scheme is

$$\frac{u_{y,x}^{n+1}-u_{y,x}^{n}}{\Delta t}-v^{n}\frac{u_{y,x+1}^{n}-u_{y,x-1}^{n}}{2\Delta x}=\kappa_r\frac{u_{y,x+1}^{n}-2u_{y,x}^{n}+u_{y,x-1}^{n}}{\Delta x^{2}}+\kappa_r\frac{u_{y+1,x}^{n}-2u_{y,x}^{n}+u_{y-1,x}^{n}}{\Delta y^{2}}. \qquad (5.77)$$

In order to use the analysis of Strikwerda (50), solving Equation (5.77) for $u_{y,x}^{n+1}$ helps to examine and analyze the stability of Equation (5.77). The solution of Equation (5.77) for $u_{y,x}^{n+1}$ is

$$\begin{aligned}u_{y,x}^{n+1}=&\kappa_r\frac{\Delta t}{\Delta x^{2}}(1+\frac{v^{n}\Delta x}{2\kappa_r})u_{y,x+1}^{n}+\kappa_r\frac{\Delta t}{\Delta x^{2}}(1-\frac{v^{n}\Delta x}{2\kappa_r})u_{y,x-1}^{n}\\&+(1-2\kappa_r\frac{\Delta t}{\Delta x^{2}}-2\kappa_r\frac{\Delta t}{\Delta y^{2}})u_{y,x}^{n}+\kappa_r\frac{\Delta t}{\Delta y^{2}}(u_{y+1,x}^{n}+u_{y-1,x}^{n})\end{aligned}. \qquad (5.78)$$

John C. Strikwerda in *Finite Difference Schemes and Partial Differential Equations* (50) discussed the stability condition for the convection-diffusion equation, $\frac{\partial u}{\partial t}+a\frac{\partial u}{\partial x}=b\frac{\partial^{2}u}{\partial x^{2}}$. He found the ratio $\frac{\Delta x a}{2b}$ describes that where this ratio is greater than 1, the solution will be oscillatory. This result is same for both positive and negative a so it is convenient to use the absolute value $|a|$. For Equation (5.78) $a=-\frac{v^{n}}{2}$ and $b=\kappa_r$. Accordingly the ratio is $\frac{\Delta x v^{n}}{2\kappa_r}$.

From his conclusion, the condition $\frac{\Delta x v^n}{2\kappa_r} \le 1$ is a condition on the mesh spacing that must be satisfied in order for the solution to the scheme to behave qualitatively as that of a parabolic differential equation.

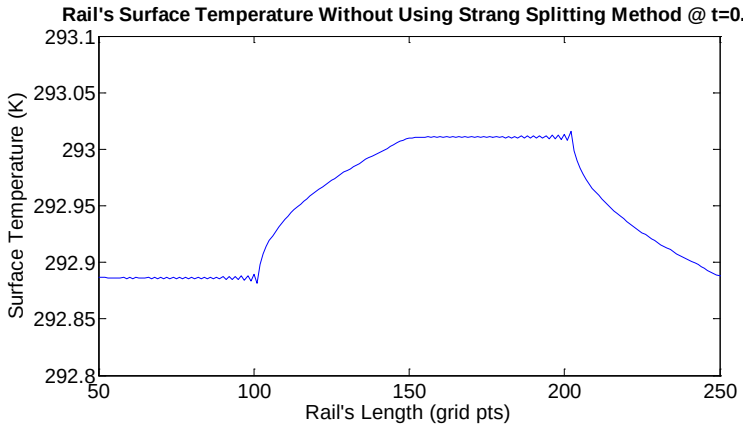

Figure 20. Rail's Surface Temperature Distribution at t=0 for v(t)=1 m/sec

Figure 20 is the numerical result for $\frac{\Delta x v^n}{2\kappa_r} < 1$ where $\Delta x = 0.002$, $\kappa_r = 7.44 \times 10^{-3}$ and $v^n = 1$. The *x*-axis represents the surface along the rail. The slipper contacts the rail between 100th grid point and 200th grid point. At the time $t = 0.1$ second, the frictional heat is generated due to sliding event and the surface temperature of the interface area along the rail rises. Because the rail is effectively moving right with first contact at the 100th grid point a steady temperature rise is seen looking left to right in the direction of motion. Figure 20 indicates that the solution does not oscillate notably when the sled's velocity is 1 m/sec. However, if $\frac{\Delta x v^n}{2\kappa_r} \ge 1$ where $v_n = 10$ m/sec, then the solution becomes oscillatory, see Figure 21.

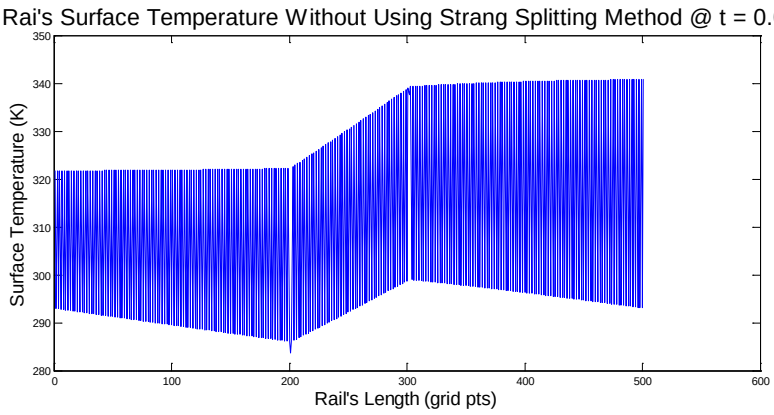

Figure 21. Rail's Surface Temperature Distribution at t=0.004 for v(t)=10 m/sec

John C. Strikwerda in *Finite Difference Schemes and Partial Differential Equations* (50) states that the oscillations do not grow excessively, i.e. the amplitude of oscillations maintains the same length as time progresses. He indicates they are not the result of instability.

One numerical technique used to remediate this oscillation is the operator splitting method. In Chertock and Kurganov's paper *On Splitting-Based Numerical Methods for Convection-Diffusion Equations* (51) they describe that computing solutions of convection-diffusion equations is an important and challenging problem, especially in the convection dominated case. This is because viscous layers (melt layers) are so thin that one is forced to use under-resolved methods that may be unstable. If a numerical convection method dominates over a physical diffusion process, the under-resolved method is typically stable, but the resolution may be severely affected.

If an insufficient amount of physical diffusion is compensated by an excessive numerical viscosity, the under-resolved method is typically stable, but the resolution may be severely affected. At the same time, the use of dispersive schemes may cause spurious oscillations that

may trigger numerical instabilities. Their approach to overcome these difficulties was an operator splitting technique which numerically preserved a delicate balance between the convection and diffusion terms.

Operator or time splitting is often used in the numerical solution of initial boundary value problems for differential equations. Lanser and Verwer (52) stated that virtually all processes modeled by time-dependent partial differential equations split additively in subprocesses for which simpler PDEs exist. This leads to the use of operator splitting or time splitting. An early influential paper on this subject is Gilbert Strang's paper, *On The Construction and Comparison of Difference Schemes* (53). In his paper, he used nonlinear initial value problems in two space variables. The methods to solve these nonlinear initial value problems in two space variables were either too crude to be accurate for first order or too complicated for third order methods. The computations were expensive either by the fine mesh required by a first order scheme in order to provide enough detail, or by the delicate differencing which maintained a high order of accuracy. So he proposed a new device for the construction of accurate difference schemes, which was an alternating direction scheme with the half-steps ordered for maximum accuracy.

Figure 21, shows that oscillation appears when the sled velocity is 10 m/sec. For the 2D heat transfer problem the velocity is very large, i.e. $v(t)\ is\ 100\ -\ 3000\ \mathrm{m/sec}$, and the scheme to solve rail's heat transfer problem introduces oscillations. As such it will not be a good approximation to the true solution. Because the heat flow term, $v(t)\frac{\partial u}{\partial x}$ in Equation (5.2a), is not negligible in computing solutions of rail's heat transfer problem, the Strang Splitting technique is employed.(53)(54) The method is described as

$$u^{n+1} = S_1(\frac{dt}{2})S_2(dt)S_1(\frac{dt}{2})u^n \ . \qquad (5.79)$$

In Equation (5.79), S_1 and S_2 are the diffusion and convection processes. If the diffusion process is applied first for the half-time step then the convection process is applied for the full-time step. In order to make a full-time step with the diffusion process, the half-time step diffusion needs to be applied again. These processes show the alternating operators between the diffusion and convection processes for a single iteration.

The rail's two dimensional heat transfer problem can be rewritten as

$$u_t = \underset{\text{heat flow}}{\mathbf{v}(t)\cdot\nabla u} + \underset{\text{heat diffusion}}{\kappa_r\cdot\nabla^2 u} \qquad (5.80)$$

Using the concept of Equation (5.79) with Equation (5.80), it is possible to develop the Strang Splitting Method. For each time step, the heat diffusion process $u_t = \kappa_r\cdot\nabla^2 u$ is solved for a half time step; then the heat flow process $u_t = \mathbf{v}(t)\cdot\nabla u$ is solved for a full time step; and finally, $u_t = \kappa_r\cdot\nabla^2 u$ is solved for a half time step. As the sled is moving by the velocity $\mathbf{v}(t)$, the contact area between the rail and slipper has to be adjusted at each time as the sled moves.

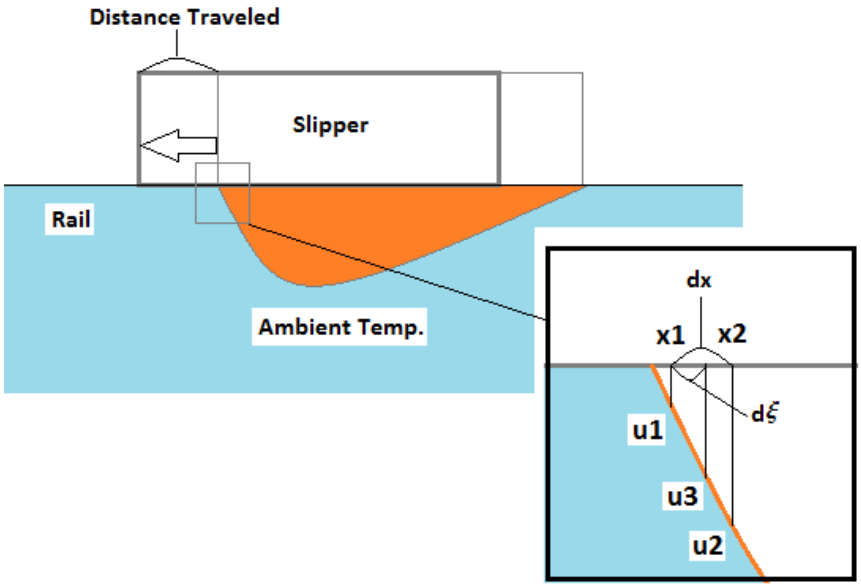

Figure 22. Rail's Domain Change Due to Sliding Velocity

Figure 22 illustrates how the contact area moves at each time step. The slipper's new domain corresponds to a new domain of rail each time. Each domain of rail has a different temperature distribution at each time step. The temperature profile under the distance traveled for some time becomes the ambient temperature T_0. Each point on the graph is mapped to the new position due to sliding velocity.

Let's consider the discrete domain and difference scheme. Let dx be the distance between x_1 and x_2 during one time interval, and $d\xi$ be the distance from x_1 to some point x_3 which lies between x_1 and x_2 as in Figure 22. Then if the rail's temperature is a linear function of time on one interval, the slope between two points u_1 and u_2 is the same as the slope between two points u_1 and u_3, i.e.

$$\frac{u_2-u_1}{\Delta x}=\frac{u_3-u_1}{\Delta \xi} \quad \Rightarrow \quad u_3=u_1+\Delta\xi\left(\frac{u_2-u_1}{\Delta x}\right). \tag{5.81}$$

In the Chertock and Kurganov's paper *On Splitting-Based Numerical Methods for Convection-Diffusion Equations* (51), they split the diffusion process into two half-time steps for the first and the third steps, and used the one-full-time step convection process for the second step. Using this idea, frictional heat energy is diffused into the rail for the first half time step. Using this relation to move the coordinate of rail in x-axis, the rail is moved by the distance traveled at a given velocity during the time step then the frictional heat energy is allowed to diffuse into rail for the second half time step. Finally the frictional heat energy diffusion is applied again to complete one iteration.

5.6 Calculating Heat Partitioning Values Numerically

In Chapter 3 the heat partition function was determined analytically using the method of Carslaw and Jaeger. First, the surface temperature distributions of two sliding materials were calculated using uniform frictional heat energy at constant velocity and then the surface temperatures were averaged along the contact region. Equating the averaged surface temperatures of the two materials gave rise the analytical solution for frictional heat partition values. As a result Equation (3.40) in Section 3.2 was derived as the analytical solution of the slipper's frictional heat partition function $\alpha(t)$, i.e.

$$\alpha(t)=\frac{1}{\pi}\int_0^{\infty} e^{-\frac{v_0}{2}tr}\,\frac{\beta^*\sqrt{r}\tilde{F}(-r)}{r(1+(\beta^*)^2 r(\tilde{F}(-r))^2)}\,dr \tag{5.82}$$

where $\beta^* = \frac{k^s}{k^r}\sqrt{\frac{\kappa^r}{\pi\kappa^s}}$ and $\tilde{F}(-r) = e^r \sum_{k=0}^{\infty}(k+1)\frac{2^{2k+3}(k+1)!}{(2k+3)!}(-r)^k$. The discrete PDE's for the two dimensional rail and slipper problem correspond to their continuous PDE's. As such, numerical representations corresponding to the analytical expressions with influences by the initial temperature and interface boundary condition must be developed.

The numerical method to determine the evolution of the heat partitioning function follows the development of the analytical solution. However, because the numerical solution allows for a continuously changing flux, $q(t)$ (i.e. non-constant velocity), along with the convective boundary conditions on either end of the slipper, a more accurate estimate of the partitioning function will be possible.

Begin by rewriting the two dimensional numerical solutions of rail and slipper as

$$\begin{aligned} u_r^{n+1}(\alpha_n) &= M_1 u_r^n + (1-\alpha_n) M_2 q^n \\ u_s^{n+1}(\alpha_n) &= N_1 u_s^n + \alpha_n N_2 q^n \end{aligned}, \qquad (5.83)$$

where $u_r^{n+1}(\alpha_n)$ and $u_s^{n+1}(\alpha_n)$ yields the numerical solutions of rail and slipper using the previous (slipper) heat partition value α_n. $M_1 u_r^n$ and $N_1 u_s^n$ can be thought of as the numerical contribution of the rail and slipper temperature distributions at time t_n. Similarly, $(1-\alpha_n)M_2 q^n$ and $\alpha_n N_2 q^n$ are the numerical contributions of the rail and slipper interface boundary condition to the temperature distribution during the time interval t_n to t_{n+1}. With the method of Carslaw and Jaeger (21), $u_r^{n+1}(\alpha_n)$ and $u_s^{n+1}(\alpha_n)$ in Equation (5.83) are averaged along the interface to produce values $\overline{u_s^{n+1}}(\alpha_n)$ and $\overline{u_r^{n+1}}(\alpha_n)$. Here the 'over bar' stands for average along the contact

interface length only. If the difference of $\overline{u_s^{n+1}}(\alpha_n)$ and $\overline{u_r^{n+1}}(\alpha_n)$ is zero, then the partition value α_n was correctly chosen. If the difference between $\overline{u_s^{n+1}}(\alpha_n)$ and $\overline{u_r^{n+1}}(\alpha_n)$ is not zero, the value for α_n must be adjusted. The difference between these average values is given by

$$\overline{u_r^{n+1}}(\alpha_n) - \overline{u_s^{n+1}}(\alpha_n) = \overline{M_1 u_r^n} + (1-\alpha_n)\overline{M_2 q^n} - \overline{N_1 u_s^n} + \alpha_n \overline{N_2 q^n} \ . \tag{5.84}$$

The goal is to calculate a correction, $\Delta\alpha$, to α_n so that Equation (5.84) vanishes for $\alpha_n^c = \alpha_n + \Delta\alpha$. Accordingly, $\alpha_n^c = \alpha_n + \Delta\alpha$ is chosen such that

$$\overline{u_r^{n+1}}(\alpha_n + \Delta\alpha) - \overline{u_s^{n+1}}(\alpha_n + \Delta\alpha) = \overline{M_1 u_r^n} + (1-\alpha_n + \Delta\alpha)\overline{M_2 q^n} - \overline{N_1 u_s^n} + (\alpha_n + \Delta\alpha)\overline{N_2 q^n} \ . \tag{5.85}$$
$$= 0$$

Solving Equation (5.85) for $\Delta\alpha$ yields

$$\Delta\alpha = \frac{\overline{u_r^{n+1}}(\alpha_n) - \overline{u_s^{n+1}}(\alpha_n)}{\overline{M_2 q^n} + \overline{N_2 q^n}} \ . \tag{5.86}$$

The averaged boundary condition influences to the rail and slipper at the interface $\overline{M_2 q^n}$ and $\overline{N_2 q^n}$ can be found from the averaged temperature influences at the interface $\overline{M_1 u_r^n}$ and $\overline{N_1 u_s^n}$. The values of $\overline{M_1 u_r^n}$ for the rail and $\overline{N_1 u_s^n}$ for the slipper are calculated numerically by letting $\alpha_n = 1$ for Equation (5.83) term $\overline{M_1 u_r^n}$ and $\alpha_n = 0$ in Equation (5.83) term $\overline{N_1 u_s^n}$. With Equation (5.83), solving $\overline{u_r^{n+1}}(\alpha_n) = \overline{M_1 u_r^n} + (1-\alpha_n)\overline{M_2 q^n}$ and $\overline{u_s^{n+1}}(\alpha_n) = \overline{N_1 u_s^n} + \alpha_n \overline{N_2 q^n}$ for $\overline{M_2 q^n}$ and $\overline{N_2 q^n}$ produces the following

$$\overline{M_2 q^n} = \frac{1}{1-\alpha_n}\left[\overline{u_r^{n+1}}(\alpha_n) - \overline{M_1 u_r^n}\right]$$
$$\overline{N_2 q^n} = \frac{1}{\alpha_n}\left[\overline{u_s^{n+1}}(\alpha_n) - \overline{N_1 u_s^n}\right] \quad . \tag{5.87}$$

Using these values in Equation (5.86), the change of slipper's heat partition value $\Delta\alpha$ is computed. With the slipper's corrected heat partition value $\alpha_n^c = \alpha_n + \Delta\alpha$, the temperature distributions for the rail and slipper are re-evaluated. The averaged temperatures of rail and slipper $\overline{u_r^{n+1}}(\alpha_n^c)$, $\overline{u_s^{n+1}}(\alpha_n^c)$ at the interface are now equal to one another. There are two major influences determining the slipper's heat partitioning value: 1) the different thermal properties of rail and slipper and 2) the surface temperature of rail and slipper.

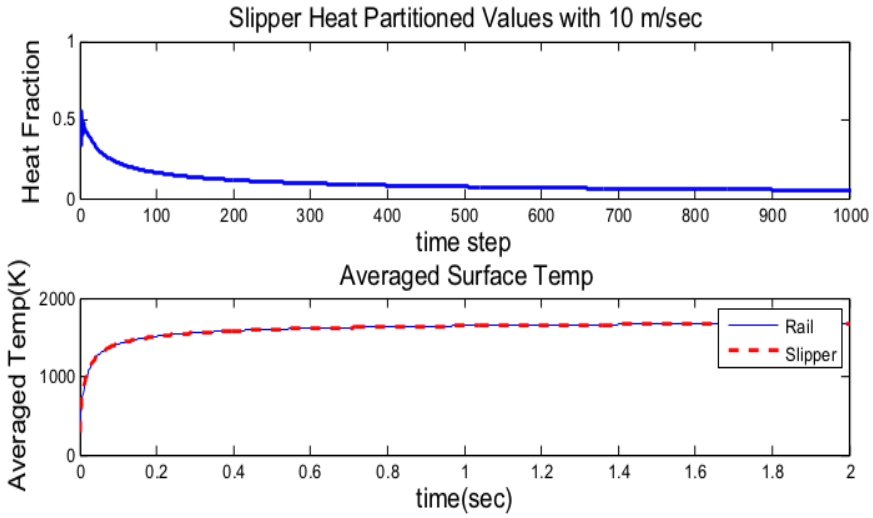

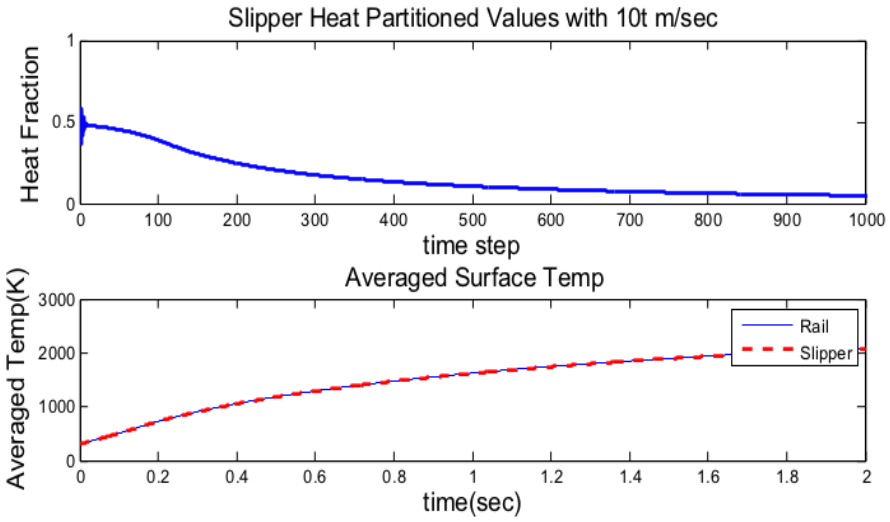

Figure 23. Slipper's Adjusted Heat Partition Values to Match Averaged Surface Temperatures of Rail and Slipper vs Sliding Time

The first two graphs of Figure 23 are (a) the slipper's heat partition value graph and (b) the averaged surface temperatures of rail and slipper when a sled is moving at constant rate 10 m/sec. The next two graphs of Figure 23 are (c) the slipper's heat partition value graph and (d) the averaged surface temperatures of rail and slipper when the velocity of a sled is increasing linearly at $10 \cdot t$ m/sec. From two graphs (b) and (d) in Figure 23, Equation (5.86) calculates the correct slipper's heat partition value at each iteration so the slipper's averaged surface temperature matches the rail's averaged surface temperature.

In graphs (a) and (b) of Figure 23, initially the sled is moving 10 m/sec, which means the friction initially heats the contact surfaces of slipper and rail. In graphs (c) and (d) of Figure 23, the velocity of the sled is increasing linearly at the rate of 10 m/sec^2, *v(t)=10t* m/sec, i.e. the velocity of the sled starts at 0 m/sec and reaches 10 m/sec at one second. The key point here is that *v(t)=10t* m/sec is starting at zero and the sled accelerates to velocity of *10* m/sec in one

second while *v(t)=10* m/sec is starting at *10* m/sec and remains at *10* m/sec for one second. The slipper's initial heat partition fraction is set to 0.488. This initial guess is based on the slipper and rail's thermal properties calculated in Equation (3.39). The heat generated with the constant velocity is greater than for accelerating velocity. From Equation (4.24)

$$\int_0^1 \mu P(t) v_1(t)\, dt \geq \int_0^1 \mu P(t) v_2(t) dt\,. \tag{5.88}$$

where $\mu = 0.2, v_1(t) = 10 m/sec$ and $v_2(t) = 10tm/sec.$ Therefore, the frictional heat generated in one second at constant velocity is more than that generated accelerating to that velocity in the same time. The averaged surface temperatures of the slipper and rail are 293K initially. Figure 23 (b) and (d) show that the slipper with the velocity *10* m/sec heats up faster and reaches higher temperature than the slipper with the velocity *10t* m/sec, which Equation (5.88) explains.

During the first time iteration the slipper receives 48.8% of the frictional heat energy as the frictional heat flux is distributed evenly to slipper and rail. For the next iteration, the slipper's sliding surface is in contact with the new region of the rail due to the coordinate change by the distance which the slipper has traveled during one iteration. So the surface temperatures of slipper and rail are not the same for the next iteration. By matching the averaged surface temperatures of rail and slipper after the first time step, the slipper's heat partitioning value needs to be corrected for the next time step. Because the slipper is moving into a cooler region of rail, the slipper accepts less heat energy at the next time step.

Figure 23 shows that the slipper's heat partitioning values fluctuate at the beginning and the difference between two iterations gets smaller as time evolves. This numerical instability is

due to the slipper's initial-guessed heat partitioning value evaluated by the relation of thermal properties of slipper to rail. Initially 48.8% of total frictional heat energy flows into slipper's interface so the rail and slipper's surface temperatures are different. Since the difference between the averaged surface temperatures of the rail and slipper is not zero, the slipper's heat partitioning value must be adjusted. With the corrected heat partitioning value, the slipper absorbs correspondingly more or less at the next iteration. By the nature of this process, the heat partitioning values seem instable at the beginning; however, after a few iterations of adjusting process, the value becomes stable, i.e. they continue to oscillate at each iteration but the amplitude of oscillation is diminishing.

After ten iterations, the slipper's heat partitioning value curve does not oscillate and produces a smooth exponentially decreasing function plot. The reason that the slipper's heat partitioning values decrease is the slipper moves continually into a cooler region of rail and more heat energy flows into the cooler rail. Once the system becomes stable, it is possible to predict the long term behavior. However, when the slipper's sliding surface starts melting, the slipper's surface temperature remains at the melt temperature and the slipper slides along the cooler region of rail (which is set to be the ambient temperature). After reaching the melting point the surface temperature difference between slipper and rail is same for each iteration and the heat partitioning value remains unchanged. The heat partitioning value after the melt time is fixed at $\alpha(t_m)$, the slipper's heat partitioning value at melt time. This melt time can be found from Figure 23 or the formulas, Equations (4.28) and (4.30), developed in Section 4.3.

From Figure 23, with the velocity 10 m/sec, the slipper's averaged surface temperature reaches the melt temperature 1685 *K* about 1.3 seconds and the slipper's averaged surface temperature with the velocity *10t* m/sec reaches the melt temperature about 1.4 seconds. Also, from Table 2 and 3 in Section 4.3, the melt time of the slipper with 10 m/sec and $\mu = 0.2$ is 1.33 seconds and the melt time of the slipper with *10t* m/sec and $\mu = 0.2$ is 1.44 seconds. This implies that the numerical model using Strang's Splitting method and ADI method verifies the solution for the melt time, Equations (4.28) and (4.30) in Section 4.3. Once the melt time found from either the numerical solution or Equations (4.28) and (4.30), the slipper's heat partitioning value after the melt time is no longer valid so the slipper's heat partitioning value is fixed at $\alpha(t_m) = 0.06$ for $t \geq t_m$.

6 Comparison and Analysis

6.1 Comparison of Analytical and Numerical Results

As the velocity of sled increases the frictional heat generated due to velocity and pressure increases. The change in the frictional heat at the interface due to the change in velocity and loading pressure influences the surface temperatures of rail and slipper and the temperature distribution inside both sliding materials. The ADI method was employed to evaluate the temperature changes given velocity and pressure. The change in surface temperature and the frictional heat at the contact surface influences the heat partitioning value. Therefore, it is necessary to calculate the heat partitioning fraction given velocity and pressure at each timestep. However, computing solutions of convection-diffusion equations is a problem fraught with complexity.

Chertock and Kurganov(51) describe that "Computing solutions of these equations is an important and challenging problem, in which viscous layers are so thin that one is forced to use under-resolved methods that may be unstable. If an insufficient amount of physical diffusion is compensated by an excessive numerical viscosity, the under-resolved method is typically stable, but the resolution may be severely affected. At the same time the use of dispersive schemes may cause spurious oscillations that may trigger numerical instabilities."

In order to overcome these difficulties by numerically preserving a balance between the convection and diffusion terms, this research employs Strang's Splitting method. When using Strang's Splitting method grid spacing size is varied in response to velocity changes. In *'Finite Difference Schemes and Partial Difference Equations'*, John C. Strikwerda (50) examined the

convection-diffusion problem with two different grid spacing values, relatively small and large numbers. He concluded, "First, there is a grid spacing limitation. If the grid spacing is too coarse, then the scheme will not compute a qualitatively correct solution. Secondly, if precise information is needed about the solution and it is not cost-effective to use a small grid spacing, then other methods should be investigated to obtain this information. In recent years a number of methods have been developed for increasing local grid refinement only in those places where the solution is changing rapidly."(50) His statement implies that changing the grid spacing size and splitting step size due to velocity changes may cause instability in the solutions if Strang's Splitting method is used. For the numerical analysis using ADI method and Strang's Splitting method, the grid spacing size has to be fixed. Since the change of the splitting step size at each time causes oscillations in the solution, the splitting step size also must remain fixed in the numerical code. Figure 24 shows the comparison of two results, the analytical solution of the heat partitioning function, and the numerical solution of the heat partitioning fraction for a constant velocity and pressure. This comparison between the two results of the constant velocity case shows that the analytical solution can be calculated only when the velocity is assumed to be constant.

From Figure 24, it is apparent that the analytical solution is slightly larger than the numerical solution. First, a system of partial differential equations for finding the analytical solution was simplified. In Section 3.2, the slipper's PDE $\frac{\partial w^s}{\partial \tau} = \frac{\partial^2 w^s}{\partial \eta^2} + \varepsilon^2 \frac{\partial^2 w^s}{\partial \xi^2}$ in Equation (3.8) contains ε^2 in $\frac{\partial^2 w^s}{\partial \xi^2}$ term. Since the value of ε is approximately 10^{-2}, the heat propagation

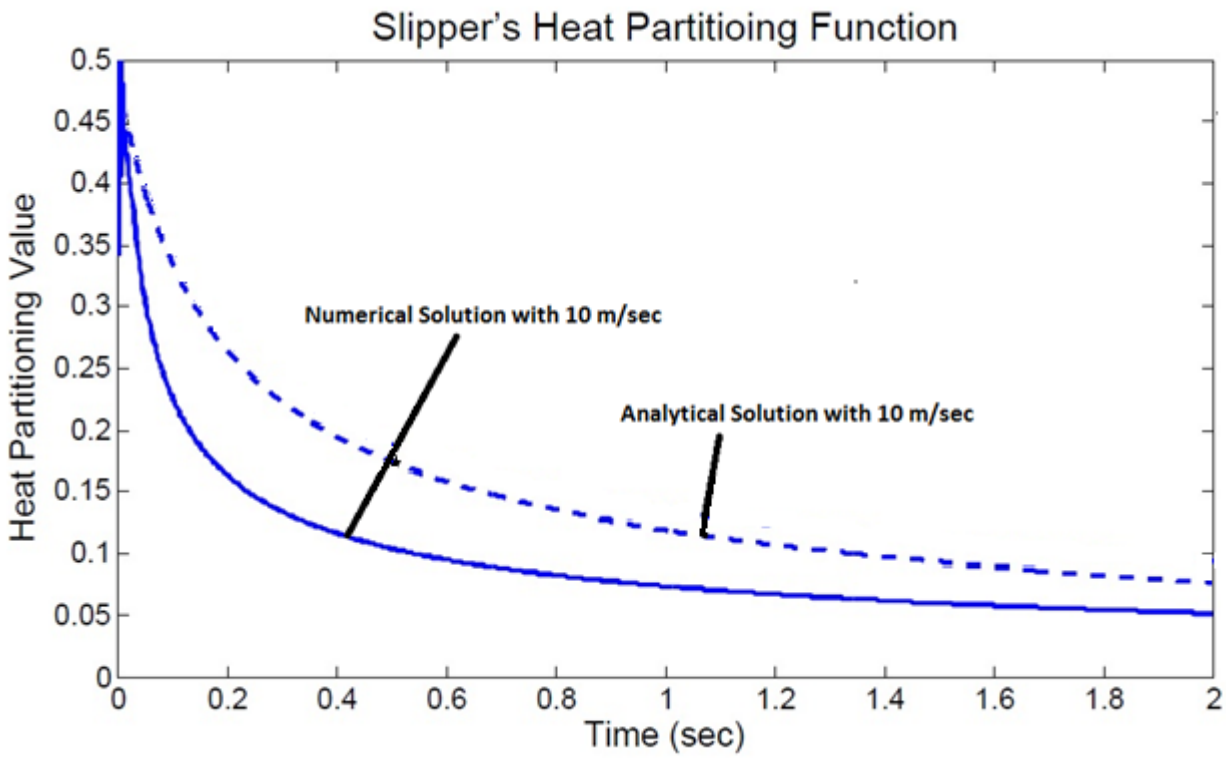

Figure 24. Comparison of Slipper's Heat Partitioning Values at v(t)=10 m/sec

in the ξ direction is considered small. So the influence of $\frac{\partial^2 w^s}{\partial \xi^2}$ term is ignored. Second, the contribution of the slipper's head and tail boundary conditions is assumed small enough to be neglected. Because $\varepsilon \ll 1$, the contribution of convective effects is neglected. Assumptions of the heat flow in the ξ direction and contact boundary conditions are key influences to the difference between the analytical and numerical solutions of the slipper's heat partitioning values and the slipper's surface temperature.

In practice, the slipper is always in contact with a cooler region of rail when sliding. As the velocity of the slipper increases, more frictional heat is generated and an increasing portion of the frictional heat flows into the rail. Once the slipper's surface temperature reaches melt

temperature, the temperature difference between the slipper and rail surfaces remains the same. With these observations, the slipper's heat partitioning function should show that the slipper's heat partitioning value is decreasing and approaching a fixed value. After the surfaces of the slipper and rail reach melting temperature, their surface temperature difference is same and the heat partitioning value remains same, i.e. $\alpha(t_m)$ the slipper's heat partitioning value at melt time. The melt time for this research was calculated by Equation (4.28) in Section 4.3 while the numerical solution was modeled and developed in Chapter 5.

A system of numerical PDEs was developed from the two-dimensional convection-diffusion problem. It considers all of the following things, which are the convective boundary conditions at the slipper and rail surfaces, the two dimensional heat energy diffusion process inside of slipper and rail, the bounce effect, and varying velocity and loading pressure profiles. Since the numerical analysis considers all of these factors, the numerical solution of the slipper's heat partitioning function with ADI method and Strang's Splitting method is expected to have the heat energy gain or loss consistent with the analytical solution.

Indeed, the numerical solution follows the qualitative behavior of the heat partitioning values. Figure 24 shows that the numerical result using ADI method and Strang's Splitting method is remarkably close to the analytical solution of the slipper's heat partitioning function. This implies that the numerical evaluation using ADI method and Strang's Splitting method can be used to verify the analytical solution of the slipper's heat partitioning function, which was developed in Section 3.2.

7 Numerical Application: Melt Wear Percentage

Conducting an experimental wear study replicating the conditions seen by the slipper at the HHSTT is economically infeasible at this time. However, the wear phenomena can still be evaluated by carefully implementing models verified for slower sliding velocity. This chapter will first discuss the generation of slipper dynamics data, which is the foundation for much of the numerical techniques used. The heat partition function will be integrated and evaluated numerically with some parameters varying with time. The graph of the heat partition fraction as a function of time will be compared with other experimental and analytical transient solutions, described in literature review section for verification. It will describe the numerical analysis method and the mathematical modeling development. The method for calculating the surface temperature of the slipper and melt wear percentage will then be described.

7.1 Numerical Analysis of Heat Partition Function

In Chapter 3, a two-dimensional mathematical model for the present application problem was developed and used to derive the surface temperature distributions of two bodies using Green's functions. After matching the averaged surface temperatures of slipper and rail at the sliding interface, the frictional heat partition fraction function is determined and expressed in Equation (3.40), i.e.

$$\alpha(t) = \frac{1}{\pi}\int_0^{\infty} e^{-\frac{v_0}{2}tr} \frac{\beta^* \sqrt{r}\tilde{F}(-r)}{r(1+(\beta^*)^2 r(\tilde{F}(-r))^2)} dr\,, \tag{7.1}$$

where $\beta^* = \frac{\beta}{\sqrt{\pi}} = \frac{k^s}{k^r}\sqrt{\frac{\kappa^r}{\pi\kappa^s}}$ and $\tilde{F}(-r) = e^r \sum_{k=0}^{\infty}(k+1)\frac{2^{2k+3}(k+1)!}{(2k+3)!}(-r)^k$. The denominator of Equation (3.40) is an infinite sum rendering the integration impossible analytically. With the help of a numerical scheme implemented in MATLAB, the integration is carried out and the frictional heat partition fraction function is evaluated numerically.

There are two major parameters in the frictional heat partition function; $\beta = \frac{k^s}{k^r}\sqrt{\frac{\kappa^r}{\kappa^s}}$ the relation of thermal properties of slipper to rail and v_0 the dimensionless constant velocity as defined in Chapter 3. Figure 25 shows the comparison among the heat partition fraction function graphs of two cases, 5 m/sec and 10 m/sec. For each velocity case, different values of β are

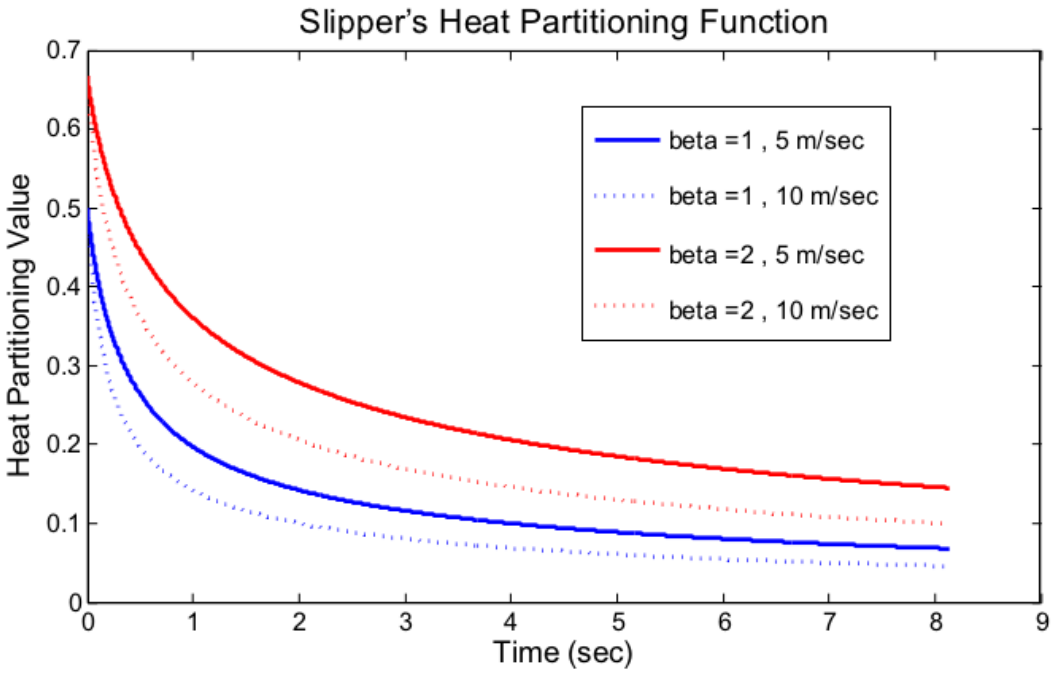

Figure 25. Slipper's Frictional Heat Partitioning Values with Various Parameters

used. The values of $\beta = 1, 2$ are tested with the two different constant velocity values.

In Figure 25, the solid line and dotted line represent the velocity 10 m/sec, and the velocity 5 m/sec respectively. Different colors represent the different values of β, the relation of the thermal properties of rail and slipper. For example, if the rail and slipper are made up of the same material, then the slipper's initial heat partitioning value $\alpha(\tau = 0)$ is evaluated using Equation (3.32), i.e.

$$\alpha(\tau = 0) = \frac{\beta}{1+\beta}. \tag{7.2}$$

The initial values for dotted and solid lines of the same color are equal because sled has not moved yet.

We may examine both plots (10 m/sec and 5 m/sec) for any of the cases shown in Figure 25 to determine trends. For an increased starting velocity, the heat partitioned to the slipper falls faster. In general the slipper's heat partition values decrease exponentially and the steady state value approaches 0. Therefore, after a certain amount of time, most of the frictional heat energy transfers to rail if the sled moves at very high speed. This observation is supported by other FEA model experiments (34)(35)(36). In these experiments a locked rail car wheel assumes the role of the slipper. In these efforts the researchers assume that the wheel and rail are made out of the same material and α is the fractional heat partitioning value flowing into rail. Figure 5 in Section 1.6.3, Heat partition factor vs. time at various positions along the contact patch, shows that initially α is approximately 0.42 so that α decreases as time progresses. After 0.1 second of sliding, the heat partition fraction approaches zero. This implies that almost all of the heat is

entering the rail. Using Figure 25, the result of comparison of heat partitioning graphs for 5 m/sec and 10 m/sec confirms my numerical results and corresponding results are reasonable.

7.2 Numerical Methods for Heat Conduction Problem

As mentioned previously in Chapter 2, the thermal gradient of the slipper is defined by the heat conduction equation given in Equation (2.4) as $\frac{\partial T}{\partial t} = \kappa \frac{\partial^2 T}{\partial x^2}$. This equation can be solved numerically, using either an explicit or implicit solution scheme. (1)

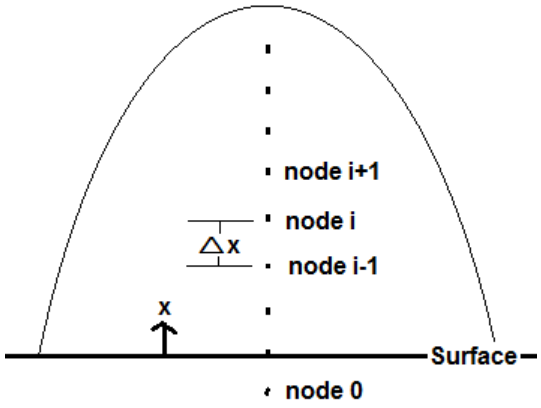

Figure 26. One-Dimensional Heat Transfer Schematic (1)

1. *Explicit Solution Scheme:* The advantage of the explicit scheme (which utilizes a forward difference for time and a central difference for space) is that the implementation is straightforward, as the temperature for each node at a given time step is a function of the surrounding nodes at the previous time step.

$$T_i^{n+1} = T_i^n + \kappa \frac{\Delta t}{\Delta x^2}(T_{i+1}^n - 2T_i^n + T_{i-1}^n) \qquad (7.3)$$

In Equation (7.3), the *n* superscript refers to the previous time step and *n+1* refers to the current time step, and the *i* subscript refers to the node location. By definition, the temperature at a node for the current time step is denoted as T_i^{n+1}, and Figure 26 shows a schematic of the one-dimensional layout. The drawback to the explicit scheme is that it is conditionally stable. The coefficient attached to the second term in the right hand side of equation above is known as the Fourier number *Fo*, and defined as $Fo = \kappa \frac{\Delta t}{\Delta x^2}$.

The stability criterion for the explicit scheme requires that the coefficient associated with the node of interest at the previous time step, T_i^n, be greater than or equal to zero, or $(1 - 2Fo) \geq 0$. This requires a Fourier number such that $Fo \leq 0.5$.(40) This limits the range of available time and space intervals, Δt and Δx, respectively. If a fine resolution temperature gradient is desired near the surface of the slipper the node spacing needs to be small. To maintain stability the time step must be small as well. This can present potential issues with computer memory allocation if the resolution requirements are too fine. This drawback can be circumvented by using an implicit scheme to solve the heat conduction equation.

2. *Implicit Solution Scheme:* The implicit scheme differs from the explicit scheme in that it uses a backward difference on time and a central difference in space. Most importantly it is unconditionally stable meaning that no restrictions are place on Δt and Δx. The implicit method is defined as

$$\frac{T_i^{n+1} - T_i^n}{\Delta t} = \kappa \left[\frac{T_{i+1}^{n+1} - 2T_i^{n+1} + T_{i-1}^{n+1}}{(\Delta x)^2} \right]. \qquad (7.4)$$

The most notable difference between Equation (7.3) and Equation (7.4) is that the "new" temperature for any node at time *n+1* is a function of the "new" temperature at the surrounding nodes. Thus, to solve the equations, the temperatures must be determined simultaneously. This complicates the programming slightly, but the relaxation of the time and space intervals allows for a fine resolution of the temperature gradient without encountering memory allocation errors.

7.3 One Dimensional Problem with Melt Front Removal

Consider the slipper as a semi-infinite solid, which is initially at a uniform temperature. During sliding process, the surface at $x = 0$ is subjected to heating at the rate of $Q(t)$ due to friction. Suppose that T is the slipper's temperature distribution. Before the slipper can generate a melt layer, the temperature at any interior point will never exceed its melt temperature T_m, i.e. $T_0 \le T(x,t) < T_m$. Once the surface temperature of slipper reaches the melt temperature, the surface undergoes a change of state from solid to liquid, called 'melt layer'. It is assumed that this melt region is removed continuously and immediately.

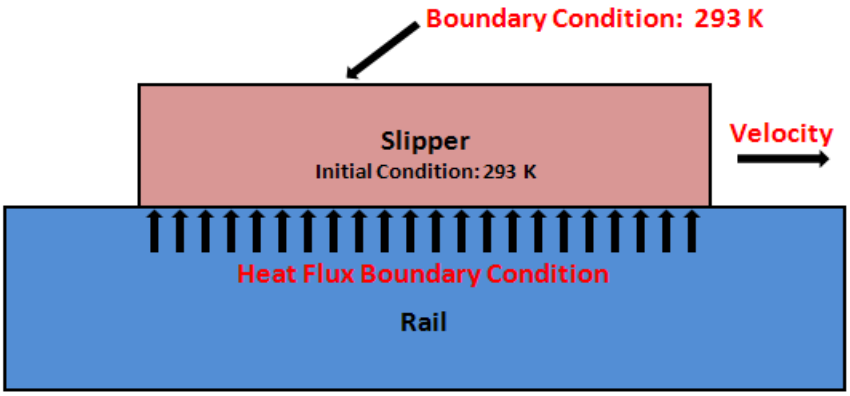

Figure 27. Heat Transfer Boundary and Initial Conditions (1)

In Section 3.2, the heat flux $Q(t)$ is assumed to be uniform along the contact surface, and the one dimensional heat transfer PDE is used to find the melt time in Chapter 4. With the same assumption in Section 3.2 and the same approach in Chapter 4, let's solve the slipper's one-dimensional finite difference heat equation approximations using the backward time difference scheme (the implicit scheme). In Figure 27, the slipper is initially at ambient temperature, $T_a = 293K$, throughout the entire the thickness. The boundary condition at the top of the slipper holds the temperature at the ambient condition for the entirety of the calculation. The second boundary condition is the frictional flux condition applied at the bottom edge of the slipper defined as

$$-k\left.\frac{\partial T}{\partial x}\right|_{x=0} = Q(t) \ . \qquad (7.5)$$

Figure 27 shows that the heat flux is uniformly applied along the contact surface.

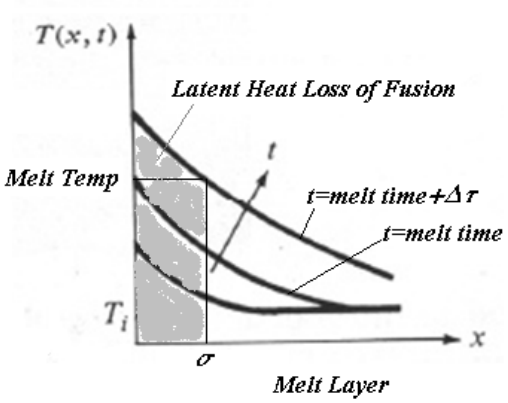

Figure 28. Slipper's Melt Layer Due to Latent Heat Loss of Fusion

Figure 28 describes the slipper's temperature distribution through the thickness. As time evolves, the surface temperature increases and the heat propagates into the slipper's body due to

the addition of frictional heat energy at the surface. When the slipper starts sliding along the rail, the heat flux shown in Equation (7.5) raises the slipper's surface temperature. Once the surface temperature reaches the melt temperature melt wear (melt removal) takes place. Therefore, a new model must be considered. First, the melt region is continuously removed and the latent heat of fusion must be included in the flux boundary condition, mathematically described as

$$-k\frac{\partial T}{\partial x}\bigg|_{x=\sigma(t)} = Q(t) - \rho\ell\frac{d\sigma}{dt} \tag{7.6}$$

where $\sigma(t)$ is the location of the melt front as a depth into the slipper, x is a depth into the slipper, and ℓ is the latent heat of fusion.

When the sled slides on the rail (with loading) the aerodynamic behavior creates the bounce effect. Two boundary conditions at the sliding contact surface have to be considered. When the loading pressure exists, the slipper is in contact with the rail. Therefore, the boundary condition has a heat flux as described in Equation (7.6). When the loading pressure does not exist, the slipper is not in contact with the rail and a convective flux boundary condition more closely approximates the true physics of not-in-contact boundary condition. The mathematical expression of this boundary condition is defined as

$$-k\frac{\partial T_2}{\partial x} = \begin{cases} Q(t) - \rho\ell\dfrac{d\sigma}{dt} & \text{in contact} \\ h(T - T_a) & \text{not in contact} \end{cases} \tag{7.7}$$

where h is the convective heat transfer coefficient. Since the slipper is not always in contact with the rail during the run, a switch function is used to indicate either the in-contact condition or not-

in-contact condition. Let the switch function be a function of a loading pressure (force) defined as

$$m(t) = \begin{cases} 1, & \text{Force} > 0 \\ 0, & \text{Force} \le 0 \end{cases} \tag{7.8}$$

where the force is the function of time and this function's output is the loading pressure. Therefore, if there exists a positive loading pressure at some time t_k, $m(t_k) = 1$. Otherwise, $m(t_k) = 0$. The convective and conductive flux boundary condition with the bounce effect, combined Equation (7.7) with Equation (7.8), can be represented by

$$-k\frac{\partial T}{\partial x} = m(t)\left(Q(t) - \rho\ell\frac{d\sigma}{dt}\right) + (1 - m(t))\left[h(T - T_3)\right] . \tag{7.9}$$

This adds the complexity of either a convective flux boundary condition or bounce effect. They assumed that the slipper was in contact with the rail for the duration of the wear event.

Once the temperature at the contact boundary reaches the melt temperature, melt removal creates boundary movement. The position of the boundary shifts with the value of $\sigma(t)$, the melt layer thickness. The boundary conditions at the melt front and the top of the slipper are

a) The slipper's temperature at the melt front is melt temperature after it starts to melt, i.e. $T(\sigma(t), t) = T_m$ where $t \ge t_m$.

b) The other end of slipper, the top of slipper, in a semi-infinite domain, is an ambient temperature, i.e. $T(x, t) \to T_a$ as $x \to \infty$.

c) The melt layer does not occur until it reaches the melt time, i.e. $\sigma(t) = 0$ for $0 \le t < t_m$.

For the purposes of truncating the computational domain, *x* has to be bounded so the boundary condition $T(x,t) \to T_a$ as $x \to \infty$ is replaced with $T(x,t) = T_a$ at $x = x^*$ where x^* is a sufficiently large distance from the contact surface. A reasonable choice of x^* may be given by the diffusion length for the total event time t^*, i.e. $x^* = \sqrt{\kappa t^*}$.

To establish a new scaled coordinate system with respect to the melt front, a new length scale is introduced and defined as $\xi = \dfrac{x - \sigma(t)}{x^*}$. The temperature $T(x,t)$ is made dimensionless by setting

$$T(x,t) = (T_m - T_a)w(\xi,t) + T_a \tag{7.10}$$

where T_m melt temperature and T_a ambient temperature. From the boundary condition, this relation implies that as $\xi \to \infty$, $w(\xi,t) = 0$ because of the boundary condition $T(x,t) = T_a$ as $x \to \infty$. The boundary conditions at the melt front $x = \sigma(t)$ and at the other end of slipper $x \to \infty$ become

$$\begin{array}{ll} \text{(a)} & w(\xi,t) = 1 \quad \text{at } \xi = 0 \text{ for } t \ge t_m \\ \text{(b)} & w(\xi,t) \to 0 \quad \text{as } \xi \to \infty \text{ for } t > 0 \end{array} . \tag{7.11}$$

With Equation (7.10) and new length scale $\xi = \dfrac{x-\sigma(t)}{x^*}$, Equation (3.6) (the heat equation) and Equation (7.9) (a convective and a conductive flux boundary condition with the bounce effect) become

$$\begin{aligned}
&\text{(a)}\quad \frac{\partial w}{\partial t} = \frac{\kappa}{(x^*)^2}\frac{\partial^2 w}{\partial \xi^2} + \frac{1}{x^*}\frac{d\sigma}{dt}\frac{\partial w}{\partial \xi}, \qquad 0<\xi<1, t>0 \\
&\text{(b)}\quad -\left.\frac{\partial w}{\partial \xi}\right|_{\xi=\sigma} = \frac{x^*}{k(T_m - T_a)}\begin{pmatrix} m(t)\left(\rho\ell\dot{\sigma} - Q(t)\right) \\ +h(1-m(t))(T_m - T_a)(w(\sigma,y,t) - \phi_3(\sigma,t)) \end{pmatrix}. \qquad (7.12) \\
&(c)\quad w(1,t) = 0
\end{aligned}$$

The next section develops a numerical finite difference scheme for Equation (7.12).

7.4 Numerical Model Development for One Dimensional Problem

With the numerical approach, let $\Delta\xi = \dfrac{1}{N}$ where N is the number of partitions taken for depth. Define $\xi_i = \Delta\xi(i-1)$ and $v_i(t) = w(\xi_i, t)$, $i = 1, \cdots, N+1$. Using a second-order difference approximation for the spatial derivatives and the temperature above the top of the slipper setting as the ambient temperature $v_{N+1}(t) = 0$, Equations (7.12a) and (7.12b) become

$$\begin{aligned}
&\text{(a)}\quad \dot{v}_i(t) = \frac{\kappa(v_{i+1}(t) - 2v_i(t) + v_{i-1}(t))}{\Delta\xi^2 (x^*)^2} + \frac{\dot{\sigma}(t)}{x^*}\frac{v_{i+1}(t) - v_{i-1}(t)}{2\Delta\xi} + O(\Delta\xi^2) \\
&\qquad\qquad \text{for } i = 1, 2, \cdots N \qquad . \qquad (7.13) \\
&\text{(b)}\quad v_0(t) = \frac{2x^*\Delta\xi m(t)}{k(T_m - T_a)}\left(Q(t) - \rho\ell\dot{\sigma}\right) + \frac{2x^*\Delta\xi h(1-m(t))}{k}(v_1(t) - \phi_3(t)) + O(\Delta\xi^2) \\
&(c)\quad v_{N+1}(t) = 0
\end{aligned}$$

Appendix A.9 shows the calculation of Equations (7.13a) and (7.13b). For simplicity, let $\alpha = \frac{\kappa}{(x^*)^2 \Delta\xi^2}$ and $\beta(t) = \frac{\dot{\sigma}(t)}{2x^* \Delta\xi}$. Note that $\beta(t)$ is a function of time. Then for $i = 1, 2, \cdots, N-1, N$,

$$
\begin{aligned}
\dot{v}_1(t) &= v_1(t)\left[-2\alpha + (\alpha - \beta(t))\left(\frac{2x^*\Delta\xi h(1-m(t))}{k}\right)\right] + 2\alpha v_2(t) \\
&\quad + (\alpha - \beta(t))\left(\frac{2x^*\Delta\xi}{k(T_m - T_a)}\right)\left[m(t)(Q(t) - \rho\ell\dot{\sigma}) + h(1-m(t))(T_a - T_m)(v_1(t) - \phi_3(t))\right] \\
\dot{v}_2(t) &= (\alpha - \beta(t))v_1(t) - 2\alpha v_2(t) + (\alpha + \beta(t))v_3(t) \qquad . \quad (7.14) \\
&\vdots \\
\dot{v}_N(t) &= (\alpha - \beta(t))v_{N-1}(t) - 2\alpha v_N(t)
\end{aligned}
$$

The matrix form of Equation (7.14) is

$$\dot{\mathbf{v}}(t) = \mathbf{A}(t)\mathbf{v}(t) + \mathbf{f} \qquad (7.15)$$

where $\mathbf{f} = (1, 0, \cdots 0)^T \left[\frac{2x^*\Delta\xi}{k(T_m - T_a)}(\alpha - \beta(t))m(t)\left(Q(t) - \rho\ell\dot{\sigma}\right) + h(1-m(t))(T_a - T_m)(v_1(t) - \phi_3(t))\right]$,

$\mathbf{v}(t) = (v_1(t), \cdots v_N(t))^T$ and

$$\mathbf{A}(t) = \begin{bmatrix} -2\alpha & 2\alpha & 0 & \cdots & \cdots & 0 \\ \alpha - \beta(t) & -2\alpha & \alpha + \beta(t) & \cdots & \cdots & 0 \\ 0 & \alpha - \beta(t) & -2\alpha & \alpha + \beta(t) & \cdots & 0 \\ \vdots & \ddots & \ddots & \ddots & \vdots & \vdots \\ \vdots & \cdots & 0 & \alpha - \beta(t) & -2\alpha & \alpha + \beta(t) \\ 0 & \cdots & \cdots & 0 & \alpha - \beta(t) & -2\alpha \end{bmatrix}.$$

To solve the matrix $\dot{\mathbf{v}}(t) = \mathbf{A}(t)\mathbf{v}(t) + \mathbf{f}$ using the forward difference time marching scheme, that is, replace $\dot{\mathbf{v}}(t)$ with $\frac{\mathbf{v}^{n+1} - \mathbf{v}^n}{\Delta t_n}$ where the superscript represents the time step number, i.e. $\mathbf{v}^n = \mathbf{v}(t_n)$ and $\Delta t_n = t_{n+1} - t_n$. In the finite difference approximation, Equation (7.15) becomes

$$\mathbf{v}^{n+1} = (\mathbf{I} + \Delta t_n \mathbf{A}(t_n))\mathbf{v}^n + \Delta t_n \mathbf{f}^n \tag{7.16}$$

with the initial condition $\mathbf{v}_i^{\,0} = w(\xi_i, 0)$.,i.e. the i^{th} component of the vector $\mathbf{v}^0$ at $t = 0$. Because $\dot{\sigma}(t_n)$ is unknown at each time step, $\beta(t_n)$ is also unknown. To mitigate this difficulty, Equation (7.16) must be solved iteratively. The steps to find the values for $\beta(t_n)$ are as follows.

First, set $\beta(t_n) = \beta(t_{n-1})$. Since $\beta(t)$ is defined as $\frac{\dot{\sigma}(t)}{2x^* \Delta\xi}$ in Equation (7.14) and no melt layer is created initially, we take $\beta(t_0) = 0$. $\mathbf{v}_1^{N+1}$ represents the first component of the vector $\mathbf{v}^{N+1}$, the temperature distribution at the contact surface boundary at $(N+1)^{th}$ time step, for $v_i(t) = w(\xi_i, t)$, $i = 1, \cdots, N+1$. If $\mathbf{v}_1^{n+1} > 1$, then the temperature at the boundary has exceed the melt temperature, the melt front boundary condition $w(0,t) = 1$ for $t > t_m$, and Equation (7.11a) is not satisfied. Thus, $\beta(t_n)$ must be corrected such that $v_i^{n+1} \geq 1$ and $v_{i+1}^{n+1} < 1$. The new approximation for $\beta(t_n)$ is determined by

$$\beta(t_n) = \frac{(i+1)\mathbf{v}_i^{n+1} - i\mathbf{v}_{i+1}^{n+1} - 1}{2x^* \Delta t_n (\mathbf{v}_i^{n+1} - \mathbf{v}_{i+1}^{n+1})} \ . \tag{7.17}$$

Now solve Equation (7.16), the corrected value for $\beta(t_n)$, in both **A** and **f** and continue this process until $\mathbf{v}_1^{n+1}$ is sufficiently close to 1. Once the converged value of Equation (7.17) is determined $\sigma(t_n)$ is found as

$$\sigma(t_n) = 2x^* \Delta\xi \Delta t_n \beta(t_n) \ . \tag{7.18}$$

Before illustrating the results of Equation (7.18) the properties of the slipper and rail as well as the DADS data are examined. The slipper begins at rest and is accelerated down the rail with a velocity profile described by the Dynamic Analysis Data System (DADS) data for the rocket sled test event. The measured contact pressures along with the velocity are used to determine the bounce influence and calculate the slipper's partitioned frictional heat energy at each time step. The next chapter presents the results using Equation (7.18) to calculate the wear percentage for the current application problem, the Holloman High Speed Test Track Wear Project with their physical and material properties.

At the Holloman High Speed Test Track, significant research has been conducted in the area of high-energy impact creating gouging at the interface of a slipper/rail boundary brought about by contact of the test sled on the track. Table 1 shows the physical properties of slipper (VascoMax 300 maraging steel) and rail (AISI 1080 Carbon Steel) materials. In Table 1, the rail and the slipper's thermal conductivity and diffusivity values are given. Using Equation (3.32), it is expected that 48.8% of the total frictional heat flux flows into slipper when the sled is not moving and just in contact, i.e.

$$\alpha(t)=\frac{\beta}{1+\beta}=0.487885 \quad \text{as} \quad v(t)\to 0 \quad \text{and} \quad \beta=\frac{k^s}{k^r}\sqrt{\frac{\kappa^r}{\kappa^s}}=0.9527 \quad . \qquad (7.19)$$

Graphs (a) and (b) in Figure 29 represent sled velocity profile and pressure profile of HHSTT.

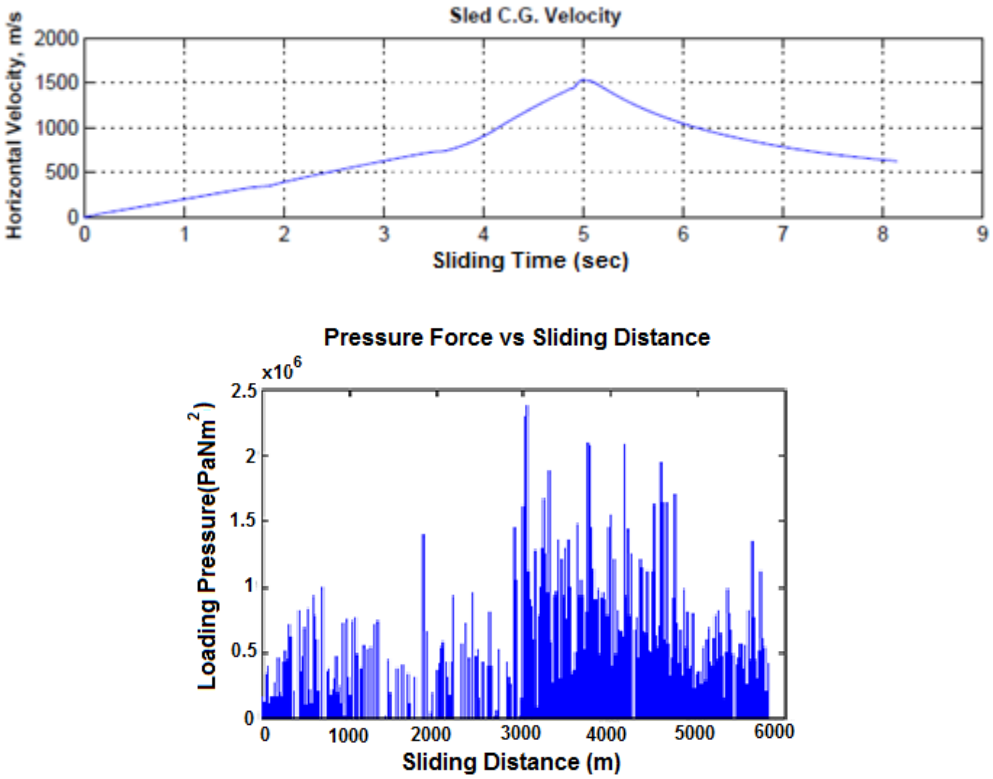

Figure 29. (a) Sled's Sliding Velocity, (b) Loading Pressure of the Wear Project (1)

Graph (a) in Figure 29, sled's velocity profile, shows that it accelerates for 5 seconds then steadily decelerates. The experiment is a three stage burn with the sled's speed increasing at a constant rate, (accelerating linearly) during each burn and leveling off as the empty stage is severed before the ignition of the next stage. With the reduced mass of the sled after each burn-out the overall effect is three increases in the slope of the time-velocity plot giving the illusion of

steadily increasing acceleration. On closer examination it is evident that it is nearly linear during a given burn. Bounce effects (chatter) become pronounced after third stage burnout due to aerodynamic effects or the loss of thrust torque. Either way, bounce effects are the result of slipper wear that occurred earlier but was not a significant factor until burnout changed forces acting on the sled (directly or indirectly). From Graph (b) in Figure 29, the loading pressure values increase substantially after passing 3000 m. In Equation (3.1), the frictional heat energy is defined as $Q(t) = \mu\alpha Pv(t)$. Since the loading pressure gets greater from the sliding distance 3000 m or sliding time 5 seconds, it is expected to generate greater frictional heat energy and to raise the slipper's surface temperature. Moreover, it significantly influences the slipper's melt layer process.

In Section 7.5, the first sub-section shows the results using different constant frictional heat partition fraction values, the second sub-section using the hypothesized frictional heat partition fraction function, and the last sub-section using the analytical solution of frictional heat partition fraction function developed in Chapter 3.

7.5 Numerical Results and Analysis

Wear is a three-dimensional phenomenon. To apply the dimensional results to this three dimensional problem, a simplifying assumption is made such that

$$\text{Melt Wear} = \int_{t_m}^{t} A(t)\frac{d\sigma}{dt}dt \ . \tag{7.20}$$

The melt depth is defined as the distance $\sigma(t)$ that the melt front moves during the sliding time and *A(t)* is the melt region. The melt wear volume was defined in section 3.1. Here the melt wear percentage is defined as

$$\text{melt wear percentage} = \frac{\text{melt wear volume}}{\text{slipper's volume}} \times 100 \ . \qquad (7.21)$$

Therefore, the melt wear percentage means the melt wear volume per slipper's total volume not the total wear volume. If the material does not reach the melt temperature then the melt layer does not yet exist and the melt front does not move.

In this chapter, the numerical data with different frictional heat partitioning scenarios is compared and discussed. Dynamics data, sled velocity, and loading pressure of the third state pusher sled for the 2008 HHSTT test mission is used to calculate the melt wear percentage. The first scenario for calculating the slipper's melt wear percentage uses three different heat partition fraction values for the slipper. The second scenario uses the hypothesized heat partition function. The last scenario uses the analytical solution of slipper's heat partition function developed in Chapter 3. For the first and second scenarios, the constant sled velocity function $v(t) = 10 \text{ m/sec}$ is used to compare the melt wear percentage result with the result of the third scenario with $(t) = 10 \text{ m/sec}$.

7.5.1 Calculating Melt Wear Percentage With Different Constant Values of α(t)

When the sled slides along the rail at high speed, it creates dynamic behaviors, of chief interest is the bounce effect. While two sliding surfaces of slipper and rail are separated, a

convective heat flow exists in the gap between the slipper and rail. Otherwise, the frictional heat flows from one body to the other body via conductive heat flux.

In Figure 29, the values of *Force* (Graph b) imported from DADS data determine whether the surfaces are in contact. Due to high velocity and loading pressure, a large amount of frictional heat energy is generated by Equation (3.1), $q(t) = \mu P(t)v(t)$. The surface temperature of the slipper will eventually reach the melting temperature.

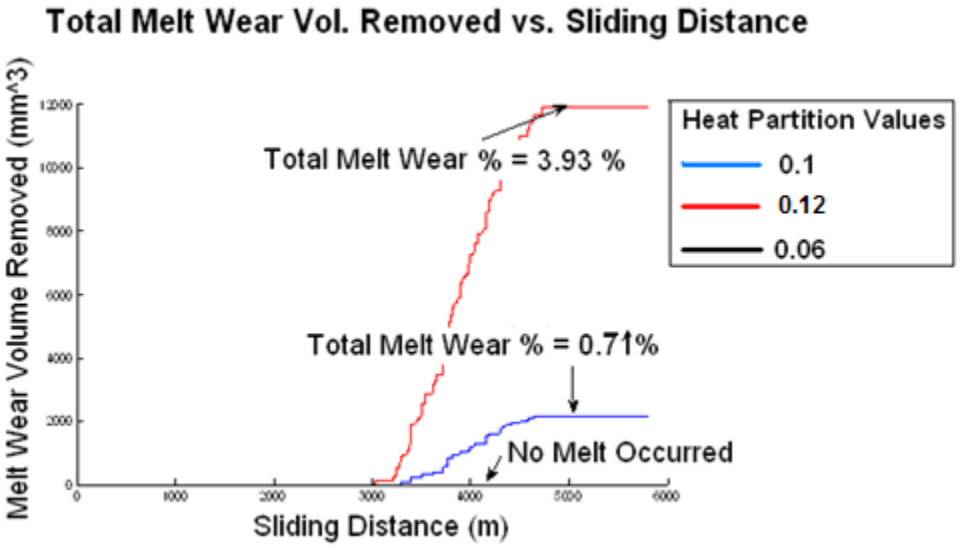

Figure 30. Melt Volume Removed for Different Heat Partition Values with Bounce

Figure 30 shows the process of melt layer removal with three different constant heat partition values for the slipper while sliding with bounce effects. Frictional heat generated during while sliding raises the slipper surface temperature. The melt layer created at the contact surface of slipper is removed immediately.

When the sled travels 3000+ *m*, slippers with constant heat partitioning values of 0.1 and 0.12 yield a melt layer. The sled's sliding velocity decreases but the loading pressure increases when the sled reaches approximately 3000 m as observed in Figure 29. This impact loading

pressure creates greater frictional heat energy which is then absorbed by the slipper and rail. With the slipper's constant heat partition value of 0.06, only 6% of total frictional heat energy flows into the slipper. The slipper's surface temperature never reaches the melt temperature and the melt layer is never created. So the slipper's melt wear percentage remains zero. However, when the slipper's constant heat partitioning values are assumed 0.1 and 0.12, i.e. 10% and 12% of total frictional heat energy flows into the slipper, 0.71% and 3.93% melt wear of total slipper's volume is observed. This illustrates a key point: a slight increase in slipper's heat partition fraction value makes a great difference in the melt wear.

Another observation of Figure 30 is the monotonic-step increase of graphs due to bounce effect. The loading pressure profile graph in Figure 29 shows that the pressure value is positive when two surfaces are in contact and zero when they are not in contact. When the slipper and rail are in contact, frictional heat is generated and creates the melt layer. However, when they are not in contact, the fraction does not apply and no heat flows into slipper which delays the melting process at the contact surface. This physical process creates the monotone-step increase behavior of graphs, which is shown in Figure 30.

7.5.2 Calculating Melt Wear Percentage With Hypothesized Function α(t)

With the consideration of few characteristics to determine the slipper's frictional heat partitioning function discussed in Chapter 3, it is hypothesized as a function of time $\alpha(t) = 0.4e^{-5t^2} + 0.1$. Because of the bounce effect, frictional heat energy is generated when in contact raising the slipper's surface temperature. However, the bounce effect produces

aerodynamic air flow between the slipper and rail surfaces (when not in contact) and the slipper's surface may lose heat energy thereby decreasing the surface temperature. As such, the slipper's surface temperature increases for $P(t) > 0$ and decreases for $P(t) \le 0$.

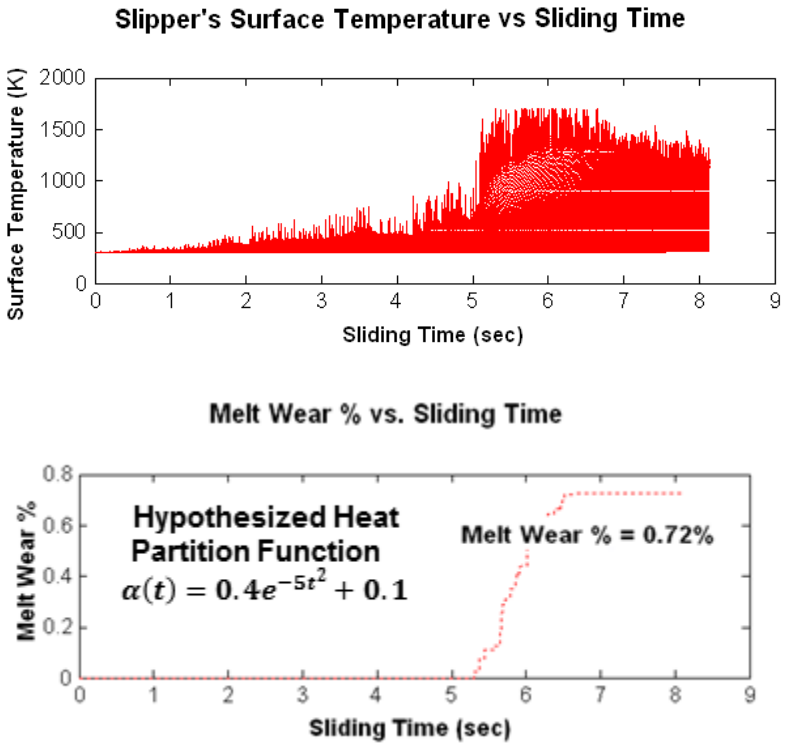

Figure 31. (a) Slipper's Surface Temperature, (b) Melt Wear % vs Sliding Time using $\alpha(t) = 0.4e^{-5t^2} + 0.1$

In Figure 31, Graphs (a) and (b) show the slipper's surface temperature change and its melt wear percentage using a hypothesized function $\alpha(t) = 0.4e^{-5t^2} + 0.1$ and bounce effect. During the first 5 seconds, the slipper's surface temperature increases and it behaves as a step-wise function due to bounce effect. Since the frictional heat flux is determined by Equation (3.1) and the difference in loading pressure is much greater than the difference in velocity change ($P(t) = k_P \times 10^6$ and $v(t) = k_v \times 10^3$ for $0 < k_p, k_v < 10$), greater frictional heat energy flows into

the slipper. Accordingly, it raises the slipper's surface temperature to melting temperature. The melt wear percentage graph shows that the slipper's surface undergoes melt layer formation after 5 seconds. The slipper's surface temperature never exceeds the melt temperature because the melt layer is removed immediately and continuously.

With a hypothesized heat partition fraction function $\alpha(t) = 0.4e^{-5t^2} + 0.1$ and bounce effect, the total melt wear percentage of the slipper's volume is 0.72%.

7.5.3 Calculating Melt Wear Percentage With Analytical Solution α(t)

The analytical solution of the heat partition function is developed in Section 3.2 and defined in Equation (3.40),

$$\alpha(t) = \frac{1}{\pi}\int_0^{\infty} e^{-\frac{v_0}{2}tr} \frac{\beta^* \sqrt{r}\tilde{F}(-r)}{r(1+(\beta^*)^2 r(\tilde{F}(-r))^2)} dr \tag{7.22}$$

where $\tilde{F}(-r) = e^r \sum_{k=0}^{\infty} (k+1)\frac{2^{2k+3}(k+1)!}{(2k+3)!}(-r)^k$, $\beta^* = \frac{\beta}{\sqrt{\pi}} = \frac{k^s}{k^r}\sqrt{\frac{\kappa^r}{\pi\kappa^s}}$ the relation of thermal properties of slipper and rail and v_0 the dimensionless constant velocity $\overline{v}(\tau) = \frac{t^*}{l} v(t^*\tau) = v_0$.

This analytical solution is derived with some assumptions. The velocity and loading pressure profiles are uniform along the contact surface and constant during the sliding time, i.e. the sled moves at the same speed from the beginning to end and the slipper and rail are continually in contact all the time. The program calculating slipper melt wear percentage considers the various velocity profiles and loading pressure profiles as a function of time. With physical and material

properties of slipper and rail listed in Table 1, the program's results for the frictional heat partition function are given below.

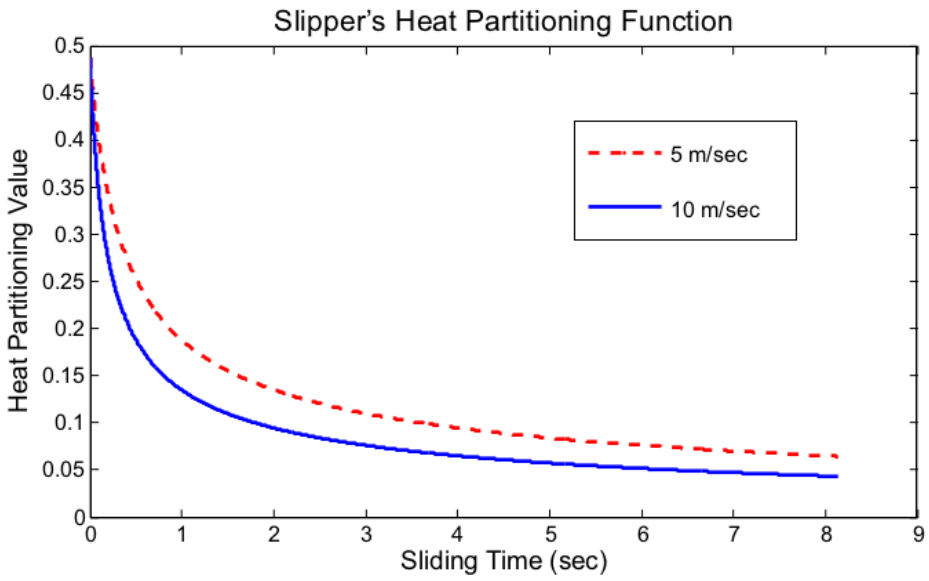

Figure 32. Graphs of Slipper's Heat Partitioning Values at v(t)=5 and 10 m/sec

From Figure 25 in Section 7.1, the fraction of frictional heat energy flowing into a slipper diminishes with higher velocities. Figure 32 shows the same behavior. Looking at the 1.5 second mark, the slipper's heat partitioning value for the velocity $v(t) = 10$ m/sec is 0.1171 while the slipper's heat partitioning value at the velocity $v(t) = 5$ m/sec is 0.1650. To be clear: the faster the sled, the smaller the fraction of heat generated flowing into the shoe. However, the total frictional heat generated by a sled traveling at the velocity $v(t) = 10$ m/sec is twice that of one traveling velocity $(t) = 5$ m/sec . This is observed in the heat flux equation defined in Equation (0.47) as $q(t) = \mu P(t)v(t)$, i.e.

$$\begin{aligned} 10\mu P(t) &\geq 5\mu P(t) \quad \text{for all } 0 \leq t \leq \text{total sliding time} \\ q_{v(t)=10}(t) &\geq q_{v(t)=5}(t) \end{aligned} \quad . \qquad (7.23)$$

The inequality in Equation (7.23) is the comparison of frictional heat flux for two different velocity profiles, $v(t) = 10$ m/sec and $(t) = 5$ m/sec . With the result in Equation (7.23), the numerical results of slipper's surface temperature and melt wear percentage for both constant velocity values are generated and presented in Figure 33.

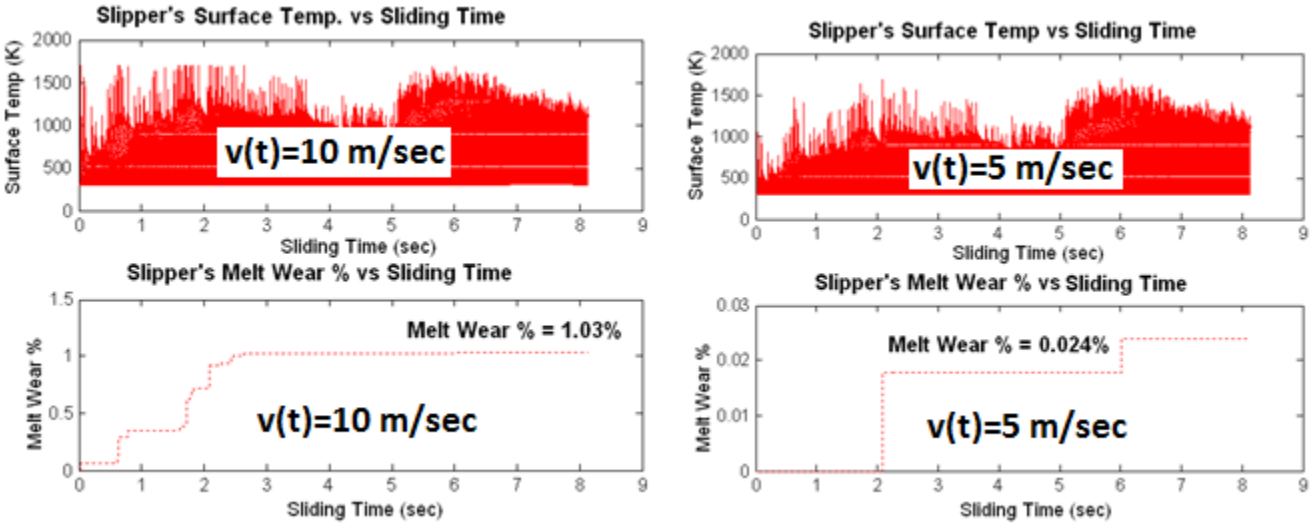

(a) (b)

Figure 33. Surface Temperature and Melt Wear % vs Sliding Time

Even though the slipper's heat partitioning function at $v(t) = 10$ m/sec is smaller than at $(t) = 5$ m/sec , Equation (7.23) shows that the sled generates frictional heat $q_{v(t)=10}(t)$ at $v(t) = 10\ m/\sec$ twice that generated $q_{v(t)=5}(t)$ at $v(t) = 5$ m/sec . This implies that the amount of heat flowing into the slipper at $v(t) = 10$ m/sec is greater than at $(t) = 5$ m/sec . For example, Figure 32 shows that at 0.1 second, 11.71% of the total frictional heat energy with the

velocity $v(t) = 10$ m/sec flows into the slipper while 16.50% of the total frictional heat energy with the velocity $v(t) = 5$ m/sec flows into the slipper, i.e.

$$\begin{gathered} q_{v(t)=10}(1.5) = 10\alpha_{v(t)=10}\mu P(1.5) = 1.171\mu P(1.5) \\ q_{v(t)=5}(1.5) = 5\alpha_{v(t)=5}\mu P(1.5) = 0.825\mu P(1.5) \\ \therefore q_{v(t)=10}(1.5) \geq q_{v(t)=5}(1.5) \end{gathered} \tag{7.24}$$

The inequality in Equation (7.24) supports the numerical results in Figure 33. The two graphs of slipper surface temperature at $v(t) = 10\ m/\sec$ and $v(t) = 5\ m/sec$ represent surface temperature changes over the sliding time based on the loading pressure profile and velocity. Since more heat energy flows into the slipper at a sliding velocity of 10 m/sec ($v(t) = 10\ m/\sec$), the slipper's surface temperature reaches melting temperature near instantaneously creating a melt layer. However, if the sled moves at $v(t) = 5\ m/sec$, the surface temperature achieves melt temperature in just over 2 seconds as illustrated in Figure 33. The loading pressure profile in Figure 29, shows that pressure values decrease after the sled travels the first 1000 m and increase significantly when it hits the 3000 m mark (3rd stage rocket burnout). This effects the amount of frictional heat energy defined in Equation (3.1) as $q(t) = \mu P(t)v(t)$.

The surface temperatures for both velocity cases decrease after 1-2 seconds when the sled crosses the 1000 m mark and increase again after 5 seconds upon crossing the 3000 m mark. We find the melt wear percentage graph in Figure 33 (a) ($v(t) = 10\ m/\sec$), which has monotonic stepwise increases, i.e. the melt layer is a transient phenomena under experimentally measured loading conditions. Figure 33 (b), the melt wear percentage graph at $(t) = 5$ m/sec, shows stepwise behavior again. (Note *y* axis scale differences on these plots.) A melt layer is created

briefly at around the 2 second mark and no melt layer is observed from 2 seconds to 6 seconds because the loading pressure decreases during this time period and the frictional heat energy is insufficient to raise the slipper's surface temperature above the melting point. After the loading pressure increases again, sufficient frictional heat energy is produced to raise the surface temperature and create a melt layer. At the end of sliding event, the slipper's total melt wear percentage with the analytical solution and experimental loads at $v(t) = 10\ m/\sec$ is 1.03% while at $v(t) = 5\ \mathrm{m/sec}$ the loss is 0.024%. In Figure 31, the values of melt wear percentage with constant heat partition fractions $\alpha(t) = 0.12$ and $\alpha(t) = 0.06$ are 3.93% and 0%. This shows that the results of analytical solutions lie between the results of two constant heat partition fraction function cases. This implies that if a simple and constant heat partition fraction value is needed, it is reasonable to say that 0.06 and 0.12 may be the lower and upper bound respectivly of the constant heat partition fraction value.

7.6 Conclusion and Further Study

The primary objective of this research was to develop an analytical solution for frictional heat partitioning. Two-dimensional conductive heat transfer partial differential equations were employed to find the surface temperature distributions of the slipper and rail with Green's functions. Using Jaeger's method, the slipper and rail surface temperature distributions were averaged and surface temperatures matched. After applying the Laplace Transform and using the Incomplete Gamma Function, the slipper's frictional heat partitioning solution was developed in integral form. Since the slipper's frictional heat partitioning solution for the two-dimensional

heat transfer problem was valid for the pre-melt state, the slipper's pre-melt problem was formulated and then the melt time formula of the pre-melt problem was found. Numerical methods yielded the slipper's frictional heat partitioning analytical function with varying parameters, such as velocity profile and thermal properties. This results of the analytical solution closely matches Komanduri and Hou's (32) discovery of the non-uniform distribution of the heat partition function using a curve-fit analysis approach with compensation terms discussed and presented in Section 1.6.2.

The second objective of this research was to develop a numerical scheme for the two dimensional convection diffusion problem using ADI method and Strang's Splitting method. With the numerical method, both internal and surface temperature distributions of slipper and rail were evaluated and the heat partitioning fraction calculated by matching the averaged surface temperature of two sliding materials. Finally the numerical solution was compared with the analytical solution in Section 6.1. The observations from Figure 24, two graphs closely approximate each other and both solutions represent the qualitative behavior of the heat partitioning values indicating that the analytical and numerical solutions are good representations of the slipper's heat partitioning function.

The last objective of this research was to produce the melt wear percentage for the present application: the Holloman High Speed Test Track slipper wear problem. In the problem, the sled's velocity is assumed to be constant at the maximum speed during the sliding time. Using the analytical solution of slipper's heat partitioning function, the slipper's melt wear percentage was evaluated and presented in section 7.5.3.

Due to practical computational limits the numerical analysis was used to find the slipper's heat partitioning values for velocity below 10 m/sec, and the analytical solution was used for velocities above 10 m/sec. For velocities above 100 m/sec, excessive memory is required forcing alternative approaches either mathematically or computationally. Daoud S. Daoud (58) encountered this problem and presented a new splitting approach for the numerical solution of the multi-dimensional convection diffusion equations. His method combines additive and multiplicative splitting. The method not only reduces the linear (or nonlinear) original problem into a series of one-dimensional and one physical operator linear problems, but also enables computation of one-dimensional problems using parallel processors.(58) This could render the numerical calculation practical, enabling the code to evaluate the heat partitioning function at a higher velocity. Studying Daoud's method and developing a different numerical analysis using additive and multiplicative splitting is the next step to overcome the technical issues for velocity above 100 m/sec.

Previous research (1) assumed constant contact and constant partitioning between slipper and rail for the entire experiment in analytical and computational work. The analytical frictional heat partitioning function in this dissertation considers the physical parameters affecting the slipper's heat partitioning value. There are three factors; (a) motion of slipper (slipper moving into cooler region of rail), (b) pressure profile and material properties, and (c) varying velocity. With these considerations this research hypothesized the physics-based frictional heat partitioning function. Using partial differential equations the analytical solution was developed with numerical methods, such as Strang's Splitting method, Crank-Nicolson method and implicit numerical scheme. The switch function was adopted to apply bounce effects to the numerical

model. When the slipper is in contact, the conductive heat transfer is used with the actual value of loading pressure. When the slipper is not in contact convective heat loss is considered.

The numerical solution to the slipper's frictional heat partitioning function represents the real nature of changes over time in a sliding system. The slipper's averaged surface temperature rises when in contact with high loading pressure and drops when the slipper is no longer in contact due to convective heat loss. It also shows that the total melt wear volume percentage increases when the slipper is in contact and remains constant when the slipper is not in contact.

The improved model using real HHSTT experimental data of loading pressure produces a more realistic demonstration of how the average surface temperature and total melt wear volume percentage evolves over time. Since the analytical solution of the slipper's frictional heat partitioning function implements physics based behavior rather than assuming a uniform constant value, the calculation of the slipper's surface temperature and total melt wear volume percentage better approximates the behavior of HHSTT experiments.

Appendix

A.1 Development of Green's Function Solution to Differential Equation of Heat Conduction

This appendix shows the derivation of the Green's function solution to Differential equation of heat conduction, Equations (2.14)-(2.16), Section 2.5. Let's consider the part of the solid bounded by an imaginary cylinder of cross-section *A* whose axis is normal to the surface of the plate. When the steady state of temperature has been reached, the quantity *q* of heat which flows up through the plate in *t* seconds over the surface *S* is equal to below

$$\frac{k(T_{lower} - T_{upper})At}{d}, \tag{10.1}$$

where *k* is defined as the thermal conductivity and T_{lower}, T_{upper}, d are the temperature of the lower surface and of the upper surface, and the thickness of the plate. Generally speaking, the thermal conductivity of the substance is a constant depending upon the material of which it is made. In other words, the flow of heat between these two surfaces is proportional to the difference of temperature of the surfaces. But, in experiments, the conductivity *k* is not constant for the same substance because it depends upon the temperature. However, the micro-scale of rubbing surfaces is of interest, so the range of temperature is limited and this change in *k* may be neglected. Therefore, in the general mathematical expression of heat conduction it is assumed that the conductivity does not vary with the temperature. (In a real application or experiment, the thermal conductivity *k* is a function of velocity and specific heat.)

In the fundamental experiment, which was used to define the thermal conductivity above, the solid is supposed to be homogeneous and of such a material that, when a point within it is heated, the heat spreads out equally well in all directions. Such a solid is said to be isotropic, that is a material whose structure and properties in the neighborhood of any point are the same relative to all directions through the point. The rate of flow of heat per unit time per unit area in the direction of *x* increasing is

$$-k\frac{\delta T}{\delta x} \;\rightarrow\; f_x = -k\frac{\partial T}{\partial x} \quad \text{as} \;\; \delta x \rightarrow 0 \; . \tag{10.2}$$

Consider the case of a solid through which heat is flowing, but within which no heat is generated. Then, the mathematical equation for the heat conduction of a homogeneous isotropic solid whose thermal conductivity is independent of the temperature is

$$\frac{\partial^2 T}{\partial x^2}+\frac{\partial^2 T}{\partial y^2}+\frac{\partial^2 T}{\partial z^2}-\frac{\rho c}{k}\frac{\partial T}{\partial t}=0 \;\rightarrow\; \kappa\left(\frac{\partial^2 T}{\partial x^2}+\frac{\partial^2 T}{\partial y^2}+\frac{\partial^2 T}{\partial z^2}\right)=\frac{\partial T}{\partial t} \; . \tag{10.3}$$

where ρ, c are the density and the specific heat, and κ is a constant called the thermal diffusivity, defined as $\kappa = \dfrac{k}{\rho c}$.

In the article *A Problem In The Theory of Heat Conduction*(2), the idea of a finite quantity of heat instantaneously liberated at a given point and time in an infinite solid has been well developed and showed the advantage of solving a large number of important physical problems to be written down from first principles. The solution for Equation (10.3) the instantaneous point source in three dimensions (Green's function) is

$$T(x,y,z,t;x',y',z') = \frac{q(t)}{8(\pi\kappa t)^{3/2}} e^{-[(x-x')^2+(y-y')^2+(z-z')^2]/4\kappa t} \qquad \text{point source in 3-D} \quad (10.4)$$

where *q(t)* is a heat flux at a point (x', y', z'). Integrating Equation (10.4) with respect to the time produces the solution for the continuous point source, and integrating the solutions for point sources with regard to appropriate space variables gives solutions for instantaneous line, plane, and spherical surface sources.

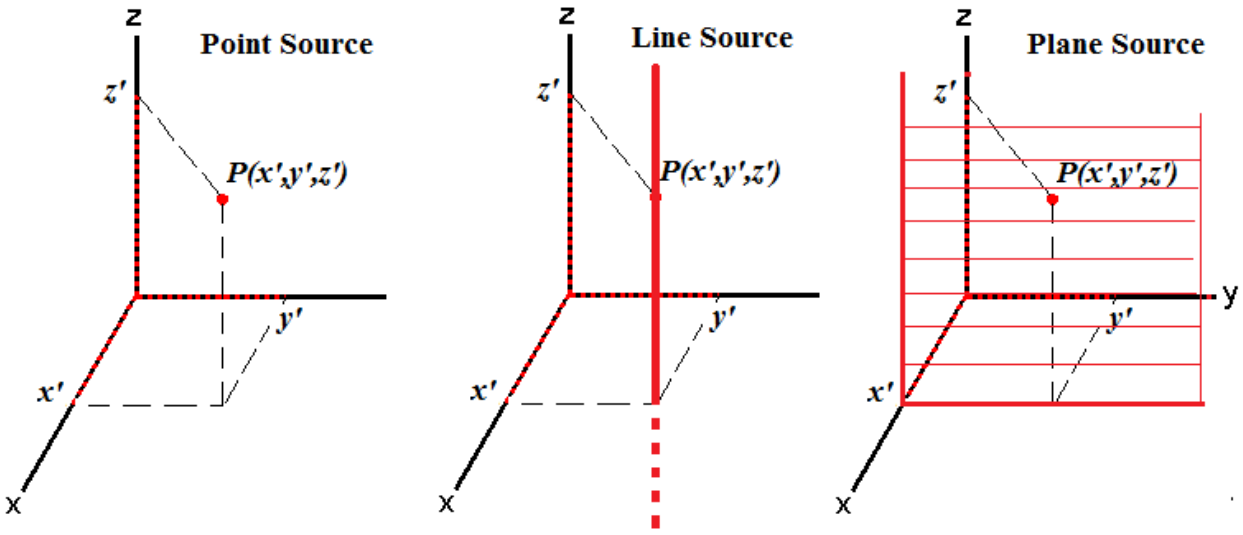

Figure 34. Different Heat Source in 3D Cartesian Coordinate System

Let's consider a distribution of instantaneous point sources, heat flux $q(t)$ in Equation (10.4). The line source is parallel to the *z*-axis and passing through the point (x', y'). The rate of heat input is $q(t)dz'$ at z' along the *z*-axis. Integrating Equation (10.4) with respect to space variable *z* gives the temperature distribution for instantaneous line source in the *x*, *y* plane $(z = 0)$,

$$T(x,y,0,t;x',y',z') = \frac{q(t)}{8(\pi\kappa t)^{3/2}}\int_{-\infty}^{\infty} dz' e^{-\{(x-x')^2+(y-y')^2+(0-z')^2\}/4\kappa t}$$
$$= \frac{q(t)}{4\pi\kappa t} e^{-\{(x-x')^2+(y-y')^2\}/4\kappa t} \qquad \text{line source in 2-D} \qquad .(10.5)$$

By integrating Equation (10.5) with respect to the space variable *y* becomes the temperature distribution of instantaneous plane source, parallel to the plane $x = 0$ at $y = 0$,

$$T(x,0,t;x') = \int_{-\infty}^{\infty} \frac{q(t)}{4\pi\kappa t} e^{-\{(x-x')^2+(0-y')^2\}/4\kappa t} dy'$$
$$= \frac{q(t)}{2\sqrt{\pi\kappa t}} e^{-(x-x')^2/4\kappa t} \qquad \text{plane source 1-D} \qquad . \qquad (10.6)$$

Let's consider a temperature distribution, Equation (10.4), of instantaneous point sources of heat flux $q(t)$. Since integrating Equation (10.4) with respect to time *t* produces the solution for the continuous point source, the temperature distribution for continuous point source is

$$T(x,y,z,t;x',y',z',t') = \int_0^t \frac{q(t')}{8(\pi\kappa(t-t'))^{3/2}} e^{-[(x-x')^2+(y-y')^2+(z-z')^2]/4\kappa(t-t')} dt' \; . \qquad (10.7)$$

Integrating Equation (10.6) with respect to time *t* produces the temperature distribution of continuous plane source, parallel to the plane $x = 0$

$$T(x,t;x') = \int_0^t \frac{q(t')}{2\sqrt{\pi\kappa(t-t')}} e^{-(x-x')^2/4\kappa(t-t')} dt' \; . \qquad (10.8)$$

Steps from Equation (10.4) to Equation (10.8) suggest that it is possible to reduce the three-dimensional heat conduction problem due to friction to component two or one dimensional problems and to express the heat source moment-to-moment as either a line or plane surface

source in steady-state conditions. Let's consider the heat line source liberated at the rate q' per unit time per unit length along the *y*-axis. It is moving parallel to the axis of *x* with a velocity *U*, then the temperature distribution in the steady state at the point *(x,y,z)* is given (21)

$$\begin{aligned} T &= \frac{q'}{4\pi k}\int_{-\infty}^{\infty}\frac{dy'}{\sqrt{x^2+y'^2+z^2}}e^{-U[\sqrt{x^2+y'^2+z^2}-x]/2\kappa} \\ &= \frac{q'}{2\pi k}e^{Ux/2\kappa}K_0[U\sqrt{x^2+z^2}/2\kappa] \end{aligned} \tag{10.9}$$

where $K_0(x)$ is the modified Bessel function of the second kind(3) of order zero.

A.2 Derivation of the Green's function solution for $w^r(\xi,\eta,\tau)$

This appendix shows the derivation of the solution to Equation (3.17), Section 3.2. Let's recall the rail's PDE system, Equation (3.7)

(a) $\rho^r c^r \dfrac{\partial T^r}{\partial t} = k^r \nabla^2 T^r$ for $t>0$, $|x_r| \le \infty$, $y<0$

(b) I.C. : $T^r(x_r, y, 0) = T_a$ for $|x_r| \le \infty$, $-\infty < y < 0$, $t = 0$

(c) B.C. : $T^r(x_r, y, t) \to T_a$ as $y \to -\infty$ or $|x_r| \to \infty$ (10.10)

(d) $$k^r \frac{\partial T^r}{\partial y}(x_r, 0, t) = \begin{cases} m(t)(1-\alpha(x_r+x(t),t))q(x_r+x(t),t) \\ \quad +(1-m(t))h_3(T^r(x_r+x(t),0,t)-T_3(x_r+x(t),t)) & \text{for } |x_r+x(t)|<l \\ h_4(T^r(x_r+x(t),0,t)-T_a) & \text{for } |x_r+x(t)|\ge l \end{cases}$$

where $T_3(x_r+x(t),t)$ and h_4 are defined as $T_3(x_r+x(t),t)-T_a = (T_m-T_a)\phi_3(\xi,\tau)$ and the thermal convective coefficient between the slipper and rail's sliding interface when not in contact. Using the Galilean coordinate transformation Equation (3.11),

$$T^r(x_r, y, t) = T^r(x_s - x(t), y, t) \ . \tag{10.11}$$

This leads to

$$\frac{\partial T^r}{\partial x_r} = \frac{\partial T^r}{\partial x_s} \quad \text{and} \quad \frac{\partial T^r}{\partial t} = -\frac{\partial T^r}{\partial x_s}\cdot\frac{\partial x}{\partial t} + \frac{\partial T^r}{\partial t} \tag{10.12}$$

Introducing the dimensionless variables used in the slipper equations (i.e. $\xi = \frac{x_s}{l}$, $\eta = \frac{y}{y^*}$ and $\tau = \frac{t}{t^*}$), then

$$\overline{v}(\tau) = \frac{t^*}{l} v(t^*\tau) = \frac{1}{l}\frac{dx}{dt}(t^*\tau) \ \text{ and } \ \overline{\xi}(\tau) = \int_0^\tau \overline{v}(\tau')d\tau' \ . \tag{10.13}$$

Along with $T^r(x_r, y, t) = T_a + (T_m - T_a)w^r(\xi, \eta, \tau)$, Equations (3.7a) are reduced to

$$\rho^r c^r (T_m - T_a)\left[\frac{\partial w^r}{\partial \tau}\frac{1}{t^*} - \frac{\partial w^r}{\partial \xi}\frac{v(t)}{l}\right] = k^r (T_m - T_a)\left[\frac{\partial^2 w^r}{\partial \xi^2}\frac{1}{l^2} + \frac{\partial^2 w^r}{\partial \eta^2}\frac{1}{(y^*)^2}\right]. \tag{10.14}$$

After multiplying this equation by $\frac{y^{*2}}{k^r(T_m - T_a)}$ and recalling $\kappa^r = \frac{k^r}{\rho^r C^r}$, Equation (3.12) is obtained. Continuing to simplify Equation (3.12) by replacing y^{*2} in the coefficient of the term $\frac{\partial w^r}{\partial \xi}$ with $y^{*2} = \kappa^s t^*$, results in

$$\frac{\kappa^s}{\kappa^r}\frac{\partial w^r}{\partial \tau} = \frac{\kappa^s}{\kappa^r}\frac{t^*}{l} v(t)\frac{\partial w^r}{\partial \xi} + \left(\frac{y^*}{l}\right)^2 \frac{\partial w^r}{\partial \xi^2} + \frac{\partial w^r}{\partial \eta^2} \ , \tag{10.15}$$

Equation (3.7 d) in Section 3.2 is the rail's boundary condition at the sliding contact surface. With the definition of $T_r(x_r + x(t), y, t) = T_a + (T_m - T_a)w^r(\xi, \eta, \tau)$ and the dimensionless variables defined in Section 3.2, this boundary condition becomes

$$\frac{\partial w^r}{\partial \eta}(\xi, 0, \tau) = \begin{cases} \dfrac{y^* h_4}{k^r} w^r(\xi, 0, \tau) & |\xi| > 1 \\ C^r m(1-\alpha(\xi,\tau))q(\xi,\tau) + \dfrac{y^* h_3}{k^r}(1-m)[w^r(\xi,0,\tau) - \phi_3(\xi,\tau)] & |\xi| < 1 \end{cases} \tag{10.16}$$

with $C^r = \dfrac{y^*}{k^r(T_m - T_a)}$. In general, the convective heat transfer coefficient for the forced air convection is in the range of 10-200 $\mathrm{W/m^2K}$. Using a typical value of h_i, say $h_i \approx 100$ $(i = 1, 2, 3, 4)$, and material properties given in Table 1, $\dfrac{y^* h_i}{k^r} \approx \dfrac{\sqrt{9 \cdot 10^{-6} \cdot 8} \cdot 100}{31} \approx 3 \cdot 10^{-2} = \mathcal{O}(\varepsilon)$. In Section 3.2, the value $\dfrac{y^*}{l} \equiv \varepsilon$ is very small so the influence of the terms with $\mathcal{O}(\varepsilon)$ is negligible. Therefore, with the consideration of neglecting term $\mathcal{O}(\varepsilon)$, this boundary condition is simplified to

$$\begin{aligned} \frac{\partial w^r}{\partial \eta}(\xi, 0, \tau) &= \begin{cases} 0 & |\xi| > 1 \\ C^r m(1-\alpha(\xi,\tau))q(\xi,\tau) & |\xi| < 1 \end{cases} \\ &= H(1-\xi^2)C^r(1-\alpha(\xi,\tau))q(\xi,\tau) \qquad |\xi| < \infty, \end{aligned} \tag{10.17}$$

where $H(\xi)$ is the Heaviside function. In this research, only the continuous contact is considered, $m = 1$. That is, it is assumed that the pressure is always positive. With Equations (3.14) and (10.17), the rail's PDE system becomes

$$Rail's\ PDE:\quad \frac{\partial w^r}{\partial \tau} = \bar{v}(\tau)\frac{\partial w^r}{\partial \xi} + \gamma\frac{\partial^2 w^r}{\partial \eta^2} \qquad |\xi| < \infty\,, \eta < 0\,, \tau > 0$$

$$I.C.:\quad w^r(\xi,\eta,0) = 0 \qquad |\xi| < \infty\,, \eta < 0 \tag{10.18}$$

$$B.C.: (a) w^r(\xi,\eta,\tau) \to 0 \qquad as \quad |\xi| \to \infty \quad or \quad \eta \to -\infty\,, \tau > 0$$

$$(b)\ \frac{\partial w^r}{\partial \eta}(\xi,0,\tau) = H(1-\xi^2)C^r\big(1-\alpha(\xi,\tau)\big)q(\xi,\tau) \quad |\xi| < \infty\,,\ \tau > 0$$

where $\bar{v}(t) \equiv \dfrac{v(t*\tau)t*}{l}$, $\gamma = \dfrac{\kappa^r}{\kappa^s}$ and $C^r = \dfrac{y*}{k^r(T_m - T_a)}$.

In order to reduce to one spatial variable, apply the complex Fourier Transform into $w^r(\xi,\eta,\tau)$ over $|\xi| < \infty$ (21), i.e.

$$\mathcal{F}[w^r(\xi,\eta,\tau)] = \widetilde{w^r}(p,\eta,\tau) = \tfrac{1}{\sqrt{2\pi}}\int_{-\infty}^{\infty} e^{ip\xi} w^r(\xi,\eta,\tau)d\xi \tag{10.19}$$

$$Inversion: \mathcal{F}^{-1}\big[\widetilde{w^r}\ (\xi,\eta,\tau)\big] = w^r(\xi,\eta,\tau) = \tfrac{1}{\sqrt{2\pi}}\int_{-\infty}^{\infty} e^{-ip\xi}\widetilde{w^r}(\xi,\eta,\tau)d\xi$$

First, consider the boundary condition (b) in Equation (10.18). In general, we shall define

$$\begin{aligned} Q(p,\tau) &= \frac{1}{\sqrt{2\pi}}\int_{-\infty}^{\infty} e^{ip\xi} H(1-\xi^2)C^r(1-\alpha(\xi,\tau))q(\xi,\tau)d\xi \\ &= \frac{1}{\sqrt{2\pi}}\int_{-1}^{1} e^{ip\xi} C^r(1-\alpha(\xi,\tau))q(\xi,\tau)d\xi \end{aligned} \tag{10.20}$$

Recall the frictional heat flux $q(\xi,\tau) = \mu P(\xi,\tau)v(\tau)$ given in Equation (4.24). Three conditions for $\alpha(\xi,\tau)$ and $P(\xi,\tau)$ will be considered for the effective heat flux. The frictional heat

partitioning function is uniform across the interface contact in ξ, the pressure profile is uniform across the interface contact in ξ, and both the frictional heat partitioning function and pressure profile are uniform across the interface contact in ξ. Using the definition of the frictional heat flux, the uniform pressure in ξ implies the uniform heat flux in ξ, i.e. $\mu P(\xi,\tau)v(\tau) = \mu P(\tau)v(\tau) = q(\tau)$. Next, let's examine the boundary condition (b) of Equation (10.18) for each of the cases in the complex Fourier Transform,

$$\mathcal{F}\left[w_\eta^r(\xi,0,\tau)\right] = \tilde{w}_\eta^r(p,0,\tau) = \frac{C^r}{\sqrt{2\pi}}\int_{-1}^{1} e^{ip\xi}\left(1-\alpha(\xi,\tau)\right)q(\xi,\tau)d\xi. \qquad (10.21)$$

First, consider the uniform frictional heat partitioning function across the interface contact in ξ, $\alpha(\xi,\tau) = \alpha(\tau)$, then

$$\begin{aligned}\tilde{w}_\eta^r(p,0,\tau) &= \frac{C^r}{\sqrt{2\pi}}[1-\alpha(\tau)]\underbrace{\int_{-1}^{1} e^{ip\xi}q(\xi,\tau)d\xi}_{=\sqrt{2\pi}\tilde{q}(p,\tau)} \\ &= C^r\tilde{q}(p,\tau)\left[1-\alpha(\tau)\right] \equiv Q_1(p,\tau)\end{aligned}. \qquad (10.22)$$

Second, consider the uniform pressure profile across the interface contact in ξ, $P(\xi,\tau) = P(\tau)$, that means the uniform frictional heat flux across the interface contact in ξ, $q(\xi,\tau) = \mu P(\tau)v(\tau) = q(\tau)$,

$$\begin{aligned}\tilde{w}_\eta^r(p,0,\tau) &= \frac{C^r}{\sqrt{2\pi}}q(\tau)\Big[\underbrace{\int_{-1}^{1} e^{ip\xi}d\xi}_{=\frac{2\sin p}{p}} - \underbrace{\int_{-1}^{1} e^{ip\xi}\alpha(\xi,\tau)d\xi}_{=\sqrt{2\pi}\tilde{\alpha}(p,\tau)}\Big] \\ &= C^r q(\tau)\left[\sqrt{\frac{2}{\pi}}\frac{\sin p}{p} - \tilde{\alpha}(p,\tau)\right] \equiv Q_2(p,\tau)\end{aligned}. \qquad (10.23)$$

Last, consider the uniform frictional heat partitioning function and pressure profile (frictional heat flux) across the interface contact in ξ, $\alpha(\xi,\tau)=\alpha(\tau)$ and $q(\xi,\tau)=\mu P(\tau)v(\tau)=q(\tau)$,

$$\begin{aligned}\tilde{w}_{\eta}^{r}(p,0,\tau) &= C^{r}q(\tau)[1-\alpha(\tau)]\underbrace{\int_{-1}^{1}e^{ip\xi}d\xi}_{=\frac{2\sin p}{p}} \\ &= C^{r}\sqrt{\frac{2}{\pi}}\frac{\sin p}{p}\left[1-\alpha(\tau)\right]q(\tau)\equiv Q_{3}(p,\tau)\end{aligned} \quad . \tag{10.24}$$

Further, using Equation (10.19) and integrating by parts, $\mathcal{F}\left(w_{\xi}^{r}\right)=-ip\tilde{w}^{r}$. Now, Equations (10.18) with the interface contact boundary conditions defined in Equations (10.22) – (10.24) become

$$\begin{aligned}&\text{Rail's PDE}: && \tilde{w}_{\tau}^{r}=\overline{v}(-ip)\tilde{w}^{r}+\gamma\tilde{w}_{\eta\eta}^{r} && |\,p\,|<\infty,\ \eta<0,\ \tau>0 \\ &\text{I.C.}: && \tilde{w}^{r}(p,\eta,0)=0 && |\,p\,|<\infty,\ \eta<0 \\ &\text{B.C.}: && \tilde{w}^{r}(p,\eta,\tau)\to 0 && \text{as } |\,p\,|\to\infty \text{ or } \eta\to-\infty,\ \tau>0 \\ & && \tilde{w}_{\eta}^{r}(p,0,\tau)=Q(p,\tau) && |\,p\,|\le\infty,\ \tau>0\end{aligned} \quad . \tag{10.25}$$

Lemma A. 1 If $\underline{f}(r)=\sqrt{\frac{2}{\pi}}\int_{0}^{\infty}f(\beta)\cos r\beta\,d\beta$ for $r\ge 0$, then $\underline{f}(r)=\underline{f}^{-}(r)$ for $\eta<0$ where

$$\underline{f}^{-}(r)=\sqrt{\frac{2}{\pi}}\int_{-\infty}^{0}f(\eta)\cos r\eta\,d\eta\,.$$

Proof Let $\mathcal{F}_{c}[f(\beta)]\equiv\underline{f}(r)=\sqrt{\frac{2}{\pi}}\int_{0}^{\infty}f(\beta)\cos r\beta\,d\beta$ for $r\ge 0$. For $\eta<0$, let $\beta=-\eta$ and $d\beta=-d\eta$. If $f(\eta)$ is only defined on $\eta<0$, then

$$\underline{f}(r) = \sqrt{\frac{2}{\pi}}\int_0^{\infty} f(-\beta)\cos r\beta \, d\beta = \sqrt{\frac{2}{\pi}}\int_0^{-\infty} f(\eta)\cos r(-\eta)\,(-d\eta)$$
$$= \sqrt{\frac{2}{\pi}}\int_{-\infty}^{0} f(\eta)\cos r\eta \, d\eta = \underline{f}^{-}(r) \qquad \text{for } \eta < 0\,. \tag{10.26}$$

Lemma A.2 The Fourier cosine Transform along with the inverse transform are given by

$$\mathcal{F}_c[f(x)] \equiv \underline{f}(r) = \sqrt{\frac{2}{\pi}}\int_0^{\infty} f(x)\cos rx \, dx \qquad (r \geq 0)$$

$$\mathcal{F}_c^{-1}\left[\underline{f}(r)\right] \equiv f(x) = \sqrt{\frac{2}{\pi}}\int_0^{\infty} \underline{f}(r)\cos rx \, dr \qquad (x \geq 0). \tag{10.27}$$

Let $h(y)$ be defined for $y \leq 0$ then the followings are true,

$$\mathcal{F}_{-c}[h^{-}(y)] \equiv \underline{h}^{-}(p) \equiv \sqrt{\frac{2}{\pi}}\int_{-\infty}^{0} h^{-}(y)\cos(py)\, dy \qquad (p \leq 0) \tag{10.28}$$

$$\mathcal{F}_{-c}^{-1}\left[\underline{h}^{-}(p)\right] \equiv h^{-}(y) \equiv \sqrt{\frac{2}{\pi}}\int_{-\infty}^{0} \underline{h}^{-}(p)\cos(py)\, dp \qquad (y \leq 0)$$

Proof Let $h(y)$ be defined for $y \leq 0$ and let $y = -x$ with $x \geq 0$. For $p \leq 0$, let $r = -p$ with $f(x) = h^{-}(y)$, then the results follow. Similarly with $\underline{f}(r) = \underline{h}^{-}(p)$.

Next, consider the Fourier cosine Transform of $\tilde{w}^{r}(p,\eta,\tau)$ over $0 < \eta < \infty$ and its inversion formula

$$\mathcal{F}_{-c}[\tilde{w}^r(p,\eta,\tau)] = \underline{\tilde{w}}^r(p,r,\tau) = \sqrt{\frac{2}{\pi}}\int_0^\infty \tilde{w}^r(p,\eta,\tau)\cos(r\eta)\,d\eta \qquad r>0$$
$$\text{Inversion Formula}: \quad \tilde{w}^r(p,\eta,\tau) = \sqrt{\frac{2}{\pi}}\int_0^\infty \underline{\tilde{w}}^r(p,r,\tau)\cos(r\eta)\,dr \qquad \eta>0 \tag{10.29}$$

By Lemma A.1 and A.2, Equations (10.30a) and (10.30b) are equivalent,

$$\text{for } \eta>0, \quad \mathcal{F}_c[g(\eta)] = \underline{g}(r) = \sqrt{\frac{2}{\pi}}\int_0^\infty g(\eta)\cos(r\eta)d\eta \qquad r>0 \quad \cdots(a)$$
$$\text{for } \eta>0, \quad \mathcal{F}_{-c}[g(\eta)] = \underline{g}^r(r) = \sqrt{\frac{2}{\pi}}\int_0^\infty g(\eta)\cos(r\eta)d\eta \qquad r<0 \quad \cdots(b) \tag{10.30}$$

If $\tilde{w}^r(p,\eta,\tau)\to 0$ and $\tilde{w}^r_\eta(p,\eta,\tau)\to 0$ as $\eta\to\infty$, applying Fourier cosine Transform to $\tilde{w}^r_{\eta\eta}$ for $\eta<0$ produces

$$\mathcal{F}_c\left[\tilde{w}^r_{\eta\eta}\right] = -r^2\underline{\tilde{w}}^r(p,r,\tau) + \sqrt{\frac{2}{\pi}}\tilde{w}^r_\eta\Big|_{\eta=0}. \tag{10.31}$$

Next, let's define the forward and inverse Fourier cosine transform for $\eta<0$,

$$\mathcal{F}_c\left[\tilde{w}^r(p,\eta,\tau)\right] = \underline{\tilde{w}}^r(p,r,\tau) = \sqrt{\frac{2}{\pi}}\int_{-\infty}^0 \tilde{w}^r(\xi,\eta,\tau)\cos(r\eta)d\eta \quad \text{for } \eta<0$$
$$\text{Inversion formula}: \qquad \tilde{w}^r(p,\eta,\tau) = \sqrt{\frac{2}{\pi}}\int_{-\infty}^0 \underline{\tilde{w}}^r(p,r,\tau)\cos(r\eta)dr \tag{10.32}$$

By Equation (10.30), Equation (10.32) is true for $\eta<0$.

Applying the cosine Fourier Transform to the rail's PDE in Equation (10.25) with Equations (10.31) and (10.32) produces the following result,

$$\sqrt{\frac{2}{\pi}}\int_{-\infty}^{0}\widetilde{w_\tau^r}\cos(r\eta)d\eta=\sqrt{\frac{2}{\pi}}\int_{-\infty}^{0}\{\bar{v}(-ip)\tilde{w}^r+\gamma\tilde{w}_{\eta\eta}^r\}\cos(r\eta)\,d\eta \tag{10.33}$$

where each term of Equation (10.33) becomes

$$\int_{-\infty}^{0}\widetilde{w_\tau^r}\cos(r\eta)d\eta=\frac{\partial}{\partial\tau}\int_{-\infty}^{0}\tilde{w}^r\cos(r\eta)\,d\eta=\sqrt{\frac{\pi}{2}}\underline{\widetilde{w_\tau}}^r$$

$$\int_{-\infty}^{0}\bar{v}(-ip)\tilde{w}^r\cos(r\eta)\,d\eta=\bar{v}(-ip)\int_{-\infty}^{0}\tilde{w}^r\cos(r\eta)\,d\eta=\sqrt{\frac{\pi}{2}}\bar{v}(-ip)\underline{\tilde{w}}^r$$

$$\int_{-\infty}^{0}\gamma\tilde{w}_{\eta\eta}^r\cos(r\eta)\,d\eta=\gamma\sqrt{\frac{\pi}{2}}[-r^2\underline{\tilde{w}}^r+\sqrt{\frac{2}{\pi}}\tilde{w}_\eta{}^r(p,0,\tau)].$$

Therefore, Equation (10.33) can be simplified as

$$\underline{\widetilde{w_\tau}}^r=\bar{v}(-ip)\underline{\tilde{w}}^r+\gamma[-r^2\underline{\tilde{w}}^r+\sqrt{\frac{2}{\pi}}\tilde{w}_\eta{}^r(p,0,\tau)] \tag{10.34}$$

Observe Equations (10.22) ~ (10.24). Each equation shows the interface boundary conditions for three different cases in the complex Fourier transform domain. Three cases are ①the uniform frictional heat partitioning value along the interface, ②the uniform pressure value along the interface, and ③ the uniform frictional heat partitioning value and pressure value along the interface. For any case, $\tilde{w}_\eta^r(p,0,\tau)=Q_i(p,\tau)$, $i=1,2,3$. After applying Fourier cosine transform over $-\infty<\eta<0$, the rail's PDE system, Equation (10.34), becomes

$$PDE:\quad \underline{\tilde{w}}_\tau^r=-ip\overline{v}\underline{\tilde{w}}^r-\gamma r^2\underline{\tilde{w}}^r+\gamma\sqrt{\frac{2}{\pi}}\tilde{w}_\eta^r(p,0,\tau)$$

$$\underline{\widetilde{w}}_{\tau}^{r} + \underline{\widetilde{w}}^{r}(ip\overline{v} + \gamma r^2) = \gamma\sqrt{\frac{2}{\pi}}Q(p,\tau) \tag{10.35}$$

$$I.C.: \underline{\widetilde{w}}^{r}(p,r,0) = 0$$

where $Q(p,\tau)$ any $Q_i(p,\tau)$ as defined in Equations (10.22) ~ (10.24). Multiplying Equation (10.35) by the integrating factor $\exp[\int_0^{\tau}(ip\overline{v} + \gamma r^2)d\tau] = \exp[ip\overline{\xi}(\tau) + \gamma r^2\tau]$ reduces it to

$$\frac{\partial}{\partial\tau}[(e^{ip\overline{\xi}(\tau)+\gamma r^2\tau})\underline{\widetilde{w}}^{r}] = (e^{ip\overline{\xi}(\tau)+\gamma r^2\tau})\gamma\sqrt{\frac{2}{\pi}}Q(p,\tau)$$

$$\underline{\widetilde{w}}^{r} = \left(e^{-ip\overline{\xi}(\tau)-\gamma r^2\tau}\right)\int_0^{\tau}\left(e^{ip\overline{\xi}(\tau')+\gamma r^2\tau'}\right)\gamma\sqrt{\frac{2}{\pi}}Q(p,\tau')\,d\tau'$$

$$= \gamma\sqrt{\frac{2}{\pi}}\int_0^{\tau}\left(e^{-ip\left(\overline{\xi}(\tau)-\overline{\xi}(\tau')\right)-\gamma r^2(\tau-\tau')}\right)Q(p,\tau')\,d\tau' \tag{10.36}$$

From *Table of Integrals, Series, and Products* (94), the formula 3.896.4 is $\int_0^{\infty} e^{-\beta x^2}\cos(bx)\,dx = \frac{1}{2}\sqrt{\frac{\pi}{\beta}}\exp\left(-\frac{b^2}{4\beta}\right)$. By letting $\beta = \gamma(\tau-\tau')$ and $b = \eta$, $\int_0^{\infty} e^{-\gamma(\tau-\tau')\,x^2}\cos(\eta x)\,dx = \int_{-\infty}^{0} e^{-\gamma(\tau-\tau')\,x^2}\cos(\eta x)\,dx = \frac{1}{2}\sqrt{\frac{\pi}{\gamma(\tau-\tau')}}\exp\left(-\frac{\eta^2}{4\gamma(\tau-\tau')}\right)$ because the integrant is an even function. Using the inversion Fourier cosine transform formula in Equation (10.32), Equation (10.36) becomes

$$\widetilde{w}^{r}(p,\eta,\tau) = \sqrt{\frac{2}{\pi}}\int_{-\infty}^{0}\underline{\widetilde{w}}^{r}(p,r,\tau)\cos(r\eta)\,dr$$

$$= \frac{2}{\pi}\gamma \int_0^{\tau} [\int_{-\infty}^{0} e^{-\gamma r^2(\tau-\tau')} \cos(r\eta)\, dr] e^{-ip\left(\bar{\xi}(\tau)-\bar{\xi}(\tau')\right)} Q(p,\tau')\, d\tau'$$

$$= \sqrt{\frac{\gamma}{\pi}} \int_0^{\tau} \frac{1}{\sqrt{\tau-\tau'}} \exp\left(-\frac{\eta^2}{4\gamma(\tau-\tau')}\right) e^{-ip\left(\bar{\xi}(\tau)-\bar{\xi}(\tau')\right)} Q(p,\tau')\, d\tau' \qquad (10.37)$$

Next, apply the inversion formula for complex Fourier transform (Equation (10.19)) to Equation (10.37) to produce

$$w^r(\xi,\eta,\tau) = \frac{1}{\sqrt{2\pi}} \int_{-\infty}^{\infty} e^{-ip\xi} \tilde{w}^r(p,\eta,\tau)\, dp$$

$$= \frac{1}{\sqrt{2\pi}} \int_{-\infty}^{\infty} e^{-ip\xi} \sqrt{\gamma\pi} \int_0^{\tau} \frac{1}{\sqrt{\tau-\tau'}} \exp\left(-\frac{\eta^2}{4\gamma(\tau-\tau')}\right) e^{-ip\left(\bar{\xi}(\tau)-\bar{\xi}(\tau')\right)} Q(p,\tau')\, d\tau'\, dp$$

$$= \frac{\sqrt{\gamma}}{\sqrt{\pi}} \int_0^{\tau} \frac{1}{\sqrt{\tau-\tau'}} e^{-\frac{\eta^2}{4\gamma(\tau-\tau')}} [\int_{-\infty}^{\infty} e^{-ip\left(\bar{\xi}(\tau)-\bar{\xi}(\tau')+\xi\right)} Q(p,\tau') dp] d\tau'. \qquad (10.38)$$

In Equation (10.20), $Q(p,\tau)$ is defined with Heaviside function. With this definition, w^r can be further simplified to

$$w^r(\xi,\eta,\tau) = \sqrt{\frac{\gamma}{\pi}} C^r \int_0^{\tau} \frac{1}{\sqrt{\tau-\tau'}} e^{\frac{-\eta^2}{4\gamma(\tau-\tau')}} \left[H(1-z^2)\left(1-\alpha(z,\tau')\right) q(z,\tau')\right] d\tau'. \qquad (10.39)$$

where $z = \bar{\xi}(\tau) - \bar{\xi}(\tau') + \xi$, $C^r = \dfrac{y^*}{k^r(T_m - T_a)}$ and $\gamma = \dfrac{\kappa^r}{\kappa^s}$.

A.3 Lemma $\frac{1}{2}\int_{-1}^{1} \mathrm{H}(1-(\mathrm{x}+\mathrm{h})^2)\mathrm{dx} = \mathrm{H}(1-\frac{|\mathrm{h}|}{2})(1-\frac{|\mathrm{h}|}{2})$ **for** $\boldsymbol{h} \in \mathbb{R}$

This appendix derives the results for Equation (3.22), Section 3.2. As observed in Figure 14 in Section 3.2, when $y(x) = 1-(x+h)^2 = 0$, the *x*-intersection points are $x = -h-1$ and $x = -h+1$. If the slipper's length is assumed to be 2, the endpoints of slipper's front and back are $-h-1$ and

$-h+1$. For $-1 \le x \le 1$, let's evaluate $\frac{1}{2}\int_{-1}^{1} H(1-(x+h)^2)dx$ in $-1 \le x \le 1$ with varying h values.

There are four cases to consider; i) $|-h| > 2$, ii) $-h = 0$, iii) $-2 < -h < 0$ and iv) $0 < -h < 2$.

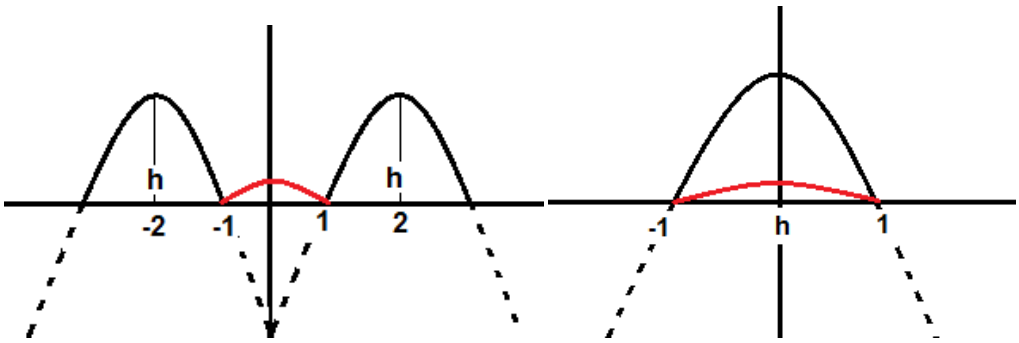

(i) **(ii)**

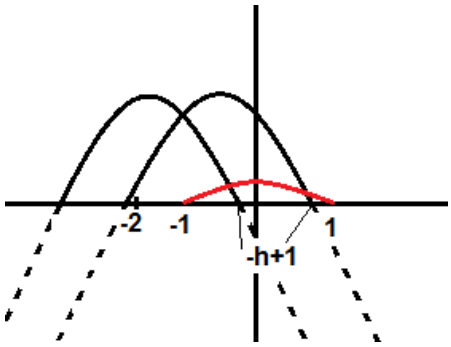

(iii)

Figure 35. Graphs of $y(x) = 1-(x+h)^2$ for the Cases of i), ii) and iii)

i) For $|-h| > 2 \rightarrow h < -2$ or $h > 2$, $\frac{1}{2}\int_{-1}^{1} H(1-(x+h)^2)dx = \frac{1}{2}\int_{-1}^{1} 0\, dx = 0$.

ii) For $-h = 0$, $\frac{1}{2}\int_{-1}^{1} H(1-(x+h)^2)dx = \frac{1}{2}\int_{-1}^{1} 1\, dx = 1$.

iii) For $-2 < -h < 0 \rightarrow 0 < h < 2$,

$$\frac{1}{2}\int_{-1}^{1} H(1-(x+h)^2)dx = \frac{1}{2}\left[\int_{-1}^{-h+1} H(1-(x+h)^2)dx + \int_{-h+1}^{1} H(1-(x+h)^2)dx\right]$$
$$= \frac{1}{2}\left[\int_{-1}^{-h+1} 1\,dx + \int_{-h+1}^{1} 0\,dx\right]$$
$$= \frac{1}{2}(-h+1+1) = 1-\frac{h}{2}$$

iv) For $0 < -h < 2 \rightarrow -2 < h < 0$, similar to upper case but the lower boundary changes,

$$\frac{1}{2}\int_{-1}^{1} H(1-(x+h)^2)dx = \frac{1}{2}\left[\int_{-1}^{-h-1} H(1-(x+h)^2)dx + \int_{-h-1}^{1} H(1-(x+h)^2)dx\right]$$
$$= \frac{1}{2}\left[\int_{-1}^{-h-1} 0\,dx + \int_{-h-1}^{1} 1\,dx\right]$$
$$= \frac{1}{2}(1+h+1) = 1+\frac{h}{2}$$

Therefore, $\frac{1}{2}\int_{-1}^{1} H(1-(x+h)^2)dx = \begin{cases} 1-\frac{|h|}{2} & \text{for } |h|<2 \\ 0 & \text{for } |h|\geq 2 \end{cases} = H(1-\frac{|h|}{2})(1-\frac{|h|}{2})$. (10.40)

A.4 Derivation of the Heat Partition Function in the Laplace Transform Domain

This appendix shows the derivation of slipper's heat partitioning function using the slipper and rail's averaged interface temperature, which is the solution to Equation (0.66) in Section 3.2.

In Section 3.2, the solutions to the rail and slipper's temperature distribution in 2 dimensions, Equations (3.10) and (3.17), were found. Equation (3.20) shows the rail and slipper's interface temperature distributions by letting $\eta = 0$ and Equation (3.21) shows that the integration along the contact interval $-1 \leq l \leq 1$ is used to calculate the averaged slipper and

rail's interface temperatures. Using the Carslaw and Jaeger assumption of matching the slipper and rail's averaged interface temperature, the slipper's heat partitioning function $\alpha(\tau)$ is found by solving Equation (3.23) in Section 3.2. This equation is further reduced by assuming the slipper is at constant velocity v_o . The resulting equation is

$$\int_0^\tau \frac{1}{\sqrt{\tau-\tau'}}\big(1+\beta K(\mathbf{h})\big)\alpha(\tau')q(\tau')d\tau' = \beta\int_0^\tau \frac{1}{\sqrt{\tau-\tau'}}K(\mathbf{h})q(\tau')d\tau' \tag{10.41}$$

where $\beta = \frac{\sqrt{\gamma}C_r}{C_s} = \frac{k^s}{k^r}\sqrt{\frac{\kappa^r}{\kappa^r}}$ and $K(\mathbf{h}) = H(1-\frac{v_0|\tau-\tau'|}{2})\left(1-\frac{v_0|\tau-\tau|}{2}\right)$.

Using the Laplace Transform as given by $\mathcal{L}\{f(t)\} = \int_0^\infty f(t)e^{-st}\,dt = F(s)$, and recognizing that Equation (10.41) is a convolution, produces

$$\mathcal{L}\{\alpha q\}\mathcal{L}\left\{\frac{1}{\sqrt{\tau}}+\beta\frac{K(\mathbf{h})}{\sqrt{\tau}}\right\} = \mathcal{L}\{q\}\beta\mathcal{L}\left\{\frac{K(\mathbf{h})}{\sqrt{\tau}}\right\}$$

$$\mathcal{L}\{\alpha q\}\left[\mathcal{L}\left\{\frac{1}{\sqrt{\tau}}\right\}+\beta\mathcal{L}\{\frac{K(\mathbf{h})}{\sqrt{\tau}}\}\right] = \mathcal{L}\{q\}\beta\mathcal{L}\left\{\frac{K(\mathbf{h})}{\sqrt{\tau}}\right\}$$

$$\mathcal{L}\{\alpha q\}\left[\sqrt{\frac{\pi}{s}}+\beta\mathcal{L}\{\frac{K(\mathbf{h})}{\sqrt{\tau}}\}\right] = \mathcal{L}\{q\}\beta\mathcal{L}\left\{\frac{K(\mathbf{h})}{\sqrt{\tau}}\right\}$$

$$\mathcal{L}\{\alpha q\} = \mathcal{L}\{q\}B(s) \tag{10.42a}$$

where

$$B(s) = \frac{\beta\sqrt{s}\mathcal{L}\left\{\frac{K(\mathbf{h})}{\sqrt{\tau}}\right\}}{\sqrt{\pi}+\beta\sqrt{s}\mathcal{L}\left\{\frac{K(\mathbf{h})}{\sqrt{\tau}}\right\}} \tag{10.42b}$$

and $\mathcal{L}\left\{\frac{K(\mathbf{h})}{\sqrt{\tau}}\right\} = \int_0^\infty e^{-s\tau}\frac{1}{\sqrt{\tau}}H\left(1-\frac{v_0|\tau|}{2}\right)\left(1-\frac{v_0|\tau|}{2}\right)d\tau.$

When the pressure and velocity are assumed to be constants P_0 and v_0 respectively, then $q(\tau) = \mu P_0 v_0 \doteq q_0$ is constant and Equation (10.42) is reduced to

$$q_0\mathcal{L}\{\alpha\} = q_0\frac{1}{s}B(s)$$

$$\mathcal{L}\{\alpha\} = \frac{1}{s}B(s) \ . \qquad (10.43)$$

A.5 Lemma $\lim_{s\to\infty}\sqrt{s}F(s) = \sqrt{\pi}$

This lemma proves the result used in Equation (3.35) in Section 3.2.

Proof: From Equation (3.31) with $x = \dfrac{2s}{v_0}$

$$\lim_{s\to\infty}\sqrt{s}F(s) = \lim_{x\to\infty}\sqrt{x}\tilde{F}(x)$$

and from Equation(3.30)

$$\sqrt{x}\tilde{F}(x) = (1-\frac{1}{x})\gamma(\frac{1}{2},x) + \frac{\mathrm{e}^{-x}}{\sqrt{x}}.$$

Hence

$$\lim_{x\to\infty}\sqrt{x}\tilde{F}(x) = \lim_{x\to\infty}(1-\frac{1}{x})\gamma(\frac{1}{2},x) + \frac{\mathrm{e}^{-x}}{\sqrt{x}} = \Gamma(\frac{1}{2}) = \sqrt{\pi} \qquad (10.44)$$

A.6 Lemma $\gamma(\frac{1}{2}, x) = x^{1/2}e^{-x}\sum_{k=0}^{\infty} A_k x^k$ where $A_k = \frac{2^{2k+1}k!}{(2k+1)!}$

This lemma is used in Equation (3.31) in Section 3.2. After applying a series of integration by parts, the result to $\gamma(\frac{1}{2}, x)$ is expressed in the infinite sum as follows:

$$\begin{aligned}
\gamma(\frac{1}{2}, x) &= \int_0^x e^{-t}t^{1/2-1}dt \\
&= \int_0^1 e^{-rx}(xr)^{-1/2}xdr \\
&= x^{1/2}\int_0^1 e^{-rx}r^{-1/2}dr \\
\text{(by parts)} &= x^{-1/2}\left\{e^{-rx}\frac{r^{1/2}}{1/2}\Big|_0^1 + \frac{x}{1/2}\int_0^1 e^{-rx}r^{1/2}dr\right\}
\end{aligned}$$

$$\begin{aligned}
\text{(by parts)} &= x^{-1/2}\left\{\frac{e^{-x}}{1/2} + \frac{x}{1/2}\left(e^{-rx}\frac{r^{3/2}}{3/2}\Big|_0^1 + \frac{x}{3/2}\int_0^1 e^{-rx}r^{3/2}dr\right)\right\} \\
&= x^{-1/2}\left\{\frac{e^{-x}}{\frac{1}{2}} + \frac{xe^{-x}}{\frac{1}{2}\cdot\frac{3}{2}} + \frac{x^2}{\frac{1}{2}\cdot\frac{3}{2}}\int_0^1 e^{-rx}r^{3/2}dr\right\} \\
\cdots &= x^{-1/2}e^{-x}\left\{\frac{1}{\frac{1}{2}} + \frac{x}{\frac{1}{2}\cdot\frac{3}{2}} + \frac{x^2}{\frac{1}{2}\cdot\frac{3}{2}\cdot\frac{5}{2}} + \cdots + \frac{x^k\Gamma(1/2)}{\Gamma(k+3/2)} + \cdots\right\}
\end{aligned}$$

$$\gamma(\frac{1}{2}, x) = x^{-1/2}e^{-x}\sum_{k=0}^{\infty}\frac{\sqrt{\pi}}{\Gamma(k+3/2)}x^k \ . \qquad (10.45)$$

Let's observe the expression $\frac{\Gamma(k+3/2)}{\sqrt{\pi}}$ in Equation (10.45). It can be rewritten as

$$\frac{\Gamma(k+3/2)}{\sqrt{\pi}} = \frac{\Gamma(k+3/2)}{\Gamma(1/2)} = (k+\frac{1}{2})(k-\frac{1}{2})\cdots\frac{1}{2}$$
$$= \frac{2k+1}{2}\cdot\frac{2k-1}{2}\cdot\frac{2k-3}{2}\cdots\frac{3}{2}\cdot\frac{2}{2}\cdot\frac{1}{2} \quad . \tag{10.46}$$
$$= \frac{(2k+1)!}{2^{2k+1}k!}$$

Therefore, using Equation (10.46), Equation (10.45) becomes

$$\gamma(\frac{1}{2}, x) = x^{1/2}e^{-x}\sum_{k=0}^{\infty} A_k x^k \quad \text{where} \quad A_k = \frac{2^{2k+1}k!}{(2k+1)!} \ . \tag{10.47}$$

A.7 Lemma $\tilde{F}(x) = e^{-x}\sum_{j=0}^{\infty}\frac{2(j+1)}{2j+3}A_j x^j = e^{-x}\sum_{j=0}^{\infty}(j+1)A_{j+1}x^j$

This lemma shows the result to Equation (3.35) in Section 3.2.

$$\tilde{F}(x) = e^{-x}\left\{\frac{1}{x}(x-\frac{1}{2})\sum_{k=0}^{\infty}A_k x_k + \frac{1}{x}\right\} \quad \text{where} \quad A_k = \frac{2^{2k+1}k!}{(2k+1)!}$$
$$= \frac{e^{-x}}{x}\left\{1+(x-\frac{1}{2})\sum_{k=0}^{\infty}A_k x_k\right\}$$
$$= \frac{e^{-x}}{x}\left\{1+\sum_{k=0}^{\infty}A_k(x^{k+1}-\frac{1}{2}x^k)\right\} \tag{10.48}$$
$$= \frac{e^{-x}}{x}\left\{1-\frac{1}{2}\sum_{k=0}^{\infty}A_k x^k + \sum_{k=1}^{\infty}A_{k-1}x^k\right\}$$

$$\tilde{F}(x) = \frac{e^{-x}}{x}\left\{1-\frac{1}{2}A_0 + \sum_{k=1}^{\infty}(A_{k-1}-\frac{1}{2}A_k)x^k\right\} \quad \text{where} \quad A_k = \frac{2^{2k+1}k!}{(2k+1)!} \tag{10.49}$$

Using the definition for A_k, and A_{k+1}, the terms $(1-\frac{1}{2}A_0)$ and $(A_{k-1}-\frac{1}{2}A_k)$ in Equation (10.49) become as follows:

$$\text{(a) } 1-\frac{1}{2}A_0 = 1-\frac{1}{2}\frac{2^{2\cdot 0+1}0!}{(2\cdot 0+1)!} = 1-\frac{1}{2}\cdot 2 = 0$$

$$\text{(b) } A_{k-1}-\frac{1}{2}A_k = A_{k-1}(1-\frac{1}{2}\frac{A_k}{A_{k-1}}) = A_{k-1}(1-\frac{1}{2}\cdot\frac{2}{2k+1}) = \frac{2k}{2k+1}A_{k-1} \qquad (10.50)$$

$$\text{(c) } A_{k+1} = \frac{2^{2k+3}(k+1)!}{(2k+3)!} = \frac{2^2(k+1)}{(2k+3)(2k+2)}\frac{2^{2k+1}k!}{(2k+1)!} = \frac{2}{(2k+3)}A_k$$

With Equations (10.50a) ~ (10.50c), Equation (10.49) is $\tilde{F}(x) = \frac{e^{-x}}{x}\sum_{k=1}^{\infty}\frac{2k}{2k+1}A_{k-1}x^k$.

Let $k = j+1$, then Equation (10.49) becomes

$$\tilde{F}(x) = e^{-x}\sum_{j=0}^{\infty}\frac{2(j+1)}{2j+3}A_j x^j = e^{-x}\sum_{j=0}^{\infty}(j+1)A_{j+1}x^j \quad . \qquad (10.51)$$

A.8 Evaluating $\alpha(t)$ using Branch Cut Integral

This appendix shows the derivation of the slipper's heat partitioning function, Equation (3.38) in Section 3.2, by inverting the Laplace Transform. The Inverse Laplace Transform given in Equation (3.37) reduces to the evaluation of a branch cut integral. Recalling Equations (3.35) and (3.32)

$$\mathcal{L}\{\alpha q\} = \mathcal{L}\{q\}\,B(s) = \mathcal{L}\{q\}\frac{\beta^*\sqrt{s}F(s)}{1+\beta^*\sqrt{s}F(s)}. \qquad (10.52)$$

Where $\beta^* = \frac{k^s}{k^r}\sqrt{\frac{\kappa^r}{\pi\kappa^s}}$. Assuming a non-zero constant heat flux function $q(\tau) = q_0$, the heat partition function $\mathcal{L}\{\alpha\}$ in Laplace Transform domain was given in Equation (3.26b) as

$$\mathcal{L}\{\alpha\} = \frac{\beta^* \sqrt{s} F(s)}{s(1+\beta^* \sqrt{s} F(s))} \ . \tag{10.53}$$

Equation (10.53) is a rational function with a removeable simple pole at *s=0*. Further, the function $1+\beta^* \sqrt{s} F(s)$ has no roots in complex plane. Using the inverse Laplace Transform formula on Equation (10.53), the heat partition function is then given by

$$\alpha(t) = \frac{1}{2\pi i} \int_{Br} \frac{e^{st}}{s} \frac{\beta^* \sqrt{s} F(s)}{(1+\beta^* \sqrt{s} F(s))} ds \tag{10.54}$$

where $F(s) = s^{-1/2} \gamma(\frac{1}{2}, \frac{2s}{v_0}) - s^{-3/2} \frac{v_0}{2} \gamma(\frac{3}{2}, \frac{2s}{v_0})$. Set $s = \frac{v_0}{2} x$ then, as observed in Equation (3.31),

$$F(s) = F(\frac{v_0}{2} x) = (\frac{v_0}{2})^{-1/2} \tilde{F}(x) \tag{10.55}$$

With Equation (10.55), Equation (10.54) becomes

$$\alpha(t) = \frac{1}{2\pi i} \int_{Br} e^{\frac{v_0}{2} xt} \frac{1}{x} \frac{\beta^* \sqrt{x} \tilde{F}(x)}{1+\beta^* \sqrt{x} \tilde{F}(x)} dx \tag{10.56}$$

Because Equation (10.56) contains $\sqrt{x}$, it has a branch point at *x=0* and we shall take the branch cut along the negative real axis in the complex *x* plane. Thus, introducing a loop contour around the branch cut integral along the negative real axis in the complex *x* plane is equivalent to evaluating Equation (10.56) for the heat partition function $\alpha(t)$.

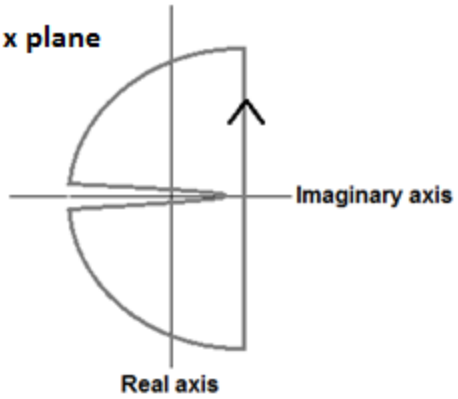

Figure 36. Branch Cut Integration Along the Negative Complex Axis

$$\begin{aligned} &\text{For upper branch,} \quad x = e^{i\pi} r \quad \text{then } x = -r,\ dx = -dr\ ,\ \sqrt{x} = i\sqrt{r} \\ &\text{For lower branch,} \quad x = e^{-i\pi} r \quad \text{then } x = -r,\ dx = -dr\ ,\ \sqrt{x} = -i\sqrt{r} \end{aligned} \tag{10.57}$$

Using the upper and lower branches in Equation (10.57), Equation (10.56) becomes

$$\begin{aligned} \alpha(t) &= \frac{1}{2\pi i}\left\{ \int_{\infty}^{0} \frac{e^{-\frac{v_0}{2}tr}}{-r} \frac{\beta^*(-i)\sqrt{r}\tilde{F}(-r)}{1+\beta^*(-i)\sqrt{r}\tilde{F}(-r)}(-dr) + \int_{0}^{\infty} \frac{e^{-\frac{v_0}{2}tr}}{-r} \frac{\beta^*(i)\sqrt{r}\tilde{F}(-r)}{1+\beta^*(i)\sqrt{r}\tilde{F}(-r)}(-dr) \right\} \\ &= \frac{1}{2\pi}\int_{0}^{\infty} e^{-\frac{v_0}{2}tr} \frac{\beta^*\sqrt{r}\tilde{F}(-r)}{r}\left(\frac{1}{1-i\beta^*\sqrt{r}\tilde{F}(-r)} + \frac{1}{1+i\beta^*\sqrt{r}\tilde{F}(-r)} \right) dr \\ &= \frac{1}{\pi}\int_{0}^{\infty} e^{-\frac{v_0}{2}tr} \frac{\beta^*\sqrt{r}\tilde{F}(-r)}{r(1+(\beta^*)^2 r(\tilde{F}(-r))^2)} dr \end{aligned} \tag{10.58}$$

where $\beta^* = \dfrac{\beta}{\sqrt{\pi}}$ and $\tilde{F}(-r) = e^r \sum_{k=0}^{\infty} (k+1)A_{k+1}(-r)^k$ for $A_k = \dfrac{2^{2k+1}k!}{(2k+1)!}$.

Some observations about the function $\tilde{F}(z)$ would be useful here. Using Equation (3.27b) with the substitution $z = \dfrac{2s}{v_0}\xi^2$, we find $F(s) = \sqrt{\dfrac{2}{v_0}} 2\int_0^1 \exp(-\dfrac{2s}{v_0}\xi^2)(1-\xi^2)d\xi$.

Referring to Equation(10.55) and replacing $2s/v_0$ with z results in the equation

$$\widetilde{F}(z) = 2\int_0^1 e^{-z\xi^2}(1-\xi^2)d\xi = \frac{e^{-z}}{z} + \frac{1}{2z^{3/2}}(2z-1)\sqrt{\pi}erf(\sqrt{z}) \qquad (10.59)$$

Integrating this representation for $\widetilde{F}(z)$ by parts also leads to the series given in Equation (10.51). Further, we see that for all real values of x, $\widetilde{F}(x)$ is real and $\widetilde{F}(x) > 0$. Now by the Schwarz Reflection Principle, it follows that $\widetilde{F}(z^*) = \widetilde{F}^*(z)$. Here, * is the complex conjugate operator.

A.9 Derivation of $\dot{v}_i(t)$ *and* $v_0(t)$

This appendix derives to the expression for $\dot{v}_i(t)$, $v_0(t)$ and $v_{N+1}(t)$ in Equation (7.13), Section 7.4 from Equation (7.12). First let $v_i(t) = w(\xi_i, t)$, then

$\dot{v}_i(t) \equiv \frac{d}{dt}v_i(t) = \frac{\partial w}{\partial t}(\xi_i, t)$ for $i = 1, \ldots, N+1$. Substituting the second order difference approximations for the spatial derivatives,

$$\frac{\partial w}{\partial \xi}(\xi_i, t) = \frac{\delta_x^c w(\xi_i, t)}{2\Delta\xi} + \mathrm{O}(\Delta\xi^2) = \frac{v_{i+1}(t) - v_{i-1}(t)}{2\Delta\xi} + \mathrm{O}(\Delta\xi^2)$$

and

$$\frac{\partial^2 w}{\partial \xi^2}(\xi_i, t) = \frac{\delta_x^2 w(\xi_i, t)}{\Delta\xi^2} + \mathrm{O}(\Delta\xi^2) = \frac{v_{i+1}(t) - 2v_i(t) + v_{i-1}(t)}{\Delta\xi^2} + \mathrm{O}(\Delta\xi^2)$$

Into Equation (7.12a) produces

$$\dot{v}_i(t) = \frac{\kappa(v_{i+1}(t) - 2v_i(t) + v_{i-1}(t))}{(\Delta\xi)^2 (x^*)^2} + \frac{\dot{\sigma}(t)}{x^*}\frac{v_{i+1}(t) - v_{i-1}(t)}{2\Delta\xi} + O(\Delta\xi^2) \ . \qquad (10.60)$$

From the boundary condition in Equation (7.12c) $v_{N+1}(t) = w(\xi_{N+1}, t) = w(1,t) = 0$, and from Equation (7.12b)

$$-\frac{v_2(t) - v_0(t)}{2\Delta\xi} = \frac{2x^* m(t)}{k(T_m - T_a)}\left(Q(t) - \rho\ell\dot{\sigma}\right) + \frac{2x^*}{k}h(1-m(t))(v_1(t) - T_a) \ . \tag{10.61}$$

Solving Equation (10.61) for $v_0(t)$ produces

$$v_0(t) = \frac{2x^*\Delta\xi m(t)}{k(T_m - T_a)}\left(Q(t) - \rho\ell\dot{\sigma}\right) + \frac{2x^*}{k}h(1-m(t))(v_1(t) - T_a) + v_2(t) \ . \tag{10.62}$$

A.10 Time to Reach the Melt Temperature Formulas

In this appendix the solution to the problem of time required to reach the melt temperature at the interface at the interface is developed. Two different velocity cases are considered and Equations (4.28) and (4.30) in Section 4.3 are derived. The numerical results using the material's with physical and thermal properties given in Table 1, are presented in Table 2 and 3 in Section 4.3.

Equation (4.25) states

$$\int_0^\infty T_0(\xi)G(0,\xi,t_m)d\xi + \int_0^{t_m}\frac{\kappa}{k}Q(\tau)G(0,0,t_m-\tau)d\tau = T_m . \tag{10.63}$$

If $T_0(\xi) = T_a$, then

$$\int_0^\infty T_0(\xi)G(0,\xi,t_m)d\xi = T_a\int_0^\infty G(0,\xi,t_m)d\xi = T_a$$
$$\Rightarrow \frac{\kappa}{k}\int_0^{t_m} Q(\tau)G(0,0,t_m-\tau)d\tau = T_m - T_a \tag{10.64}$$

With $Q(t) = \alpha\mu P(q_0 + at)$ and $G(0,0,t_m-\tau) = \dfrac{1}{\sqrt{\kappa\pi(t_m-\tau)}}$, Equation (10.64) becomes

$$\frac{\kappa}{k}\int_0^{t_m} \alpha\mu P(q_0 + a\tau)\frac{d\tau}{\sqrt{\kappa\pi(t_m-\tau)}} = T_m - T_a \tag{10.65}$$

Let $t_m - \tau = \beta$, which implies $d\beta = -d\tau$ and $\tau = t_m - \beta$. Then, Equation (10.65) is rewritten as the following

$$\int_0^{t_m} \frac{\kappa\alpha\mu P}{k\sqrt{\kappa\pi}}(q_0 + a(t_m-\beta))\frac{d\beta}{\sqrt{\beta}} = \frac{\alpha\mu P}{k}\sqrt{\frac{\kappa}{\pi}}[2(q_0+at_m)\beta^{1/2} - \frac{2}{3}a\beta^{3/2}]\Big|_0^{t_m} = T_m - T_a \tag{10.66}$$

$$\frac{\alpha\mu P}{k}\sqrt{\frac{\kappa}{\pi}}(2q_0t_m^{1/2} + \frac{4}{3}at_m^{3/2}) = T_m - T_a\ .$$

(10.67)

If $a = 0$, then

$$t_m = \frac{\pi}{\kappa}\left[\frac{(T_m - T_a)k}{2\alpha\mu P q_0}\right]^2\ . \tag{10.68}$$

If $a \neq 0$, then let $t_m = s^2$. Then, Equation (10.67)

$$\frac{4}{3}as^3 + 2q_0 s - \frac{T_m - T_a}{\alpha\mu P}k\sqrt{\frac{\pi}{\kappa}} = 0$$
$$\Rightarrow\ s^3 + \frac{3q_0}{2a}s - \frac{T_m - T_a}{\alpha\mu P a}\frac{3k}{4}\sqrt{\frac{\pi}{\kappa}} = 0 \tag{10.69}$$

Bibliography

1. Hale, Chad. *Consideration of Wear Rates At High Velocities*. Ph.D. Dissertation, AFIT/DS/ENY/10-08. Air Force Institute of Technology (AU), Wright-Patterson AFB OH, September 2009 (ADA515123).

2. D.W.Minto. "Recent Increases in Hypersonic Test Capabilities at the Holloman High Speed Test Track," *AIAA, The 38th AIAA Aerospace Sciences Meeting and Exhibit*, Reno, Nevada: AIAA, 2000.

3. D.W.Minto. "The Holloman High Speed Test Track Hypersonic Upgrade Program Status," *AIAA, The 22nd AIAA Aerodynamic Measurement Technology and Ground Testing Conference,* Saint Louis, Missouri: AIAA, 2002.

4. Laird, D.J. *The Investigation of Hypervelocity Gouging*. Ph.D. Dissertation, AFIT/DS/ENY/02-01. Air Force Institute of Technology (AU), Wright-Patterson AFB OH, January 2002 (AD-A398636).

5. Laird, D.J. and A. N. Palazotto. "Gouge Development During Hypervelocity Sliding Impact," *International Journal of Impact Engineering*, 30: 205-223 (February 2004).

6. Szmerekovsky, A. G., A.N. Palazotto, and J. D. Cinnamon. "An Improved Study of Temperature Changes During Hypervelocity Sliding High Energy Impact," *The 47th AIAA/ASME/ASCE/AHS/ASC Structures, Structural Dynamics and Materials Conference*. Newport, Rhode Island: AIAA, May 2006.

7. Baker, W.P., A.N. Palazotto, and D.J. Laird. "Thermal Diffusion and Associated Stress Field due to High Speed Source," *Journal of Aerospace Engineering*, 15:.3.118-124 (July 2002).

8. Bayer, R.G. *Engineering Design for Wear*. New York: Marcel Dekker, Inc., 2004.

9. Bayer, R.G. *Mechanical Wear Fundamentals and Testing*. New York: Marcel Dekker Inc., 2004.

10. Bayer, R.G. *Wear Analysis for Engineers*. New York: HNB Publishing, 2002.

11. Kato, K. Chichester. *Classification of Wear mechanisms/Models, Wear-Materials, Mechanisms and Practice*. England : John Wiley & Sons, 2005.

12. Nichols, E.L. and W.S. Franklin. *The Elements of Physics: Mechanics and heat*. London : MacMillan & Co., Ltd, 1898.

13. Dowson, Duncan. *History of Tribology.* 2nd.: Professional Engineering Publishing, 1997.

14. Hibbeler, R.C. *Engineering Mechanics*. 11th.: Pearson, Prentice Hall, 2007.

15. Soutas-Little, Robert W., Inman, Balint. *Engineering Mechanics*.: Thomson, 2008.

16. Kennedy, F.E. and Karpe, S.A. "Thermocracking of a mechanical face seal," *Wear*, 79: 21-36 (1982).

17. Banerjee, B.N. and R.A.Burton. "Experimental studies of thermoelastic effects in hydrodynamically lubricated face seals," *J. Lubr. Technol*., 101: 275-282 (1979).

18. Uetz, H. and Fohl, J. "Wear as an energy transformation process," *Wear*, 49: 253-264.

19. Kennedy, Francis E. and Bharat Bhushan. *Modern Tribology Handbook Vol. 1*. Boca Raton, FL: CRC Press LLC, 2001.

20. Kakac, Yaman Yener and Sadik. *Heat Conduction*. (4th Edition). New York: Taylor & Francis Group, LLC, 2008.

21. Jaeger, H.S. Carslaw and J.C. Jaeger *Conduction of Heat in Solids*. New York : Oxford University Press, 1989.

22. Cannon, John Rozier. *One Dimensional Heat Equation, Encyclopedia of Mathematics and Its Applications*. (1st Edition). New York: Cambridge University Press, 1984.

23. Wikipedia contributors. "Normal distribution," *Wikipedia, The Free Encyclopideia*. May 17, 2012. http://en.wikipedia.org/w/index.php?title=Normal_distribution&oldid=492963537.

24. Farrell, R.M. and T.S. Eyre. "The Relationship Between Load and Sliding Distance in the Initiation of Mild Wear in Steels," *Wear*, 15: 359-372 (May 1970).

25. Lim, S.C. and M.F.Ashby. "Wear-Mechamism Maps," *Aca Metallurgica.*, 35: 1-24 (January 1987).

26. Blok, H. "Les Temperatures de Surface dans des Conditions de Graissage Sous Extreme Pression," *Proc. Sd. World Petrol. Cong*. 3: 471-486. 1937.

27. Tian, X. and F.E. Kennedy. "Maximum and average flash temperatures in sliding contact," *ASME J. Tribol*., 116: 167-174. 1994.

28. Komanduri, R. and Z.B.Hou. "Tribology in metal cutting - some thermal issues," *ASME J. Tribol*., 123: 799-815. 2001.

29. H.A.Francis. “Interfacial temperature distribution within a sliding Herzian contact,” *ASLE Trans*. 14: 41-54. 1970.

30. Iwand, H.C., D.H.Stone, and G.J.Moyar. *A thermal and metallurgical analysis of martensite formation and tread spalling during wheel skid. Rail Transportation*. New York: ASME, 1992.

31. Sun,J., K.J.Sawley, D.H.Stone, and D.F.Teter. “Progress in the reduction of wheel spalling,” *12th International Wheelset Congress.* 18-29. Qingdao China: 1998.

32. Hou, Z.B. and R. Komanduri. “Analysis of heat partition and temperature distribution in sliding systems,” *Wear*, 251: 925-938 (2001).

33. Gupta, V., G.T.Hahn, P.C.Bastias, and C.A.Rubin. “Calculations of the frictional heating of a locomotive wheel attending rolling plus sliding,” *Wear*, 131: 237-241 (1996).

34. Kennedy, T.C., C.Plengsaard, and R.F.Harder. “Transient heat partition factor for a sliding railcar wheel,” *Wear*, 261: 932-936 (2006).

35. Malinowski, Z., J.G.Lenard, and M.E.Davies. “A Study of The Heat-Transfer Coefficient As A Function of Temperature and Pressure,” *J Materials Processing Technology*, 41: 125-142 (1994).

36. Iqbal, S.A., P.T.Mativenga, and M.A.Sheikh. “An investigative study of the interface heat transfer coefficient for FE modelling of high speed machining,” *Ned University J of Research*, 1: 44-58 (2009).

37. Bhushan, Bharat. *Modern Tribology Handbook.* Boca Raton: CRC Press LLC, 2001.

38. Haberman, Richard. *Elementary Applied Partial Differential Equations* (2nd Edition). Englewood cliffs : Prentice-Hall Inc., 1987.

39. Paek-Spidell, Gracie Y., William Baker, and Anothony Palazotto. “Surface Temperature and Melt Profile due to Frictional Heating,” *AIAA-Dayton-cincinnati aerospace science symposium*. Dayton OH : 2010.

40. Kennedy, F.E. and S.Traiviratana. “Transient effects on heat conduction in sliding bodies,” *Numerical Heat Transfer*, 47: 57-77 (2005).

41. Beck, J.V., K.D.Cole, A.Haji-Sheikh, and B.Litkouhi. *Heat Conduction Using Green's Functions.* : Hemisphere Publishing Corporation, 1992.

42. Abramowitz, M. and I.A.Stegun. *Handbook of Mathematical Functions with Formulas, Graphs, and Mathematical Tables.* New York: Dover, 1972.

43. G.Arfken. *Mathematical Methods for Physicists* (3rd Edition). Orlando : Academic Press, 1985.

44. Incropera, F P. and David P. Dewitt. *Fundamentals of Heat and Mass Transfer* (4th Edition). : John Wiley & Sons, Inc., 1996.

45. Lakoba, T. "The Heat equation in 2 and 3 spatial dimensions," *University of Vermont*. Math 337 Class Notes 140-166. June 2011 www.cems.uvm.edu/~**tlakoba**/math337/notes_15.pdf .

46. Li, Jichun and Yi-Tung Chen. *Computational Partial Differential Equations Using MATLAB.* Boca Raton : Taylor & Francis Group, 2009.

47. Peaceman, D.W. and H.H.Jr. Rachford. "The numerical Solution of Parabolic and Ellliptic Differential Equations," Journal of the Society for Industrial and Applied Mathematics, 65: 28-41 (1955).

48. Crank, J. and P. Nicolson. "A Practical method for numerical evaluation of solutions of partial differential equations of the heat-conduction type," *Advanced in Computational Mathematics*, 6: 207-226 (1996).

49. Morton, K.W. and D.F. Mayers. *Numerical Solution of Partial Differential Equations* (2nd Edition). Cambridge: Cambridge University Press, 2005.

50. Strikwerda, John C. *Finite Difference Schemes and Partial Differential Equations. Pacific Grove* : Wadsworth & Brooks/Cole Advanced Books & Software, 1989.

51. Chertock, Alina and Alexander Kurganov. "On Splitting-Based Numerical Methods for Convection-Diffusion Equations," *Quaderni di Matematica*, 2010. www4.ncsu.edu/~acherto/papers/**Chertock-Kurganov**.pdf

52. Lanswer, D. and J.G.Verwer. "Analysis of operator splitting for advection-diffusion-reaction problems from air pollution modeling," *Journal of Computational and Applied Mathematics*, 201-216 (1999).

53. Strang, Gilbert. "On the Construction and Comparison of Difference Schemes," *SIAM J. Numer. Anal.* 3: 506-517 (1968).

54. Novak, Kyle. Class handout, Math 676, Numerical Methods for Partial Differential Equations. School of Mathematics and Statistics, Air Force Institute of Technology, Wright-Patterson AFB OH, Summer Quarter 2008.

55. Goshtasby, A. and W.D. O'Neill. "Curve fitting by a sum of Gaussians," *Graphical Models and Image Processing*, 56: 281-288 (1994).

56. Jocobs, D. *The State of the Art, Numerical Analysis*. New York : Academic Press, 1977.

57. McLain, D.H. *Mathematical Methods, Computer Graphics Design.* New York : Academic Press, 1980.

58. Daoud, Daoud S. "On combination of first order Strang's splitting and additive splitting for the solution of multi-dimensional convection diffusion problem," *International Journal of Computer Mathematics*, 84: 1781-1794 (December 2007).

59. Nicholson, J.W. "A problem in the theory of heat conduction," *Proceedings of the Royal Society of London, Series A*, 100: 226-240 (December 1921).

60. Abramowitz, M. and I.A. Stegun. *Handbook of mathematical functions* (9th Edition). Washington, D.C. : U.S. Government Printing Office, 1970.

61. Ludema, Kenneth and Bharat Bhushan. *Modern Tribology Handbook Vol.2.* Boca Raton, Florida : CRC Press LLC, 2001.

62. Gahr, Karl-Heinz Z. Microstructure and Wear of Materials. Elsevier Science Ltd., 1987.

63. Damdakizi, F., P. Le Tallec, and J.P. Perlat. "Multiscale thermomechanical modeling of shock-driven dry friction in hydrodynamics," *Computer Methods in Applied Mechanics and Engineering*, : 25 (2009).

64. Parker, F. Stefani and J.V. "Experiments to Measure Wear in Aluminum Armatures," *IEEE Tans. Magnetics*, 35: 100-106 (January 1999).

65. Ling, Frederick F. "A quasi-iterative method for computing interface temperature distributions," *Zeitschrift für angewandte Mathematik und Physik (ZAMP)*, 10.5: 461-474 (1959).

66. Tanvir, M.A. "Temperature rise due to slip between wheel and rail - an analytical solution for hertzian contact," *Wear*, 61: 295-308 (1980).

67. Knothe, Martin Ertz and Klaus. "A Comparison of analytical and numerical methods for the calculation of temperatures in wheel/rail contact," *Wear*, 253: 498-508 (May 2002).

68. Karlsson, Birger and Johan Ahlstrom. “Analytical 1D model for analysis of the thermally affected zone formed during railway wheel skid,” *Wear*, 232: 15-24 (May 1999).

69. Trigger, K.J. and B.T. Chao. “Temperature distribution at the chip-tool interface in metal-cutting,” *Trans. ASME*, 77: 1107-1121 (1955).

70. Ling, F.F. “A quasi-iterative method for computing interface temperature distributions,” *Zeitschrift fur Angewandte Mathematik*, 10: 461-474 (1959).

71. Hou, Z.B. and R. Komanduri. “Thermal analysis of dry sleeve bearings - a comparison between analytical, numerical(FEM), and experimental results,” *Tribol. Int.*, 34: 145-160 (2001).

72. Kennedy, Jr., F.E. “Surface temperature in sliding systems - a finite element analysis,” *Trans. ASME J. Tribol.*, 103: 90-96 (1981).

73. Floquet,A., D. Play, and M. Godet. “Surface temperatures in distributed contacts - application to bearing design,” *Trans. ASME J. Lubric. Technol.*, 99: 277-283 (1977)

74. McGraw-Hill and S.P. Parker. *McGraw-Hill Dictionary of Scientific and Technical Terms* (6th Edition). New York: The McGraw-Hill Company Co., 2003.

75. Landau, H.G. “Heat Conduction in a Melting Solid,” *Quarterly of Applied Mathematics*, 8: 81-94 (1950).

76. Stefani, R.E. Kothmann and F. *A thermal Hydraulic Model of Melt Lubrication in Railgun Armature: Tech. Report, 2003*. Institute for Advanced Technology, The University of Texas at Austin. 2003.

77. Nastac, Laurentiu. “On the Validity of the Quasi-Steady State Equation for Heat or Mass Transfer Problems with an Axially Moving Boundary,” *Int. Comm. Heat Mass Transfer.*, 25: 407- 416 (1998).

78. Laraqi, N., N.Alilat, J.M.Garcia de Maria, and A.Bairi. “Temperature and Division of Heat in a pin-on-disc Frictional Device-Exact analytical Solution,” *Wear*, 266: 765-770 (2009).

79. Challita, J.P. Barber and A. “Velocity Effects on Metal Armature Contact Transition,” *IEEE Trans. On Magnetics*, 29: 733-737 (January 1993).

80. Dreizin, J.P. Barber and Y.A. “Model of Contact Transitioning with Realistic Armature Rail Interface,” *IEEE Trans. On Magnetics*, 31: 96-100 (January 1995).

81. Johnson, K.L. *Contact Mechanics*. Cambridge, U.K. : Cambridge University Press, 1985.

82. Evans, G.W., E. Isaacson, and J.K.L. MacDonald. “Stefan-Like Problems,” *Quart. Appl. Math.*, 8: 312-319 (1950).

83. Ruoff, A.L. “An Alternate Solution of Stefan's Problem,” *Quart. of Appl. Math*., 116: 197-201 (July 1958).

84. Ingersoll, L.R. and Zobel, O.J. *An introduction to the Mathematical Theory of Heat Conduction*. New York : Ginn and Co., 1913.

85. Lightfoot, N.M.H. “The Solidification of Molten Steel,” *The London Mathematical Society, Series 2*, 31: 97-116 (1930).

86. White, F.M. *Viscous Fluid Flow* (3rd Edition). : McGraw-Hill, 2006.

87. Goodman, T.R. “Aerodynamic Ablation of Melting Bodies,” *The third U.S. National congress of Applied Mechanics.* Brown University : 1958.

88. Citron, Stephen J. “Heat Conduction in a Melting Slab,” *Journal of the aero/space sciences*, 27: 219-228 (March 1960).

89. Meador, S. P. *Consideration of Wear at High Velocities*, MS Thesis, AFIT/GAE/ENY/10-M16. School of Engineering and Management Air Force Institute of Technology (AU), Wright Patterson AFB, OH, March 2010.

90. Pritchett, Michael and Peter J. Blau. *Friction Science and Technology* (2nd Edition). Boca Raton : CRC Press, 2009.

91 Morton, K.W. and D.F. Mayers. *Numerical Solution of Partial Differential Equations* (2nd Edition). Cambridge : Cambridge University Press, 2005.

92. Strikwerda, John C. *Finite Difference Schemes and Partial Differential Equations*. Pacific Grove : Wadsworth & Brooks/Cole Advanced Books & Software, 1989.

93. Kaplan, Wilfred. *Operational Methods For Linear Systems*. Reading, Massachusetts : Addison-Wesley Publishing Company, INC., 1962.

94. Gradshteyn, I.S. and I.M. Ryzhik. *Table of Integrals, Series, and Products* (7th Edition). Massachusetts, USA : Academic Press, Elsevier Inc., 2007.

REPORT DOCUMENTATION PAGE

Form Approved
OMB No. 0704-0188

PLEASE DO NOT RETURN YOUR FORM TO THE ABOVE ADDRESS.

1. REPORT DATE *(DD-MM-YYYY)*	2. REPORT TYPE	3. DATES COVERED *(From - To)*
27 Mar 2014	Dissertation	01 Sep 2007 - 27 Mar 2014

4. TITLE AND SUBTITLE

Analysis of Heat Partitioning During Sliding Contact At high Speed and Pressure

5a. CONTRACT NUMBER

5b. GRANT NUMBER

5c. PROGRAM ELEMENT NUMBER

6. AUTHOR(S)

Paek-Spidell, Gracie Y.

5d. PROJECT NUMBER

5e. TASK NUMBER

5f. WORK UNIT NUMBER

7. PERFORMING ORGANIZATION NAME(S) AND ADDRESS(ES)

Air Force Institute of Technology
Graduate School of Engineering and Management (AFIT/EN)
2950 Hobson Way
Wright-Patterson AFB OH 45433-7765

8. PERFORMING ORGANIZATION REPORT NUMBER

AFIT-ENC-DS-14-M-02

9. SPONSORING/MONITORING AGENCY NAME(S) AND ADDRESS(ES)

Air Force Office of Scientific Research
875 Randolph St. Suite 325, room 3112
Arlington, VA 22203
PM: Michael Kendra

10. SPONSOR/MONITOR'S ACRONYM(S)

AFOSR/NA

11. SPONSOR/MONITOR'S REPORT NUMBER(S)

12. DISTRIBUTION/AVAILABILITY STATEMENT

DISTRIBUTION STATEMENT A. APPROVED FOR PUBLIC RELEASE; DISTRIBUTION UNLIMITED.

13. SUPPLEMENTARY NOTES

This material is declared a work of the U.S. Government and is not subject to copyright protection in the United States.

14. ABSTRACT

This research develops a mathematical formulation and an analytical solution to frictional heat partitioning in a high speed sliding system. Frictional heating at the interface of sliding materials impacts temperature and the wear mechanisms. The heat partition fraction for a sliding system is an important parameter in calculating the distribution of frictional heat flux between the contacting surfaces. The solution presented in this dissertation considers the characteristics of the slipper's frictional heat partition values along with the experimental loading data. With a physics based, rather than a phenomenological approach, this solution improves the estimate for the slipper's heat partition function. Moreover, this analytical solution is practical in calculating the average surface temperature and estimating the total melt wear volume. The heat partition function compares favorably with existing experimental and analytical data. Using the Strang's Splitting and ADI methods, a numerical method for surface temperature and corresponding wear percentage under dynamic bounce conditions was extensively developed.

15. SUBJECT TERMS

Frictional Heat Partitioning, Heat flux distribution, Sliding Contact

16. SECURITY CLASSIFICATION OF:			17. LIMITATION OF ABSTRACT	18. NUMBER OF PAGES	19a. NAME OF RESPONSIBLE PERSON
a. REPORT	b. ABSTRACT	c. THIS PAGE			Dr. William P. Baker, AFIT/ENC
U	U	U	UU	219	19b. TELEPHONE NUMBER *(Include area code)* (937) 255-3636 x4517 william.baker@afit.edu

Reset

Standard Form 298 (Rev. 8/98)
Prescribed by ANSI Std. Z39.18